REPORT DOCUMENTATION PAGE

Public reporting burden for this collection of information is estimated to average 1 hour per response, including the time for reviewing instructions, searching existing data sources, gathering and maintaining the data needed, and completing and reviewing the collection of information. Send comments regarding this burden estimate or any other aspect of this collection of information, including suggestions for reducing this burden, to Washington Headquarters Services, Directorate for Information Operations and Reports, 1215 Jefferson Davis Highway, Suite 1204, Arlington, VA 22202-4302, and to the Office of Management and Budget, Paperwork Reduction Project (0704-0188), Washington, DC 20503.

1. AGENCY USE ONLY *(Leave blank)*	2. REPORT DATE 23.May.03	3. REPORT TYPE AND DATES COVERED DISSERTATION

4. TITLE AND SUBTITLE
CHARACTERIZING MOTOR VEHICLE FLEET EMISSIONS BY OPEN-PATH
SPECTROSCOPY

5. FUNDING NUMBERS

6. AUTHOR(S)
CAPT BRANAN DANIEL M

7. PERFORMING ORGANIZATION NAME(S) AND ADDRESS(ES)
UNIVERSITY OF DENVER

**8. PERFORMING ORGANIZATION
REPORT NUMBER**

CI02-966

9. SPONSORING/MONITORING AGENCY NAME(S) AND ADDRESS(ES)
THE DEPARTMENT OF THE AIR FORCE
AFIT/CIA, BLDG 125
2950 P STREET
WPAFB OH 45433

**10. SPONSORING/MONITORING
AGENCY REPORT NUMBER**

11. SUPPLEMENTARY NOTES

12a. DISTRIBUTION AVAILABILITY STATEMENT
Unlimited distribution
In Accordance With AFI 35-205/AFIT Sup 1

12b. DISTRIBUTION CODE

13. ABSTRACT *(Maximum 200 words)*

DISTRIBUTION STATEMENT A
Approved for Public Release
Distribution Unlimited

20030604 068

14. SUBJECT TERMS

	15. NUMBER OF PAGES 233
	16. PRICE CODE

17. SECURITY CLASSIFICATION OF REPORT	18. SECURITY CLASSIFICATION OF THIS PAGE	19. SECURITY CLASSIFICATION OF ABSTRACT	20. LIMITATION OF ABSTRACT

CHARACTERIZING MOTOR VEHICLE FLEET EMISSIONS BY
OPEN-PATH SPECTROSCOPY

———————

A Dissertation

Presented to

the Faculty of Natural Sciences, Mathematics, and Engineering

University of Denver

———————

In Partial Fulfillment

of the Requirements for the Degree
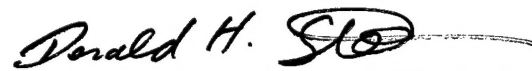
Doctor of Philosophy

———————
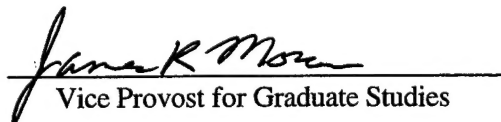
by

Daniel M. Branan

August 2002

GRADUATE STUDIES

AT

THE UNIVERSITY OF DENVER

Upon the recommendation of the chairperson of the
Department of Chemistry this dissertation is hereby
accepted in partial fulfillment of the requirements for the
degree of

Doctor of Philosophy

Donald H. Sto
_____
Professor in charge of dissertation

James R More
_____
Vice Provost for Graduate Studies

_1/31/03_
_____
Date

TABLE OF CONTENTS

LIST OF FIGURES

LIST OF TABLES

CHAPTER 1. - INTRODUCTION

1.1 Statement of Thesis

In this thesis, I present the conceptual combination of the tunnel study with remote sensing. In other words, I present a technique for measuring fleet-averaged modal emissions from a large aggregate population of vehicles (as in a tunnel study), which employs relatively simple and rugged spectroscopic techniques (as in remote sensing). In combining these two ideas, even more flexibility in measurement location and traffic conditions is achieved, ensuring as random and representative a sampling of the vehicle population as is possible. In that sense, this approach could be referred to as "A Tunnel-less Tunnel Study," since it combines the inherent fleet-averaging ability of the tunnel study with the mobility of remote sensing. Specifically, this method combines both OP-FTIR and OP-UV spectroscopy and uses some local meteorological data collection to filter the data for appropriate weather conditions. The OP-FTIR spectra are analyzed using Griffith's synthetic calibration approach, while the OP-UV spectra are currently analyzed by single-component least-squares fitting of actual calibration spectra. Because very few instruments are needed,

many of the potential maintenance and calibration difficulties inherent to the tunnel study are avoided as well. Additionally, this method, which I have named **O**pen-**P**ath **I**nfrared/UV **E**missions **M**onitoring (OPIEM), could either be employed as a permanently installed unattended monitor, or may be moved to many locations to sample different vehicle populations and/or modes of operation.

What is actually measured in this approach is the absolute path-independent mixing ratio of CO_2, CO, N_2O, CH_4, NH_3 and NO. These data (with the exception of CO_2) are all regressed against the mixing ratio of CO_2 and the slope of the resulting line is taken to be the relationship between the pollutants of interest and CO_2. This is done because the change in carbon dioxide close to the roadway is assumed to be due to vehicles passing the measurement site. If a correlation exists between ΔCO_2 and ΔX, then it can be assumed that the source of X and the source of CO_2 are identical. These ratios are used to produce an emission factor that represents the contribution of the entire fleet of vehicles that passed the measurement site during data collection. In this case, this is done for all quantities except hydrocarbons (HC), which are known to be a small contribution to the

8

total exhaust of the average vehicle. Instead, the assumption is made that HC/CO_2 is equal to approximately $1/12$ of the CO/CO_2 ratio.[98]

The usefulness of this approach lies mainly in the fact that it directly produces fleet-averaged, modal emission factors (*modal* because the factor should be proportional to the mode of vehicle operation near the measurement site) without the need to use large suites of instruments (as in most tunnel studies) or to collate, weight and average a huge number of individual vehicle readings (as with most remote sensing applications). Using only two long-path spectrometers, you can obtain data that are automatically weighted to the actual distribution of vehicles and proportional to the mode of operation of those vehicles.

1.2 History

Transportation and pollution have always gone hand-in-hand. Mankind's faithful servants, the horse, the ox and the internal combustion engine, have all contributed to pollution in their own way. In fact, the internal combustion engine was originally hailed as the savior of the urban lifestyle and the large metropolis. At the turn of the twentieth century, livestock-based transportation had so polluted the

9

landscape of the modern cities of New York, Chicago and the like, that it had become a major health concern and a cause for alarm. Streets were literally choked with waste, which had to be hauled out to the countryside in tonnage quantities every day. This was a problem in every industrialized nation, but especially so in America, where large expanses of available land had led to the building of enormous cities that needed large transportation systems. In New York City, for example, the horse population in 1900 was around 10,000[1] animals. When multiplied by the average waste production rate of a horse, which is 20 kg/day,[2] the result is that 73,000 metric tons of manure had to be either hauled away or trodden underfoot each year – not the healthiest scenario imaginable. In contrast, the almost invisible exhaust from the combustion of petroleum fuels was seemingly inconsequential, and at least it didn't pile up in the streets.

1.3 Air Quality Regulation in the United States

We no longer take such a benign view of automotive emissions today, or of man-made emissions in general. Since 1970, with the passage of the Clean Air Act[3] and the establishment of National Ambient Air Quality Standards (NAAQS), the United States has put major effort into reducing the impacts of both fixed and mobile sources

of pollution, with excellent results. The national trends in the United States' annual emissions of carbon monoxide (CO), volatile organic carbon (VOC), sulfur dioxide (SO2), and particulate matter (PM10), have been steadily downward since about 1970.[4] The 1990 amendments to the Clean Air Act established updated NAAQS's for seven criteria pollutants:[5] nitrogen oxides (NOx), sulfur oxides (SOx), CO, particulate matter smaller than 10 microns (PM_{10}), particulate matter smaller than 2.5 microns ($PM_{2.5}$), airborne lead, and tropospheric ozone (O_3), which are listed in Table 1. According to the EPA, "Primary standards set limits to protect public health, including the health of "sensitive" populations such as asthmatics, children, and the elderly. Secondary standards set limits to protect public welfare, including protection against decreased visibility, damage to animals, crops, vegetation, and buildings."[5] Of these pollutants, all but two, SOx and O_3, are directly emitted by automobiles, although tropospheric O_3 has been shown to be produced thorough a photochemical cycle involving organic carbon species and NOx.[6,7] Additionally, newer automobiles with catalysts designed to control NOx and CO emissions may contribute further to the particle loading in the troposphere by emitting ammonia (NH_3), which forms solid particles of ammonium sulfate and ammonium nitrate through chemical reactions with airborne

11

sulfuric and nitric acids.[8,9,10,11] There is mounting evidence that anthropogenic emissions are affecting not just the quality of the air we breathe, but also possibly the radiative balance of the earth itself.

1990 National Ambient Air Quality Standards			
POLLUTANT	**STANDARD VALUE**		**STANDARD TYPE**
Carbon Monoxide (CO)			
8-hour Average	9 ppm	($10 \, mg/m^3$)	Primary
1-hour Average	35 ppm	($40 \, mg/m^3$)	Primary
Nitrogen Dioxide (NO_2)			
Annual Arithmetic Mean	0.053 ppm	($100 \, \mu g/m^3$)	Primary & Secondary
Ozone (O_3)			
1-hour Average	0.12 ppm	($235 \, \mu g/m^3$)	Primary & Secondary
8-hour Average *	0.08 ppm	($157 \, \mu g/m^3$)	Primary & Secondary
Lead (Pb)			
Quarterly Average	$1.5 \, \mu g/m^3$		Primary & Secondary
Particulate (PM 10) *Particles with diameters of 10 micrometers or less*			
Annual Arithmetic Mean	$50 \, \mu g/m^3$		Primary & Secondary
24-hour Average	$150 \, \mu g/m^3$		Primary & Secondary
Particulate (PM 2.5) *Particles with diameters of 2.5 micrometers or less*			
Annual Arithmetic Mean	$15 \, \mu g/m^3$		Primary & Secondary
24-hour Average	$65 \, \mu g/m^3$		Primary & Secondary
Sulfur Dioxide (SO_2)			
Annual Arithmetic Mean	0.03 ppm	($80 \, \mu g/m^3$)	Primary
24-hour Average	0.14 ppm	($365 \, \mu g/m^3$)	Primary
3-hour Average	0.50 ppm	($1300 \, \mu g/m^3$)	Secondary

* The ozone 8-hour standard is included for information only. A 1999 federal court ruling blocked implementation of these standards, which EPA proposed in 1997. The U.S. Supreme Court has ruled that the implementation plan for the new ozone standards is unlawful. The case has been remanded to the Court of Appeals for the District of Columbia Circuit.[12]

Table 1 - U. S. EPA National Ambient Air Quality Standards

Since 1988, the Intergovernmental Panel on Climate Change (IPCC), formed by the United Nations Environment Program (UNEP) and the World Meteorological Organization (WMO), has attempted to compile the most reliable, peer-reviewed data and scientific analysis regarding human impacts on the global environment that are available. Using this information, the IPCC publishes an exhaustive report about every five years. There is no doubt that the concentrations of certain gases in the atmosphere, such as carbon dioxide (CO_2), tropospheric ozone (O_3), nitrous oxide (N_2O), and others have risen steadily since the beginning of the industrial revolution (see Table 2).[13] In their 2001 report, the IPCC states that the transportation sector alone accounted for 22% of the global energy-related CO_2 emissions in 1995.[14] The United States Environmental Protection Agency (EPA) national pollutant emission estimate for 1999 shows that both on and off-road vehicles were responsible for more than 77% of total CO, 56% of nitrogen oxides (NOx), and 47% of VOC emissions.[15] Estimates of anthropogenic sources of methane and nitrous oxide were characterized by the IPCC as uncertain, but the transportation sector certainly contributes to each of these greenhouse gas emissions. This is confirmed by the U. S. EPA and in a number of recent publications.[16-20] The EPA's estimate of recent greenhouse gas

emission trends shows that mobile sources are the second largest

contributor,[21] albeit only 16% in 1997, to N_2O emissions in the United

States.

Indicator	Observed Changes
Concentration indicators	
Atmospheric concentration of CO_2	280 ppm for the period 1000-1750 to 368 ppm in year 2000 ($31\pm4\%$ increase).
Terrestrial biospheric CO_2 exchange	Cumulative source of about 30 Gt C between the years 1800 and 2000; but during the 1990s, a net sink of about 14 ± 7 Gt C.
Atmospheric concentration of CH_4	700 ppb for the period 1000-1750 to 1,750 ppb in year 2000 ($151\pm25\%$ increase).
Atmospheric concentration of N_2O	270 ppb for the period 1000-1750 to 316 ppb in year 2000 ($17\pm5\%$ increase).
Tropospheric concentration of O_3	Increased by $35\pm15\%$ from the years 1750 to 2000, varies with region.
Atmospheric concentrations of HFCs, PFCs, and SF_6	Increased globally over the last 50 years.

Table 2 - IPCC Summary of Greenhouse Gas Changes

The United States also has international obligations when it

comes to reporting emissions of many of these gases. In 1992, the

U.S. became a signatory to the United Nations Framework Convention

on Climate Change (UNFCCC). By signing on to this international

agreement, the U. S. agreed to "develop, periodically update, publish

and make available...national inventories of anthropogenic emissions

by sources and removals by sinks of all greenhouse gases not

controlled by the Montreal Protocol, using comparable

methodologies."[22] The "Montreal Protocol on Substances that Deplete

the Ozone Layer" is another international agreement established in

1987 to reduce the production and use of halocarbons.[23] In fulfillment

of this obligation to the UNFCCC, the U.S. EPA publishes a report

entitled "Inventory of U.S. Greenhouse Gas Emissions and Sinks:"

each year. The greenhouse gases of interest (those not covered by

the Montreal Protocol) are hydrofluorocarbons (HFC's),

perfluorocarbons (PFC's), sufur hexafluoride (SF_6), H_2O, N_2O, CO_2,

and CH_4. Because there are so many natural sources of water vapor

in the atmosphere, it is not considered a result of anthropogenic

interference, even though a large number of man-made processes

produce water vapor. The "comparable methodologies" have been

established by the IPCC in the publication entitled: "IPCC Guidelines

for National Greenhouse Gas Inventories."[24]

1.2.1 Distance-Based Emissions Inventories

In an effort to manage fixed-source and mobile-source

emissions responsibly, the EPA requires that areas in the United

States that violate the NAAQS maintain a plan to curtail their

16

emissions. Each state with areas not in attainment with the NAAQS must submit a "State Implementation Plan" (SIP) to indicate what measures they are taking to achieve attainment with the standards. The SIP must be approved by the EPA, and must be developed by the state Department of Health, with input from the metropolitan planning organizations (MPO) in each affected area. For example, in Colorado Springs, Colorado, where a major portion of the research for this thesis was performed, the MPO is the Pike's Peak Area Council of Governments, which oversees all metropolitan planning projects in the city and surrounding areas. The EPA's *Procedures for Preparing Emissions Projections* document stipulates that a "zonal travel demand model" must be employed in the determination of mobile source emissions. This model should be based on actual traffic counts, where they are available. These estimates of vehicle miles traveled (VMT) in the non-attainment area are then combined with modeled emission factors from the EPA's MOBILE modeling program to produce an estimate of total emissions, which is called the "mobile emissions inventory".[25,26] The mobile and fixed-source emissions inventories are combined to produce an area-wide emissions inventory. As part of the SIP, the state must show what measures it will take to annually decrease the total annual inventory of any pollutant exceeding the

17

standards. Any new metropolitan planning must be weighed against the SIP by estimating any impact to the emissions inventory by either fixed or mobile sources. If it is estimated that the new project will cause the total emissions inventory to rise so that the area will degrade its non-attainment status even further, then the project will not be undertaken.[25] According to the 1990 amendments to the Clean Air Act (section 108(f)(1)(A)), there are many ways that a state can show that a transportation-related project may decrease the emissions inventory, but virtually all of them are based upon the unproven idea that decreased traffic congestion results in decreased mobile source emissions.[25]

As an example of an actual SIP, I will discuss the methods, results and recommendations from the Colorado Springs, Carbon Monoxide plan. Colorado Springs is a quickly growing community in the foothills of the Rocky Mountains where I have attempted to measure fleet-averaged modal emission factors over the past few years. The city is located approximately 60 miles south of Denver, and is the predominant population center in El Paso County. In calendar year 2000, El Paso County had a population of 519,774 people over the age of 1 year, according to the Colorado Department of Health.[27]

18

The total number of registered vehicles for the same time period and location was 455,764, according to the Colorado Department of Revenue's annual report.[28]

According to the Colorado Department of Public Health and Environment, Air Pollution Control Division, Technical Services/Planning and Policy Program Office,[29] Colorado Springs was in non-attainment of national CO concentration standards from the 1970's until 1989. Due to the fact that CO levels have not exceeded
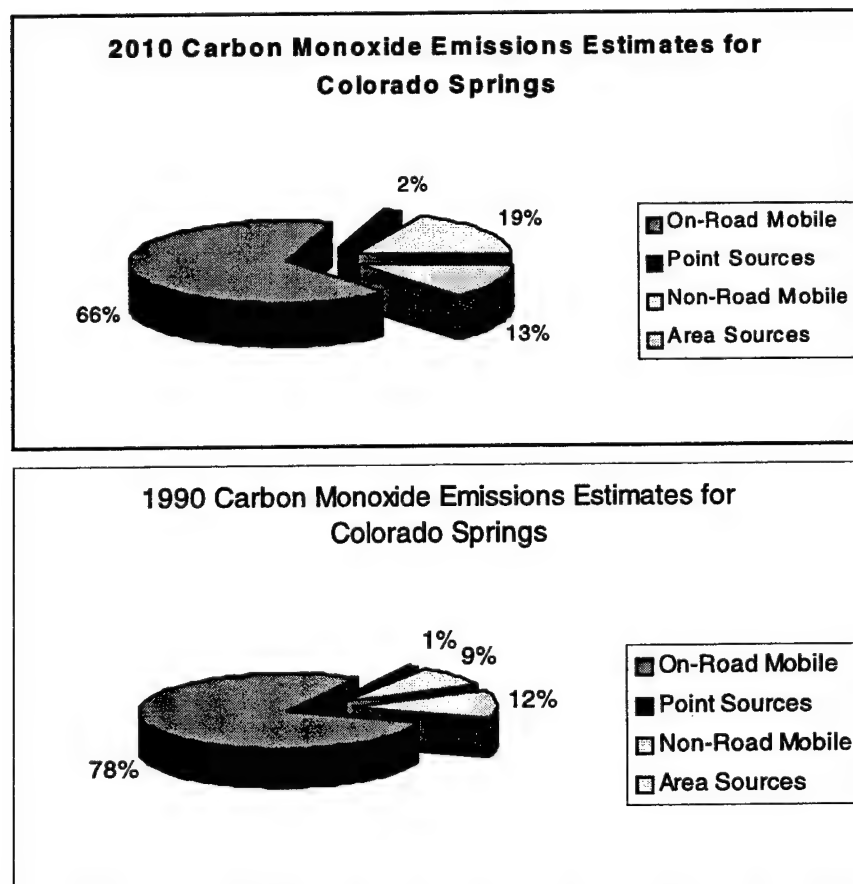
Figure 1 - CO Emission Estimates for Colorado Springs

the NAAQS since that time, the state requested a redesignation of Colorado Springs to "attainment" status in 1999. In order to support this request, the state had to make the case that the CO emissions are less now than in the recent past, and that they were likely to be even less in the future. The methods employed to do this will be described below and held out as a general example of how states determine emission inventories for the criteria pollutants, and how they determine what future emissions are likely to be. Later, these methods will be compared and contrasted with the methods proposed in this thesis.

In order to show continued improvement and satisfy the EPA's requirements, the state of Colorado had to calculate CO inventories both for a baseline year when Colorado Springs was in compliance, which they chose to be 1990, and for a period of time at least ten years later. Therefore, the redesignation request included complete inventories of CO emissions for 1990 and 2010, the results of which are represented in Figure 1. It is important to note that these inventories were both calculated from EPA approved models, and were not the results of actual measurements. Both years (1990 and 2010) were modeled in 1998 when the work for the redesignation request was performed.

In comparison to stationary sources, which can be well characterized, the contribution of mobile sources is difficult to quantify. The EPA categories of sources in Colorado Springs are listed in Table 3. The accuracy of the state's estimate of mobile source emissions relies entirely on the accuracy of the estimated VMT and the estimated

On-Road Mobile	Non-Road	Point Sources	Area Sources
Cars and Trucks	Aircraft, Railroads, Lawn and Garden, Airport Service, Recreational, Recreational Marine, Light Commercial, Industrial, Construction, Agricultural, Logging	Major Industrial Plant (>= 100 tons per year) Minor Industrial Plant (< 100 tpy)	Fireplaces, Woodstoves, Natural Gas, Forest Wildfires, Managed Burning, Charcoal Grilling, Structural Fires, Firefighter Training, Aircraft/Rocket Motor testing, Orchard Heaters

Table 3 - EPA Source Categories Present in Colorado Springs

(modeled) emission factors. In both cases, accuracy is difficult to gauge because neither estimation method gives quantified errors. In the case of the latter, emission factor models have been shown many times to deviate from actual measurements of real-world vehicle emissions, sometimes by factors of 3 or 4.[30 - 33, 100] In addition, emission factor models are statistically based and have traditionally been unable to adequately represent high emitting vehicles.[34] Stedman, *et al.*, have shown that high-emitters dominate roadway

21

emissions and are highly variable, making them difficult to model statistically. This merely points out the need for accurate measurement technologies and techniques in order to realistically measure the actual emissions from the real-world fleet.

1.2.2 Fuel-Based Emissions Inventories

Using actual measurements of vehicle emissions also gives the opportunity to calculate (as opposed to model) a mobile-source emissions inventory. This can be done because the basic assumption can be made that virtually all of the carbon in the fuel is emitted as either CO_2, CO or hydrocarbons. This assumption is accurate to at least a level of 98%. Assuming that this is true, both Stedman[39] and Harley[35] have shown that CO_2 can essentially be used as a tracer gas. If the ratio to CO_2 of each of the other emitted gases is calculated, the following equation can be used to calculate the grams of pollutant X (where 'X' is some other emitted gas) emitted per liter of gasoline burned. By Stedman's method, one must first determine the ratio of X to carbon on a mole basis:

$$\frac{moles_X}{moles_C} = \frac{[X]\big/[CO_2]}{([CO_2]+[CO]+[HC])\big/[CO_2]} \qquad (1)$$

This ratio is then used to calculate the fuel-based emission factor, which takes into account the average density of gasoline and the average number of moles of carbon per kilogram of gasoline:

$$emission\_factor_X = \frac{moles_X}{moles_C} * \left[\frac{g}{mole}\right]_X * \frac{71.43\_molesC}{kg_{fuel}} * \frac{0.73\_kg_{fuel}}{L_{fuel}} \qquad (2)$$

Using these equations along with real-world measurements and knowledge of fuel use within a certain geographic area, it is possible to calculate a fuel-based emissions inventory. Even though there is a large amount of literature regarding emissions factors for various pollutants, they have only recently been used, initially by Harley and Singer, for the purposes of calculating fuel-based inventories.[35-39]

A majority of the emissions factors listed in the literature can be found in Appendix F. One of the problems plaguing those who would like to make comparisons between emission factors measured and calculated by various methods is the wide difference in units used to report these factors. Groups interested in mileage-based modeling usually report emission factors in units of grams/kilometer (or mile), while those interested in fuel-based calculations usually report in units of grams/liter (or gallon). Tunnel studies often report factors in a distance-based unit because the emissions are actually measured over

23

a specific distance inside the tunnel. Sometimes, the factors are reported in energy units such as grams/brake-horsepower. There is no simple way of converting between distance and volume-based units, but I have made a rudimentary attempt in Appendix F, which is at least consistent if not entirely accurate. In order to truly convert from a volume-based unit to a distance-based unit, one needs to know the exact fuel economy for the vehicle(s) when the factor was measured. In lieu of being that specific, I instead attempted to determine an average fleet-wide fuel economy for a random fleet of vehicles within the United States, and then used that number to convert from distance to fuel volume. Therefore, the factors in Appendix F are reported in g/km, g/mi, g/L and g/gal, no matter what their original units of measurement happened to be.

To determine an average fleet-wide fuel economy, I used model year distribution data gathered by our research group in Austin, Texas; Chicago, Illinois; Denver, Colorado; Los Angeles, California and Phoenix, Arizona, between 1997 and 2000. These data sets consist of makes and models of vehicles identified from their license plates. Using the US EPA's data on fuel economy by model year, I calculated a weighted average for the entire fleet in each city. The result was

24

surprisingly coherent, with a standard deviation of less than 1% of the

average value. The result (with an assumed error of 3*sigma) is:

21.48 ± 0.58 miles per gallon. This analysis took into account the

makes, models and age-adjusted fuel economy of 162,112 vehicles.

1.3 Air Pollution of Interest from Mobile Sources

If we could measure the real-world emissions from automobiles directly, what would we need to measure and why? A discussion of this topic necessitates an explanation of the combustion process in order to understand how automotive pollutants are produced. Engines in on-road vehicles in the United States can generally be separated into one of two different classes: spark ignition gasoline engines, and compression ignition diesel engines. Both classes are reciprocating piston engines, but there are many different variations of each kind with different numbers of cylinders or fuel/air mixing systems, etc. However, the principles of combustion are the same in any kind of internal combustion engine, so I will not differentiate between the different classes unless there is some reason to do so based on combustion product differences.

Principally, when discussing air quality standards, the highest

degree of concern is with the troposphere, since that is the layer that

has the most direct impact on plant and animal life. Figure 2 illustrates

the layers of the atmosphere with corresponding height, pressure and

temperature profiles of each. The lowest 18 km of the atmosphere (the
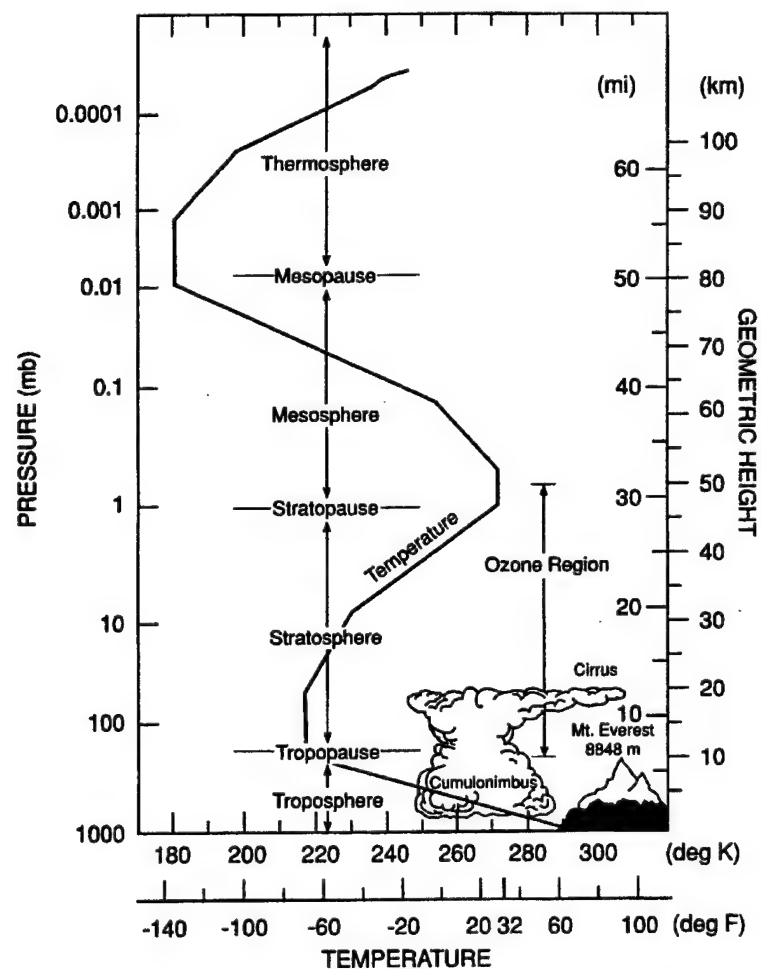
Figure 2 – Layers of the Atmosphere[23]

troposphere) contains 85 – 90% of the total mass of the atmosphere, which amounts to approximately 4.6 x 10^{15} metric tons.[23] The lowest kilometer, or so, of the troposphere is called the atmospheric boundary layer, and is responsible for the exchange of chemical compounds between the surface and the free troposphere.[23] The composition of the atmosphere is relatively stable, even though the concentrations of some compounds have been increasing slowly, as mentioned above. Nevertheless, it is a chemically dynamic environment, with a myriad of competing chemical equilibria. The average mixing ratios of major components of the atmosphere are listed in Table 4, along with the major source of each compound.

Chemical Composition of the Atmosphere

Constituent	Chemical Formula	Volume Mixing Ratio in Dry Air	Major Sources and Remarks
Nitrogen	N_2	78.084%	Biological
Oxygen	O_2	20.948%	Biological
Argon	Ar	0.934%	Inert
Carbon dioxide	CO_2	360 ppmv	Combustion, ocean, biosphere
Neon	Ne	18.18 ppmv	Inert
Helium	He	5.24 ppmv	Inert
Methane	CH_4	1.7 ppmv	Biogenic and anthropogenic
Hydrogen	H_2	0.55 ppmv	Biogenic, anthropogenic, and photochemical
Nitrous oxide	N_2O	0.31 ppmv	Biogenic and anthropogenic
Carbon monoxide	CO	50-200 ppbv	Photochemical and anthropogenic
Ozone (troposphere)	O_3	10-500 ppbv	Photochemical
Ozone (stratosphere)	O_3	0.5-10 ppm	Photochemical
Nonmethane hydrocarbons		5-20 ppbv	Biogenic and anthropogenic
Halocarbons (as chlorine)		3.8 ppbv	85% anthropogenic
Nitrogen species	NO_y	10 ppt-1 ppm	Soils, lightning, anthropogenic
Ammonia	NH_3	10 ppt-1 ppb	Biogenic
Particulate nitrate	NO_3^-	1 ppt-10 ppb	Photochemical, anthropogenic
Particulate ammonium	NH_4^+	10 ppt-10 ppb	Photochemical, anthropogenic
Hydroxyl	OH	0.1 ppt-10 ppt	Photochemical
Peroxyl	HO_2	0.1 ppt-10 ppt	Photochemical
Hydrogen peroxide	H_2O_2	0.1 ppb-10ppb	Photochemical
Formaldehyde	CH_2O	0.1-1 ppb	Photochemical
Sulfur dioxide	SO_2	10 ppt-1 ppb	Photochemical, volcanic, anthropogenic
Dimethyl sulfide	CH_3SCH_3	10 ppt-100 ppt	Biogenic
Carbon disulfide	CS_2	1 ppt-300 ppt	Biogenic, anthropogenic
Carbonyl sulfide	OCS	500 pptv	Biogenic, volcanic, anthropogenic
Hydrogen sulfide	H_2S	5 ppt-500 ppt	Biogenic, volcanic
Particulate sulfate	SO_4^{2-}	10 ppt-10 ppb	Photochemical, anthropogenic

Table 4 – Composition of the Atmosphere[23]

What compounds does an internal combustion (IC) engine emit, and by what processes are they made? The answer to that question begins with the basis of operation for any IC engine: the oxidation of a hydrocarbon fuel. This can be generally represented by the following chemical equation.[6]

$$C_x H_y + (x + \frac{1}{4} y)O_2 \rightarrow xCO_2 + \frac{1}{2} yH_2O \qquad (3)$$

29
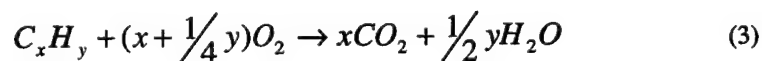
The situation where there is exactly enough oxygen to completely oxidize the hydrocarbon is called a *stoichiometric* air/fuel ratio. Because hydrocarbon fuels are a mixture of a variety of different-length carbon chains, x and y in the above equation for an actual fuel are not necessarily integers. For example, a common test fuel mixture in the United States is "indolene," which has $x=7$, and $y=13.02$.[6] For this fuel, applying equation (3), the stoichiometric amount of oxygen would be 10.3 moles, or 329.6 grams. Because oxygen and nitrogen comprise more than 99% of the dry atmosphere, we can consider the combined amount of oxygen and nitrogen to be the "air" in the air/fuel ratio. Also, because nitrogen is present in a relatively fixed ratio to oxygen (3.76:1), we know there will be 38.7 moles (1085.2 grams) of nitrogen in the air containing the 10.3 moles of oxygen, which is to be mixed with the fuel. This gives a total stoichiometric air/fuel ratio (by mass) of 14.6, which is the standard air/fuel ratio set in most automobiles today.[40] If the air/fuel ratio were higher than stoichiometric, it would be called "lean," and if it were lower, it would be called "rich." Modern, computer controlled engines continuously vary fuel flow (by mass) in order to maintain the air/fuel mixture at close to stoichiometric levels. When excess load is placed on the engine, the computer may cause the fuel flow to increase in order to maximize power. This condition is referred

to as "commanded enrichment." The variation in engine emissions as

a function of air/fuel ratio is illustrated in both Figure 3, and Figure 4.
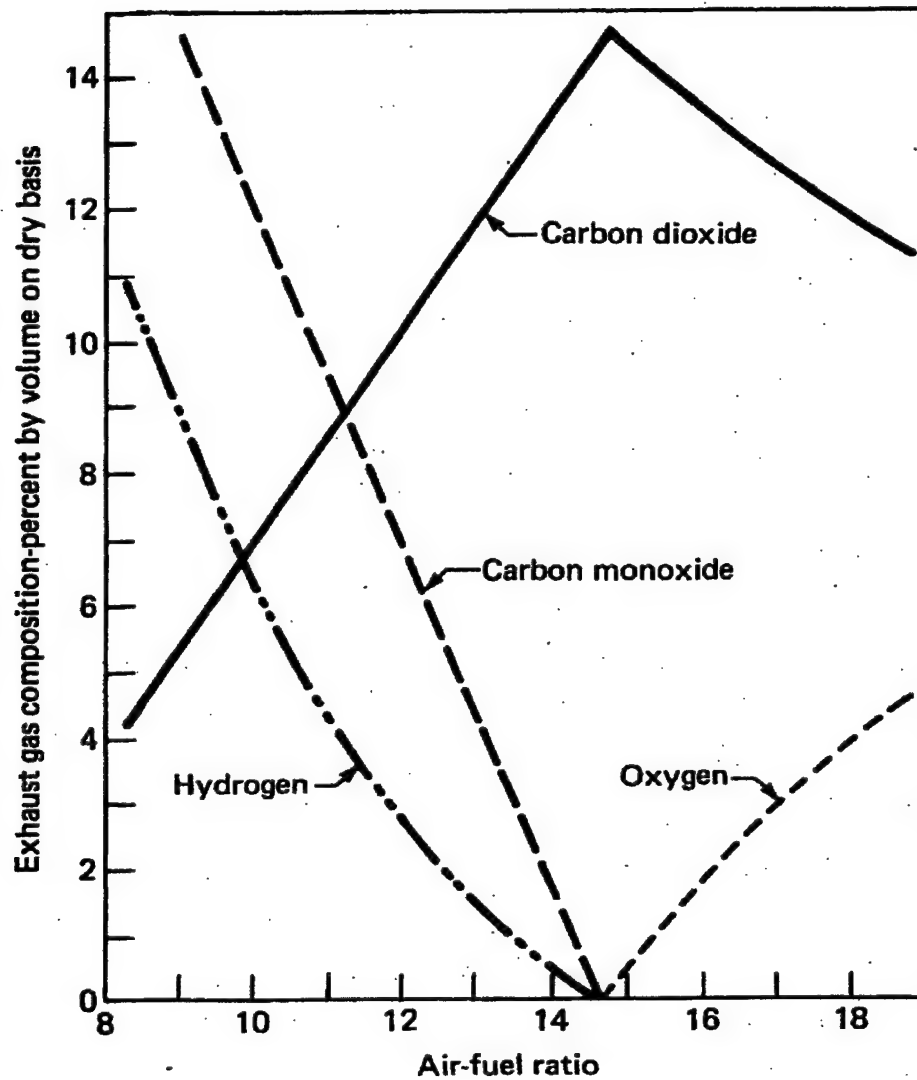
Figure 3 – Approximate Emission Variation with A/F ratio (#1) [6]
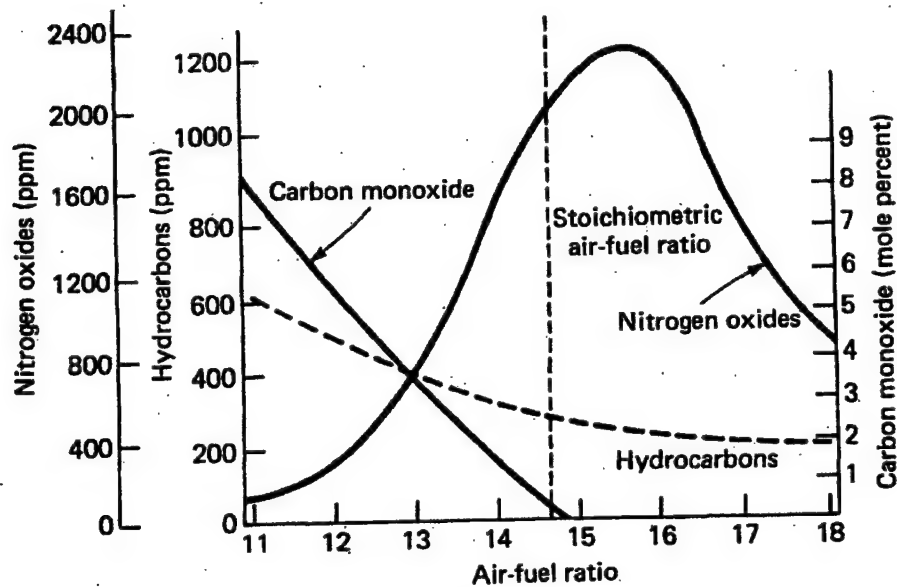
Figure 4 – Emission Variation with A/F ratio (#2) [6]

The direct products of the complete oxidation of hydrocarbons
are carbon dioxide and water, as indicated in equation (3). However, if
the air/fuel mixture is not exactly stoichiometric, or if conditions are not
ideal, there are other products that may be formed. The most
predominant of these is carbon monoxide, which is formed under rich-
burn (high-load) and high temperature conditions. Rich conditions
result in partial oxidation of the fuel due to a lack of oxygen, but even
under slightly lean conditions, high temperatures induce the
dissociation of CO_2 into CO and atomic oxygen.[41,6] Carbon monoxide
is also a deadly poison to humans when present in high enough
concentrations, due to the fact that hemoglobin has a higher affinity for
CO than for oxygen. In the atmosphere, CO is a moderately long-lived

gas, with a lifetime on the order of 10 months.[23] Its primary reaction in the lower atmosphere is to serve as a sink for the hydroxyl radical ($HO\cdot$), which oxidizes it according to this equation: [23]

$$CO + HO\bullet \rightarrow CO_2 + HO_2 \bullet \tag{4}$$
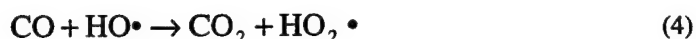
The resulting hydroperoxy radical ($HO_2\cdot$) proceeds to react predominantly with oxides of nitrogen, which will be covered in the following paragraph. Because nitrogen is such a large component of ambient air, and because the hydrocarbon combustion takes place in a high-temperature, high-pressure environment, there exists the possibility for the formation of nitrogen oxides. Molecular nitrogen is very stable, having a bond dissociation energy of 225 kcal/mol.[6] Formation of nitrogen compounds requires high temperatures, with maximum formation rate of nitrogen oxide (NO) occurring at about 3500 K.[40] This is due to the fact that the chemical reactions governing both the formation and destruction of NO are strongly temperature dependent. As can be seen in Figure 4, the production of NO peaks at a slightly lean air/fuel ratio. This is because there are lower temperatures and insufficient oxygen at low air/fuel ratios, but as the ratio exceeds about 16, even though there is excess oxygen,

temperatures again begin to fall due to the dilution of the hot combustion gases with excess air.

The generally accepted mechanism for the formation of nitrogen oxides (NOx) was proposed by Zeldovich in 1946, and later modified by Lavoie, Heywood and Keck in 1970 (Figure 5). The forward rate constant for the second step shown in Figure 5, as well as the reverse

$$O_2 + M \rightleftharpoons 2O + M$$

$$O + N_2 \rightleftharpoons NO + N$$

$$N + O_2 \rightleftharpoons NO + O$$

$$N + OH \rightleftharpoons NO + H$$
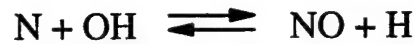
Figure 5 - Zeldovich Mechanism for NO Formation

reaction rates for steps three and four, have very high activation energies, resulting in a very strong temperature dependence for the rate of formation of NO. Most of the NO formation actually takes place after combustion.[40] Even though the temperatures in the flame front are very high and are conducive to NO formation, the duration of these conditions is very short. After combustion takes place, however, the gases are further compressed by the action of the piston, and their temperature is maintained in a range favorable to further NO formation.

After the compression/ignition stroke is completed, the piston rapidly moves downward and lowers the pressure and temperature of the gases in the cylinder dramatically. Because of the strong temperature dependence of the kinetics of the Zeldovich mechanism, the NO formation and destruction processes are said to be "frozen" during the expansion stroke of the piston. Finally, the exhaust stroke vents the mixture of gases to the atmosphere. In the exhaust gases, there is actually a mixture of both NO and NO_2. In spark-ignition gasoline engines, NO_2 usually comprises on the order of 1% of the total NOx, whereas in diesels operating under light load, up to 30% of NOx is in the form of NO_2. According to Hilliard and Wheeler,[42] this is consistent with the fact that diesels under light load have multiple low-temperature regions in the cylinder, which more rapidly quench the back conversion of NO_2 to NO.

The lifetime of NOx in the atmosphere is on the order of one day.[23] The atmospheric chemistry of NOx is very complex, and will not be dealt with in depth here. However, a primary result of this chemistry cycle is the formation of tropospheric O_3, which, as was pointed out above, has been increasing over the past few decades. Figure 6 gives some indication of the complexity of the multiple other cycles in which

NOx is involved within the troposphere. A full discussion of these cycles and their interactions is outside the scope of this thesis.

The health effects of NOx are not as severe as those of CO, [43] but they still impact human, animal and plant life. Though there is no evidence that NO is a health concern at present levels, NO_2 has been shown to cause emphysema in several animal studies. Other animal studies have shown a negative effect by NO_2 on the immune system. In addition to the direct effects of NOx, the adverse effects from one of

Figure 6 – Tropospheric Chemistry of NOx [23]

its primary atmospheric products, O_3, are also of concern.[6] Levels of O_3 typical in polluted urban environments (100 - 500 ppbv) have been shown in studies to cause lesions and necrosis in plants and eye irritation in humans. Levels only 2 to 5 times this much have been proven to cause irreversible lung damage in animal studies.[6]

Another component of automotive exhaust is unburned or partially burned hydrocarbons. Hydrocarbons are not on the EPA's list of criteria pollutants (Table 1), but they are of interest in the chemistry of the troposphere, as can be seen from the numerous organic "R" groups represented in Figure 6. As shown in Figure 4, the unburned hydrocarbon (HC) fraction of the exhaust increases nearly linearly as the air/fuel ratio decreases. There are several proposed mechanisms for this, nearly all physical, rather than chemical, in nature. These are listed in Table 5.

1.	Flame quenching at the combustion chamber walls, leaving a layer of unburned fuel-air mixture adjacent to the wall.
2.	The filling of crevice volumes with unburned mixture which, since the flame quenches at the crevice entrance, escapes the primary combustion process.
3.	Absorption of fuel vapor into oil layers on the cylinder wall during intake and compression, followed by desorption of fuel vapor into the cylinder during expansion and exhaust.
4.	Incomplete combustion in a fraction of the engine's operating cycles, occurring when combustion quality is poor.

Table 5 - Mechanisms for Production of Unburned Hydrocarbons [40]

Since all of these processes are essentially unrelated to combustion, and can all be expected to vary with individual engine designs, HC emissions can be expected to be non-uniform. The unburned HC components then leave the exhaust system in one of two forms: gaseous or particulate (soot). The latter is especially prevalent in diesel engines, which burn HC fuel with much higher boiling points (longer carbon chains) than the fuels burned in gasoline engines.[40] The precise nature and reactions of the wide variety of hydrocarbons that are directly emitted by, or formed in post-combustion processes in, an internal combustion engine is a topic too wide to cover here. However, it has been shown that many forms of organic particulate matter, especially those containing polynuclear-aromatics, are potential carcinogens.[6,40] In general, hydrocarbons are oxidized by approximately the same types of processes in the atmosphere, although different hydrocarbons have vastly different lifetimes. Methane can persist for years in the troposphere, whereas some longer-chain hydrocarbons only last a few hours.[23] The basic processes by which hydrocarbons are oxidized are represented in Figure 7. Methane is also a relatively potent greenhouse gas, being approximately 25 times more effective than CO_2 at trapping heat in the atmosphere.[23] The "radiative forcing" coefficient of a gas is a quantity

defined in Brasseur as: "the response in the net radiative energy flux at

the tropopause to changes in the concentration of a given trace gas."[23]

The magnitude of this number is calculated by complex atmospheric

radiative transfer computer models, and is proportional to the molar

absorptivity of the gas as well as it's current concentration and lifetime

in the atmosphere.
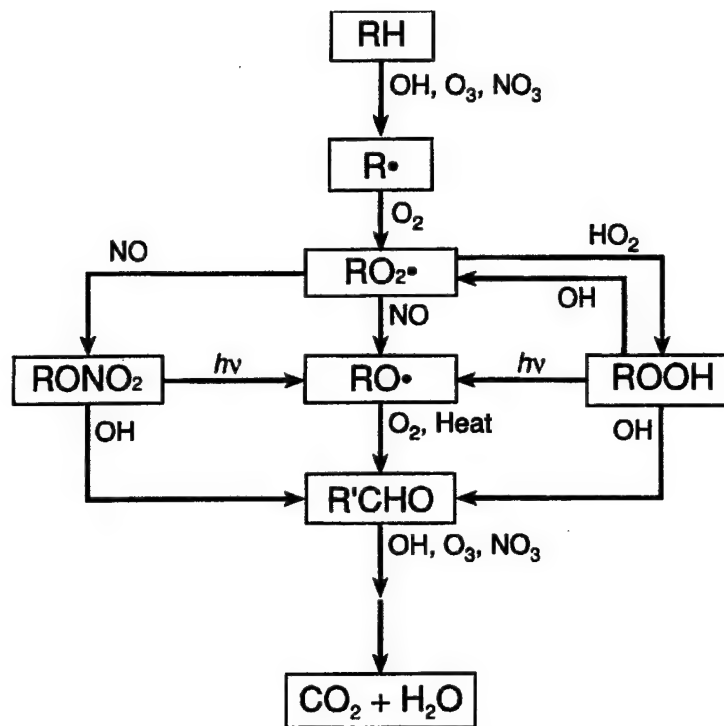
Figure 7 - General Oxidation Sequence of Hydrocarbons [23]

A very minor, but potentially significant component of automotive exhaust is nitrous oxide (N_2O). Since the mid-1980's, it has been known that automotive exhaust gases contain small amounts of N_2O.[44,45] Furthermore, it has been shown that newer vehicles possessing three-way (oxidizing and reducing) catalytic converters emit higher levels of the gas.[46] As discussed above, the predominant oxide of nitrogen created inside an internal combustion engine is NO, where

40

the nitrogen has a formal oxidation state of +2. It is certainly conceivable that, in the environment of a reducing catalyst, the nitrogen could be reduced to a formal oxidation state of +1, as in N_2O, although this has not been clearly proven.[47] Nitrous oxide production is not strictly combustion related, but has been shown to be positively correlated to engine rotation speed and inversely related to the condition of the catalyst.[48,49] Therefore, all things remaining equal, under slightly lean conditions, the production of N_2O should increase with increased use of fuel.

As a health concern, there is no evidence linking current ambient levels of N_2O with any health effects in humans. In concentrated form, N_2O is known as "laughing gas" and is still used as a general anesthetic in dentistry. However, it is almost completely unreactive in the troposphere and therefore is relatively long-lived, having a total atmospheric lifetime between 120 and 130 years.[23] The major source of N_2O is primarily biological processes in the soil and ocean which result in "denitrification," which is the conversion of nitrate salts back into gaseous nitrogen products such as N_2, NO and N_2O.[23] According to the IPCC, the total annual global production of N_2O amounts to 14.7 million metric tons per year, expressed as nitrogen.

41

Approximately 65% of this amount is emitted from soils and another 20% is emitted from the ocean. Of the 9.5 million metric tons emitted from soils, 37% is due to fertilized agricultural activities, which is 61% of the total anthropogenic source of N_2O. In the United States, the EPA estimates that 16% of all N_2O emissions come from mobile sources.[50] Once in the troposphere, N_2O is gradually transported into the stratosphere, where it becomes the major source of NO by reaction with an excited-state of atomic oxygen:[6]

$$O(^1D) + N_2O \rightarrow 2NO \qquad (5)$$

In this capacity, N_2O acts as a reservoir from which "active" nitrogen compounds are formed. Because of its long atmospheric lifetime and ability to strongly absorb infrared radiation, N_2O has a relative radiative forcing that is about 300 times that of CO_2.[51] In other words, for a one-kilogram increase of both CO_2 and N_2O, the latter would trap 300 times more heat in the atmosphere. Thus, N_2O is a very effective "greenhouse gas." In fact, even though it is only present in a mixing ratio of about 300 ppb (0.00003 %) in the troposphere, the IPCC estimates that the increase in N_2O concentration since 1900 has accounted for 6% of the total influence of all greenhouse gas increases

during that time. In this context, the "greenhouse gases" under consideration are: CO_2, CH_4, N_2O, and chloro-fluorocarbons.[52]

Finally, one fairly recent addition to the list of internal combustion engine emissions is ammonia (NH_3). After molecular nitrogen and nitrous oxide, ammonia is the third most abundant nitrogen-containing gas in the atmosphere. It is a very reactive gas and only has an average residence time in the atmosphere of about ten days. Animal waste, soil emission, biomass burning and fertilizers account for approximately 85% of all ammonia in the atmosphere. Even though it is a relatively minor component, ammonia plays a very important role as the only naturally occurring base in the atmosphere, neutralizing acidic constituents such as nitric and sulfuric acids in heterogeneous gas/liquid phase reactions.[23] As with nitrous acid, ammonia has only become a measurable constituent of automotive emissions within the last decade, as vehicles equipped with three-way, oxidation/reduction catalysts have begun to comprise more of the fleet. The emission of ammonia from a three-way catalyst equipped car is not strictly related to combustion, but is closely tied to combustion conditions, such as air/fuel ratio.[53] As it has become apparent that

vehicles are producing more ammonia, people have become interested in quantifying this additional source of ammonia.[54-59]

1.4 Air Pollution Measurement Technologies

In general, analytical techniques make measurements of two types: point measurements and path-integrated measurements. For example, mass spectrometry, atomic absorption or emission, and gas chromatography are all techniques that sample at a single point. If the concentration of a particular pollutant is to be measured along a particular path by one of these methods, point samples of the air at spatially-distributed locations along the path must be collected and analyzed. Light absorption spectrometry is naturally a path-averaging technique because light is passed through a path of some known length. In the laboratory, these path lengths are usually quite short, basically approximating a point measurement. However, there is no reason that light absorption techniques should be confined to the realm of short paths, as long as adequate light can be passed through the sample of interest. Path-averaged measurements are useful for detecting and quantifying chemical species along the path of interest, but cannot distinguish between homogenous and non-homogenous samples. In other words, a spectroscopic measurement along a path

44

of 100 meters cannot distinguish between a sample of analyte evenly distributed along the path and one where an equivalent amount of analyte is concentrated within only ten meters of the total pathlength (see Figure 8).[60] However, in situations where the distribution of the analyte is unknown, such as beside a roadway, this is actually an advantage. For example, taking point samples beside a roadway may lead to inaccurate results if the analyte of interest is not homogenously distributed in the air along the roadway. The inherent path-averaging ability of absorption spectroscopy is derived from one of its governing principles: the Beer-Lambert Law. Expressed for a single wavelength of light, the Beer-Lambert Law (often called Beer's Law) is stated as:

$$A = -\log(\frac{I}{I_0}) = \varepsilon bc \qquad (6)$$

Where A is the unitless absorbance, I and I_0 are the final and initial intensity of light at the detector, ε is the molar absorptivity in appropriate units of (pathlength*concentration)$^{-1}$, b is the pathlength of the light, and c is the concentration of the analyte. This equation only holds true for the absorbance of one chemical species at one wavelength of light, and only if the width of the absorbance peak exceeds the resolution of the spectrometer. If an absorbance spectrum

is measured for several chemical species across several wavelengths, the total absorbance at each wavelength is described by:[60]

$$A_\lambda = \sum_i \varepsilon_i(\lambda) \cdot \int_0^L c_i(x) \cdot dx \qquad (7)$$

In the above equation, the integral is what is referred to as the "path-integrated" concentration, and is just equal to the average concentration multiplied by the total pathlength, L. In usual practice, the absorbance is measured, the absorption coefficients are known, and equation (7) is rearranged to solve for concentration.

Long-path IR spectroscopy has been applied to the investigation of air pollution since the ground-breaking work of Stephens and Hanst[61-66] in the 1950's. At that time, the instruments were dispersive, prism-based systems with very limited resolution. Nevertheless, path-lengths of up to 400 meters were achieved and new discoveries were made. For example, in 1956, Stephens and Hanst first reported
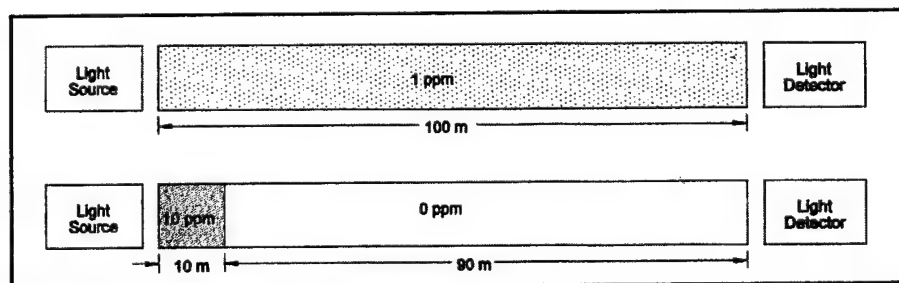
Figure 8 – Illustration of Path-Averaged Concentration Measurement

46

spectroscopic evidence for the presence of ozone in photochemical smog, and soon afterward discovered a previously unknown, highly toxic component of smog – peroxyacetyl nitrate (PAN).[67]

It was not until the mid-1970's that digital computers were powerful enough, in conjunction with the use of the Fast Fourier Transform[123], to make Fourier Transform Infrared spectroscopy a practical addition to the analytical chemist's repertoire of techniques. This technique vastly improved the ability of scientists to probe the infrared region of the spectrum, improving, among other things, the possible resolution of infrared instruments by at least a factor of 100. In 1973, P. L. Hanst was again at the forefront in application of this technique, using an FTIR spectrometer to identify the presence of high concentrations of formic acid in a smog cloud, and later (1976) collaborating with James N. Pitts at the University of California, Riverside, to build an enclosed long-path FTIR chamber with a folded path-length of greater than 1 km![69] This remarkable system was used in 1976 to confirm, for the first time, the presence of nitric acid in a polluted urban atmosphere. Additionally, evidence collected at this time indicated that nitric acid was combining with ammonia to form ammonium nitrate particulate matter.[67] Hanst [68-76], Pitts and

Tuazon [77-82] and others continued to develop long-path FTIR (LP-FTIR) techniques throughout the 1970's and 80's.

Throughout the 1970's and 80's and into the mid-1990's, the standard method of performing LP-FTIR analysis of gaseous components was basically the same as that employed in bench-top FTIR analysis in the laboratory:

1. Collect a background spectrum.

2. Ratio a sample spectrum to the background.

3. Apply Beer's law to calculate component concentrations.

While this worked very well in the laboratory, or in sealed sampling cells, in which temperature, pressure, and humidity could be controlled, and which could be filled with nitrogen for clean reference spectra, it does not work terribly well under ambient, open-air conditions. Primarily for this reason, open-path LP-FTIR (OP-FTIR) had essentially been relegated to the role of searching for fugitive emissions from industrial plants or waste disposal sites. For instance, since 1990, 84% of open-path FTIR related publications identified by SciFinder™ relate to this type of application. In these applications, sometimes referred to as "fence-line monitoring," the pressure, temperature and humidity

changes throughout the sampling period can be mitigated by taking new background spectra throughout the day. This can be done because more than 99% of the time, the relatively concentrated component being looked for (methane or some process chemical, for example) is not present in the ambient air to any great degree. Because of water's ubiquitous absorption lines in the infrared, even small changes in humidity between the background and sample spectra can cause great difficulties in calculating an absorbance spectrum for the sample. Another difficulty was in calibrating the spectrometer. Normally, to calibrate such a system so that quantitative measurements can be performed, a background spectrum containing either none, or a known concentration, of the component of interest is needed, along with a series of samples of known concentration. This is needed to correct for imperfections in the instrument; otherwise, if the molar absorptivity and pathlength were known, it would be possible to directly calculate the concentration of the desired component, providing that a completely clean background is obtained. In an open-path system, with no containment of the sample, these requirements are difficult to meet, at best.

The use of OP-FTIR and OP-Ultraviolet (OP-UV) spectroscopy
to measure automotive emissions has been attempted in the past, but
not with great success, due to the difficulties mentioned above.
Several attempts to employ these techniques were made in Denver,
Colorado by Don New[83] and Scott McClaren,[60] between 1993 and
1995. These studies employed the use of sulfur hexafluoride (SF_6) as
a tracer gas to allow calculation of the effective dispersion coefficient of
the pollutants from the roadway. In theory, if the tracer emission rate is
known, and if the tracer concentration is measured simultaneously with
the pollutant of interest, and if the tracer is emitted in a manner
representative of the pollutant emissions, then the pollutant emission
rate (R_p) can be calculated by:[60]

$$\sigma = \frac{R_T}{[T]}; \quad R_P = \sigma * [P] \qquad (8)$$

In the above equation, R indicates the emission rate of either
the tracer (T), or the pollutant (P), and square brackets indicate the
concentration of each. In these studies, it was found that the
positioning of the tracer emission device had some influence on the
apparent emission rate of the pollutant, and that it was difficult to make
the measurements due to wind and traffic flow variation. Often, the
pollutants being measured were below the detection limits of the

50

instruments. Also, because individual measurements of pollutant concentrations were used, variation in background concentrations often seemed to mask the influence from the roadway. Nevertheless, New and McClaren did show the ability to make measurements of carbon monoxide emissions that, at the low end of their range, agreed with accepted values.[60]

Another open-path spectrometric method that may be applied is that of flux measurement. While a complete discussion of gas flux measurement is outside the scope of this thesis, I will briefly outline what it is and why it would not be practical for roadway studies of automotive emissions. A "flux" is defined as "the rate of transfer of a quantity per unit area per unit time."[84] Within the troposphere, which is the lowest 11 km of the atmosphere,[84] heat fluxes from the surface to the air, as well as the reverse, cause turbulent eddies which result in a well mixed layer of air over time. Because gross air movement dominates the transport mechanisms in the troposphere, gases are diffused predominately by eddies, and not by molecular diffusion in this portion of the atmosphere.[84] Furthermore, the lowest portion of the troposphere tends to be very turbulent compared with the rest of the atmosphere, and is called the "Atmospheric Boundary Layer," or ABL.

The ABL varies in height from 200 to 4000 meters.[84] Within a well-mixed ABL, it is assumed that there is no net flux in the horizontal (x and y) directions, and that concentrations vary only with height. Thus, it is generally assumed at every point in the ABL, that:[84]

$$\frac{\Delta F_x}{\Delta x} \approx \frac{\Delta F_y}{\Delta y} \approx 0 \qquad (9)$$

Where ΔF_x and ΔF_y are the horizontal fluxes. By process of elimination, then, the only important flux in the ABL is in the vertical (z) direction. Therefore, if there is a source of some gaseous chemical species on the surface of the earth, and if that chemical species is not absorbed significantly by the surface of the earth, there will be a net upward flux of that chemical driven by ABL eddy diffusion. By extension of this idea, long path FTIR has been employed in studies of plant and animal production rates of various gases by measuring the net upward flux (F_z) over a defined area.[85-88] It might seem that this technique could be used to study automotive emissions from roadways as well, but there are several reasons why this is not the case. First is that the assumptions in this method dictate that the F_z is driven by random thermal eddy motion. For this reason, flux studies must assume an infinite, homogenous ABL so that any air parcel that moves

horizontally out of the area being measured will be replaced by an equivalent parcel from the x or y directions. Over a roadway, the vehicles are constantly perturbing the air and the roadway itself is too small to fulfill the requirement of an "infinite," homogenous ABL. For these reasons, I did not pursue the flux method for my OP-FTIR studies of roadway emissions.

It was not until 1996, that a method was introduced by David W. T. Griffith, of the University of Wollangong, Australia, which could make many of the traditional problems with OP-FTIR obsolete.[89] In this method, which will be detailed in the section 2.4 Data Analysis, on page 107 and following, instrumental and environmental variables are used, in conjunction with a high-resolution database of infrared absorption line parameters, to create a set of synthetic calibration spectra. This is done without the need for a clean background or any actual calibration cells of known concentration. The sample spectra can then be fit to the database of calibration spectra by a multivariate algorithm, such as the classical least squares (CLS) method. Since the introduction of this method, the accuracy and precision of OP-FTIR have been improved to allow quantitative analysis of air pollutants in a number of different matrices. Examples of these applications are:

analysis of biomass fire plumes,[90,91,92] flux measurements of trace gases,[85] direct precision analysis of volcano emissions,[93] preliminary analysis of motor-vehicle fleet emissions by our research group,[94] and even studies of methane emissions from free-ranging sheep.[95]

1.5 Tunnel Studies

Before the development of synthetic calibration methods, as mentioned above, how were real-world automotive emissions measurements collected? Historically, this type of data collection has been performed almost exclusively through the use of the "tunnel study." In such studies, most notably those performed by William Pierson,[96-99] Alan Gertler,[31,99-101] and Robert Harley,[102-105] as well as others,[106-110] a roadway tunnel is employed as the "sample chamber." A collection of analytical instruments is placed in (or samples are collected from) the overhead access-way and/or ventilation ducts of the tunnel, and air samples are drawn through tubes and analyzed. Often, measurements are made at two points: near the entrance and near the exit of the tunnel. These measurements are used to determine the concentration increase of the species of interest, and, combined with a measurement of the dilution induced by airflow through the tunnel, emission factors are calculated. This has been, and still is, a very

valuable method for measuring real-world emissions from cars and trucks. Large suites of scientific equipment may be employed to give a very wide range of quantifiable chemical species, although these instruments must then be maintained and calibrated. However, the major weakness of the method is that there aren't very many traffic tunnels in the United States, or elsewhere, which can be employed for this kind of study. Also, the placement of the tunnel may influence the makeup of the vehicle population that is using it on a regular basis and thus may make the measured vehicles a non-representative sample of the local population. For example, if the tunnel primarily provides access to an area of mostly white-collar (higher wage) industry, then the vehicle population using the tunnel may not be representative of the local population as a whole. In addition, tunnels may only afford the opportunity to measure a single mode of driving when traffic loading is high enough to give measurable readings. This may tend to influence the measured emission factors either high or low, depending on the situation in the tunnel.

1.6 Remote Sensing

A more flexible technique is that of remote sensing of automotive tailpipe emissions, first employed by Donald Stedman and

Gary Bishop at the University of Denver.[111,112] In this technique, a narrower range of chemical species is usually measured, but it can be employed in a much broader set of locations. The other major difference between remote sensing and tunnel studies is that remote sensing measures individual cars, whereas the tunnel study measures the aggregate effect of the entire measured population of vehicles. Therefore, remote sensing can produce similar fleet-averaged data by weighted averaging, but tunnel studies cannot provide information on individual vehicles. Remote sensing is based on the absorption of either IR or UV light by the chemicals of interest, and is performed by shooting beams of light through the tailpipe plume of a passing vehicle and measuring the decrease in intensity of specific regions of the spectrum, which correspond to absorption peaks of specific chemical species. Remote sensing has been used in many countries around the world, and is currently being developed as a means of identifying high-emitting vehicles in actual use. A major strength of this method is its high mobility. When placed in a single location, it potentially suffers from the same possible sampling bias suffered by the tunnel study. However, since it is very mobile and can be placed in several successive locations, or even in multiple simultaneous locations when using several systems, this potential bias can be mitigated. While a

56

robust, relatively simple, and accurate technique, remote sensing has its own drawbacks as well. Most notably, it can only be used across a single lane of traffic, and is restricted to measuring vehicles that have tailpipes in standard positions. For example, in order to measure emissions from vertical stack diesel trucks, special placement of the equipment must be made so that the light may be passed through the plume exiting above the truck cab.[113] Because tailpipe plume remote sensing is restricted to single lanes, suitable measurement locations are fairly limited, although not as much as with a tunnel study. However, using off and on-ramps to highways, or blocking traffic lanes to induce single-lane traffic flow may also influence the measured emission factors, much like in the tunnel study, because it restricts the modes of operation that may be sampled.

CHAPTER 2. – THEORY OF OPERATION AND EQUIPMENT

2.1 Introduction

This chapter details the equipment and methods used in my research. Principally, I have used two spectrometers, a Fourier-Transform Infrared (FTIR) system, and an Ultraviolet/Visible (UV/Vis) monochromator. In this introductory section, I will discuss the theory of operation of each of these systems, before proceeding to detail their specifications in the following section (2.2). After describing the equipment, I will describe the methods used to collect and analyze the FTIR and UV-Vis spectra to produce the data used in the "Tunnel-less Tunnel Study" mentioned in the Statement of Thesis (Section 1.1).

2.1.1 Beer's Law

Because absorption spectroscopy of any type is primarily based on the application of Beer's Law, I will begin with a detailed discussion of this topic. In 1852, when August Beer first published his research on light absorption by various materials, he did not relate it to chemical concentration, but instead to material thickness.[114,115] His expression for the exponential decrease of light intensity as it moves through an absorbing medium was restated to take the pathlength of light and the

concentration of the absorbing species into account almost 40 years later by B. Walter.[114,116]

There are six basic assumptions involved in the modern statement of Beer's Law,[117] and the deviation of reality from these assumptions will cause a lack of adherence to it. After listing these assumptions, I will discuss the more important specific causes of deviation from Beer's Law, also called "non-linearity," later in the section. The assumptions are as follows:

1. The incident radiation is monochromatic.
2. The absorbers act independently of each other.
3. The incident radiation consists of parallel rays, which are perpendicular to the surface of the absorbing medium.
4. The pathlength traversed is uniform over the cross section of the beam, yielding identical path lengths for all beams of light.
5. The absorbing medium is homogenous and does not scatter the radiation.
6. The incident flux of light is not large enough to cause saturation of the detector.

The first assumption leads to the most glaring cause of non-linearity in real spectroscopy, especially in FTIR spectroscopy: the beam of light is clearly not monochromatic. Even in the case of UV/Visible spectroscopy where a "monochromator" is used, the result is always a range of wavelengths, the width of which depends upon the

resolution of the monochromator. The first problem imposed by polychromatic light is that different wavelengths of light are not propagated through the system and detected equally. For the sake of argument, we will consider only two wavelengths, λ_1 and λ_2, realizing that the situation can be extended to cover all wavelengths incident on the sample. In this case, λ_1 is the absorption wavelength of interest and λ_2 is a nearby wavelength of light that influences the detector's response to λ_1 in some unspecified manner. This changes the apparent intensity recorded at λ_1 by some function that is dependent of the instrument's optics and detector.[118] Therefore, only considering two wavelengths of light, we no longer have a strictly linear relationship between absorbance and concentration. The situation becomes more complex when more wavelengths of light are included, as in real spectroscopy. Usually, the actual impact of this effect is very small. In the case of very sharp, closely spaced absorption features, however, this effect will be enhanced because the absorption coefficient changes rapidly in a short space of frequencies, and can contribute substantially to deviations from Beer's Law.[117] This is the case for many gaseous species measured by OP-FTIR because the very narrow lines due to rotational fine structure are present. If the resolution is larger than the width of these lines (sometimes less than a tenth of a wavenumber),

the effect of polychromatic light will be to cause individual peak heights

to vary non-linearly with concentration.[89] However, the MALT/HITRAN

software I used in my studies to create synthetic calibration spectra

(see pages 109 and 110), and to calculate mixing ratios in the sample

spectra, has been shown by David W. T. Griffith to correctly account for

this effect.[89] For example, in the case of N_2O, Griffith reports that the

errors introduced by uncompensated non-linearity over a 600 ppbv

range were on the order of 3 ppbv.

Another major contributor to non-linearity in relation to Beer's

Law results from increased concentrations of analytes, and

correspondingly high absorbances. As the light absorbance by a

particular analyte becomes greater (i.e. – the transmittance

approaches zero), incremental increases in concentration will cause

non-linear increases in absorbance. For example, a recent study of

CO using OP-FTIR determined that CO is highly non-linear when

present in optical densities greater than 0.3 atm-cm, or 3000 ppm-m.

As will be discussed below, normal conditions for the studies

undertaken in this thesis resulted in CO optical densities of less than

1000 ppm-m, which is well within the linear range. Just as in the

previous case of non-linearity, the MALT/HITRAN software I used to

generate synthetic calibration files based on high-resolution absorption lines, can adequately account for and correctly model this non-linearity.

2.1.2 FTIR Spectroscopy

The advantages of using FTIR over dispersive IR techniques are threefold: multiplex data collection, light throughput, and resolution. The multiplex advantage is achieved by the fact that all the wavelengths of light are collected at the same time. On a dispersive instrument, there is uncorrelated noise introduced into the signal for each wavelength of light collected, as the device scans through the spectrum. This gives the FTIR instrument a superior signal-to-noise in a much shorter period of time. Related to this is the fact that there is no need for narrow slits for wavelength selection, and more light can enter the instrument unimpeded. Finally, high resolution is more easily achieved with an FTIR than with a dispersive IR instrument. This is because resolution in an FTIR system is only dependent on the maximum optical path difference, whereas a dispersive instrument is limited in practice by the slit width of the monochromator, and in principle by the number of lines on the grating used to disperse the light. This has led to FTIR resolutions of less than 0.001 cm^{-1}, which would be impossible with dispersive instruments.

2.1.2.1 *Interferometry*

As with any form of spectrometry, FTIR is predicated on the phenomenon of molecular absorption of light. In the region of the so-called mid-IR, from 650 cm^{-1} to 4000 cm^{-1}, molecules undergoing vibrational and rotational transitions absorb the light energy. This absorption only occurs strongly if the vibrational motion of the molecule results in a nonzero transition dipole moment. For vibrational motion, the electric dipole moment (μ) can be approximated as:[119]

$$\mu = \mu_0 + (r - r_e)\left(\frac{\partial \mu}{\partial r}\right)_0 \tag{10}$$

Where r is the internuclear distance, and r_e is the equilibrium bond distance, and μ_0 is the permanent dipole moment. Since μ_0 is a constant, the transition dipole moment (R) can be calculated with equation 11:

$$R = \int \psi_i^* \left[(r - r_e)\left(\frac{\partial \mu}{\partial r}\right)_0 \right] \psi_j \, d\tau \tag{11}$$

From this expression, a change in the molecular dipole moment with respect to r ($\delta\mu/\delta r$) is necessary to have a non-zero value of R. Thus, it is not sufficient, or even necessary, to have a permanent dipole moment in the molecule in order to observe the absorption of infrared

radiation. For example, carbon dioxide has no permanent dipole moment, but absorbs in the infrared due to asymmetric stretching and bending modes, which induce a transition dipole in the molecule. This also makes it clear why homonuclear diatomic molecules cannot absorb strongly in the infrared.

An FTIR spectrometer collects broadband infrared radiation very quickly, without the need for isolating or scanning through the wavelengths being collected. This is made possible through a device known as an interferometer, and is most commonly a Michelson interferometer, named after its inventor, Albert A. Michelson, who first introduced the device in 1881.[120] A diagram of an interferometer is shown in Figure 9. This device initially splits incoming light into two equal parts that are initially in phase with one another. These two parts recombine at the output of the interferometer, which is where the detector is located. When the two mirrors in the interferometer are equidistant from the beam splitter, they are said to be at the point of zero path difference, or "zpd". At this point, all wavelengths of light are perfectly in phase, and constructively interfere with each other to give maximum intensity. As the moving mirror moves away from zpd, the light reflected off of it must travel farther than the light reflected off the

stationary mirror, and the two beams are no longer in phase. In the case of monochromatic light, the resulting graph of signal vs. mirror displacement would be a cosine curve, with maxima corresponding to
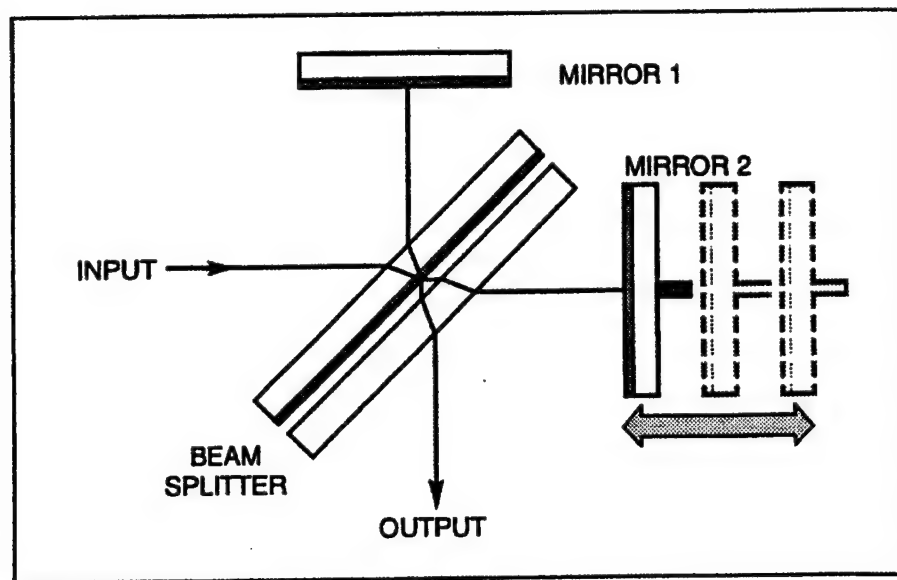
Figure 9 - Michelson Interferometer[121]

optical path differences equal to integer multiples of the wavelength. Since the change in the light path is twice the displacement of the mirror, then every time the mirror moves a multiple of 0.5λ, there will be a maximum in the cosine curve because the two halves of the light beam will be in phase again.

Consider the case of polychromatic light, such as the infrared radiation produced by a hot filament. At zpd, the situation is the same

as that for monochromatic light, except that the overall signal is comprised of the sum of the constructive interference of each discrete wavelength of light. The only mirror position where all wavelengths of light are constructively interfering is at zpd, and this results in a signal that is very large compared to any other mirror position. This is commonly called the "centerburst." When displacement from zpd occurs, only the light having a wavelength that is a multiple of twice the displacement will have maximum constructive interference. As the mirror continues to move, each wavelength of light creates a unique cosine wave, which has a frequency (f) dependent on both the wavelength (λ) of the original radiation and the speed (r) of the moving mirror:[119]

$$f = 2r(\frac{1}{\lambda}) \tag{12}$$

Since the speed of the mirror is conveniently expressed in terms of cm/sec, it is also convenient to express the inverse wavelength of the light in terms of cm^{-1}, also referred to as "wavenumbers." The other convenient aspect of these units is that since they are the inverse of the wavelength, they are directly proportional to the energy of the light. The signal at the detector is the sum of all these individual cosine waves. The resulting "interferogram" looks something like the wave-

form shown in Figure 10. Contained in this complex waveform is the information about each of the individual wavelengths of light that was passed through the interferometer, expressed as intensity vs. mirror position. This intensity spectrum, $I'(\delta)$, varies as:[122]

$$I'(\delta) = 0.5I(\overline{v}) + 0.5I(\overline{v})\cos(2\pi\overline{v}\delta) \qquad (13)$$

In this expression, δ is the mirror displacement, $\overline{v}$ is the wavenumber, and $I(\overline{v})$ is the intensity of the light at a given wavenumber. When δ is an integer multiple of a particular wavelength, the intensity at the detector equals the full intensity of that wavelength because the cosine term equals 1. It is the modulated portion of equation (13) that is commonly called the interferogram. In a perfect instrument, the interferogram would simply be equal to the cosine term in equation (13). However, there are instrument-dependent quantities such as beamsplitter efficiency, electronic characteristics and detector
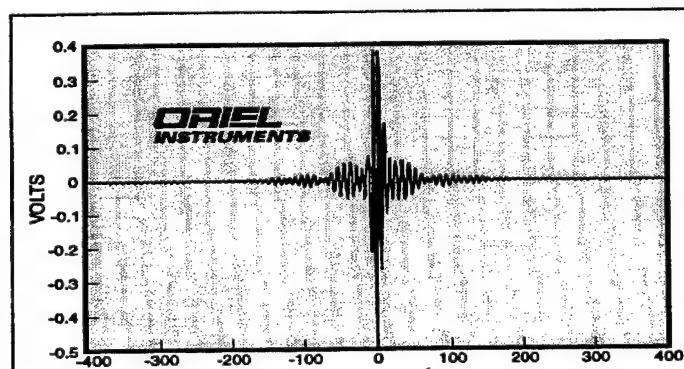
Figure 10 – Interferogram (V vs. Displacement)[121]

67

response, which modify the intensity of the detected light. All of these wavelength-dependent instrumental effects may be combined with the factor of 0.5 and the pure intensity spectrum to give an instrument-dependent spectrum, $B(\overline{\nu})$, so that the interferogram, $I(\delta)$, is expressed as:

$$I(\delta) = B(\overline{\nu})\cos(2\pi\overline{\nu}\delta) \qquad (14)$$

2.1.2.2 Fourier Transform Pairs

When $I(\delta)$ is integrated over all wavelengths, equation (15) is the result. The interferogram, $I(\delta)$, and the spectrum, $B(\overline{\nu})$, are a Fourier transform pair. This means that equation (15) may be rearranged to give equation (16).[122]

$$I(\delta) = \int_{-\infty}^{+\infty} B(\overline{\nu})\cos(2\pi\overline{\nu}\delta)\cdot d\overline{\nu} = 2\int_{0}^{+\infty} B(\overline{\nu})\cos(2\pi\overline{\nu}\delta)\cdot d\overline{\nu} \qquad (15)$$

$$B(\overline{\nu}) = \int_{-\infty}^{+\infty} I(\delta)\cos(2\pi\overline{\nu}\delta)\cdot d\delta \qquad (16)$$

In the case of Equation (15), the equivalence is made because it is physically impossible to have negative wavenumbers. When making a spectroscopic measurement, the interferogram is actually the measured quantity, but the wavenumber-dependent spectrum is the

desired quantity. Mathematically, it is possible to convert the interferogram into the spectrum via the process of the Fourier Transform. However, we must consider a few important factors before we arrive at that step.

2.1.2.3 Truncation, Apodization and Phase Errors

As evidenced by the above equations, a true representation of the spectrum, $B(\overline{v})$, requires that the displacement of the mirror in a Michelson interferometer be moved through an infinite range of motion. This is impossible, but implies that any range of motion that is less than infinite will somehow compromise the quality of the resulting spectrum. This effect is called "truncation" and has the effect of superimposing a boxcar function on the interferogram. In other words, in relation to the actual interferogram, the truncated interferogram is multiplied by a factor of 1 for the interval [-δ,+δ], but by a factor of 0 for the intervals of [-∞, -δ) and (+δ, +∞]. If the boxcar function is represented by $D(\delta)$, then the result is:

$$B'(\overline{v}) = \int_{-\infty}^{+\infty} D(\delta)I(\delta)\cos(2\pi\overline{v}\delta) \cdot d\delta \qquad (17)$$

Since the Fourier Transform of a product is equal to the convolution of the Fourier Transform of each function, then the following is true:

$$B'(\overline{V}) = B(\overline{V}) * f(\overline{V}) \tag{18}$$

In the above expression, $f(\overline{V})$ is the Fourier Transform of the boxcar function, $D(\delta)$. Convolution of functions can be depicted graphically as the modification of one continuous function by another continuous function.

This is illustrated in Figure 11. Figure 11 (a) shows the Fourier Transform of just the boxcar function itself (also see Figure 12 a). This
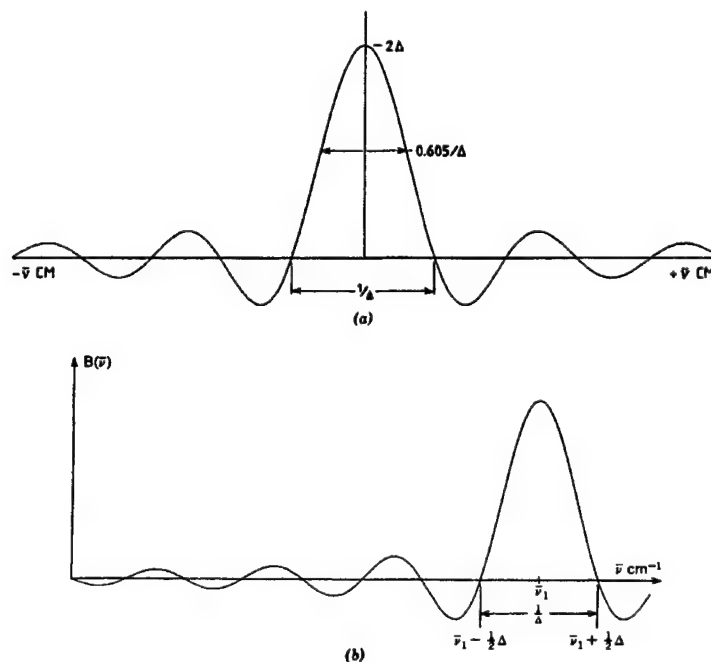
Figure 11 - Convolution of Monochromatic Spectrum with Boxcar Function[122]

70

is known as the "sinc" function. Figure 11 (b), shows the Fourier

Transform of the convolution of a monochromatic interferogram with

the boxcar function. Without this convolution, Figure 11 (b) would

merely be vertical line centered at $\bar{\nu}_1$. The boxcar function due to

truncation of the interferogram imparts the familiar "ringing" in the tails

of the spectral peaks, as well as increasing the width of the peaks.

"Ringing" can obscure small spectral features, so steps must be taken

to minimize this effect if these features are to be discerned. Since

convolution of the spectrum in this way is, to some extent, unavoidable,

the combination of the truncation effect and the instrumental effects on

the resulting interferogram is often referred to as the instrument line-

shape, or ILS.

Reduction of the effects of interferogram truncation is called "apodization", which literally means "without feet", referring to the minimization of the oscillations in the tails of spectral features. This is normally done by convolving the interferogram with yet another function which, when it's Fourier Transform is convolved with the ILS, will reduce the side-lobes in the spectral features. All available methods of apodization will broaden spectral features, but, since the side-lobes are part of the random variation in the baseline of the
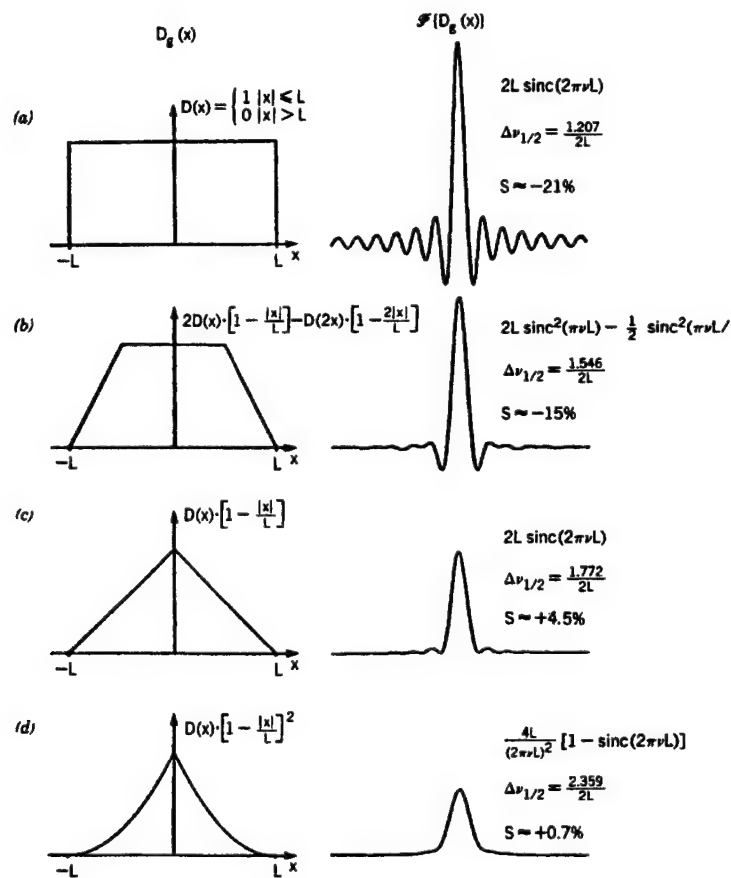
Figure 12 - Apodization Functions[122]

72

spectrum, these methods actually increase the signal to noise ratio. Some common apodization functions are shown in Figure 12.

One final consideration in the Fourier Transform of an interferogram is that of phase error. There are two primary causes of phase errors in interferograms.[122] One is caused by the collection of the first data point prior to the zpd. The second primary cause is induced by electronic filters in the equipment designed to remove high frequency noise. Both of these effects result in an offset ($\theta_{\bar{v}}$) of the phase angle ($2\pi\bar{v}\delta$) of the interferogram. Thus, the expression for the symmetric interferogram becomes:[122]

$$I(\delta) = 2\int_{0}^{+\infty} B'(\bar{v})\cos(2\pi\bar{v}\delta - \theta_{\bar{v}}) \cdot d\bar{v} \qquad (19)$$

Taking the cosine of a difference introduces sine terms into the expression, and all real interferograms contain both cosine and sine terms. It can be shown, but the proof is again outside the scope of this thesis, that equation (19) may be rewritten as:[122]

$$I(\delta) = 2\int_{0}^{+\infty} B'(\bar{v})e^{-2\pi i \bar{v}\delta} \cdot d\bar{v} \qquad (20)$$

Because the Fourier Transform pair is now described by a complex expression, the spectrum can now be described in terms of real and imaginary parts:[122]

$$B'(\overline{V}) = \mathrm{Re}(\overline{V}) + i\,\mathrm{Im}(\overline{V}) \qquad (21)$$

The phase error ($\theta_{\overline{v}}$) is related to these transforms by the following equation:[122]

$$\theta_{\overline{v}} = \arctan\left(\frac{\mathrm{Im}(\overline{V})}{\mathrm{Re}(\overline{V})}\right) \qquad (22)$$

The most common form of phase error correction is called the Mertz method,[122] and is accomplished by excising a double-sided interferogram near the centerburst and using the real and imaginary Fourier Transforms to calculate the phase error. Once the phase error is calculated, it can be separated into real and imaginary parts and used to phase-correct the real and imaginary parts of the full spectrum.[122] Table 6 explains the steps taken in each part of the Mertz phase correction process, which is pictured in Figure 13 - Figure 15.[122]

2.1.2.4 The Fast Fourier Transform

Transforming a large interferogram is a very labor-intensive process and was practically impossible until the advent of the digital computer. Even then, the time to perform a Fourier transform was prohibitive until 1969, when Cooley and Tukey proposed the Fast Fourier Transform (FFT),[123] which reduces the number of computations considerably. The FFT reduces the number of computations from n^2, where n is the number of points to be transformed, to something on the order of $n \log_2(n)$.

Part	Explanation
A	Full Interferogram
B	Excised portion of interferogram (A) for phase error determination
C	Triangular apodization function used to modify (A) and (B)
D	Apodized interferogram (B)
E	Real and Imaginary portions of complex Fourier Transform of (B)
F	Phase error curve determined from (E) and (F)
G	Cosine and Sine values of (F)
H	Apodized interferogram (A)
I	Real and Imaginary portions of complex Fourier Transform of (A)
J	Spectra (I) multiplied by the cosine and sine phase error curves
K	Transmittance spectrum: Sum of phase-corrected spectra in (J)

Table 6 – Key to Figure 13 through Figure 15

a

b

c

d

i

e

Real

imaginary

Fig. 3.7. (continued)
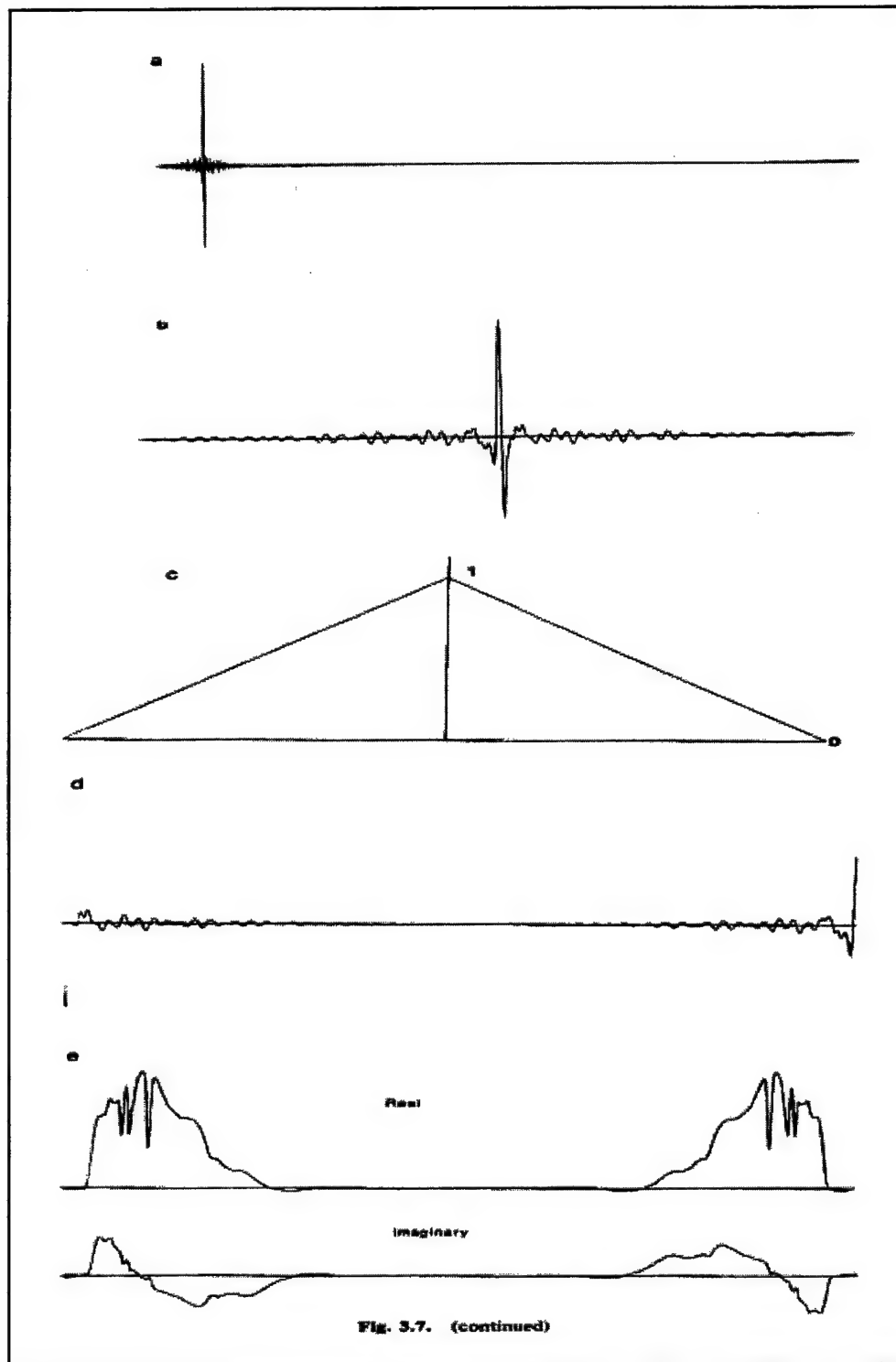
Figure 13 - Mertz Phase Correction, Part 1[122]
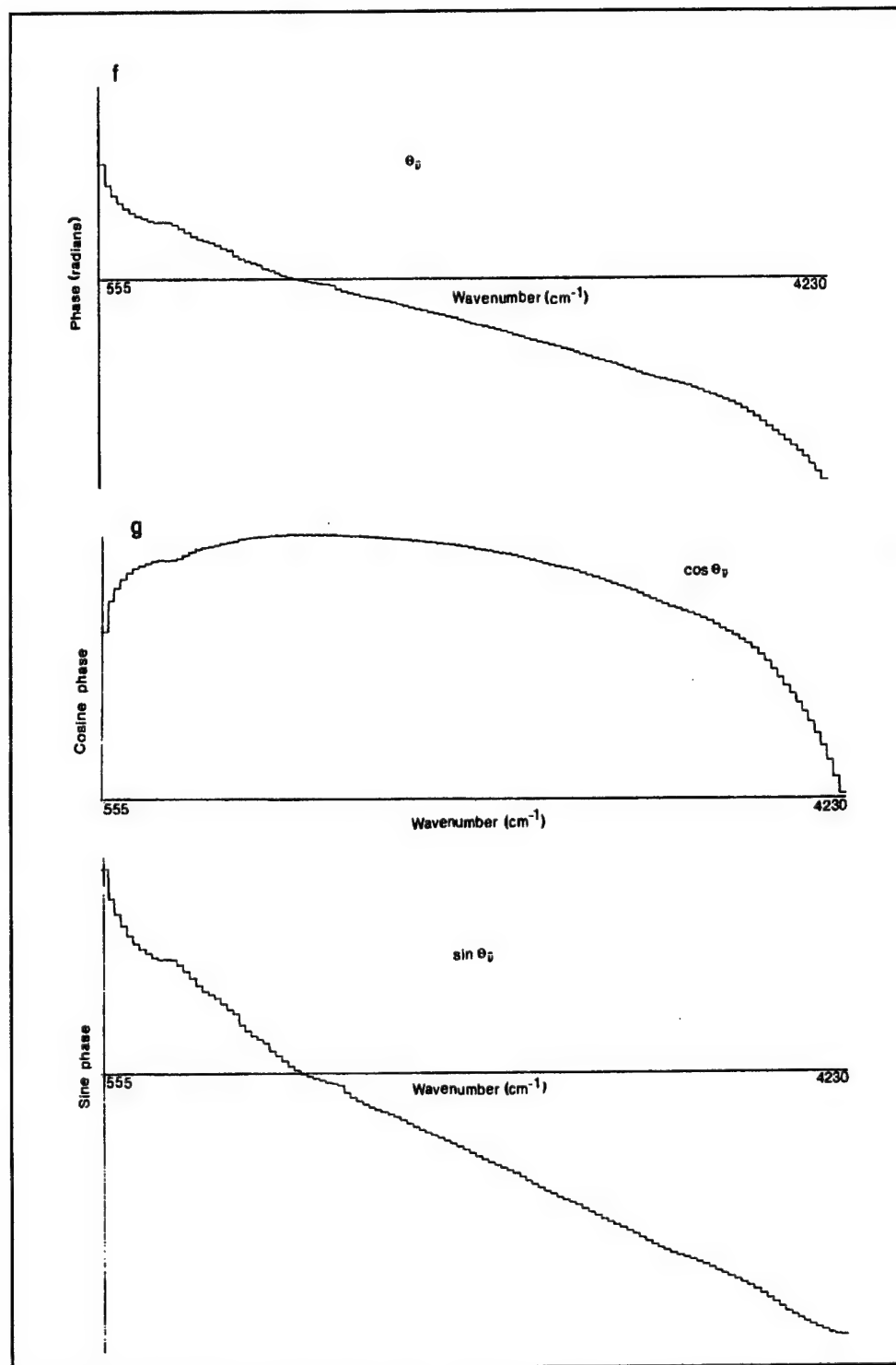
Figure 14 - Mertz Phase Correction, Part 2[122]

Figure 15 - Mertz Phase Correction, Part 3[122]
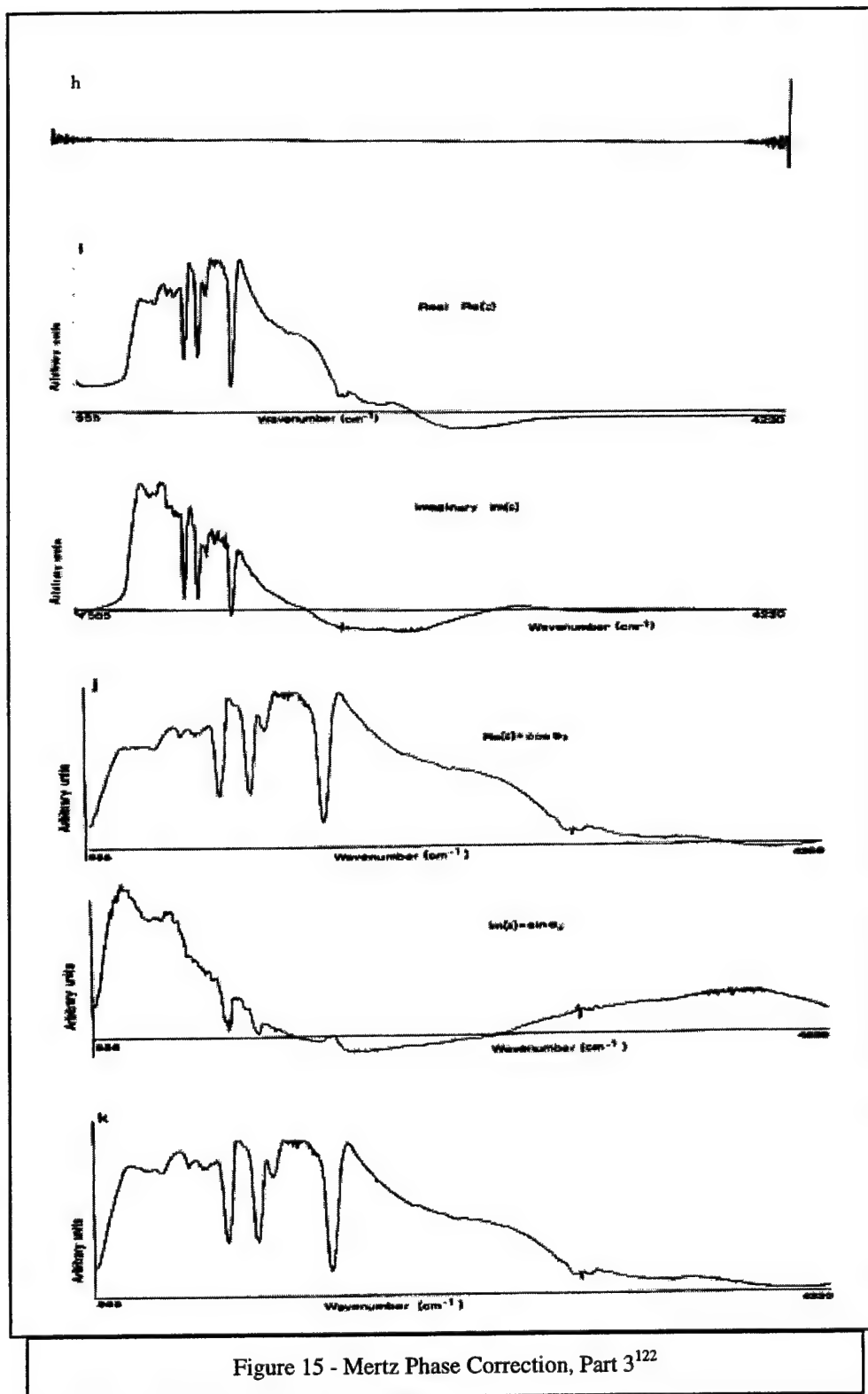
The pertinent facts regarding the Fast Fourier Transform are: that it can be done; that all the information needed to generate the spectrum is contained in the interferogram; and that the limits of integration to obtain the "true" spectrum are infinite. There are two major limitations, then, in obtaining the true spectrum from the interferogram. One is that the limits of mirror displacement are not infinite, which was discussed above, and the other is that the smooth and continuous interferogram must be sampled and digitized in order to produce the spectrum using a computer.

In order to digitize the interferogram, it must be sampled at a high enough rate to ensure an accurate representation of the real spectrum is achieved. According to the Nyquist Theorem,[120] any sinusoid can be restored exactly from its digital representation as long as the sampling frequency is at least twice that of the highest frequency component of the signal. In most FTIR spectrometers, the interferogram sampling rate is dictated by the frequency of a cosine wave set up by a Helium/Neon (He/Ne) laser passing through the same interferometer as the infrared light. The principal wavelength of the He/Ne beam is 632.8 nm. If the computer is triggered to sample the interferogram each time the He/Ne sinusoid crosses zero, one sample

will be taken every time the mirror moves 316.4 nm. By the Nyquist Theorem, the shortest wavelength of light that can be adequately sampled at such a rate is 632.8 nm long (15,803 cm^{-1}). It is common to only use positive zero crossings of the laser sinusoid, which corresponds to one sample every 632.8 nm. This would put the high frequency limit at 1.266 microns, or 7,899 cm^{-1}. In my work, I limited my investigation to a high frequency of about 4000 cm^{-1}, or 2.5 microns, meaning that either He/Ne-driven sampling rate was more than adequate for accurate digital representation of the interferogram.

However, having adequate information to reproduce the interferogram accurately does not insure that there will be enough data points in the proper locations to ensure adequate reproduction of each absorption peak in the spectrum. After all, the location of each data point is dictated by the zero-crossings of the reference laser, and has only a fortuitous relationship, if any, to the location of a particular absorption feature. It is a likely scenario that data points may fall on either side of a peak, but there may be no information about the actual height of the feature. This could be remedied by gathering more data points, which necessitates a longer range of motion for the moving mirror in the interferometer. This is not possible if the interferometer is

already operating at maximum resolution, but may also not be desirable if the spectrum must be collected within a specific time interval, since lengthening the optical path difference means a longer collection time for each interferogram. Another alternative is to interpolate more points into the interferogram without collecting any new information. This is done by a technique known as "zero-filling" the interferogram.

In fact, some degree of zero-filling is usually necessary when performing the Fast Fourier Transform. This is because the FFT algorithm requires that the total number of data points be equal to 2^n, where "n" is any integer. For example, if there are only 1000 data points in an interferogram, a minimum of 24 zeros must be added to bring the total to 1024 (n=10), before the FFT can be performed. In addition to this, more zeros may be added to bring the total number of points up to any power of 2. This is effectively the same as moving the mirror over a longer OPD, but without any additional information being added. This may seem a curious effort, since putting a zero into equation (20) will only result in a value of zero when it is transformed.

However, the zero-filled portion of the interferogram is still a truncated version of the "actual" interferogram, and is also convolved with the boxcar function as a result. When transformed, even though there is no new information, the zero-filled portion will be convolved with the sinc function, as illustrated in Figure 11(a). The result is that the peaks become smoother, even though the resolution has not changed because there is no new information in the spectrum. This is illustrated in Figure 16. It is important to realize that, when processing a zero-filled interferogram, that only the actual data be apodized, since apodizing the zero-filled portion would eliminate the advantage of using this technique in the first place.
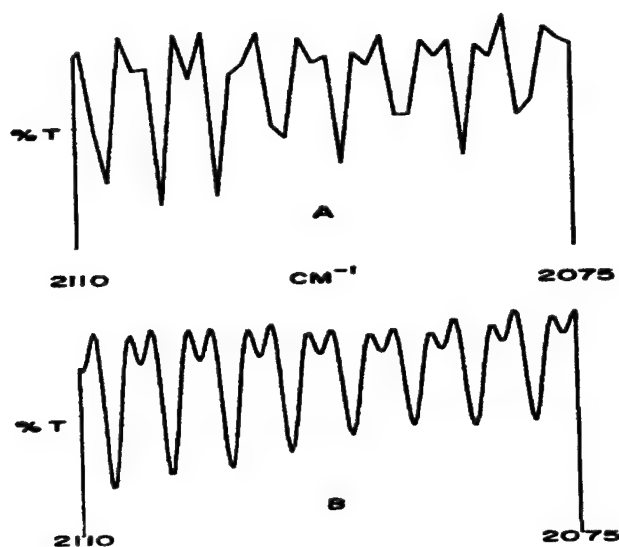
Figure 16 - Effect of Zero-filling on Spectrum of CO^{122}
A. – Raw Spectrum   B. – Zero-Filled Spectrum

2.1.3 UV/Visible Absorption Spectroscopy

Like FTIR, this type of spectroscopy is also based on the principle of molecular absorption. In the UV/visible region, however, the light is absorbed through the phenomenon of electronic transitions. Since electronic transitions require more energy, the corresponding absorption is in the ultraviolet region of the electromagnetic spectrum. This region of wavelengths, as it applies to molecular absorption, is from roughly 180 nm to 350 nm. This corresponds to an energy range of approximately 55,000 cm^{-1} to 28,000 cm^{-1}, for comparison to the previously discussed infrared region.

In UV spectroscopy, the absorption of energy is due to the shift of electrons from the lowest lying electronic state to a higher electronic state. Each of these states can be represented by a wavefunction, and each wavefunction can be thought of as the combination of an electronic, spin, vibrational and rotational wavefunction. We can consider the time-independent form of the wavefunctions because of the Born-Oppenheimer approximation, which states that electronic motion is so much faster than nuclear motion that we can consider it independently.[117] Thus, the transition moment for a given electronic band can be represented by the following equations:

83

$$R = R_e O_s O_v O_r \qquad (23)$$

and

$$R_e = \int \psi_e^{'} \mu_e \psi_e^{''} d\tau_e \qquad (24)$$

In the above equations, R_e is the electronic transition moment, given by equation (24), and the remaining elements are the spin, vibrational and rotational overlap integrals between the two electronic states, respectively. For example, the spin overlap integral is defined as:

$$O_s = \int \Phi_{spin}^{'*} \Phi_{spin}^{''} d\tau \qquad (25)$$

UV/Visible spectroscopy, like infrared spectroscopy, can be performed using either dispersive methods such as gratings or prisms, or by high throughput methods such as Fourier transform spectroscopy. However, the same limitation imposed by the Nyquist theorem would still apply. By usual methods, in order to ensure adequate sampling at the high-frequency end of the spectrum, around 200 nm, an FT-UV system would require a continuous-wave laser reference with a wavelength of around 200 nm. Since there is currently no low-cost laser with this kind of output, most UV instruments employ dispersive elements to separate the radiation into wavelength ranges and observe the intensity as different wavelength regions are selected.

To minimize, or eliminate, the need to scan through the spectrum, however, multi-channel detectors have been developed.[117] These detectors consist of an array of light sensitive diodes. After absorption by the sample, the light is focused through a slit, collimated, dispersed by a grating, refocused, and allowed to fall on the diode array. In this case, the resolution is determined by the slit width, the number of lines on the grating and possibly by the number and spacing of the diodes in the array. This results in a spectrometer with no moving parts and higher throughput of light. Refer to Figure 17 for a schematic representation of a multi-channel UV spectrometer.
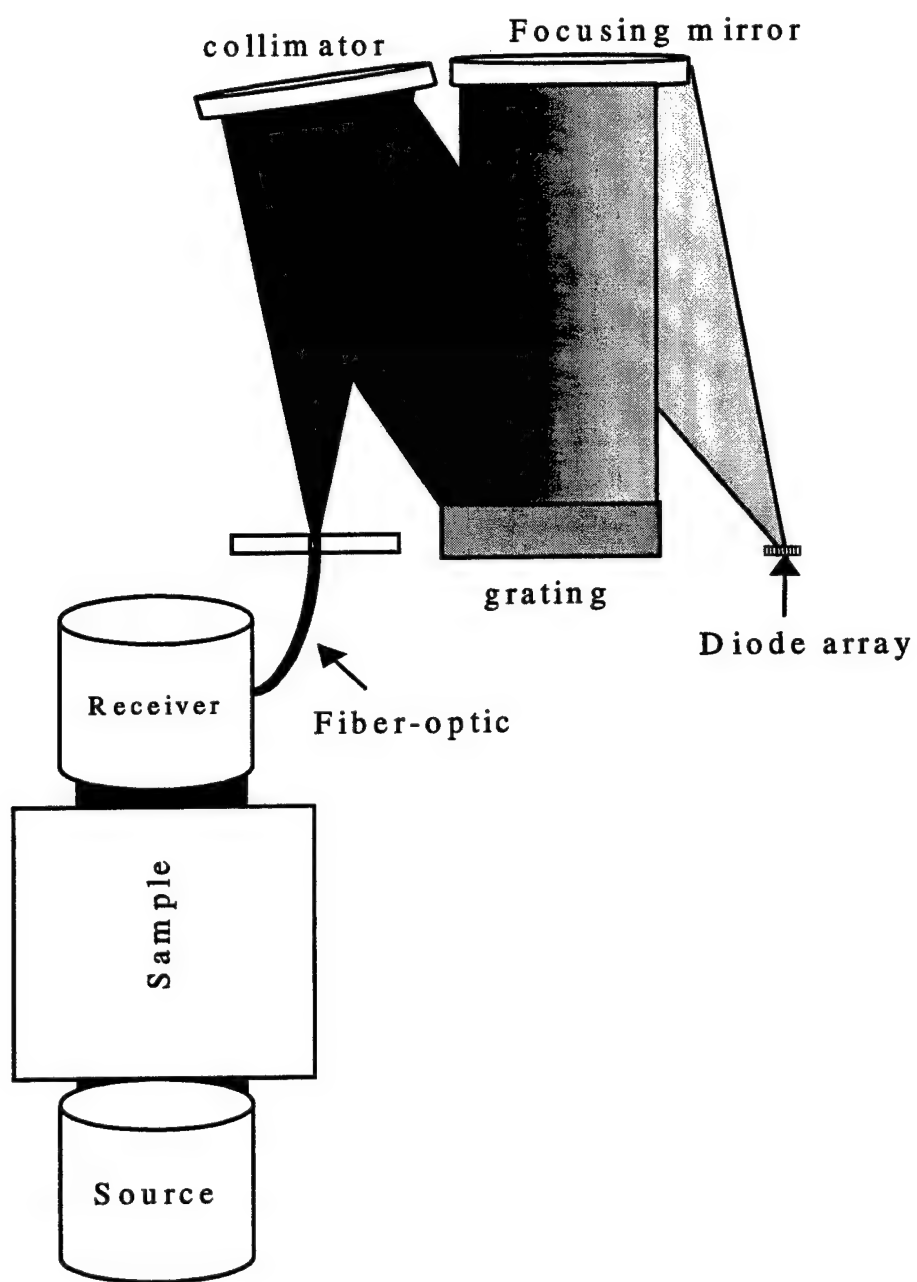
Figure 17 - Schematic Diagram of UV/Vis Monochromator

2.1.4 Open-Path Spectroscopy

Open-path spectroscopy differs from traditional spectroscopy mainly in the fact that the sample is not placed in a closed cell of any sort. As the name implies, the sample path is open to the environment and the composition of the sample can change with time. Frequently, the sample path is also very long, being in the hundreds or even thousands of meters. Mitigating the major disadvantage of this technique, difficulty in preparing and measuring standard solutions, is discussed in a later section (2.4 Data Analysis). The principle advantage of open-path spectroscopy is precisely that there is no sample containment. When measuring the concentration of reactive species in the air, collecting and containing the sample often results in the species of interest being adsorbed by or reacting with the container itself. Therefore, if other types of analytical methods are used to analyze for reactive gaseous species such as ammonia, mineral acids, radicals, etc., considerable effort must be made to minimize, control or quantify the reactions of the analytes.[124,125] On the other hand, open-path methods do not suffer from this shortcoming, and are able to produce data in minutes or hours, instead of taking days or weeks to

transport the sample and analyze it in a laboratory. Other field

analytical instruments can offer quick results as well, but still require

the sample to come into contact with some sort of sampling equipment.

When measuring light absorption over a very long path, whether

open or closed, there is always uncertainty in the exact location of the

substance being measured. Therefore, an open-path instrument

measures a path-integrated concentration, which does not guarantee a

particular concentration at any given point along the path. An example

of this is the measurement of gaseous concentrations in a stack plume.

For the sake of argument, let us assume that the light path is 100

meters long, that the plume in question occupies 10 meters of that

length, and that there is a pollutant of interest, for which Beer's Law

holds true, present in the plume at a mixing ratio of 100 parts per

million (ppm). An open path spectrometer would not be able to

distinguish between this situation, and one in which the same pollutant

was well mixed at a ratio of 10 ppm along the entire light path.[60] In

some cases, this might be a disadvantage, but in the case where the

location of the plume is uncertain, it could be a great advantage over

point sampling techniques. In the case where the air mass is well

mixed, open-path systems offer the advantage of increased sensitivity,

because the measurements are integrated along the entire length of the optical path.

2.2 Equipment

2.2.1 Open-Path Fourier Transform Spectrometer

All data were collected with one of two infrared spectrometers built by MIDAC Corporation. Both of these spectrometers use flat mirror Michelson interferometers, and have on-board computers for data preparation. Interferograms are transmitted in ASCII format through a data cable to a personal computer. One of them (hereafter called MIDAC "A") is a high-speed model, which is capable of a maximum data output rate of 120 kHz. MIDAC A has a zinc selenide (ZnSe) window for light entry or exit. The other unit (MIDAC "B") is a standard Illuminator-2500 model, which has a maximum data output rate of 80 kHz, and a potassium bromide (KBr) window. These systems are designed to provide a maximum resolution of 0.5 cm^{-1} in
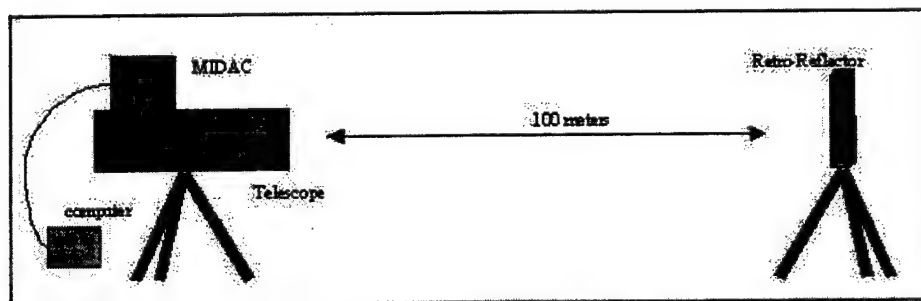
Figure 18 – Monostatic Open-Path Configuration

the mid-IR range of 800 – 4000 cm^{-1}. These spectrometers were used in one of two configurations: a monostatic open-path arrangement (Figure 18), or a large open-path White Cell manufactured by Infrared Associates (Figure 19). The "White cell" is named for its inventor, J. U. White.[126] The monostatic configuration was the more simple and flexible of the two, and was accordingly used for all outdoor field studies. The telescope used in this configuration is an 8" double-Newtonian with a ZnSe beamsplitter, which allows the light to be sent and received with the same optics. The retro-reflector is an array of 19 gold-plated corner cube reflectors. The White Cell allowed for long pathlengths to be used in the relatively confined space of the laboratory, but was much more difficult to set up and align. The White cell also had the advantage that it could be sealed up relatively well to allow the atmosphere it was sampling to be manipulated. This was not possible with the monostatic configuration due to the large distance between the source and reflector. Another major advantage of White optics is that they theoretically eliminate geometric losses of light, since the mirrors are configured to capture all the light on each pass through the system. Therefore, much higher light throughput is possible, limited only by reflective losses at the mirrors. Figure 19 shows the MIDAC sending light through a notch in mirror "A", and one pass of the light

90

from mirror "B", back to "A", on to "C" and finally out through another notch to the detector. In reality, the system was usually adjusted to allow 72 passes of the light and an effective path length of 462 meters. For a few of my studies, this was reduced to 212 meters. The alignment process for both configurations is discussed in the "Methods" section, below. Both configurations used externally mounted optics for steering the light into the EG&G liquid nitrogen-cooled mercury/cadmium/telluride detector.
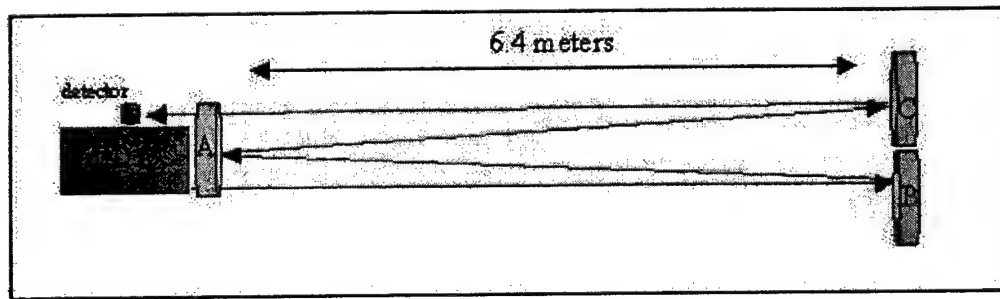
Figure 19 - Open-Path White Cell Configuration

2.2.2 *Open-Path Ultraviolet/Visible Spectrometer*

The UV/Visible spectrometry was performed using a unit that was designed and built at the University of Denver, for use with the Fuel Efficiency Automotive Test (F.E.A.T.) remote-sensing system.[127] It was designed specifically for quantifying nitric oxide concentrations and uses an on-board computer to fit light transmission profiles to a pre-stored calibration table. It is a multi-channel spectrometer, using a 128-element photo-diode array (PDA) manufactured by Hammamatsu, Inc. Light is delivered to the unit by a bundled 37-element quartz fiber optic cable (CeramOptec Industries). One end of the cable has the fibers arranged in a linear configuration, effectively forming a 4.2 μm slit through which light enters the unit. This "slit" is then collimated by the first mirror and projected onto a holographic grating. A focusing mirror directs an image of the entrance slit onto the diode array. In this way, it is possible to image a wavelength range of 16 nm onto the 128 diodes, giving an potential resolution of 0.125 nm. However, due to the fact that the optic fiber is twice this wide, the resolution is limited to 0.25 nm. When aligned for nitric oxide detection, the spectral range from

218 nm to 234 nm is on the diode array, and the gamma band of NO, located at 226.5 nm, is the peak that is measured.

2.2.2.1 Conversion and Alignment of UV-Monochromator for NH₃ Detection

This section combines information from the Hammamatsu user's manual for the PDA, existing documented procedures used by our research group, and personal experience.

An additional capability of this instrument is the ability to use a number of different photo-diode arrays. In an effort to use this instrument to look for ammonia, as well as NO, I replaced the 128-element PDA with a 512-element unit, which expanded the spectral coverage from 16 nm to 64 nm, since the diode spacing and size were the same for each array. Knowing that the fiber optics had a UV cut-off at about 190 nm, I reasoned that I should be able to see the 8 ammonia peaks that occur between 190 and 220 nm. I hoped that it would be possible to resolve these peaks sufficiently from the lower-lying peaks of NO so I could measure both species. The overall process involved was fairly straightforward:

1. Replace the 128-element PDA with the 512-element PDA.
2. Align the optics of the system so both the NH_3 and NO peaks are within the spectral window.

3. Make an ammonia calibration cell.
4. Use measurements from NH_3 and NO calibration cells to modify the software and be able to report concentrations of both species.

Because of its complexity, the process for implementing step one is attached as Appendix A. Aligning the optics of the monochromator is done using the 228 nm spectral line of a cadmium lamp. See Appendix B for the full procedure. Because I wanted to look at ammonia lines beginning at about 190 nm, and still be able to see the NO absorption band at 226.5 nm, I decided to place the 228 nm cadmium line at diode number 360, giving a spectral window of 183 nm to 247 nm.

The ammonia cell was created by filling an empty quartz cell with 1000 ppm ammonia in nitrogen. Dr. Stedman sealed the cell by heating it with a torch and pulling it until it collapsed on itself and formed a seal. A simultaneous spectrum of the ammonia cell was taken along with an NO cell, which had previously been determined to contain 28.4 ppm-m of NO. This spectrum is shown in Figure 20. Based on their separation from the other peaks, we determined that the best peaks to use would be the NO band located at diode 346, and the ammonia peak located at diode 206. The software previously used to measure only the NO peak was modified by Dr. Gary Bishop to locate

each of these peaks and to calculate a least-squares fit of the
calibration spectrum to the sample spectrum for each peak. The
results of these calculations are then output to the serial port of the UV-
monochromator's computer and can be captured on an external
computer for later analysis.
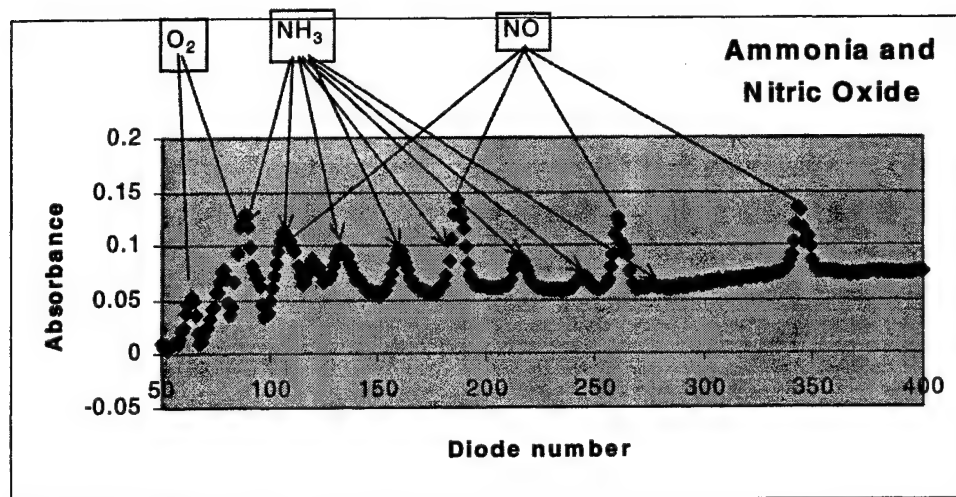
Figure 20 - Spectrum of NH$_3$ and NO from UV-monochromator

2.2.3 Meteorological Equipment

The equipment used to collect weather data consists of two
units: a three-axis anemometer, and a circuit board with a pressure
and temperature sensor wired onto it. These are described individually
in the following sections

95

2.2.3.1 Anemometer

The anemometer is a Gill-type system manufactured by R. M. Young Corporation. It has three four-blade polystyrene foam propellers, each of which drives a small direct-current generator in each arm[128]. The propellers are set at right angles to one another. They are designated as U, V and W, by meteorological convention. Traditionally, meteorologists set up Cartesian coordinates with X pointing east, Y pointing north, and z pointing up. The U, V and W designations correspond to x, y and z in this convention.[84] The mean horizontal wind speed (M) can be calculated by the following equation:

$$M = (U^2 + V^2)^{1/2} \qquad (26)$$

Compass direction (α) can be calculated by:

$$\alpha = 90° - \arctan(V/U) + \alpha_0 \qquad (27)$$

Where α_0 is 180°, if U>0 (wind is out of the east), but is zero otherwise. The anemometer blades are designed not to rotate at all if the wind is perpendicular to their axis of rotation, and their rotation speed (indicated by the magnitude of d. c. voltage generated) must be corrected by a mathematical formula if the wind is not parallel to their axis of rotation. The deviation of these propellers from true cosine response is detailed by Gill.[128]

96

The horizontal components, U and V, can be corrected

simultaneously, because they are fixed at 90 degrees from one another

in the same plane. The variable used in correcting the horizontal

components is the ratio of the smaller of the two to the larger. The

correction factors are listed in five-percent increments in Gill, page 71.

For use in my data collection program, I plotted these data and fitted a

6-degree polynomial function to the plot. I use this function to calculate

the correction factors for the U and V components, as they are

collected. For the vertical component (W), a correction of

Figure 21 - Three-axis Anemometer

1.25*(voltage) is used because the cosine response is nearly a straight line in the range of wind angle ±30° from the vertical. Since the vertical wind is very seldom out of this range, this is a good approximation for the vertical wind speed correction.[128] For conversion of voltage to wind speed, the calibration curves in the owner's manual are used, under the assumption that the characteristics of the propellers and generators have changed very little since their manufacture. The data are output to an analog-to-digital converter board in the computer that is accepting FTIR data. The data collection software performs the cosine-law corrections and conversion from milli-volts to wind speed. Before and after each FTIR spectrum is collected, 1000 data points from each axis are averaged and stored in an output file.

2.2.3.2 Temperature and Pressure

Temperature data are collected with an LM-135 integrated circuit temperature sensor, manufactured by National Semiconductor. The manufacturer claims an operational temperature range of –55 to 150 °C, with a linear response and less than 1 °C error between 0 and 100 °C, when calibrated at 25 °C. This integrated circuit is soldered onto a circuit board and provided with the necessary +5 V and ground

connections by the analog-to-digital converter in the data collection computer.

Pressure data are collected with an MPX5100-AP piezoelectric transducer manufactured by Motorola. This device is temperature compensated from 0 to 85 °C, and has a differential range of 0 to 15 PSI, which is roughly ± 1 atmosphere. This transducer is mounted on the same circuit board as the temperature sensor, and is provided with +5 V and ground connections by the analog-to-digital converter in the data collection computer.

Both of these devices were calibrated in the laboratory by plotting their output against temperature and pressure readings from standard equipment in the lab. Based on calibration and observation in the field, accuracy and precision are better than ± 2 °C for the temperature and ± 2 Torr for the pressure.

2.3 Data Collection Methods

2.3.1 Open-Path Fourier Transform Spectroscopy

This section describes the general procedures followed for use of the FTIR spectrometers after selection of appropriate locations and conditions have been made.

2.3.1.1 *Monostatic Open-Path Configuration*

The MIDAC was set up on a heavy-duty tripod and all electrical

connections were made. Figure 22 shows a cartoon of the usual

arrangement of the instruments and equipment parallel to the roadway.

The computer was connected and both it and the MIDAC were

powered with a portable generator, which was placed roughly 15

meters downwind from the MIDAC. The detector's dewar was filled

with liquid nitrogen and allowed to cool for approximately 30 minutes,

while the remainder of the equipment was set up. Next, the retro-

reflector was placed 100 meters ($\pm$ 1 meter) from the MIDAC, also on a

tripod. Liquid nitrogen was added to the detector's dewar until it was

full and cold. After this, the source was warmed and the detector

cooled enough to produce a small interferogram, instead of just
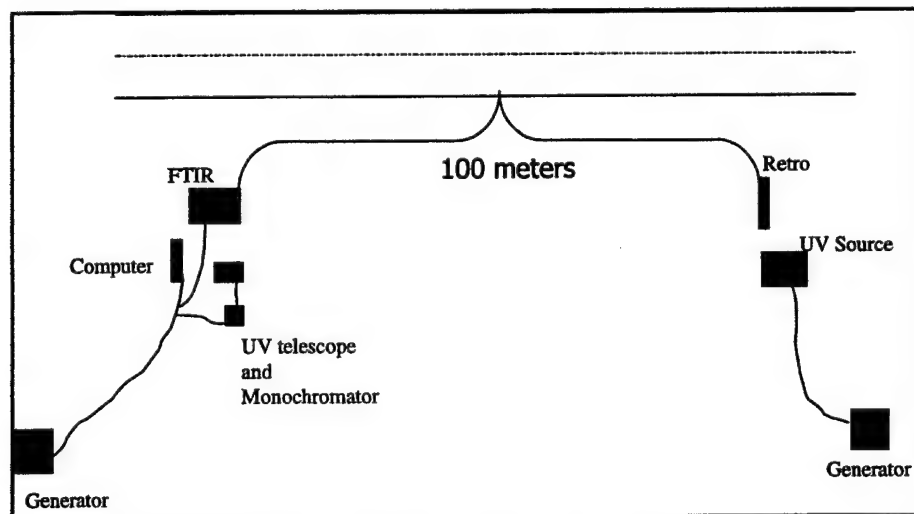
Figure 22 - Schematic Diagram of Road-side Setup of OPIEM Equipment

100

showing thermal noise. A rough alignment was made by merely

visually pointing the telescope at the retro-reflector. The alignment

process consisted of a rectangular search pattern using the azimuth

and pitch controls on the tripod. Due to the fact that the acceptance

angle of the telescope with respect to the retro-reflector was very small,

and therefore the appropriate alignment was easily missed, this

process had to be very slow and methodical. The process of finding

the retro-reflector usually took between 15 and 45 minutes. Once the

retro-reflector was in the field of view of the telescope, as indicated by

an increase in signal of a factor of 10 or more, fine alignment was

performed by making very small changes in the azimuth and pitch of

the telescope so as to maximize the signal. Some typical signal

strengths (arbitrary scale output by the control software) throughout this

process were: 0.05 (rough alignment), 1 (Retro-reflector capture), and

15 (Fine alignment). Changing the jumper settings on the detector

preamplifier could increase these signal strengths, but we always tried

to use the lowest setting that would give us signal strength between 10

and 20 without any further software amplification of the signal. This

process ensured an adequate signal-to-noise ratio while ensuring a

reasonably strong signal.   Once the system was aligned properly, the

data collection program was started and a collection of 25 spectra was

initiated. Usually, 100 scans were co-added, which gave a collection time of about 3 minutes per spectrum. After each collection was completed, the alignment was checked, and another set of 25 spectra was collected. This was usually continued for between four and six hours.

2.3.1.2 White Cell Configuration

The White cell was set up in our laboratories and sometimes used with a plastic cover in order to allow the atmosphere in the chamber to be manipulated. The MIDAC was bolted to the platform behind mirror A (refer to Figure 19) and lined up with some reference marks for a rough initial placement (Figure 23). A mask was placed on mirror B to cover all but the center 1-inch of the mirror. This was to ensure that the alignment laser was pointed at the center of mirror B before any adjustments were made to the mirror settings. Then, the same mask was transferred to mirror C. Mirror B was adjusted, if necessary, to illuminate the center of mirror C. This resulted in a laser spot in the upper left-hand corner of mirror A, and one in the lower right-hand corner of mirror A. A mask with precut holes for these two laser spots was then placed on mirror A, and mirror C was adjusted to cause the light to fall in these two holes.

The mask was removed from mirror A, and the result was two rows of laser spots across the top and bottom of the mirror. Depending on the desired pathlength, mirror C was adjusted to give the desired number of spots across the top of mirror A. The following formula was used to determine the total number of spots on mirror A needed to give the desired pathlength:

$$L = (2N + 6)(6.42) \tag{28}$$

Where L is the total pathlength in meters, N is the number of spots on mirror A, 6 is a constant representing the four passes resulting from the "bookend" mirrors (Figure 24), and one pass each for the entrance and exit of the beam of light, and 6.42 is the distance between the mirror sets. Rearranging and combining terms, the formula for determining the total number of spots actually on mirror A for a given pathlength (rounded to the nearest whole integer) is:

$$N = \frac{L - 38.52}{12.84} \tag{29}$$

These mirrors, when properly adjusted, always result in six rows of laser spots, forming a rectangle with one extra spot at the end of each of the three bottom rows. Therefore, the number of spots (R) in each of the three top rows on mirror "A" may be calculated by:

103

$$R = \frac{(N-3)}{6} \qquad (30)$$

The mask on mirror C was then removed and further small adjustments were made to achieve the most evenly spaced pattern possible, based on the observer's judgment (Figure 25). This constituted a rough alignment of the system. After the detector was sufficiently cooled with liquid nitrogen, the MIDAC was turned on and alignment proceeded using the interferogram signal strength, much as discussed in the preceding section. The difference in fine alignment of this configuration is that only small adjustments are made to mirror C, and the signal strength is much greater, owing to the unique optical properties of the White cell. Usually, the detector preamp gain jumper
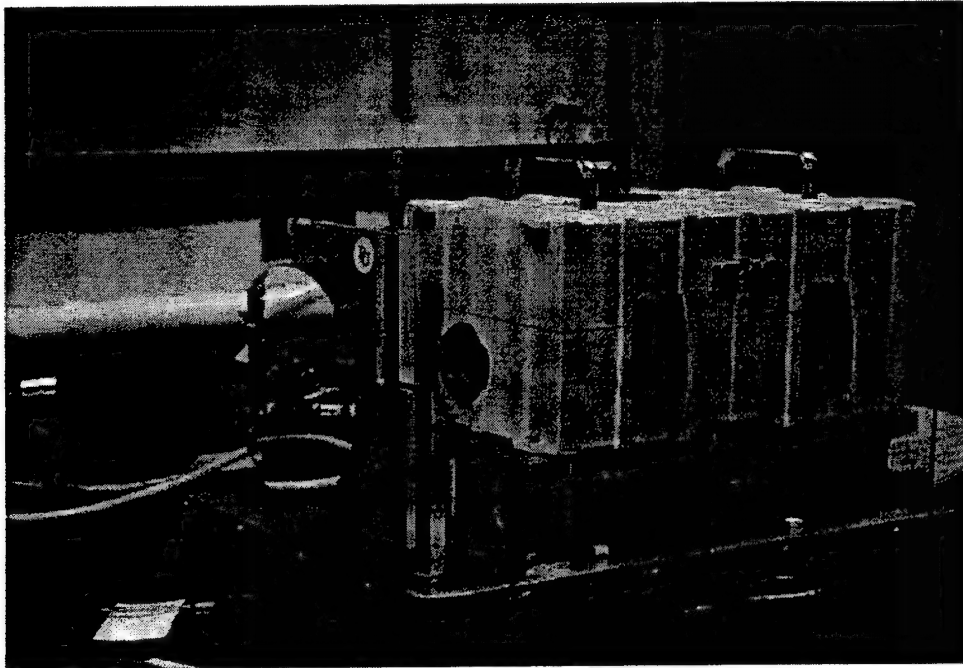
Figure 23 – MIDAC on White Cell

104

can be set two to three decades lower than when in the monostatic

open-path configuration, and signal intensities, measured in GRAMS,

as before, usually exceed 50%.
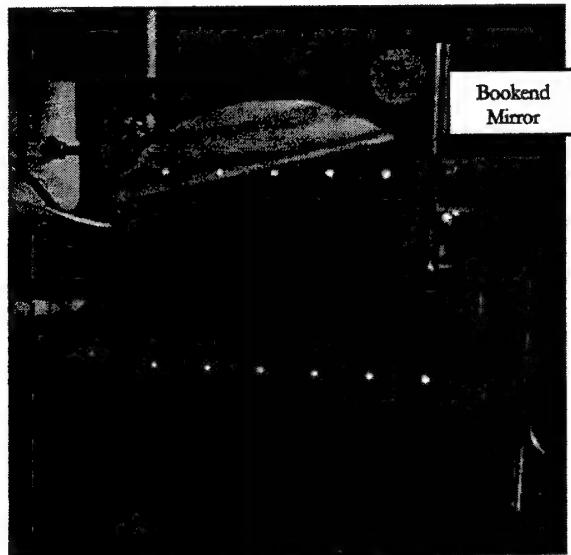
Figure 24 – Rough initial alignment of White Cell
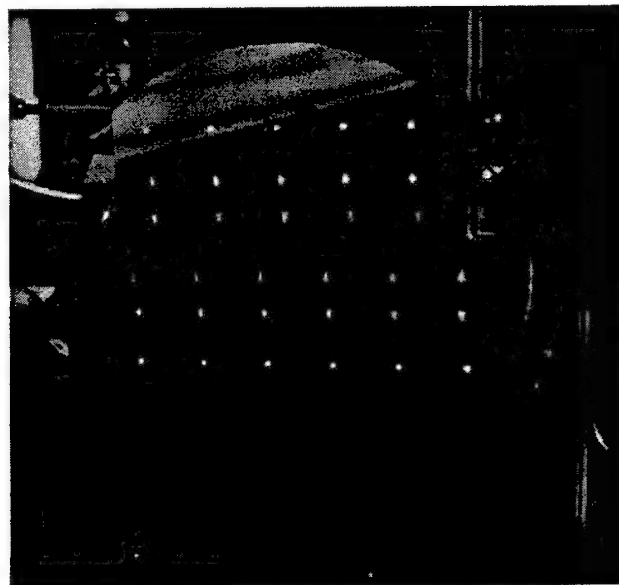
Figure 25 – Final Initial Alignment of White Cell

2.3.2 Open-Path Ultraviolet/Visible Spectroscopy

This technique was always used in conjunction with the monostatic open-path FTIR technique. After setting up the FTIR instrument, the UV/Vis monochromator and associated receiving telescope were set up next to the MIDAC. The light source, powered with a portable generator, was placed next to the retro-reflector, which was 100 meters away. This was usually done in dark, or partially dark, conditions to enable the visible light to be seen and aid in alignment of the system. First, the light source was locked into place on its three-legged platform so that the UV receiving telescope was illuminated as well as possible. Then, this telescope was adjusted so that the visible light from the source was focused on the end of the quartz fiber optic leading to the monochromator. This constituted a gross alignment, but was not sufficient for calibration. At this point, the monochromator was turned on and went automatically into alignment mode. This provided a readout of relative intensity on the monochromator's L.E.D. screen. The intensity level was then maximized to a reading of about 1000. The program was then advanced to the calibration phase, which consists of a dark scan (blocked beam), a blank scan (open beam), and a calibration scan (calibration cell in the beam). This unit could be calibrated to detect either NO, or NH_3. The scan from the calibration

106

cell was matched against a previously loaded calibration table, which was standardized to a one-meter pathlength. The concentration readings were then divided by the actual pathlength at the time of data collection, usually 100 meters. After calibration, the unit is run continuously. The unit has a 0-5 volt output, which can be connected to an analog-to-digital data card in the same computer that collects the FTIR data, or in a separate computer. The collection software we modified gives the option of either collecting UV/Vis data on the same computer as the IR, or on a different computer. During data collection, NO concentration readings from the UV/Vis system were averaged for 1 second, and these data were saved in an output file.

2.4 Data Analysis

2.4.1 FTIR Software

2.4.1.1 Introduction

The analysis of FTIR spectra is the most difficult and critical step in the process of analyzing our results. The ability to analyze our data for many different compounds, even compounds that were not looked for initially, and to do so without the need for actual calibration measurements is the greatest strength of this method. This section details the computer software that we used for collecting and analyzing

our FTIR and UV/Visible data. The actual code for all locally written or edited software is presented in Appendix C.

2.4.1.2 GRAMS/32

This commercially available package was used for controlling the FTIR, and for merging the data from all other instrumentation into a time-tagged output file for later analysis. It is written and maintained by Thermo Galactic Corporation, formerly Galactic Industries Corporation, located in New Hampshire at 395 Main Street, Salem, NH 03079. This product is the result of developing the older Lab Calc and Spectra Calc software into a multi-purpose, customizable data management software package for use in the Microsoft Windows environment. We currently use version 4, but Thermo Galactic has newer versions of the package that claim new and improved capabilities. Our version is customized for driving the MIDAC FTIR spectrometers used in this study, but GRAMS can also be customized to drive many different analytical instruments. The GRAMS package can also interface with many standard spectral databases for performing searches and matches to your data.

Another feature of GRAMS is the ability to automate data collection and manipulation by the use of Thermo Galactic's proprietary

Array Basic programming language. Array Basic is similar to Basic, with added features that allow it to interface with GRAMS to control instruments and to manipulate large arrays of spectral data. In the course of our research, we wrote and/or modified many of the Array Basic programs to suit our own purposes. Functions such as interfacing with analog-to-digital conversion hardware, controlling the timing of spectra collection, and choosing calibration files to match the spectra against were all done with Array Basic programs.

2.4.1.3 High Resolution Transmission Database

At the core of our FTIR data analysis is the High Resolution Transmission (HITRAN) database developed in 1973, and continually updated by a multi-disciplinary, international team of scientists. How we use this database will be explained further in the next section. This section will merely explain the origins and nature of the database itself. The HITRAN database has been updated many times since its initial introduction, most recently in 2000.

The goal of HITRAN is to allow users to "accurately model the simulation of transmission and radiance from the microwave through ultraviolet spectra regions."[129] The database contains information on more than one million molecular transitions for 37 molecular species.

The database also contains extensive IR cross-sections at different pressures and temperatures.

2.4.1.4 Multi-Atmospheric Layer Transmission (MALT) Program

MALT was developed at the University of Wollongong, Australia by Dr. David W. T. Griffith. The details of this program were first published in *Applied Spectroscopy* in 1996.[89] MALT is a program that uses a database, such as HITRAN, to create synthetic calibration spectra for the purpose of calculating atmospheric concentrations of analytes from real FTIR spectra. Since it's creation, MALT has been used in this fashion a number of times in a variety of applications.[90,92,94,95,131-138] Griffith, *et. al.*[130] have shown that the analytical precision of this method in analyzing spectra collected along a 22 meter pathlength at 1 cm^{-1} is as good or better than standard analytical methods for CH_4, CO and N_2O. For CO_2, the MALT method yielded a precision that was an order of magnitude worse than standard methods, but was still quite good, with $\sigma\% = 0.04\%$, versus 0.006% for the standard methods.

Because we are not using solar IR, and are only measuring in the troposphere, we actually used the "SALT," or Single Atmospheric Layer Transmission option available in MALT. This is slightly more

simple than the full atmospheric modeling available in MALT, but is still a very complex process. The IR spectrum modeling process begins with the basic premise that the optical depth of the atmosphere contributed by a single molecule at any discrete frequency is composed of the sum of the contributions from each absorption line of each molecule at each frequency. If the molecular absorptions were the only things to consider, modeling the atmospheric IR spectrum would be very simple. However, in the real atmosphere there are processes that contribute to "line broadening," causing a real spectrum to have absorption curves instead of lines. There are two major types of line broadening mechanisms: pressure broadening and Doppler broadening.

Pressure, or collisional, broadening is due to the excitation or de-excitation of the absorbers through collisions with other absorbers or chemical species. The close proximity of molecules to one another slightly influences each molecule's energetic ground-state, leading to slight differences in the actual quantity of energy that is absorbed. Pressure broadening is directly proportional to both temperature and the total number of available collision partners. This results in a broadening effect that causes the absorption line to take on a

111

Lorentzian shape, with a width at half height on the order of 10^{-3} to 10^{-2} cm^{-1}.[117]

Doppler broadening arises from the fact that absorbing molecules or atoms are likely to be moving in either a positive or negative direction along the axis of absorption. Because all absorbers have an equal probability of moving in either direction, the resulting distribution of absorbed frequencies is Gaussian in shape. The width at half height due to Doppler broadening is on the order of 10^{-2} cm^{-1}.[117]

The combination of these broadening processes imposes a convolution on the absorption line that is a mixture of Gaussian and Lorentzian, and the combined line shape is referred to as a Voight profile.

Figure 26 illustrates a variety of possible Voight profiles, depending on relative amounts of Doppler and pressure broadening. The parameter *a* shown in the bottom-half of Figure 26 indicates the relative amount of the Lorentzian function in the Voight Profile. In the simplest terms, pressure broadening is proportional to the total pressure, and Doppler broadening is proportional to molecular mass and temperature. These factors can be measured and used to

determine actual spectral line shapes in a simulated spectrum, which is exactly what the MALT program does.
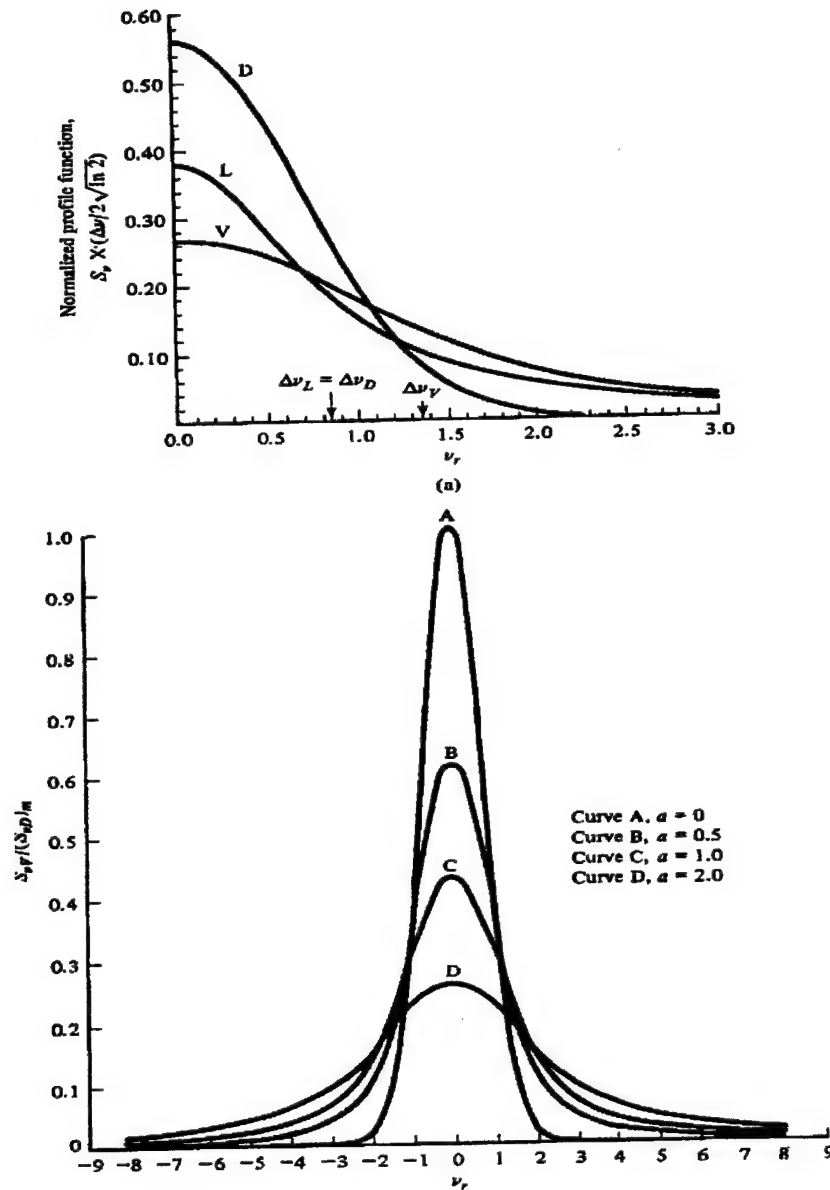
Figure 26 - Gaussian, Lorentzian and Voight Curves[117]

113

In addition to these effects on line shape, there is also an instrument-dependent effect. Any real instrument has characteristics and limitations that impose a convolution function onto the natural, broadened line shape of a spectrum. The two major instrument-dependent influences on line shape are apodization and beam divergence.[89] The shape of the apodization function varies, but is selected by the operator, as discussed previously. The divergence of the collimated infrared beam is related to the finite aperture of the light-gathering optics, and convolves the spectral line shape with an additional rectangular line shape.[89] The width of this rectangular function is often referred to as the field of view (FOV), is frequency dependent, and can be calculated by:

$$FOV = \frac{v\left(\frac{\phi}{2f}\right)^2}{2} \tag{31}$$

In this equation, ϕ is the diameter of the entrance aperture of the spectrometer and f is the focal length of the collimator.

As part of the MALT process, a finite spectral window must be defined, and all of the known absorbers within that window must be specified in order to retrieve the appropriate data from HITRAN. Once the temperature-corrected line spectra obtained from the HITRAN database are appropriately broadened, calibration spectra may be created. This is done by randomly varying the amount of each absorbing component within the bounds of the concentration range input by the user. This results in a number (also specified by the user) of unique spectra resulting from random amounts of each absorbing species. Since this is a very fast process on modern microcomputers, the standard procedure is to calculate the maximum number (60) of calibration spectra. The spectra are stored in a GRAMS-compatible multi-file format. After calculation of these calibration spectra, a real spectrum may be fitted using the Classical Least Squares algorithm.[139] This entire process is illustrated in the flow diagram in Figure 27.
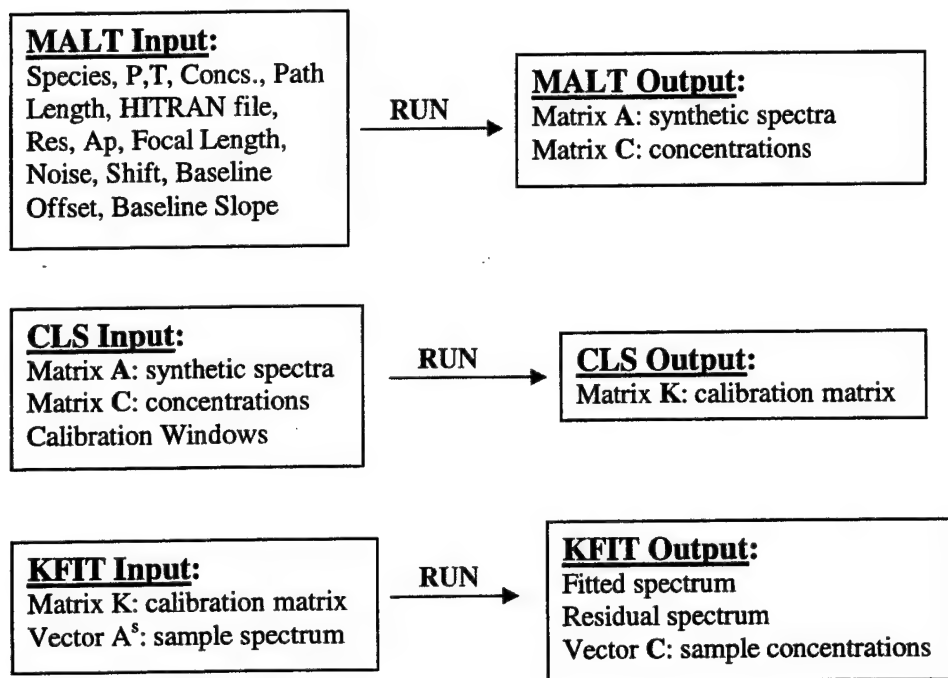
Figure 27 - MALT/CLS Process

2.4.2 The FTIR Data Collection and Analysis Process

Because of its complexity, it is instructive to put this entire process together into an illustrated flow diagram. This process is what lends the unique qualities that enable me to perform a "Tunnel-less Tunnel Study."

The first challenge in applying this method is to find a relatively narrow spectral range where there is as little interference from strong water or CO_2 peaks. This is often difficult due to the fact that both of these molecules have strong features throughout many different parts

116

of the IR spectrum. Starting with the spectral regions used by Dr. David Griffith,[130] I used real spectra to determine the best ranges to use for each species I was analyzing for. Spectral window selection was also made on the basis of goodness of fit by the MALT program and, in the case of CO_2, limiting regions of strong absorption and possible non-linearity. Griffith, *et al.* have found no problems with Beer's Law non-linearity with absorptions of less than about 0.4 absorbance units.[130]

For the purposes of illustrating the process, I will use the spectral region of $2140 - 2250$ cm^{-1}. This is the region in which the features due to CO, CO_2 and N_2O are found. The other windows I used were for CH_4 ($2980 - 3150$ cm^{-1}) and NH_3 ($900 - 970$ cm^{-1}). After the spectra are collected, the calibration files must be built to match, as closely as possible (see pressure and temperature study above), the barometric pressure and temperature of the sample spectrum.   One reason that it is preferable to have a fairly narrow spectral window is that all the absorbing species that are likely to be present must be known. This is because MALT is currently based on the Classical Least Squares technique, which cannot account for unknown species in the spectrum (130, pg. 210). If there is an absorbing chemical that is

unaccounted for within the spectral window, it will usually result in a poor fit and a relatively high root-mean-squared error. This was generally the case for methane, because there were no other simple hydrocarbons in the HITRAN database that MALT could use to build the calibration files, and there are a number of hydrocarbons that absorb in this region of the spectrum.

When building the calibration files, instrument-specific parameters must be entered to account for the way the light passes through the system. These parameters are described in the previous section on FTIR. For our MIDAC instrument, the parameters were as follows:

- Resolution = 0.5 (for normal operation)
- Collimator Aperture = 19.0 mm
- Collimator Focal Length = 762 mm
- Effective Apodization = 0.25*
- Phase Error = 0
- Misalignment = 0.25*

The quantities marked with an asterix have a range of possible values between 0 and 1, but I found that the above values generally gave the most consistent results with the instrument being used. Phase error should be zero, since the Fourier Transform routine in the

GRAMS software package automatically produces phase-error corrected spectra. Temperature, pressure and pathlength are also input into the program that eventually builds the calibration files. Finally, you must input the approximate central value of the mixing ratio expected for each absorber, and a range of values over which to calibrate. It was not unusual, for example, to encounter an average of 500 ppm of CO_2, with an approximate range of 400 to 600 ppm. If it was determined later that this range or central value was very much different from the actual values, they could be adjusted to more closely match reality. For example, if the sample spectra actually measured 900 ppm of CO_2, the CLS program would still calculate approximately 900 ppm, even if the calibration files were built for a range of 400 to 600 ppm. However, a more accurate value would be achieved if the calibration files were re-built for a higher median mixing-ratio of CO_2.

Once all of this information is entered, the MALT program builds a set of calibration spectra, as described in the previous section.

Figure 28 shows the 2140 to 2250 cm^{-1} region of an actual spectrum I collected at a pathlength of 200 meters. The reason for the non-zero baseline is that this absorbance spectrum is simply the inverse log of as single-beam transmission spectrum. When
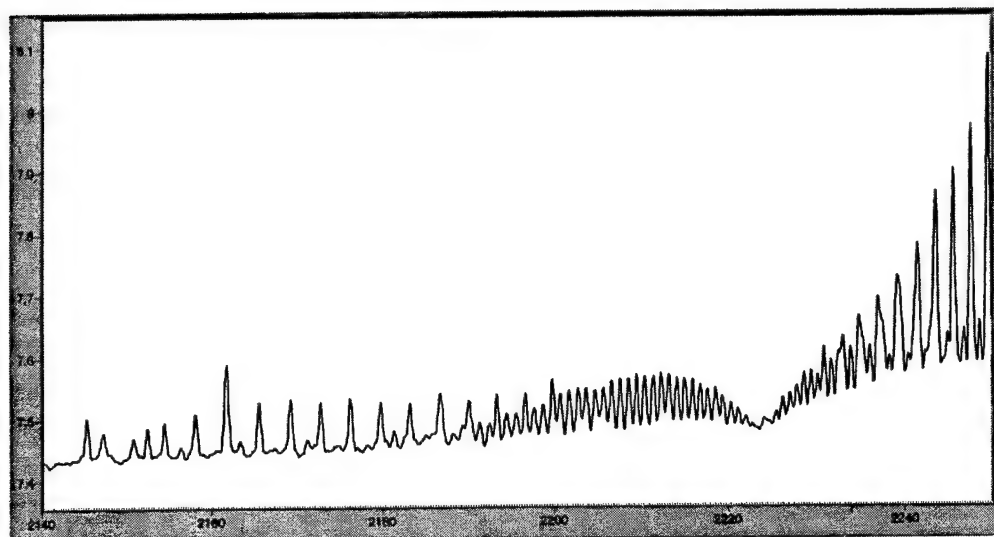
Figure 28 - CO_2, NO and CO Region of the Real Spectrum
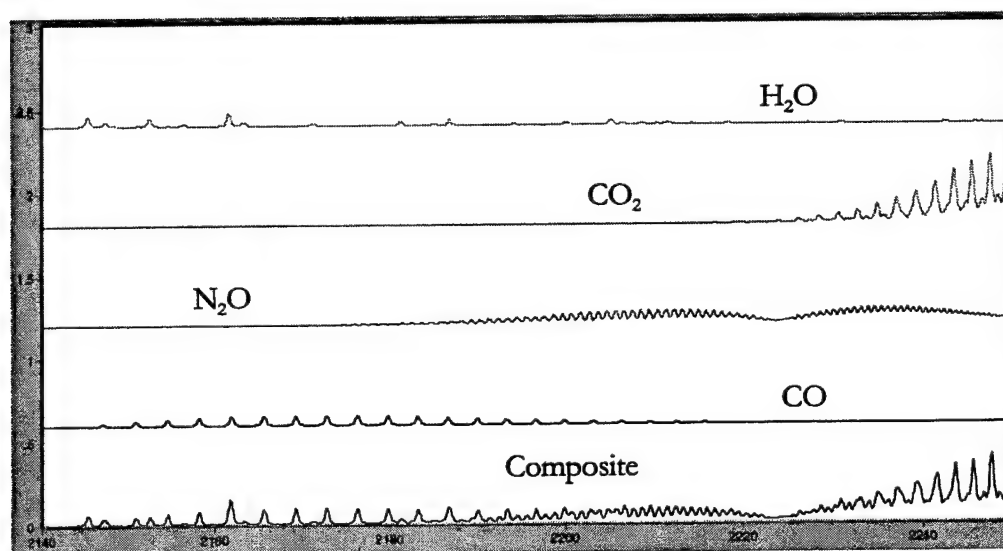
Figure 29 - Output of MALT program: median value component spectra
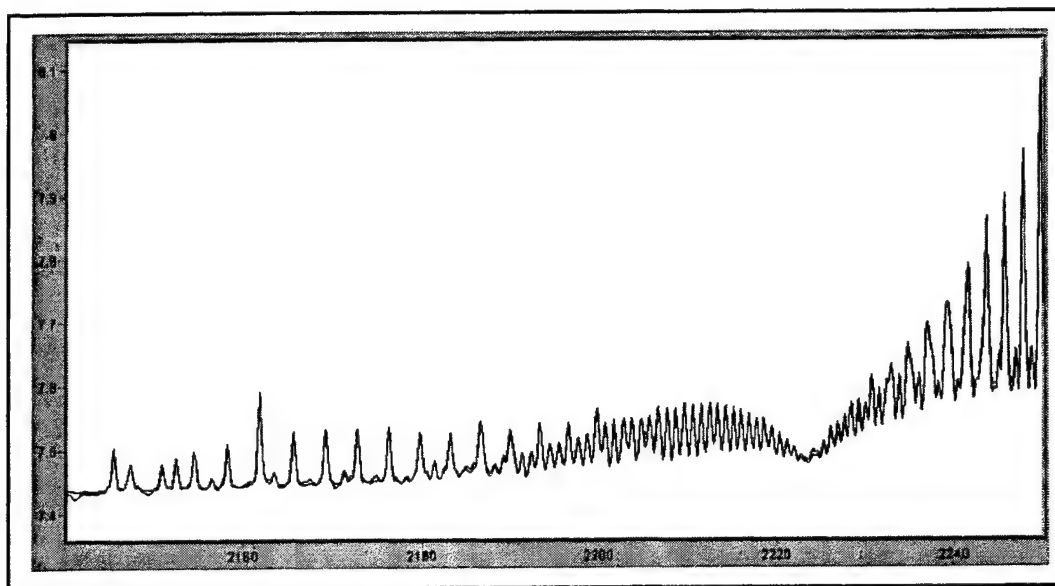
Figure 30 - CLS fit of synthetic calibration spectra to real spectrum
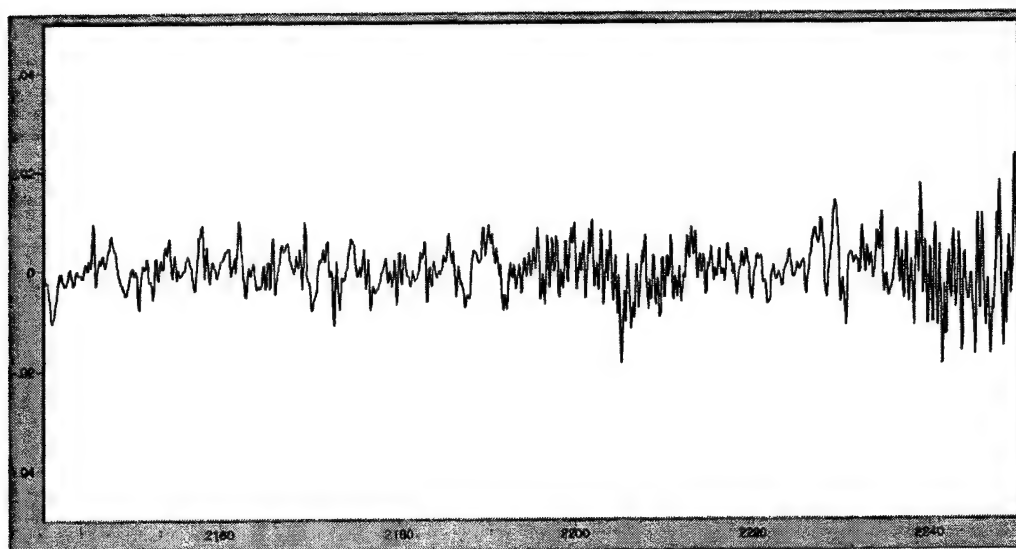
Figure 31 - Residual after CLS fit of spectrum

122

The residual spectrum shows no recognizable features and appears to be mostly noise. For this particular spectrum, the calculated mixing ratios of each component are:

- H_2O: 0.45734 %
- CO_2: 445.36 ppm
- N_2O: 0.34972 ppm
- CO: 0.72329 ppm

This summarizes the normal procedure I used for analyzing FTIR spectra. Since there were usually between 25 and 200 spectra to analyze, I actually used a GRAMS/32 array basic program to automate the process to an extent. The results for each spectrum were output to a comma-delimited file. This allowed for wholesale manipulation of the results for purposes such as graphing or further analysis. After all the spectra for a given experiment were treated in this manner, adjustments were made to the CO and N_2O results, based on some experiments described later in this thesis (sections 3.1.5 and 3.1.6). After that, the data were examined for the presence of autocorrelation (section 2.4.4.1)

2.4.3 UV/Visible Monochromator Software

The software used to collect all UV/Vis spectra is written and maintained by Dr. Gary Bishop of the University of Denver Department

of Chemistry and Biochemistry. The program used to collect spectra and calculate concentrations of ammonia and nitric oxide uses a Least Squares fitting routine to match the measured spectrum with the calibration spectrum, which is collected using a cell of known concentration. The programs are printed out and included with this thesis in Appendix D.

2.4.4 Statistics and Numerical Methods

2.4.4.1 Autocorrelation Analysis

One of the basic assumptions in the application of statistical analysis to a set of data is that the data points are independent and have uncorrelated errors associated with them. If, in fact, the data points are dependent upon one another, or the error in each point is correlated to other points in the data set, then the data are said to be "autocorrelated". Data that are influenced by a common source and that have a "natural" sequential order over time are usually autocorrelated[140]. As an example, consider the average speed of cars on an interstate on-ramp. If the cars are widely spaced, then the average speed of car "A" is unlikely to be correlated to that of car "B." In other words, each car's speed is an independent quantity. However, if the ramp becomes congested, and cars are closely spaced, then their average speeds are likely to be very similar. Even though there is

no real connection between the vehicles, they are influenced by a common source (the congestion on the ramp), and their speeds become autocorrelated. The data we collected in our roadside studies certainly fits that profile, since concentrations of the various species rise and fall in a fairly predictable manner associated with increases and decreases in traffic flow, changes in wind direction and speed, temperature and other environmental factors. Upon further examination, nearly all our data was observed to contain some degree of autocorrelation. The presence of autocorrelation in the data has three primary effects:[141]

1. Least squares estimates are said to be "inefficient" because they no longer have minimum variance.

2. The estimate of σ^2 and the standard errors of the regression coefficients may be drastically understated, giving the appearance of accuracy.

3. Confidence intervals and tests of significance are no longer strictly valid.

The presence of autocorrelation may be tested for in a number of different ways, but a popular test is the calculation of the Durbin-Watson statistic.[142] This test is based on the assumption that the

errors in a set of data form a first-order autoregressive series.[141,142] In

other words, that the error in each data point (u_t) consists of an

uncorrelated component (ε_t) and a correlated component (ρu_{t-1}) that is

a function of the error in the previous data point:

$$u_t = \rho u_{t-1} + \varepsilon_t \qquad (32)$$

If the value of ρ is zero, then there is no autocorrelation and the errors

are truly random. For this test, two statistics are calculated. The first is

called the d statistic and is used to test the null hypothesis -- the case

that there is no autocorrelation. The second statistic is denoted r and is

an estimate of ρ. They are defined as follows:

$$d = \frac{\sum\limits_{2}^{n}\left(e_t - e_{t-1}\right)^2}{\sum\limits_{1}^{n} e_t^2} \qquad (33)$$

$$r = \frac{\sum\limits_{2}^{n} e_t e_{t-1}}{\sum\limits_{2}^{n} e_{t-1}^2} \qquad (34)$$

The following approximate relationship exists between d and r.

$$d \approx 2(1-r) \qquad (35)$$

126

In Equations (33) and (34), e is the residual from the linear regression. Durbin and Watson calculated lower and upper limits (d_L and d_U) for the value of d for various degrees of confidence. These values are commonly tabulated for a 95% confidence level. See Appendix E for values of d_L and d_U. Once the value of d has been calculated, it is used in the following manner:

1. $d < d_L$, reject null hypothesis

2. $d > d_U$, accept null hypothesis

3. $d_L > d < d_U$, test is inconclusive

When autocorrelation has been identified by the Durbin-Watson test, it can then be removed from the data, since an estimate of ρ has been made in the process. The value of each individual data point loses physical significance in the process, but the results of the linear regression will be improved, as well as the estimate of error in the data. With the method derived by Cochrane and Orcutt,[141] The value of r from the Durbin-Watson test is used to transform the original data points (x_t and y_t) with the following formula:

$$x_t = x_t - r x_{t-1}; \quad y_t = y_t - r y_{t-1} \tag{36}$$

The Durbin-Watson test is performed on the transformed data set and examined for the presence of autocorrelation. This process may be repeated until the null hypothesis is accepted, but in practice, if it does not work after one attempt, then it will usually be fruitless to iterate further. This has been the case in my experience, and it is also stated in the text by Chatterjee and Price.[141]

2.4.4.2 Error Analysis

There are two basic results from our data analysis in which we must track errors: values of detection limits, and ratios of various air components to CO_2. In the case of detection limits, multiple measurements were made and the value of three times the standard deviation was used as an estimate of the total error in the number. In the case of ratio values, the ratio was obtained by linear regression of each species against CO_2. The error in this value was taken to be the standard error of the slope of the line, as calculated by the linear regression tool in Microsoft Excel®. Any additional error analysis will be described as necessary in the pertinent sections.

CHAPTER 3. - LABORATORY EXPERIMENTS AND FIELD STUDIES

3.1 FTIR Laboratory and Preliminary Experiments

This section details the laboratory experiments I undertook to establish the operational ranges and limitations of my instruments, as well as the field campaigns to collect data for proving the concept of the Tunnel-less Tunnel Study.

3.1.1 Calibration of Temperature and Pressure Instruments

I set the unit outside for one hour to get cold, and then recorded temperature (with a mercury thermometer marked in tenths of a degree) and sensor output (in data acquisition board units), as the system warmed to room temperature. Using a digital barometer to measure barometric pressure, I collected data from the pressure transducer at three pressures: 590, 591, and 618 Torr, over a three-day period. From these data, I plotted the temperature and pressure against data acquisition board units (counts), and derived the following calibration equations:

$$T = \frac{counts - 3155.5}{4.4837} \tag{37}$$

$$P = (0.3915)counts - 705.18 \tag{38}$$

During field studies, readings from these units were compared to other temperature and pressure measuring devices and found to be in good agreement.

3.1.2 Dark Spectrum Test

One cause for concern in any application of FTIR spectroscopy is the possible presence of a bias due to internally reflected light giving a non-zero dark spectrum. As shown in Figure 32, this was not a problem in our field studies. The screen shot in this picture shows two
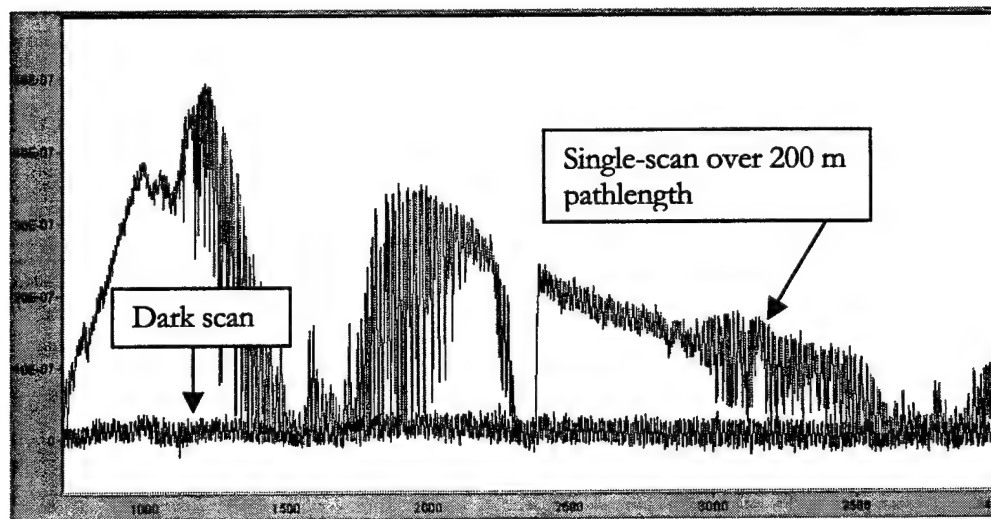
Figure 32 - Dark Scan from FTIR Spectrometer

spectra: a single-scan transmittance spectrum taken over a 200-meter path, while pointing at the retro-reflector, and a "dark scan"

130

transmittance spectrum collected while the FTIR telescope was angled approximately 45 degrees away from the retro-reflector. Both of these were collected in the field. The dark scan shows no recognizable spectral features and appears to oscillate about a value of zero.

3.1.3 Detection Limits: CO_2, CO, N_2O, CH_4, NH_3

This began as a study to determine the minimum detection limit of ammonia with the FTIR instrument. I set the open-path White cell to the closest approximation of our normal working pathlength with the long-path system: 231 meters. Then, a heavy plastic chamber was put over the White cell and sealed as well as I was able to. The MIDAC was set to collect 10-scan spectra at a rate of one 10-scan spectrum every 8 seconds. This was done continuously for almost one hour after a 1.0 mL aliquot of gaseous anhydrous ammonia was injected into the chamber. The gas concentrations were determined later by the MALT/CLS method described earlier in this thesis. Because the chamber has a calculated volume of 1680 liters, this should have given a maximum concentration of 0.6 ppmv of NH_3. However, the maximum observed concentration was 1.42 ppm, which I cannot explain except to say that the syringe I used and chamber are both relatively crude and I was not attempting to deliver extremely

precise amounts of gas. I was only interested in having enough ammonia to observe initially, observing the exponential decay of the ammonia and determining a minimum detection limit from the data. The initial decay rate of the ammonia was indeed exponential, with an R^2 value of 0.92 for an exponential curve fit to the first 21 data points (80 seconds). I expected that, at some point, the standard error of the measurement, as reported by MALT, would exceed the reported concentration of ammonia. In fact, the standard error never exceeded 50% of the calculated concentration, and was usually below 20%. Upon examination, it became obvious that the NH_3 concentration began to take on a random profile after it reached about 10 ppbv absolute (2.31 ppm-m). Analysis of the decay rate of the ammonia concentration revealed that, the half-life was only about 56 seconds. At the point in the study where the concentration of ammonia began to appear randomly distributed about avalue of 10 ppbv, approximately 10 half-lives had passed, meaning that only about 0.01% of the original concentration of ammonia remained in the chamber. This value of 2.31 ppm-m is the apparent concentration of NH_3 measured with this system when there is actually no ammonia present. This positive bias should be subtracted from any measurement obtained with this system. This

corresponds to 11.5 ppbv (absolute) when measured over the 200-meter path I normally used in the field.

Plotting the concentrations of other gases in the chamber (CO_2, CO, N_2O, CH_4, H_2O) against time revealed flat lines with slight deviations as the air in the chamber exchanged with the air in the room. This was as expected. I chose the flattest portions of the concentration curves, containing no fewer than 50 data points (covering a span of 5 minutes) to analyze for variance in concentration during times when it appeared to be stable. Figure 33 shows the region used for CO_2. The exception was ammonia, for which I used a portion of the curve where I expected that there was none remaining in the chamber. Analysis of these data was the closest I could come to making repeated measurements of a stable sample. The results are reported in Table 7, and are adjusted to reflect the 200 meter pathlength I normally use in the field. The minimum detectable change in concentration is reported as 3 times the standard deviation of the portion of the data that was analyzed. After removal of any constant bias, this also represents the minimum detection limit of the system.

	[CO2] ppm	[CO] ppm	[N2O] ppm	[CH4] ppm	[NH3] ppm
3-sigma	1.28	0.0033	0.0017	0.0132	0.0032

Table 7 – Results of FTIR Detection Limit Experiment, 04 Oct 01

A similar experiment, without the injection of ammonia, was performed on 11 Sep 01, and the results were very similar. In this case, the chamber was sealed as tightly as possible and allowed to stabilize and equilibrate with the room for several hours. After some trial and error with the spectrometer settings, the MIDAC was set to collect 10-scan spectra, which took about 8 seconds each. A total of 480 spectra were collected over a period of approximately one hour. Even though the chamber was relatively stable, there was still a general downward drift in the reported concentrations of each species. Therefore, a region of the data was chosen for which the CO_2
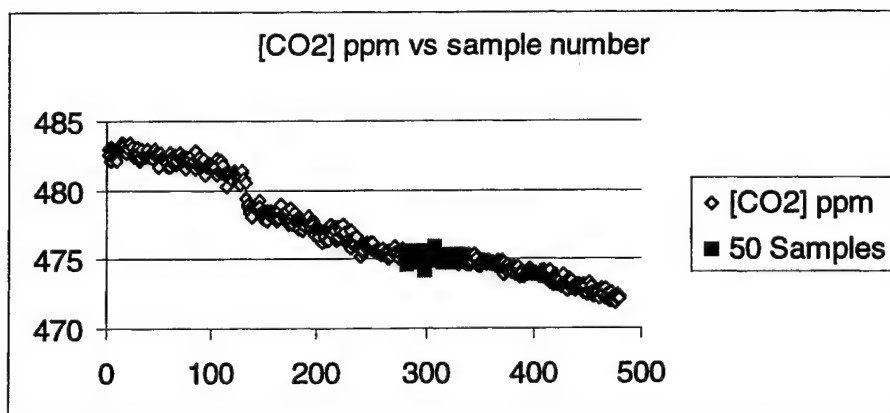
Figure 33 - Region of data analyzed for detection limits

concentration curve was the flattest, with a total number of 50 samples. The same data points were used for each of the measured gaseous species. This is illustrated in Figure 33, below. Part of the selection criteria for this region of data was to examine the point-to-point change in concentration for each gas and attempt to minimize this value. For all gases except ammonia, the point-to-point change in this region of data was on the order of 0.01% of the average concentration. The variation in measured ammonia was 1.3%, but this was most likely indicative of the variability of the system to measuring ammonia, since there should have been very little ammonia in the room. As with the data collected on 4 Oct, the standard deviation of the concentration for each gas was calculated and three times that value was taken to be the minimum detectable change in concentration. These results are summarized in Table 8, and are adjusted to reflect the 200 meter pathlength I normally use in the field.

	$[CO_2]$ ppm	$[CO]$ ppm	$[N_2O]$ ppm	$[CH_4]$ ppm	$[NH_3]$ ppm
3-sigma	0.89	0.0038	0.0017	0.0101	0.0043

Table 8 – Results of FTIR Detection Limit Experiment, 11 Sep 2001

The values determined in this study are roughly the same as those determined in the study done in October, and are smaller in every case except for CO and ammonia, which are still very close in value. The lower values determined in this experiment can probably be explained by the fact that the chamber was allowed to stabilize for a much longer time in this experiment. Therefore, the gas concentrations could be expected to be more constant during the time of the experiment. This is further supported by analysis of the October CO_2 data, which shows that the point-to-point variability for the region of data analyzed in October is nearly 3 times that for the September data. The September data are also free of any possible interference imposed by injection of ammonia into the chamber, and because of these reasons are probably more indicative of the actual limits of the FTIR system.

3.1.4 HNO_3 Detection Limit

Using the synthetic calibration method for this species proved to be difficult because there is so much data for HNO_3 in the HITRAN database at such a fine resolution that the MALT program had difficulty processing more than a very small portion of the spectrum. I was able to process a calibration spectrum for a peak between 870 and 910

cm^{-1}, which was free from water and other interferences.[79] I took 32 spectra of 100 scans each over a total pathlength of 12.6 meters in the laboratory, where there was assumed to be a nitric acid mixing ratio of 0 ppm. I then created a calibration set with $[HNO_3]$ ranging from 0 to 10 ppm, and analyzed the spectra. The average of these results was 0.27 ppm HNO_3. This was taken to be "noise" level in this region of the spectrum, and the detection limit was assumed to be three times that number. Adjusting for a typical field pathlength of 200 meters, the detection limit of HNO_3 with this system was calculated to be 51 ppb. Since HNO_3 occurs in mixing ratios of 3 to 50 ppb in polluted air,[73,80] this is not a useful detection limit for the purposes of detecting changes in HNO_3 mixing ratios.

3.1.5 Initial Investigation of Possible $N_2O/CO/CO_2$ Cross-talk

This set of experiments was instigated because I had observed

from time to time that when was an occasional anomaly which caused

the CO_2 concentration to spike very high (>10,000 ppm), the apparent

N_2O concentration became extraordinarily high as well. This led me to

believe that perhaps there was some interference (cross-talk) between

CO_2 and N_2O, since the peaks of each species are interleaved in the

region where I analyze for them, as can be seen in Figure 34.
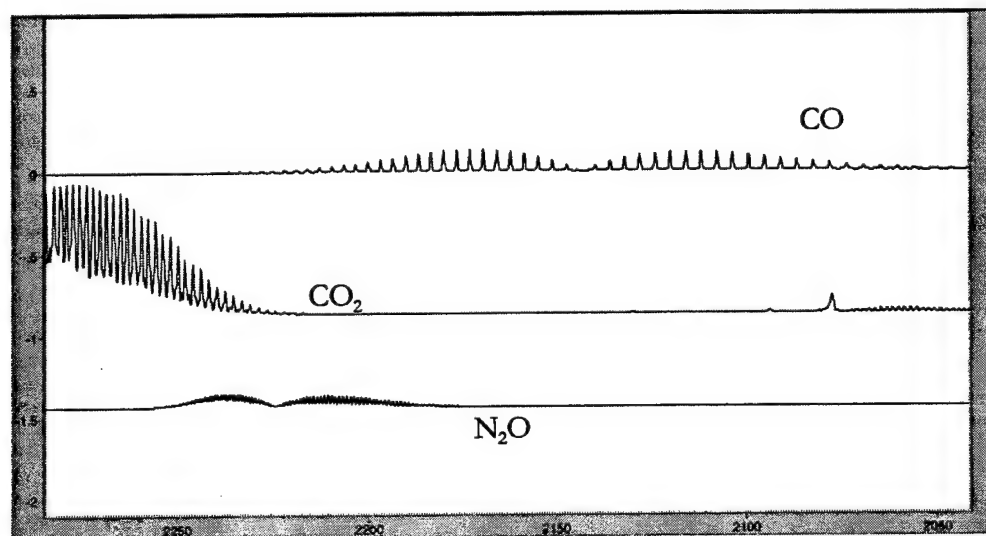
Figure 34 - CO, CO_2 and N_2O spectral features at 0.5 cm^{-1} resolution

These experiments were conducted using the bench-top

chamber in our laboratory, in conjunction with the open-path White cell

configured for a total path-length of 462 meters. In these experiments,

138

various gases were injected into the chamber, and the gas mixture

inside was allowed to exchange with the air in the room while the

constitution of the mixture was monitored by FTIR. No special care

was taken to seal the chamber very tightly.

For the first experiment, 2.0 mL of anhydrous ammonia were

injected into the chamber. The rise in ammonia, which was 10 to 20

times the level normally seen in our field studies, had no apparent

influence on any other gaseous species. The results are shown in

Figure 35.
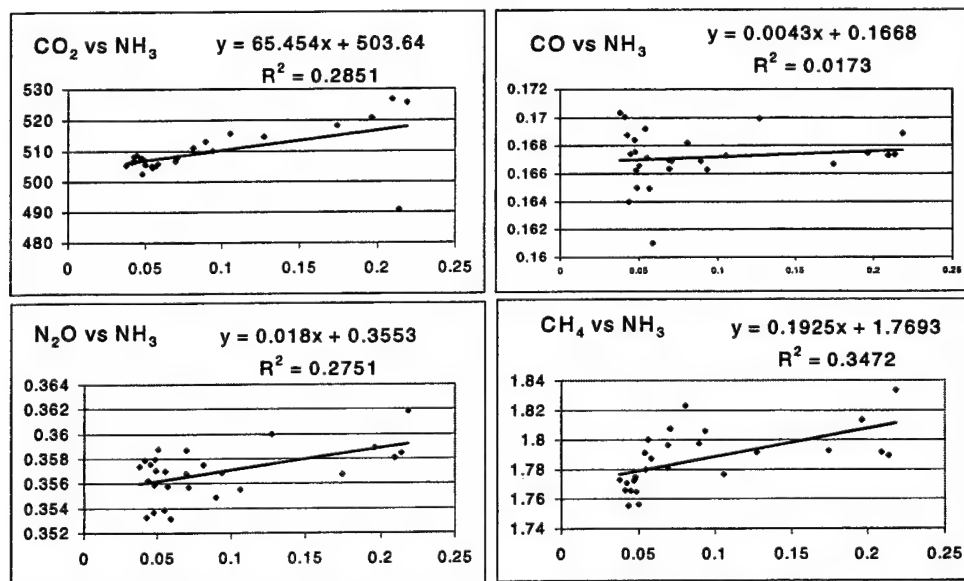
Figure 35 - Results of NH_3 Injection Experiment, 20 April 01

In the second experiment, 10 mL of N_2O were injected. This produced a total concentration of N_2O of more than 3 ppm, which is on the order of 10 times the levels seen in our field studies. Unlike ammonia, nitrous oxide had a very obvious effect on the apparent concentration of both CO_2 and CO. These results are shown in Figure 36. Since ammonia and methane do not share nitrous oxide's spectral window, there is no possibility of any software-based cross-talk
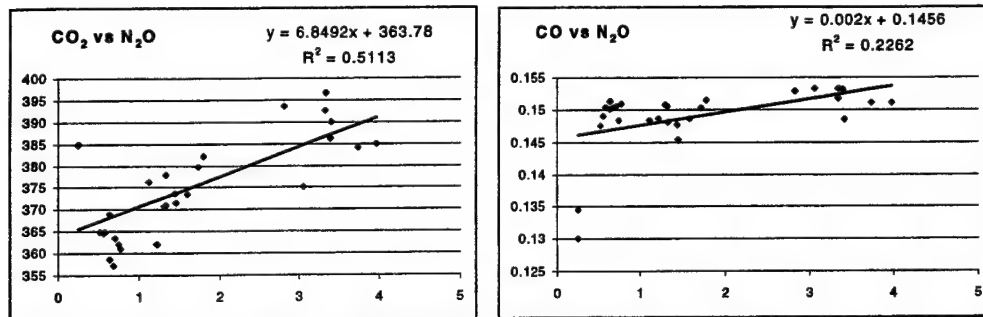
Figure 36 - Results of N_2O Injection Experiment, 20 Apr 01

between nitrous oxide and these gases. Therefore, only CO_2 and CO were examined in this case and the next. While there seems to be a real effect here, it is relatively small in magnitude. The normally measured amounts of N_2O, for example, would only account for an apparent increase of about 0.8 ppb of CO, on top of a commonly seen level of 1 to 2 ppm. Similarly, N_2O might account for as much as 2.7 ppm of the apparent CO_2 concentration, which is less than 0.8% of the background concentration of 350 ppm. Both these effects are smaller

140

than the standard errors in these measurements, and are much smaller

than the final errors in the calculated emission factors, and are

therefore negligible.

In the third experiment, 10 mL of CO was injected. There was

no obvious influence upon the apparent concentration any of the other

gases in the chamber. These results are shown in Figure 37. In the

final part of this experiment, 1 L of CO_2 was injected. This had an

obvious effect on the apparent concentration of N_2O, an unusual effect

on CO, and a possible effect on CH_4. These results can be seen in

Figure 38. The effect upon CO is unusual because it appears to fit to a

second-order polynomial. It is difficult to explain what may be the

cause of this effect, although the strong non-linearity of CO_2 at high

absorbances could impose this non-linear result. Even though the

relationship to N_2O is much more linear, it actually fits better to a

polynomial equation as well, so this explanation may be correct.
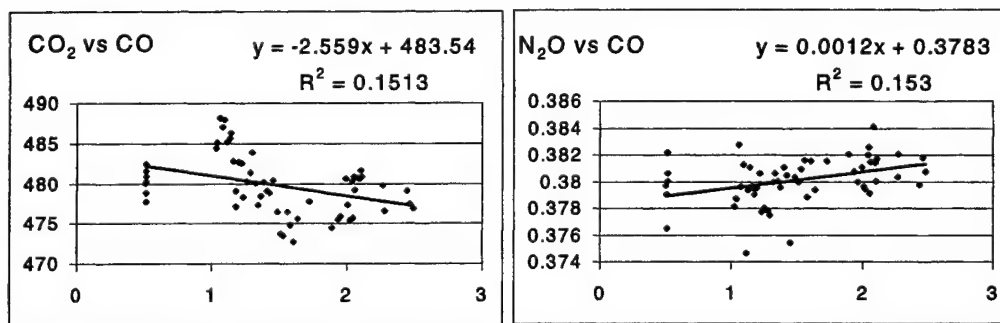
Figure 37 - Results of CO Injection Experiment, 20 April 01

141

N$_2$O vs CO$_2$ y = -0.0006x + 0.6036   R^2 = 0.9799

y = -9E-07x^2 + 0.0005x + 0.2617   R^2 = 0.9892

CO vs CO$_2$ y = -0.0061x + 9.5995   R^2 = 0.6416

y = -6E-05x^2 + 0.0674x - 13.005   R^2 = 0.9323
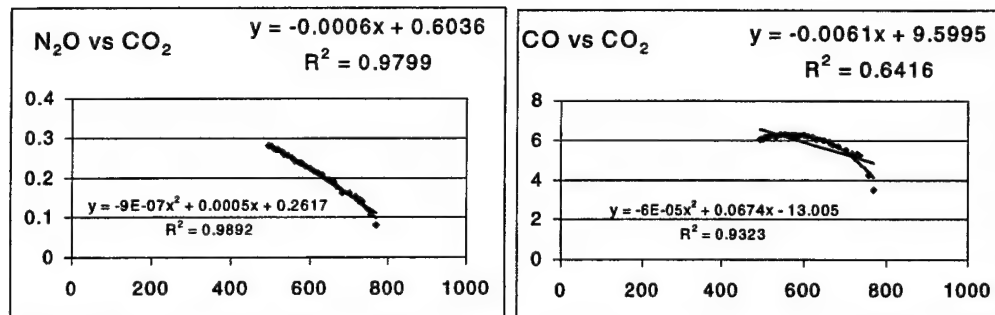
Figure 38 - Results of CO$_2$ Injection Experiment, 20 April 01

It seems unlikely that the observed relationships between N$_2$O, CO and CO$_2$ from these experiments are correct. The leaky chamber and potentially changing concentrations due to influences from ambient gases make these data suspect at best. Taken to their logical conclusion, they would imply that somewhere between 60 – 100% of the N$_2$O normally measured in roadside studies was due only to the influence of CO$_2$. These effects were studied further in the following experiment.

3.1.6 Further Investigation of CO$_2$/N$_2$O Cross-talk

In light of the fact that the concentrations of the various gases in the room air could have been changing during the course of the previous experiment, I decided to perform a new experiment using a well-sealed chamber to minimize any effect that the room air might have on the results. Also, since MALT calculates the concentration of CO$_2$ based on many absorption lines which lie far from the relatively

142

small peaks of N_2O and CO, it seems very unlikely to me that either of these gases influence the apparent concentration of CO_2. Therefore, CO_2 was the only gas injected for the new set of experiments. The bench-top enclosed chamber described earlier was sealed to the best of our ability and the open-path White cell was used along with a MIDAC FTIR. Aliquots of CO_2 (General Air Service and Supply, Denver, CO) were delivered using a 1 Liter syringe. After each injection, the chamber was allowed to equilibrate without additional mixing for about 5 minutes. After this step, some number of IR spectra were collected and analyzed at a later date. For the August experiment, 6 aliquots of 500 mL each were added to the chamber, and ten 10-scan spectra were taken after each injection. In the September experiment, 10 aliquots of 250 mL each were injected, and five 40-scan spectra were collected after each injection. The other difference between the two experiments is that the first one was performed using a total folded path of 462 meters, and the second with a path of 231 meters. However, all mixing ratios are given as absolute, path-independent figures.

The results of these two experiments (in August and September) were quite similar. Essentially, no relationship to CO_2 was detected for either ammonia or methane. This was not surprising, since the spectral regions for these gases are well separated from that of CO_2. However, CO_2 did seem to influence the apparent concentrations of both CO and N_2O. These results are summarized graphically in Figure 39 and Figure 40. For both methane and ammonia, the correlation coefficient of the relationship between these
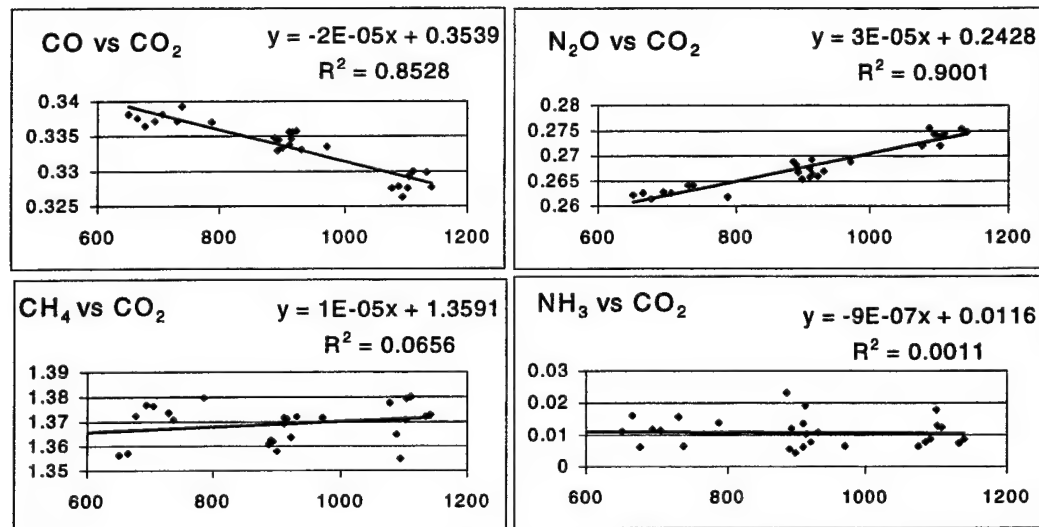
Figure 39 - Results from CO_2 Cross-talk Experiment, 31 August 01

gases and CO_2 are less than 0.1. In both experiments, a slight negative relationship was seen for CO, and a slightly positive one for N_2O. The slopes of these relationships are summarized in Table 9.

144

Date	CO vs CO_2	N_2O vs CO_2
31 August 01	$(-2 \pm 0.16) \times 10^{-5}$	$(3 \pm 0.21) \times 10^{-5}$
05 Sept. 01	$(-4 \pm 0.20) \times 10^{-5}$	$(2 \pm 0.22) \times 10^{-5}$

Table 9 - Linear Regression Slopes from Cross-talk
Experiments

In these experiments, the stepped-nature of the injections and the
more tightly sealed chamber improves the data, since each step can be
viewed as a separate quantity. The linear regression tends to fit the
line through the group of points located at each step, and there is a
reasonably good linear regression fit in each case. This process also
decreases any non-linearity due to leaks and reduces potential
contamination from changing concentrations in the room air. Since the
concentration is being successively increased, any influence from
changing ambient concentrations outside the chamber is
proportionately smaller as the experiment proceeds. Thus, I may be
able to use the linear slopes to estimate the amount of apparent
change in CO or N_2O due to the presence of CO_2. However, the fact
that the April experiment resulted in negative slopes for both gases,
while the August and September experiments gave a positive slope for
N_2O, is concerning.

Dr. D. W. T. Griffith's Group has reported a discrepancy

between modeled and experimental precision of N_2O measurements,

but has attributed it to the fact that the N_2O region is broad and

relatively featureless at the 1 cm^{-1} resolution they were using.[130] It may

be that they are seeing some effect of CO_2 on this region as well.

However, no problems with CO were reported.
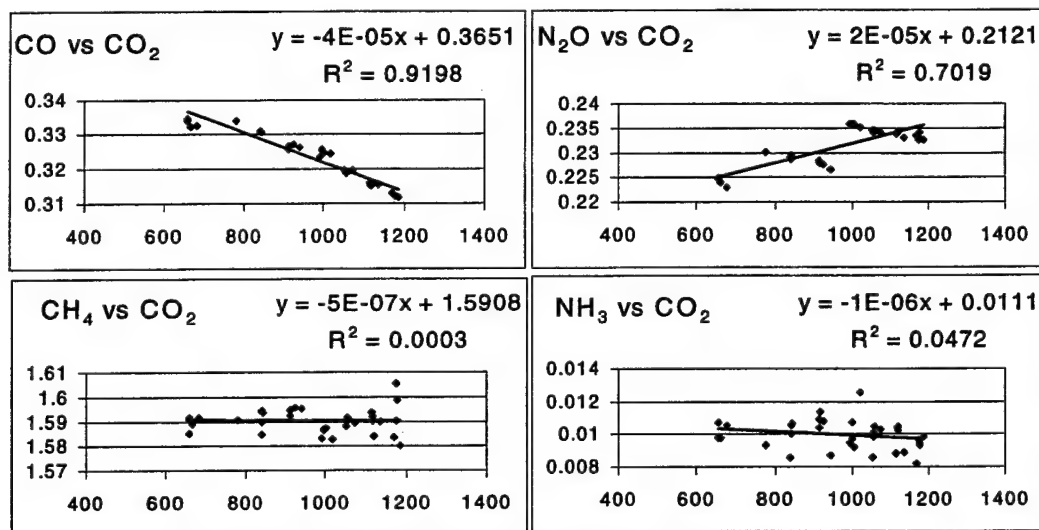
Figure 40 - Results for CO_2 Cross-talk Experiment, 5 Sept. 01

In conclusion, I believe this bears further investigation, but it

appears that I should correct any field measurements of N_2O and CO

based on the above relationships. Based upon the amounts of N_2O,

CO and CO_2 I normally measure in field studies, there could be a

possible influence of 3% to 5% of the N_2O concentration and 0.5% to

1.5% of the CO concentration.

3.1.7 Temperature/Pressure Calibration Sensitivity

Initially, I was under the impression that I could create calibration sets with MALT at any temperature and pressure and merely correct the results using the ideal gas law. This turned out to be a gross oversimplification and this experiment had the purpose of determining the boundaries within which calibration files could be created, and still obtain reasonably good results. The findings here dictated part of my eventual spectral analysis protocol.

I began by selecting a single spectrum to work with, and creating a calibration file set to match the exact temperature and pressure under which the spectrum was collected. I then used the calibration files to calculate the CO_2, N_2O and CO concentrations for this spectrum. These were taken to be the true values and all other concentrations in this experiment are referenced to them. The concentrations are representative of the values normally measured in our field studies, and the spectrum was collected under our standard operating conditions of 100-scans/spectrum taken over a 200 meter folded path. This particular spectrum was collected at our North I-25 site in Colorado Springs on 09 July 2001. The actual temperature and pressure for this spectrum was 292 K and 580 T, which are fairly

147

common conditions for the Colorado Springs area. For comparison,

calibration files were also created with a temperature of 298 K and a

pressure common to the Denver area of 630 T. Finally, calibration

files were created with standard temperature and pressure of 273 K

and 760 T. The RMS error in each fit ranged from 0.007 to 0.009

absorbance units. This indicates that any error in the calculated

concentration is due to improper calibration conditions and not due to a

poor fit. The results of this portion of the experiment are listed in Table

10.

	Calculated Concentrations at Indicated T/P				
	292/580	298/580	292/630	298/630	273/760
CO_2 (ppm)	459.41	455.79	397.83	394.64	284.62
N_2O (ppm)	0.36383	0.36359	0.34060	0.34078	0.28218
CO (ppm)	0.41305	0.41976	0.37869	0.38417	0.30022
	"Corrected" with Ideal Gas Law				
	292/580	298/580	292/630	298/630	273/760
CO_2 (ppm)	459.41	446.61	432.13	420.03	398.91
N_2O (ppm)	0.36383	0.35626	0.36996	0.36271	0.39549
CO (ppm)	0.41305	0.41131	0.41133	0.40889	0.42077
	Relative Error from Actual Concentrations				
	292/580	298/580	292/630	298/630	273/760
CO_2 (ppm)	0.0%	2.8%	5.9%	8.6%	13.2%
N_2O (ppm)	0.0%	2.1%	1.7%	0.3%	8.7%
CO (ppm)	0.0%	0.4%	0.4%	1.0%	1.9%

Table 10 - Ideal Gas Law Correction Results

For the next part of the experiment, I wanted to determine the maximum deviation from the actual pressure that was possible, while still maintaining at least 99% of the actual value of the concentration. In order to determine this, I created successive calibration file sets with gradually increasing pressures. After the pressure had been deviated 4 Torr from the original pressure of 580 T, the error in the calculated concentration of CO_2 was a little more than 1%, although for N_2O and CO, the error was still less than 1%. I then created a calibration file 4

Torr below the original pressure, just to make sure the trend held in that direction. These results are presented in Table 11.

	Calculated Concentrations at Indicated T/P				
	292/576	292/581	292/582	282/583	282/584
CO_2 (ppm)	464.83	458.07	456.73	455.40	454.07
N_2O (ppm)	0.36584	0.36343	0.36285	0.36236	0.36183
CO (ppm)	0.41607	0.41231	0.41157	0.41083	0.41009
	Relative Error from Actual Concentrations				
	292/576	292/581	292/582	282/583	282/584
CO_2 (ppm)	1.2%	0.3%	0.6%	0.9%	1.2%
N_2O (ppm)	0.6%	0.1%	0.3%	0.4%	0.5%
CO (ppm)	0.7%	0.2%	0.4%	0.5%	0.7%

Table 11 - Effect of Changing Calibration Pressure

Next, I wished to determine what the maximum variation in temperature could be, while maintaining at least 99% of the actual values. Holding the calibration file pressure at the actual value of 580 T, I varied the temperature from two degrees below to 2 degrees above the actual value. The results were still within the range of less than 1% error at this point. It was apparent, then, that the calibration file temperature could be varied by as much as two degrees from actual while still maintaining better than 99.5% accuracy. The temperature was clearly not as large an influence on calculated concentrations as pressure was, but pressure routinely varies by only a

small amount during normal sampling in the field. These data are

listed in Table 12.

	Calculated Concentrations at Indicated T/P				
	290/580	291/580	293/580	294/580	295/580
CO_2 (ppm)	457.595	460.023	458.78	458.19	457.60
N_2O (ppm)	0.363815	0.363811	0.36386	0.36385	0.36382
CO (ppm)	0.416335	0.411961	0.41416	0.41522	0.41634
	Relative Error from Actual Concentrations				
	290/580	291/580	293/580	294/580	295/580
CO_2 (ppm)	0.4%	0.1%	0.1%	0.3%	0.4%
N_2O (ppm)	0.004%	0.005%	0.008%	0.004%	0.004%
CO (ppm)	0.8%	0.3%	0.3%	0.5%	0.8%

Table 12 - Effect of Changing Calibration Temperature

Finally, I wished to see what the combined effect of temperature

and pressure differences would be. I created a series of calibration

files with combinations of high and low temperatures and pressures.

Except for the first set, the temperature was only varied by 2 K and the

pressure by 1 T. Both these restrictions are easy to adhere to in my

fieldwork, since I monitor both parameters at a frequency of 1 Hz. As

shown in Table 13, this restriction assures that there will be an error

induced by temperature and pressure differences of no more than

0.7%, which is a small portion of the 10 – 30% uncertainties in our final

results.

In conclusion, I have determined that ideal gas law corrections to the calculated concentrations produced by the MALT/CLS method are not accurate for our purposes. Errors induced by this technique can be in excess of 10%. By monitoring temperature and pressure while collecting real-world data, calibration sets can be built that have temperatures within 2 K of actual and pressures within 1 T of actual, ensuring that the error induced by this process should be no more than 1% of the actual values.

	Calculated Concentrations at Indicated T/P				
	296/584	294/581	294/579	290/581	290/579
CO_2 (ppm)	451.691	456.848	459.531	459.276	461.971
N_2O (ppm)	0.361085	0.363352	0.36434	0.363232	0.364232
CO (ppm)	0.41443	0.414462	0.415972	0.410138	0.411615
	Relative Error from Actual Concentrations				
	296/584	294/581	294/579	290/581	290/579
CO_2 (ppm)	1.7%	0.6%	0.03%	0.03%	0.6%
N_2O (ppm)	0.8%	0.1%	0.1%	0.2%	0.1%
CO (ppm)	0.3%	0.3%	0.7%	0.7%	0.3%

Table 13 -Effect of Combined Temperature/Pressure Changes

3.1.8 *Effect of Autocorrelation on Data Analysis*

As noted above in section 2.4.4.1, autocorrelation is of some concern in the analysis of field data. I wanted to quantify the effect of autocorrelation on the final results in order to determine if the effort expended to remove it was worthwhile, and also to see if there was some consistent effect due to autocorrelation of the data. The slope of linear regression was calculated for the various relationships between pollutants and CO_2, as described above. The values of these slopes, before and after removal of autocorrelation, were compared to one another. The results from a representative sample of experiments are listed in Table 14. The actual amount of increase (or decrease) in the

Date	15-Dec-99			16-Dec-99			25-Jul-01		
Autocorrelation	with	without	% change	with	without	% change	with	without	% change
CO	0.0250	0.0268	-7%	0.0280	0.0166	41%	0.0232	0.0228	2%
N_2O	0.00009	0.00009	-5%	0.00018	0.00018	-3%	0.00025	0.00024	3%
CH_4	0.0111	0.0060	46%				0.0056	-0.0002	104%
NH_3	0.0002	0.0001	56%				0.00006	0.00011	-100%
NO							0.0057	0.0048	16%
Date	1-Aug-01			28-Aug-01			9-Oct-01		
Autocorrelation	with	without	% change	with	without	% change	with	without	% change
CO	0.0152	0.0163	-7%	0.0069	0.0166	-141%	0.0200	0.0200	0%
N_2O	0.0003	0.0003	-4%	0.0003	0.0003	0%	0.0003	0.0002	28%
CH_4	0.0044	0.0033	26%	0.0010	-0.0066	780%	0.0011	0.0004	63%
NH_3	0.0004	0.0003	30%	0.0002	0.0002	0%	0.00020	0.00018	11%
NO	0.0022	-0.0005	124%	0.0027	0.0036	-34%			

Table 14 - Effect of Autocorrelation

slope of the line due to autocorrelation was highly variable. I deduced

from these results that it was absolutely necessary to remove

autocorrelation from our data, and that neither the direction nor amount

of change induced by this process could be predicted.

3.1.9 Pathlength vs. Spectral Noise Study – 14 June 2002

This study was undertaken to determine the relationship

between pathlength and increased spectral noise for the FTIR

spectrometer. As the pathlength is increased, less light is collected

due to divergence of the beam. As less light illuminates the detector, it

is expected that its contribution to the spectral noise will increase.

Also, if everything else remains constant, as the pathlength increases,

the absorption of individual chemical species will increase due to

increased optical density. The real question is whether the signal to

noise ratio increases or decreases due to the increase in pathlength.

Since absorbance increases linearly with pathlength, according to

Beer's law, it must only be shown that the increase in noise is at a

lower multiple than the increase in pathlength.

To accomplish this, three spectra were collected at each of the

following pathlengths (meters): 30, 61, 91, 122, 152, 200. The three

spectra were: two single-scan spectra collected as quickly as possible

(generally within 10 seconds of each other) and a 100-scan spectrum. The noise in each spectrum was measured in two wavenumber regions that are expected to show no absorbance features: 979 – 991 cm^{-1} and 2494 – 2506 cm^{-1}.[143] At each pathlength, the noise in each location was computed for the single-beam pseudo-absorbance (-log[T]) spectrum, the hundred-scan pseudo-absorbance spectrum, and the actual absorbance spectrum (-log[T_0/T]) for the single-scan spectrum.

The noise was approximated by calculating the root-mean squared (RMS) deviation over the ranges indicated above. However, it was apparent that the differences in baseline height had some influence on the calculated value of the RMS noise, so I applied a standard baseline routine in order to be as consistent as possible. Essentially, each region of the spectrum was excised, using GRAMS/32's "zap" function, and the spectrum was leveled and baselined to zero using each end of the range as a zeroing point. The portion of the spectrum was then exported in ASCII format to a spreadsheet and the RMS noise was calculated. This process is illustrated in Figure 41 through Figure 43.
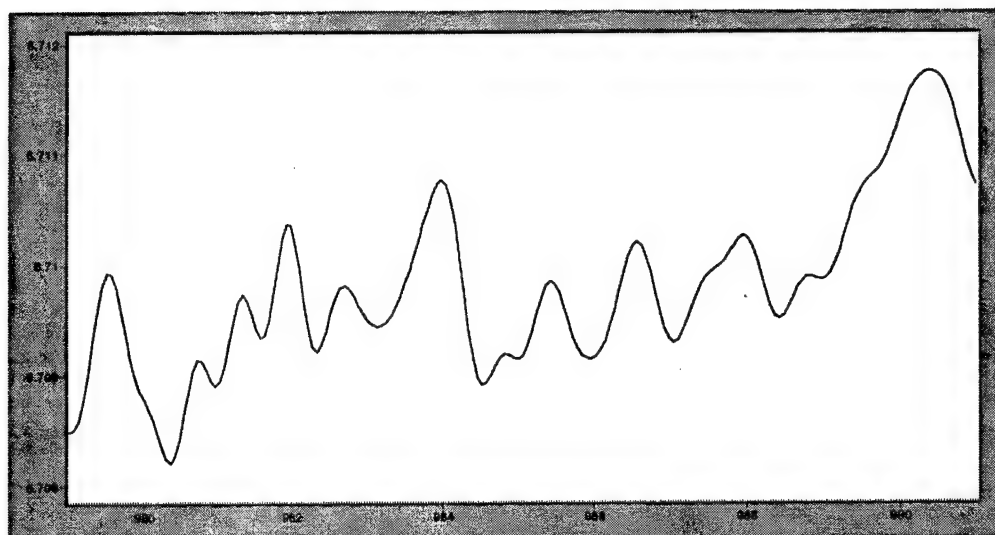
Figure 41 - Excised Portion of Spectrum, 979 - 991 cm^{-1}
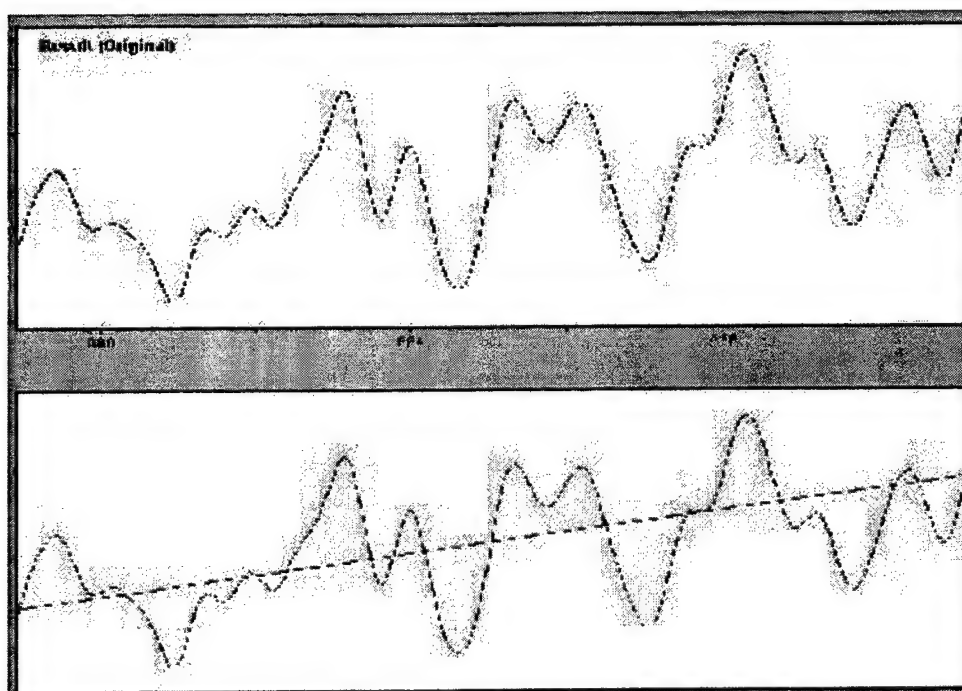
Figure 42 - Selecting Baseline Points for Spectrum
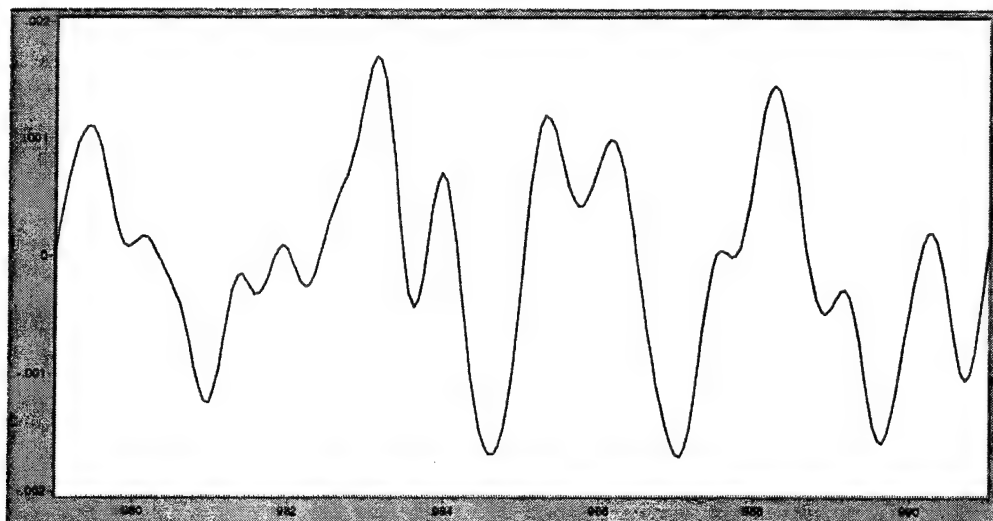
Figure 43 - Baselined Portion of Spectrum, ready for export

The results for both regions of the spectrum and for all pathlengths are shown in Table 15. In this table, "ss" indicates single-scan spectra, "Abs." Indicates actual absorbance spectra, and "100 scan" is self-explanatory. The results in the "Average" column are just the arithmetic averages of the previous two columns. These data are represented graphically in Figure 44.

While the single-scan spectral noise wanders around a bit, the noise in the 100-scan spectra falls on a line with a slope of 3×10^{-5}, and an intercept very close to zero. So, for every 100 meters increase in pathlength, the 100-scan spectral noise only increases about 0.003 absorbance units. From my experience, 200 meters works very well with the space constraints normally encountered in fieldwork. It would

157

be interesting, however, to continue extending the path and find out

where the noise becomes a mitigating factor.

	979 - 991 cm^{-1}			2494 - 2506 cm^{-1}			Average		
Pathlength (meters)	ss noise	Abs. noise	100 scan noise	ss noise	Abs. noise	100 scan noise	ss noise	ratioed noise	100 scan noise
30	0.0079	0.0082	0.0015	0.0117	0.0168	0.0035	0.0098	0.0125	0.0025
61	0.0086	0.0111	0.0019	0.0162	0.0278	0.0057	0.0124	0.0195	0.0038
91	0.0080	0.0120	0.0018	0.0186	0.0227	0.0058	0.0133	0.0174	0.0038
122	0.0114	0.0149	0.0021	0.0260	0.0333	0.0092	0.0187	0.0241	0.0056
152	0.0095	0.0136	0.0020	0.0208	0.0234	0.0093	0.0151	0.0185	0.0056
200	0.0114	0.0158	0.0024	0.0229	0.0252	0.0118	0.0172	0.0205	0.0071

Table 15 - Results of Pathlength vs. Spectral Noise Study
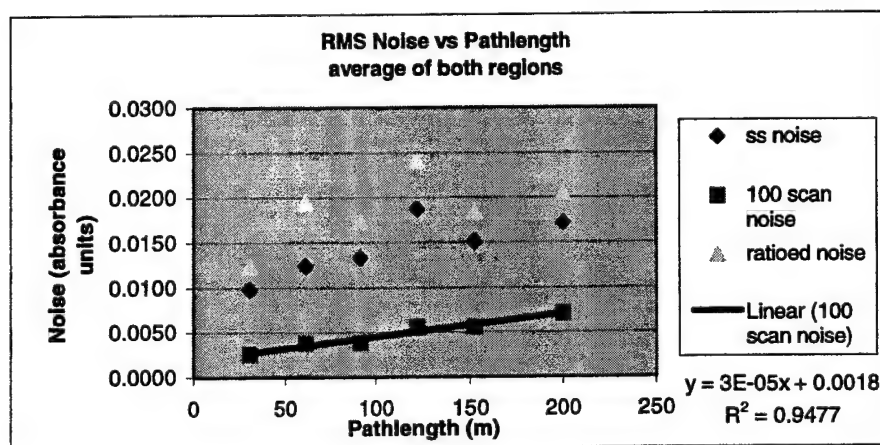
Figure 44 - Average Noise vs. Pathlength data

3.2 UV-Vis Laboratory and Preliminary Experiments

3.2.1 NH₃ Detection limit

In light of the poor detection limit of ammonia with the FTIR, I altered the UV-Vis system to make it useful for this purpose (see section 2.2.2.1). The initial tests with the modified unit were very promising. The bench-top chamber formerly used with the open-path White cell was set up and the UV system placed inside. The chamber was measured to have an approximate volume of 1724 L, and the effective light path was 5.5 meters. Initially, the calibration software was set to read 1000 arbitrary units when measuring the calibration cell of ammonia. However, the light intensity is dependent on the path length, and the path-independent concentration of the cell is 10 ppm-m. Therefore, the apparent concentration over the pathlength in this study would be:

$$\frac{10\,ppm \cdot m}{5.5m} = 1.8\,ppm \tag{39}$$

This, in turn, gives an equivalence of 1.8 ppb per arbitrary unit. After calibration, a 20 mL aliquot of anhydrous ammonia (11.6 ppm) was injected into the center of the chamber and allowed to mix and dissipate. No great care was taken to seal the chamber tightly. The

159

data fell on an apparently exponential curve, and the initial decay fit

nicely to this exponential function with an R^2 value of 0.9885:

$$y = 6434.6e^{-0.0413x} \qquad (40)$$

The y-intercept (in arbitrary units) is equivalent to 11.6 ppm, which is

exactly what was predicted.

As the concentration of the ammonia dwindled, the relative error

in the measurements became larger and larger. The point at which the

absolute value of the error began to exceed the measurement was at

about 18 arbitrary units. At this point, the apparent concentration was

32.4 ppb (18 units * 1.8 ppb/unit). The path independent concentration

over the 5.5-meter path was then 178.2 ppb-m, which is a bias that is

about 13 times lower than the bias in the FTIR system. Analysis of a

flat portion of the data (331 points) near the end of the experiment gave

a 3-sigma value of 0.91 units, which equates to a concentration of 1.6

ppb of ammonia. However, this was only over a pathlength of 5.5

meters, so the path-independent concentration would be 8.8 ppb-m.

Over the 100 meter path I normally use for the UV system in field

studies, this is equates to an absolute concentration of only 0.088 ppb

of ammonia. This detection limit is approximately 36 times more sensitive than the FTIR system.

3.2.2 NO Detection Limit, and NO/NH3 Cross-talk

This began as an attempt to determine the detection limit of NO with the modified UV-Vis system. In the process, it became obvious that the presence of NO produces an apparent concentration of NH_3. Initially, the bench-top chamber was set up as in previous experiments, and a 1 L syringe of 1270 ppm NO (Scott Specialty Gases, cyl. #ALM018141) was injected. The NO data were seen to exhibit an apparently exponential decay, as expected. Then, a mixture of gases containing 5.98% CO2, 6.09% CO, 6173 ppm propane and 2910 ppm NO (Praxair certification, serial #CC27982) was delivered with the same 1 L syringe used previously. This time, the ammonia data were examined as well and a peak was discovered that corresponded precisely with the NO peak. Suspecting contamination of the syringe, which had been used a few days earlier for an ammonia experiment, the device was flushed well with nitrogen and the experiment was attempted again, with the same result. Consulting Okabe's text on photochemistry,[144] I determined that a possible culprit was CO_2, although it is only very weakly absorbing in the region near the

161

ammonia peaks. To test this theory, a total of 20 liters of CO_2 (~1.2% by volume) was syringed into the chamber, with no discernible disturbance of the system. Next, I suspected that the ozone produced by the UV light source was perhaps converting a significant amount of NO to NO_2, which is known to have peaks very close to those of ammonia. The chamber was modified to include two cardboard baffles in one end, and the light source was positioned to shine through the holes in these baffles. Furthermore, a fan was positioned to blow perpendicularly to the opening of the outermost baffle, and thus keep any ozone emanating from the light source from entering the chamber. Data collected with this configuration showed the same phenomenon as the others, with a slight difference, which will be elucidated later. This told us that ozone could not be the cause of the problem, and the conclusion was made that the NO itself was somehow distorting the baseline of the ammonia region of the spectrum or otherwise interfering with the ability of the software to properly calculate the ammonia concentration.

In order to quantify this effect, the NH_3 data were plotted against the NO data and a regression line was plotted through the points. The result was that all of the experiments resulted in a very similar slope,

with the exception that the experiment with the light source outside the

chamber had a slope that was 13% smaller than the other experiments.

The other three slopes all agreed to within 4% of each other. This may

indicate the magnitude of the effect of having ozone produced inside

the chamber. The experiments with ozone present would be expected

to have a larger $[NH_3]/[NO]$ slope, which they actually do, if the NO_2

that is formed increases the apparent ammonia concentration without

altering the apparent NO concentration.

In conclusion, taking the last experiment as the most indicative

of real-world conditions, since there is usually relatively little ozone

beside roadways, measurements of ammonia with this system should

be modified by this formula:

$$[NH_3]_{actual} = [NH_3]_{apparent} - 0.23[NO] \tag{41}$$

3.3 Field Studies

3.3.1 Small Engines (2 and 4 stroke)

In the interest of determining whether this technique might be

useful in off-road applications, I undertook a study of two small gasoline

powered engines. One of these was a 4-stroke, 6.5 horsepower Briggs

and Stratton lawn-mower engine, which burned unleaded gasoline.

The other was a 2-stroke Weedeater® (model XT-40T) engine, which

burned a mixture of oil and unleaded gasoline. Neither of these engines had any post-combustion treatment of the exhaust other than a muffler to reduce noise. The study took place at my house, located on the United States Air Force Academy grounds in Colorado Springs. At the time of the study, the weather was clear and sunny, with a temperature of about 25 °C, and an atmospheric pressure of 595 T. I took advantage of the high deck and sloping side yard to position the Midac spectrometer to sample the air above the yard. The folded light path was 60 meters long, as measured with a 30.5-meter tape. This is illustrated in the cartoon in Figure 45.

This location is many miles from any major roadway, and there was no traffic within sight during the entire study. Also, there were no other small engines running within earshot. Before the engines were started, ten 25-scan background spectra were collected in order to ascertain whether there were any measurable sources of emissions present. The wind was very light, and background conditions were presumed to be stable and constant during the course of the study.

3.3.1.1 Lawn Mower

The lawn mower exhaust was measured in two modes: cold-start and stabilized. The cold-start emissions were measured by placing the mower under the beam from the spectrometer, starting it, and allowing it to warm-up for about 5 minutes. During this period, 25-
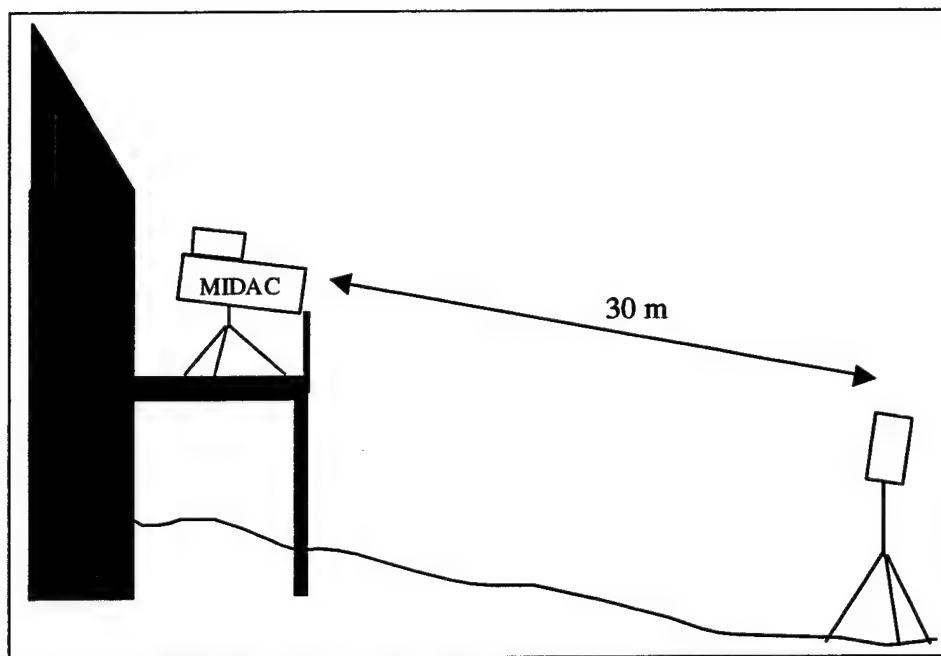
Figure 45 - Cartoon of Equipment set-up for Small Engine Study

scan spectra were collected continuously. After the mower had reached operating temperature, it was pushed back and forth parallel to the beam, with care taken not to block the light. The mower was stopped and restarted 3 times during this time. During this period, 100-scan spectra were collected for approximately an hour.

3.3.1.2 Weedeater®

The 2-stroke engine was measured in the same two operating modes as the 4-stroke engine. The cold-start emissions were measured in the same way, but the stabilized emissions were measured under two different conditions. The first set of spectra was collected while the unit was actually being used to cut grass under the light beam. The second set was collected while the unit was run, but without any grass being cut. The engine was at full throttle in both circumstances. There are some differences between these two sets of data, as will be seen below. The total running time for this phase of the study was only about 10 minutes.

3.3.1.3 Results and Discussion

The results of this study are summarized in Table 16. The

	slope vs CO_2	error	emission factor (g/gal)	+/-
Background				
CO	-0.0059	-169%	-33.00	55.86
N_2O	0.0024	74%	21.28	15.66
CH_4	0.0030	113%	26.03	29.44
NH_3	-0.0017	-167%	-14.56	24.37
Lawn Mower				
Cold-Start CO	0.0458	32%	241.33	76.48
Cold-Start N_2O	0.0017	7%	13.84	0.94
Cold-Start CH_4	0.0006	97%	1.82	1.76
Cold-Start NH_3	0.0001	36%	0.47	0.17
Running CO	0.0072	32%	39.54	12.73
Running N_2O	0.0017	4%	14.57	0.60
Running CH_4	0.0024	8%	20.80	1.66
Running NH_3	0.0010	23%	8.86	2.04
Weedeater				
Cold-Start CO	-0.0071	-75%	-39.76	29.88
Cold-Start N_2O	0.0006	161%	5.39	8.67
Cold-Start CH_4	0.0002	2552%	0.59	15.06
Cold-Start NH_3	0.0002	440%	0.72	3.15
Running CO	0.0225	48%	121.38	58.64
Running N_2O	0.0028	14%	23.64	3.25
Running CH_4	-0.0079	-26%	-66.60	17.45
Running NH_3	0.0035	26%	11.36	2.98

Table 16 - Results of Small-engine Study

167

background spectra showed essentially no relationship between CO_2 and anything else I measured. The regression lines between the different species and CO_2 all have very low correlation coefficients, as evidenced by the high error in each slope.

3.3.1.3.1 Four-stroke Engine Results

For the 4-stroke engine, there are definite relationships between CO_2 and both CO and N_2O. The results for CO show that the cold start emissions are roughly 6 times those for the stabilized mode, whereas N_2O has the same slope versus CO_2 for both modes. It is surprising that there is any correlation of N_2O to CO_2, since it is generally assumed that nitrous oxide is produced by conversion of NOx on a catalyst.

Methane shows no correlation to CO_2 during the cold-start phase, but there is a positive slope during the stabilized phase. Assuming that the mechanisms for producing unburned hydrocarbons are the same for this engine as for an automotive engine, this could be explained by the need for the engine to warm up sufficiently to begin producing hydrocarbons and perhaps in order for there to be enough energy to break down the larger hydrocarbons into smaller ones such as CH_4.

There is also a positive relationship between ammonia and CO_2 during the stabilized phase, which is 3 to 5 times that seen in my road-side automotive studies. It seems unlikely that the mower engine is actually a source of ammonia, since there is no catalyst on which ammonia might be formed. This may actually be due to the fact that the mower was actively cutting grass during this period, and the ammonia may be released from either the grass or the fertilizer, which was present. During the cold-start portion of the study, there were indeed high levels of ammonia (as much as 17 times the background levels), but it showed no correlation to CO_2. It could be that the apparent correlation during the running phase was due to spatial variations as the mower was moved closer to and farther away from the spectrometer.

3.3.1.3.2 Two-stroke Engine Results

The cold-start phase of operation for the 2-stroke engine shows no apparent correlation between any of the gases and CO_2. It could be that the relatively small engine plume did not actually cross the spectrometer's beam, but this seems unlikely, since I was standing directly underneath it, and CO_2 is elevated above ambient levels. It is more likely that the black smoke, which the engine emitted when it was first started, caused interference across the entire spectrum.

169

The stabilized phase shows three times the CO emissions and nearly twice the N_2O, as compared to the 4-stroke engine. This is unexpected, since two-stroke engines generally operate at lower internal temperatures, which does not favor NOx production, so the assumed source of N_2O should be present at much lower levels than in the 4-stroke exhaust.

There is apparently no correlation between CH_4 and CO_2, although there was a slightly higher mixing ratio of CH_4 during this phase. A two-stroke engine is normally a much higher producer of un-burned hydrocarbons than a four-stroke engine, due to the fact that oil is actually added to the fuel. It may be that the other hydrocarbons present in the 2-stroke exhaust interfere with our software's ability to analyze for methane appropriately. Possible evidence of this is found in Figure 46. Here, I have excised a region from each of three spectra, which corresponds to the region in which we analyze for methane. I have then subtracted from each region the corresponding region of a background spectrum. Each of these spectra has a calculated methane concentration (~1.61 ppm) that is comparable to the background spectrum subtracted from each one.
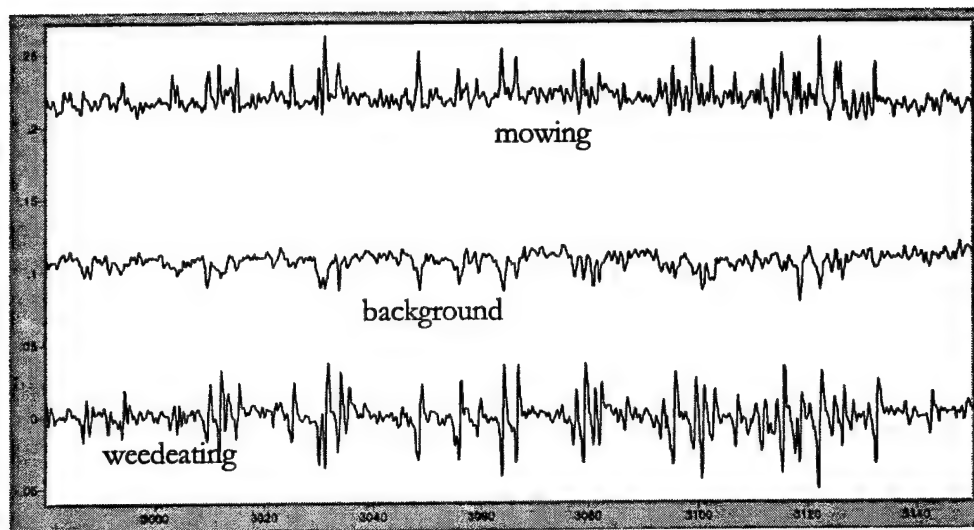
Figure 46 - Possible Hydrocarbon Interference in Methane Region

It is apparent that the "weedeating" spectrum contains possible

spectral features extending below the baseline, which are not present

in the other spectra. These may be due to spectral shifting, or possibly

to the presence of other hydrocarbons that may contribute to this

region of the spectrum. In the region from 2980 cm^{-1} to 3150 cm^{-1},

many longer-chain hydrocarbons have features due to C-H stretching.

It is also true that 2-stroke engines have been found to produce a lower

percentage of methane than 4-stroke engines, due to the fact that large

amounts of long-chain hydrocarbons tend to short-circuit through 2-

stroke engines[145]. The 2-stroke engine is also more prone to

incomplete combustion and mis-fires, which also contribute to a higher

percentage of longer chain hydrocarbons in the exhaust. This is also

171

consistent with the findings of Tsai, et al., in a study of in-use 2- and 4-stroke motorcycles. They report that the 2-stroke engines produced 5 to 7 times more total hydrocarbons, but only 2 to 3 times more volatile organics than 4-stroke engines.[146] However, this study did not report percentages of methane in the exhaust.

During the two parts of the stabilized phase, there is an obvious change in ammonia concentration. During the first collection period, when grass is actually being cut, there are elevated levels of ammonia, but no correlation to CO_2 ($R^2 = 0.0003$). During the second portion, when no grass is being cut, the levels of ammonia are actually negative. If taken as a single data set, there is an apparent correlation to CO_2, but only because these two groupings of data form two smeared "points" which the linear regression algorithm connects with a straight line.

3.3.2 *Parking Lot Study*

I made two attempts to measure the emissions from vehicles in
a small parking area near an Elementary school. I chose this particular
lot because it was fairly well separated from most other possible
sources of automotive emissions, being well off of a major roadway
and approximately one mile from the interstate. The location was also

Figure 47 - Map of Parking Lot Location (Mapquest.com)

relatively remote from densely populated areas so there should be very
little influence from any residential combustion such as lawn mowers or
furnaces. Figure 47 and Figure 48 show a map and a photograph,
respectively, of the Mountain View Elementary school parking lot and

173

the surrounding area. The spectrometers were set up approximately

40 meters south of the lot, on the south edge of a sandy playground.

For both studies, the FTIR was configured with a total folded

pathlength of 192 meters, while the UV-Vis spectrometer had a straight

pathlength of 60 meters. On the first day (February 13, 2002), the

temperature ranged from 270 to 281 K, and barometric pressure

ranged from 576 to 579 Torr. The second day (February 19, 2002),

was similar to the first, with the temperature ranging from 275 to 280 K,

and the pressure from 569 to 570 Torr.
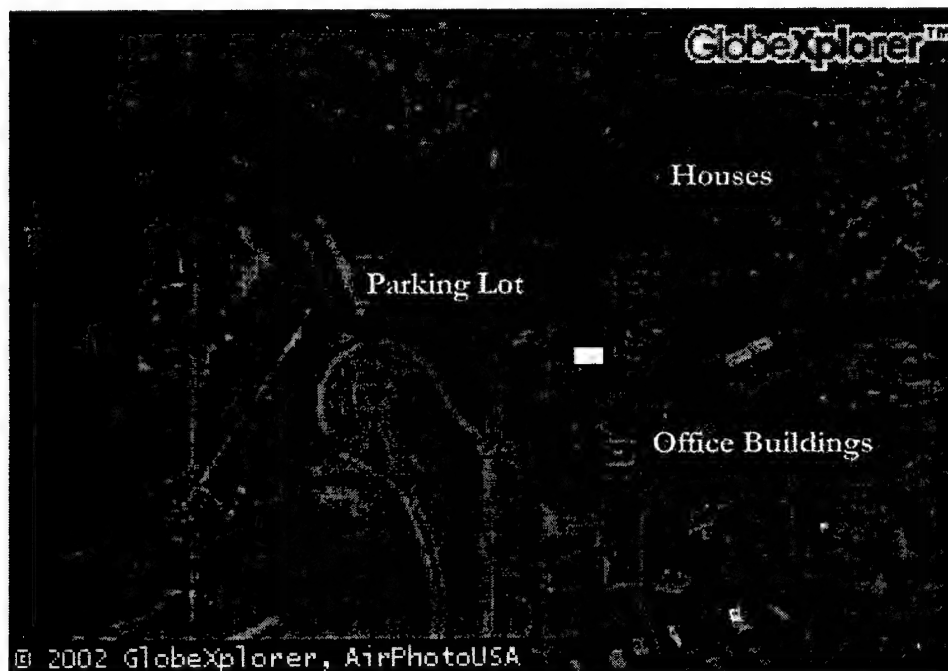
Figure 48 - Aerial Photograph of Parking Lot Location (Mapquest.com)

The traffic flow at this site is quite consistent, but very low-level. Between 7:00 and 9:00 AM, 8 diesel school buses and about 300 cars and light trucks arrive, drop off students, and then leave. Another 30 to 40 cars and light trucks park in the lot and most do not leave until after 3:30 PM. In the afternoon, the buses and cars arrive for student pick-up at approximately 2:30. Therefore, there is an opportunity to measure background conditions between 9:00 AM and 2:30 PM. Also, normal wind patterns make this location very good, because morning winds are usually from the north/northwest, which should bring the emissions from the parking lot directly to the paths of the spectrometers. Afternoon winds are usually light and variable, so are not as favorable as the morning conditions. However, on the second day of the study, the winds were out of the south/southwest most of the day, meaning that it was unlikely that my instruments would be able to measure the parking lot emissions. Over the course of the two days, 355 spectra (of 100 scans each) were collected and analyzed. The results are summarized in Table 17. The distinction between background and automobile-influenced data is made solely on the basis of wind direction. Data points collected when the wind from compass points between 300 degrees and 60 degrees (inclusive), with 0 degrees being north, are taken to be those that are influenced by the

vehicles, providing it is during a time when traffic is present. All other

data is designated as "background" although it was not clear whether

there would be any commonality between these data points. In fact, I

expected that there might be no correlation at all between the

pollutants and CO_2 in the background data.

	With cars		Background		Background	
Linear Regression vs. CO_2	13-Feb-02	+/-	13-Feb-02	+/-	19-Feb-02	+/-
CO	0.0155	27%	0.0028	27%	0.0043	15%
N_2O	0.0002	52%	0.0005	7%	0.0003	11%
CH_4	-0.0003	312%	0.0041	12%	0.0052	7%
NH_3	-0.00005	169%	-0.00008	39%	-0.00001	891%
NO	0.0027	11%	0.0004	82%	0.0015	5%
Emission Factors (g/gal)	13-Feb-02	+/-	13-Feb-02	+/-	19-Feb-02	+/-
CO	84.18	22.31	15.31	4.16	23.56	3.48
N_2O	1.56	0.81	4.68	0.35	2.96	0.34
CH_4	-1.06	3.31	13.04	1.51	16.41	1.09
NH_3	-0.15	0.26	-0.28	0.11	-0.02	0.21
NO	15.72	1.75	2.07	1.70	8.63	0.47

Table 17 - Results of Parking Lot Studies

What I noticed was that there were some strong correlations,

and they were distinctly different that those found when vehicles were

present. The emission factors calculated for CO, N_2O and NO for the

vehicle emissions are consistent with the results seen in my roadside

traffic studies for similar conditions of low acceleration and for an

essentially flat roadway. There was no correlation detected for CH_4 or NH_3 in this case. For the background conditions, there are also relationships between CO, N_2O and NO that are different from the vehicle-influenced relationships, and also a correlation between CH_4 and CO_2. I have calculated emission factors for the background data, but this may be invalid if the source of the measured gases is not a combustion process. For the two different days, the CO emission factors in the background data are statistically equivalent. However, all of the other emission factors are statistically different.

I suspect that the combustion product source for the background data may be natural gas heating systems in the houses and office buildings nearby. The CO emission factors are lower than for the automotive emissions, and the CH_4 emission factors are higher. From a qualitative assessment, this is what would be expected from a natural gas-fired boiler or heater. However, if it is indeed true that these emissions are from the combustion of methane, rather than from the combustion of gasoline, the emission factors must be calculated in a different manner. Here is the fairly simple equation, based on Equation (2) that I derived for this purpose:

$$emission\_factor_X = \frac{moles_X}{moles_C} * \left[\frac{g}{mole}\right]_X * \frac{0.04172\_moles\_C}{L\_fuel} \qquad (42)$$

177

The amount of carbon for each liter of fuel was calculated from the density of a standard liter of methane (0.7178 g/l).[147] Using this relationship, and assuming that the emissions in the background are due to methane combustion, the appropriate emission factors were calculated and are listed in Table 18. Compared to the USEPA emission factors for methane combustion, these numbers are generally quite high, although no uncertainty is reported in the EPA values, it seems unlikely that there is much agreement between their numbers and mine. The EPA distinguishes between residential heating

	Background		Background	
Linear Regression vs CO_2	13-Feb-02	+/-	19-Feb-02	+/-
CO	0.0028	27%	0.0043	15%
N_2O	0.0005	7%	0.0003	11%
CH_4	0.0041	12%	0.0052	7%
NH_3	-0.00008	39%	-0.00001	891%
NO	0.0004	82%	0.0015	5%
Emission Factors (g/m^3 of methane)	13-Feb-02	+/-	19-Feb-02	+/-
CO	3.53	0.96	5.44	0.80
N_2O	1.08	0.08	0.68	0.08
CH_4	3.01	0.35	3.79	0.25
NH_3	-0.06	0.02	-0.01	0.05
NO	0.48	0.32	1.99	0.11

Table 18 - Emission Factors for Methane Combustion

systems, small industrial boilers and large industrial boilers for both CO and NOx. No such distinction between classes of equipment is made for N_2O or CH_4, however. These values are listed in Table 19.[148] Since there are some arterial roads in the area from which the "background" emissions were measured, it is certain that there is some degree of automotive influence in these emission factors, which may account for the fact that, with the exception of the factor for NO, they are larger than the accepted values for pure methane combustion. However, since automobiles generally produce very little methane, it is very likely that this high emission factor (100 times the EPA value) is due to either a methane leak or an improperly operating system or group of systems. It is precisely this kind of disagreement, between accepted emission factors and real-world measurements, which makes a good case for periodic measurement campaigns to determine the reality of the situation. This also points out the dangers inherent in calculating an emissions inventory based on tabulated, averaged factors, since equipment in the real world is highly variable and unpredictable. Presumably, such an inventory is valid for the "average" location, but, as is so often the case, the "average" may not actually exist anywhere.

A very interesting feature of these data is that the automotive emissions overwhelm the background, even though there is a very low traffic flow. This seems to indicate that, under similar circumstances, automotive emissions from a heavily traveled roadway should dominate even if there is a measurable background component. I will address this idea further in the descriptions of my highway and arterial roadway studies.

	Residential Furnaces	Small Boilers	Large Boilers
CO	0.64	1.3	1.3
N_2O	.035	.035	.035
CH_4	.037	.037	.037
NO	0.98	1.0	2.0

Table 19 - USEPA Emission Factors for Methane Combustion, g/m^3. [148]

3.3.3 On-road Vehicle Emissions in and near Denver, CO

My first attempts to measure actual real-world automotive emissions on the highway were in Denver. This was principally because our research group had extensively studied and characterized emissions data in Denver over the years. This afforded me with the
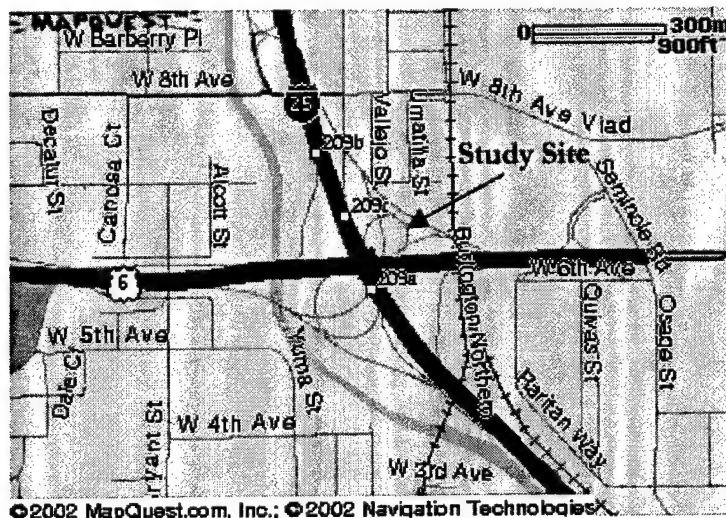
Figure 49 - Map of 6th Ave. and I-25 (Mapquest.com)
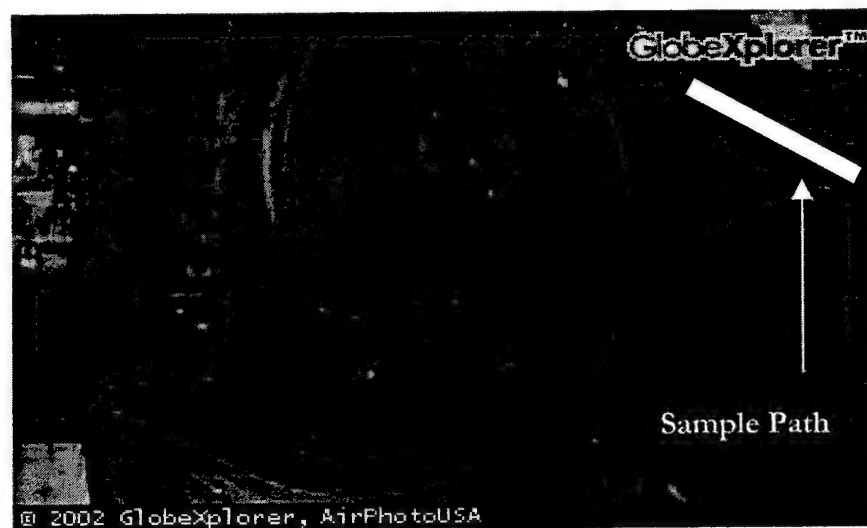
Figure 50 - Aerial Photograph of 6th Ave. and I-25 (Mapquest.com)

181

opportunity to compare my method with an established remote-sensing method. The location I chose was at 6th Avenue and Interstate 25. Figure 49 and Figure 50 show a map and photograph of the site. It is apparent that roadway emissions should dominate the air quality around our study site, since there is an abundance of heavily-traveled roadways next to and above the site. The location is also surrounded by businesses and manufacturing facilities, so there is undoubtedly a background contribution from these sources as well. However, since I am ultimately computing ratios, as long as the background is either very small or remains constant during the measurement period, it will not pose a source of interference. Evidence from my parking lot study in Colorado Springs seems to indicate that, even if a strong correlation to CO_2 exists in the background, the emissions from the automobiles should overwhelm it.

Traffic flow at and around this site is very heavy. Manual vehicle counts result in a flow of 500 to 1500 cars and trucks per hour on the 6th Avenue on-ramp, where my equipment was located. However, the total traffic flow past the site, counting all the other roadways in the vicinity is more like 4000 to 6000 vehicles per hour. Because my measurement method does not allow me to measure individual

182

vehicles, I cannot separate the contributions of vehicles on the ramp and those on the surrounding roadways. The majority of vehicles passing this site are traveling at a high rate of speed with very little load, since most of the surrounding roadways are relatively flat. The vehicles directly passing my equipment are accelerating up an 8% grade somewhere between 20 and 40 miles per hour. Data were collected on six days at this site, between December 1999 and November 2000. A total of 275 spectra were collected and analyzed.

The results of these studies are listed below in Table 20 and Table 21. Table 20 lists the values for the slopes of the linear regression against CO_2, after any autocorrelation has been removed.

Linear Regression vs CO_2	7-Dec-99	+/-	14-Jan-00	+/-	6-Sep-00	+/-
CO	0.02955	6%	0.02392	3%	0.01771	12%
N_2O	0.00019	19%	0.00013	27%	0.00045	19%
CH_4	0.00084	43%	0.00415	11%	0.00321	17%
NH_3	0.00031	10%	0.00024	10%	0.00031	41%
Linear Regression vs CO_2	8-Dec-00	+/-	10-Nov-00	+/-	17-Nov-00	+/-
CO	0.00802	30%	0.02258	7%	0.02146	16%
N_2O	0.00032	16%	0.00022	22%	0.00009	93%
CH_4	xxxx		xxxx		0.00241	25%
NH_3	0.00007	43%	0.00043	10%	0.00040	31%

Table 20 - Linear Regression results for On-road Data in Denver, Colorado

Table 21 lists the emission factors calculated from the line slopes. The
results of these studies, as well as those from other parts of the state,
will be discussed in more detail and compared with literature values in
the Chapter 4. Any results that were of particularly poor quality, as
indicated by the fact that the error in the slope of the regression line
was greater than 100%, were not reported as useful data and are
instead represented by "xxxx".

Emission Factors (g/gal)	7-Dec-99	+/-	14-Jan-00	+/-	6-Sep-00	+/-
CO	158.30	9.91	128.97	3.49	96.07	11.87
N_2O	1.62	0.30	1.15	0.31	3.83	0.71
CH_4	2.58	1.11	12.80	1.41	9.96	1.71
NH_3	1.02	0.10	0.80	0.08	1.04	0.42
Emission Factors (g/gal)	8-Dec-00	+/-	10-Nov-00	+/-	17-Nov-00	+/-
CO	43.95	13.04	121.86	8.60	115.97	18.74
N_2O	2.76	0.44	1.87	0.41	0.73	0.68
CH_4	xxxx		xxxx		7.44	1.89
NH_3	0.24	0.11	1.41	0.14	1.32	0.40

Table 21 - Emission Factors from On-road Data in Denver, CO

Another area of interest near the Denver area is located outside
the city limits in the foothills of the Rocky Mountains. Highway 70
passes into the mountains from Denver and is a heavily traveled road
with an extended length of highway at a grade of at least 8%. Vehicles

184

on this road are traveling at speeds between 50 and 70 miles per hour and could possibly be in commanded enrichment mode because of the high acceleration. To attempt to measure roadway emissions at this site, I set up my instruments in an area at Matthews/Winters Park, which is just down a slope to the south of the highway. A map and an aerial photograph of this site can be seen in Figure 51 and Figure 52.

My hope was to be able to sample air from the roadway when the cold air from the mountains was moving down slope in the late night or early morning. I camped out in this park for December 28th and 29th and collected and analyzed 272 FTIR spectra. During the afternoon and evening of December 28th, the winds were not from the
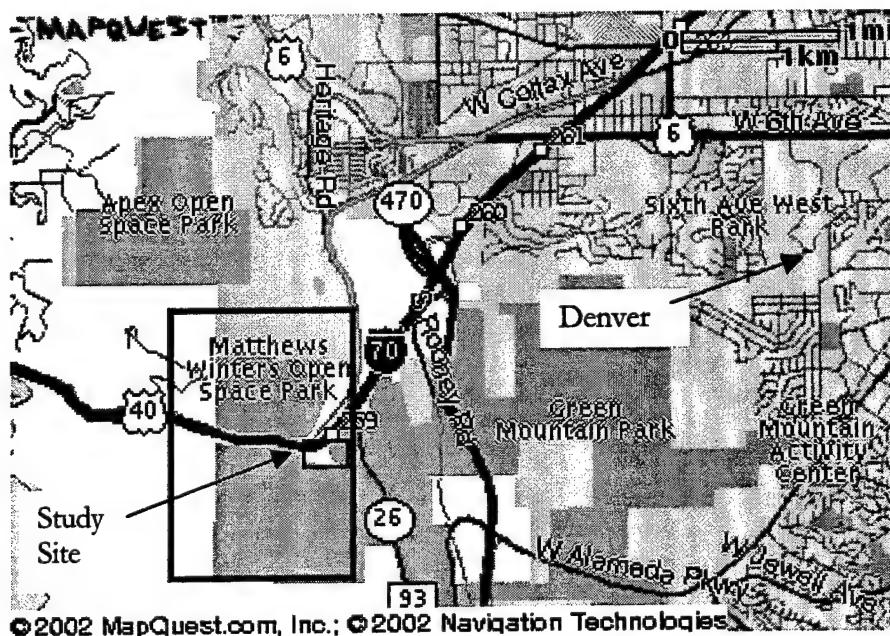
Figure 51 - Map of Matthews/Winters Park Area (Mapquest.com)

185

roadway, so I was essentially sampling the "background", even though it was not the background from the roadway, but from the surrounding areas. From midnight on the 28th to the evening of the 29th, the wind was either blowing from the roadway or was almost non-existent. However, I had some degree of trouble with the FTIR, and a large number of spectra were corrupted and were unusable. These were noticeable during data analysis because they have very high residual values and consequently high standard errors. The corrupted files were eliminated and the remainder plotted to determine the ratio of each pollutant versus CO_2.

The results of these two days are listed in Table 22. These results will be discussed in the next chapter, as mentioned above.
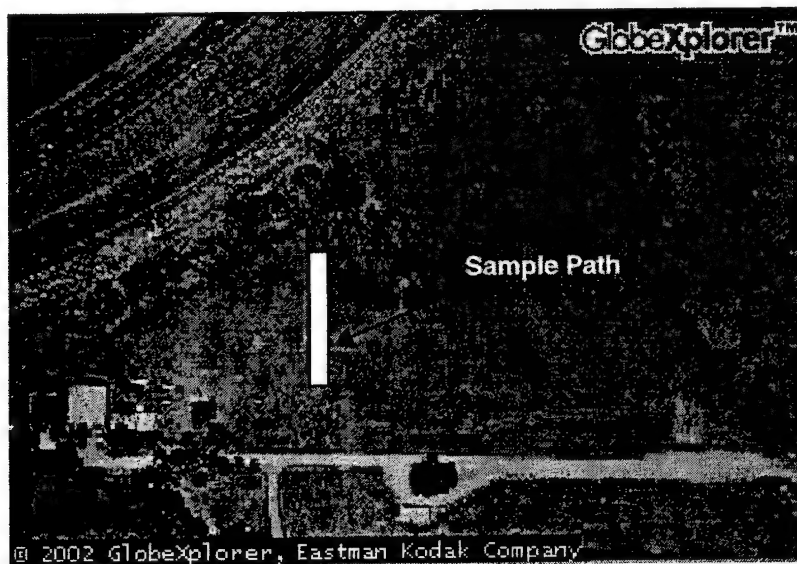
Figure 52 - Aerial Photograph of Matthews/Winters Park Sampling Site
(Mapquest.com)

186

Linear Regression vs CO_2	28-Dec-99 (background)	+/-	29-Dec-99 (vehicles)	+/-
CO	0.0112	49%	0.0439	12%
N_2O	0.0006	19%	0.00032	11%
CH_4	-0.0007	84%	0.00070	51%
NH_3	xxxx		0.00046	11%
Emission Factors (g/gal)	28-Dec-99	+/-	29-Dec-99	+/-
CO	61.06	29.86	232.08	27.57
N_2O	4.74	0.88	2.69	0.30
CH_4	-2.24	1.88	2.12	1.08
NH_3	xxxx		1.49	0.16

Table 22 - Results from Matthews/Winters Park Study

However, it is at least interesting to note that, in the case of CO, N_2O and NH_3, the emission factors for this site are higher than at 6th and I-25, as would be expected from a qualitative comparison of the two sites. Any results of particularly poor quality, as indicated by the fact that the error in the slope of the regression line was greater than 100%, were not reported as useful data and are instead represented by "xxxx".

3.3.4 On-road Vehicle Emissions in Colorado Springs, CO

My ultimate goal for the OPIEM system was to be able to

generate a mobile-source emissions inventory based on real-world

measurements in the Colorado Springs area. Therefore, I chose sites

that would give me the opportunity of measuring emission factors in a

variety of operational modes and traffic conditions. I have results from

four different study sites, two interstate sites and two arterial sites. The

approximate location of each site is indicated by an arrow on the map

of the Colorado Springs area in Figure 53.
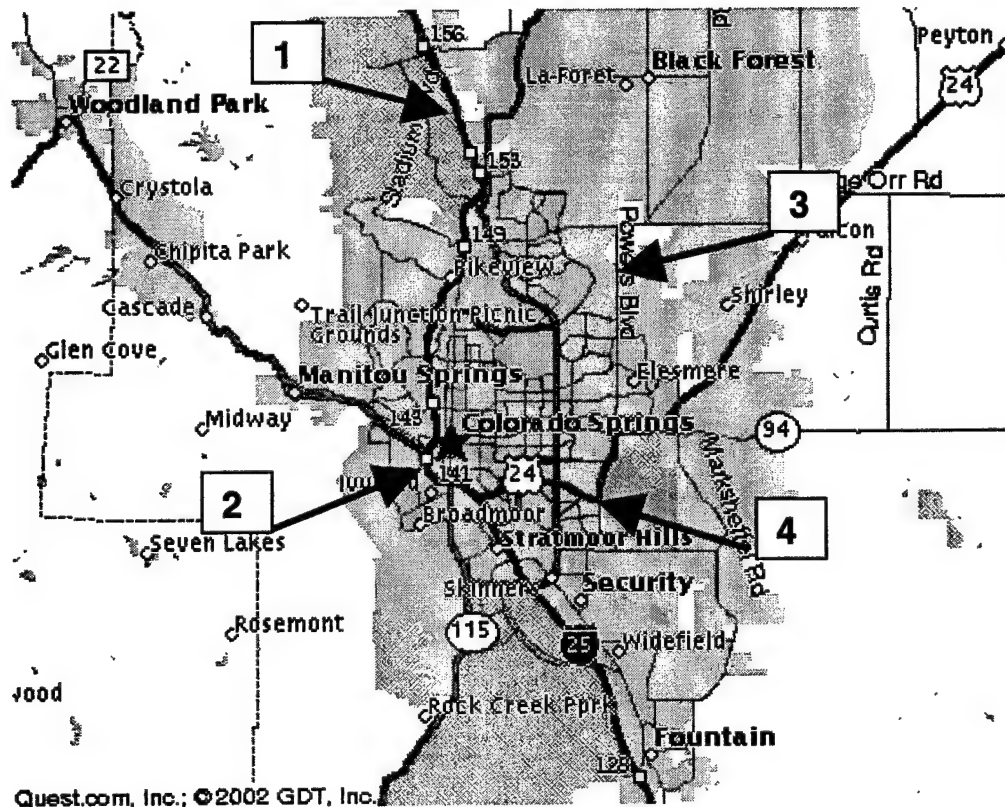
Figure 53 – Measurement Sites in Colorado Springs (Mapquest.com)

3.3.4.1 Site 1: North I-25

This site gave me the opportunity of measuring emissions in just about the worst-case scenario for making such measurements. During morning and evening rush hours, the traffic flow is normally between 4000 and 6000 cars per hour. Vehicle speeds are commonly in the 50 to 70 mile per hour range during these periods, and there is rarely a slowdown, except in the case of an accident. The grade is almost flat and there are two lanes each of north- and south-bound traffic. These conditions make for generally low emissions because the vehicles are under relatively low load and are operating very efficiently. Also, a general lack of containing geography, such as a depression or a valley,
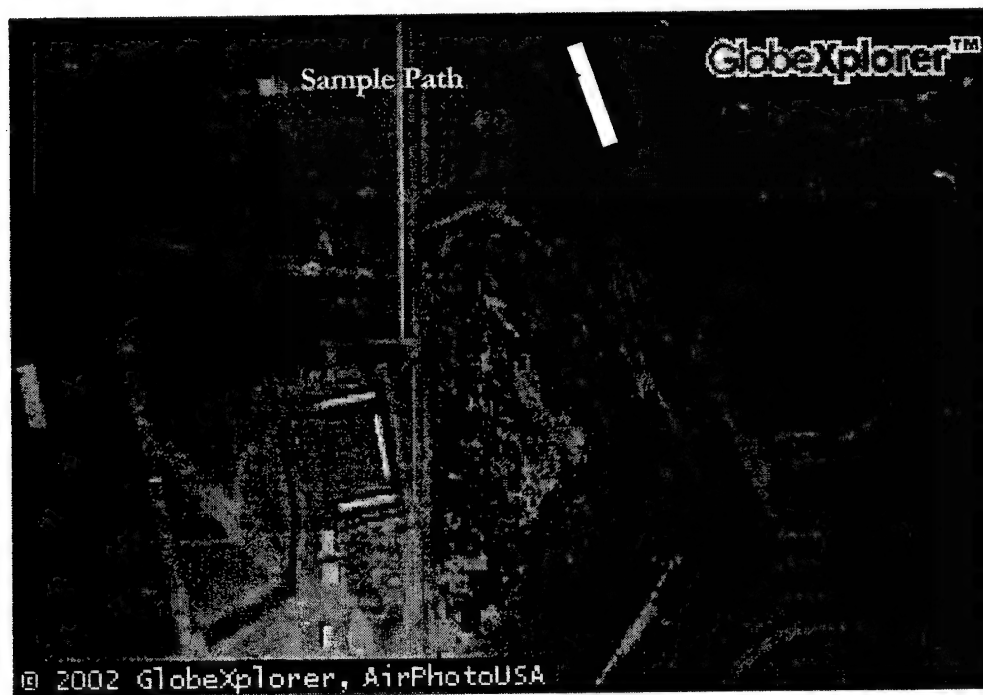
Figure 54 - Colorado Springs Site 1: North I-25 (Mapquest.com)

189

means that any change to the surrounding air composition due to vehicle emissions will be short-lived.

Figure 54 shows an aerial photograph of this site. The wind is usually from the north/northwest in the early morning, and gradually shifts to blow in from the west, which are both beneficial for measurement purposes. During 8 days of measurements at this site, between September 2000 and December 2001, a total of 540 FTIR spectra were collected and analyzed. The resulting emission factors are listed in Table 23. Any results of particularly poor quality, as

Emission Factors (g/gal)	7-Sep-00	+/-	5-Jan-01	+/-	20-Jul-01	+/-	9-Oct-01	+/-
CO	73.93	22.59	87.58	19.24	82.98	12.72	108.55	8.23
N$_2$O	1.20	1.05	2.05	0.96	1.16	0.37	1.41	0.25
CH$_4$	xxxx		4.06	0.93	3.33	1.25	1.27	0.64
NH$_3$	xxxx		0.43	0.11	0.00	0.00	0.59	0.14
NO					17.25	4.07		
Emission Factors (g/gal)	11-Oct-01	+/-	15-Nov-01	+/-	21-Nov-01	+/-	14-Dec-01	+/-
CO	97.34	9.73	130.06	12.31	98.61	11.47	71.27	12.19
N$_2$O	1.90	0.21	1.44	0.32	1.06	0.21	4.53	0.45
CH$_4$	2.56	0.78	2.35	1.42	xxxx		5.61	0.90
NH$_3$	0.48	0.07	0.68	0.09	0.88	0.07	0.32	0.10
NO							12.85	4.63

Table 23 - Emission Factors from Colorado Springs Site 1

190

indicated by the fact that the error in the slope of the regression line was greater than 100%, were not reported as useful data and are instead represented by "xxxx".

3.3.4.2 Site 2: South I-25

This site is the most heavily traveled part of the interstate in Colorado Springs. According to Colorado Department of Transportation data, an average of 90,000 vehicles per day (7500/hour) pass by the location of my measurement site. The site itself is in a bit of a swale because it is next to Fountain Creek. Unlike the north I-25 location, there are many businesses and side-roads surrounding the site, and downtown Colorado Springs is only a mile to the northeast. This location was unique because I was able to compare measurements from two locations near the same site. The first two days I took measurements were in December of 1999. I obtained permission to set up my equipment inside the fence of the Martin-Drake Power Plant (see site "A" in Figure 55). Site "A" is approximately 500 meters to the east of the highway, across the creek. The other three days of measurements at this site were performed at site "B", which is approximately 20 meters east of the highway. Although the average errors in the data collected at site "A" are slightly higher than the errors from site "B", the values are comparable.

I collected data at this location on 2 days in December 1999 and for three more days in July and August 2001. Over these five days, a total of 380 FTIR spectra were collected and analyzed. The emission factors derived from these data are listed in Table 24. Any results of particularly poor quality, as indicated by the fact that the error in the slope of the regression line was greater than 100%, were not reported as useful data and are instead represented by "xxxx".

Figure 55 – Colorado Springs Site 2: South I-25 (Mapquest.com)

Emission Factors (g/gal)	15-Dec-99	+/-	16-Dec-99	+/-	25-Jul-01	+/-	01-Aug-01	+/-	28-Aug-01	+/-
CO	143.95	14.24	78.79	6.60	123.14	9.20	88.75	13.59	99.08	29.57
N_2O	0.58	0.37	1.56	0.24	1.84	0.32	1.93	0.32	2.43	0.33
CH_4	18.42	4.92	xxxx		xxxx		10.18	3.49	-20.62	12.45
NH_3	0.26	0.12	xxxx		0.36	0.11	0.92	0.18	0.57	0.15
NO					27.68	4.59	xxxx		21.18	6.82

Table 24 - Emission Factors from Colorado Springs Site 2

3.3.4.3 Site 3: North Powers Boulevard

This was one of two locations on a busy arterial street. Powers Blvd. is one of the more heavily traveled city streets to which I could gain access for making measurements. In this location, there is a fairly steep grade, on the order of 10%, which runs for about 1000 meters. I set up my equipment approximately in the middle of this piece of road, which has two lanes in each direction. Traffic flow is highly variable, but usually averages about 1000 vehicles per hour during morning rush hour, with a peak flow of about 2400 vehicles per hour. An aerial photograph of this site is shown in Figure 56. This site is in a heavily residential area and a large business-park area lies approximately two miles to the south.

Only two days of data were collected at this location. The data

from this site and from the South Powers Blvd. site are listed together

in Table 25. One item to note is that the emission factors measured at

this location were similar to those measured at Matthews/Winters Park,

which makes qualitative sense because both of these sites are steeply

inclined.

Figure 56 - Colorado Springs Site 3: North Powers Blvd. (Mapquest.com)

3.3.4.4 Site 4: South Powers Boulevard

This site is at the south end of Powers Boulevard, near the

entrance to the Colorado Springs airport. Unlike the North Powers site,

this location has only a slight grade, but is near an intersection with a

traffic signal, so some of the vehicles are in a moderate acceleration mode. Traffic flow at this site was more consistent than at the North Powers site, and averaged about 1800 vehicles per hour. A photograph of this location can be found in Figure 57. Only two days of data were collected at this site as well, and all of the Powers Blvd. data are listed in Table 25.
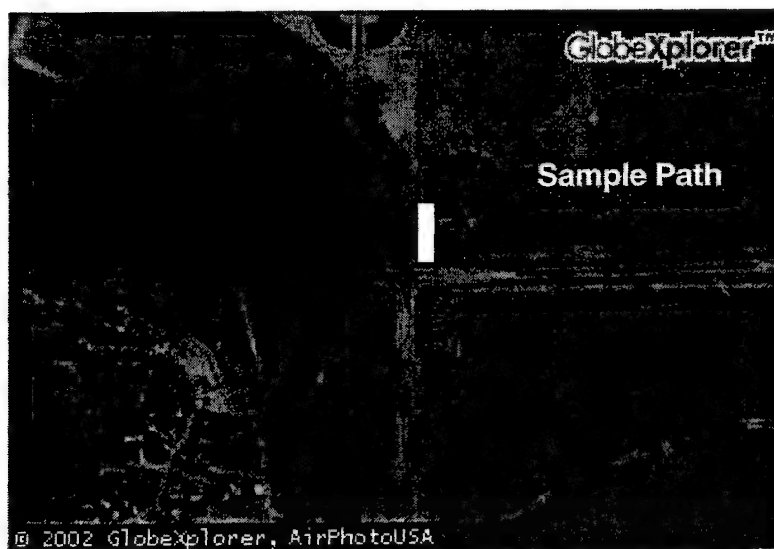
Figure 57 - Colorado Springs Site 4: South Powers Blvd. (Mapquest.com)

Emission Factors (g/gal)	North Powers				South Powers			
	23-Jun-00	+/-	1-Aug-00	+/-	3-Aug-00	+/-	8-Aug-00	+/-
CO	244.06	35.88	204.18	10.65	178.92	46.42	65.65	11.24
N_2O	xxxx		1.86	0.26	3.42	1.40	10.43	0.78
CH_4	-10.20	2.32	1.00	1.06	5.32	1.74	5.04	0.67
NH_3	2.91	0.25	1.12	0.17	1.14	0.80	0.33	0.12

Table 25 - Emission Factors from Colorado Springs Sites 3 and 4

CHAPTER 4. – CONCLUSIONS FROM AUTOMOTIVE EMISSIONS STUDIES

In the formal statement of this thesis (page 7), I proposed that this technique could combine the benefits of a tunnel study with the flexibility of remote sensing. In order to support that statement, I must show that I am able to produce equally accurate and reliable data and that it is not prohibitive in terms of money or time. I will address the question of data quality by examining the cohesiveness of my data and by comparing my results with those already reported in the literature. The literature values listed in Appendix F cover a very broad range of values. These emission factors have been measured or in a variety of different environments and modes of operation. Some of them are "real-world" numbers measured in tunnel studies and some are laboratory values measured on a dynamometer. I have listed the averages and ranges of values for each pollutant in Table 26. I have only factored those measurements made in the United States, since those figures will be more comparable to my own data. I have listed my own average values, also measured in a variety of different environmental and operational modes, in Table 27.

	g/gal	High	Low
CO	206.80	364	72.20
N_2O	1.00	1.63	0.25
Hydrocarbons (incl. Methane)	12.12	18.4	3.10
NH_3	1.73	2.52	0.34
NO	15.09	26.4	7.59

Table 26 - Average of Literature Values for Emission Factors (Appendix F)

It is apparent that my average figures fit well into the range of values listed in the literature, with the exception of nitrous oxide. Part of the reason for this may be that there are only four literature references for nitrous oxide emission factors at present, and only the two higher values are the result of actual on-road measurements. Neither of these measurements were made under high-load conditions. When only low to moderate load conditions are considered, the range of values I have measured for N_2O is 0.58 – 2.5 g/gal, with an average of 1.8 g/gal. Ammonia suffers from the same lack of data points for comparison, but perhaps it is not as sensitive to load conditions, being exclusively formed on the catalyst.

As far as the cohesiveness of the data, it is also apparent from
the values in Table 27, that there is a rather broad overall range.
However, when the data from each measurement site is examined,
one sees that the standard deviation of each emission factor is usually

	g/gal	High	Low
CO	123.19	232.08	65.65
N_2O	2.27	10.43	0.58
CH_4	3.00	18.42	1.00
NH_3	1.55	2.91	0.26
NO	14.00	27.68	12.85

Table 27 - Emission Factor Averages (g/gal) (OPIEM)

close to the error in the measurements. Furthermore, the results seem
to make sense in view of the modes of vehicle operation being
sampled. In other words, the CO emission factors are generally lower
for flat-grade, low acceleration modes of operation, and higher for
steep-grade, high-acceleration modes of operation.   When the
different measurement sites are grouped according to their grade and
acceleration characteristics, there is a definite upward trend in the
emission factors with increasing vehicle load. I have grouped the North
I-25, and Parking Lot sites together as Low Load sites, since they are

both flat and involve low acceleration modes of travel. The exception to this was the 15 Nov 01 sampling date for North I-25, when there was a traffic jam and an uncharacteristically high level of stop-and-go acceleration events. I grouped this data from the North I-25 site along with the South I-25 site and 6th and I-25 in Denver as Moderate Load sites. South I-25 is prone to traffic slowdowns and has a slight grade, and 6th and I-25 is a low speed on-ramp. Finally, I grouped the two Powers Boulevard sites and Matthews/Winters Park together as High Load sites because they either involve full-stop accelerations or prolonged grades traveled at high speeds. The results of these groupings are found in Table 28. Segregating these sites based on vehicle load is appropriate, since it has been shown, by Stedman and others, that vehicle emissions are primarily dependent upon "vehicle specific power," which is a function of the road grade, and the speed and acceleration of the vehicle.[149]

	Low Load	+/-	Moderate Load	+/-	High Load	+/-
CO	86.39	18.03	115.89	12.63	202.64	26.81
N_2O	1.69	0.66	1.70	0.40	3.96	0.56
CH_4	2.90	0.76	7.43	2.40	2.96	1.21
NH_3	0.54	0.09	0.73	0.15	1.43	0.25
NO	15.38	3.05	24.43	5.71	No Data	

Table 28 - Modal Emission Factors (g/gal) (OPIEM)

CHAPTER 5. – FUEL BASED INVENTORY FROM COLORADO SPRINGS DATA – CALENDAR YEAR 1999

In this section, I present the first attempt (to my knowledge) at constructing a fuel-based mobile-source inventory for the Colorado Springs area. I present a calculated inventory for the year 1999 because that is the most recent year for which data is available from the state of Colorado. I propose the following steps as a process by which such an inventory may be computed:

1. Determine the location of several measurement sites that are representative off the different vehicle modes of operation in the area of interest, and which offer the opportunity to sample a large portion of the local fleet.

2. Collect real-world data and calculate fleet-averaged, modal emission factors.

3. Weight these factors according to the distribution of the various driving modes within the area of interest. Combine the factors to produce one fleet and mode-averaged factor for each emission component.

4. Determine the amount of motor fuel combusted during the time-frame of the desired inventory within the area of interest.

5. Multiply the weighted emission factors by the amount of fuel combusted to obtain a total mass of each emission component produced during the inventory period.

This method has already been applied in the previously referenced emissions inventories, with one major exception: the previously used emission factors were computed from measurements taken at either one site or one type of site (i.e.- one mode of operation). Both of these situations can give rise to non-representative emission factors. The difference in this application is that I have been able to gather emission factor data about several modes of operation within the same geographic area, without much regard for geographic restrictions. I will describe, below, the way in which I accomplished each step in the above process and describe the results.

Step 1

A Colorado Springs traffic flow map is presented in Appendix G, which is a result of traffic counts performed by the Colorado Department of Transportation (CDOT).[150] It shows that, for three of the

four locations I chose, there is a high concentration of vehicle travel.

This is especially true for the interstate sites, since I-25 is the major

route for transportation between outlying areas and the city of Colorado

Springs. Additionally, these sites give a sampling point for a low load

(vehicle acceleration and/or road grade) site (North I-25), a moderate

load site (South I-25) and two high load sites (Powers Boulevard). Of

the two high load sites, one has an extended grade and the other

contains an intersection.

Step 2

The methods used to measure emission factors are described in

the preceding sections. However, the modal emission factors listed in

Table 28 combine factors for areas outside of Colorado Springs.

Therefore, the factors used to calculate the emissions inventory are

listed in Table 29:

	Low Load (g/gal)	**+/-**	**Moderate Load** (g/gal)	**+/-**	**High Load** (g/gal)	**+/-**
CO	86	18	118	19	173	26
N_2O	1.7	0.66	1.6	0.57	5.2	0.81
CH_4	2.9	0.76	8.3	1.4	3.8	1.4
NH_3	0.54	0.09	0.61	0.21	1.4	0.33
NO	15	3.1	24	5.7	No Data	

Table 29 - Modal Emission Factors from Colorado Springs

Step 3

In creating weighted emission factors, several assumptions must be made and some of these are dictated by the quality of the available data. First, I obtained the listing of roadway types and mileages in El Paso County.[150] Colorado Springs is the only major municipality in this county, with the remainder of the county being comprised mostly of farms and small rural communities. The CDOT data lists four types of roadways: Interstates, Freeways, Collectors and Arterials. My basic observations/assumptions regarding these road types is that Interstates and Freeways in El Paso County are mostly level and so are without any severe grades to consider. Interstates, according to the CDOT information, are located in rural areas, whereas Freeways are in urban locations. I decided to classify Interstates as "low load" routes and Interstates as "moderate load" routes, since they are more likely to suffer traffic slowdowns during rush hours. Finally, I decided that Arterials and Collectors should be classified as "high load," since they are more likely to resemble the Powers Boulevard sites, with relatively low speeds, stop-and-go conditions as well as intersections. El Paso County contains 677.65 centerline miles of all types of roadways. Of these, 20% are Interstates, 9% are classified as Freeways and 70% as Arterials and Collectors. I made the assumption

that the distribution of road types represented the distribution of vehicle

modes of operation. In other words, I assumed that the Arterials and

Collectors (high load) represented 70% of the average vehicle mode of

operation in El Paso County. Another way to apportion driving modes

among the vehicle population would be to use lane miles, which would

give a heavier weight to roadways capable of carrying more vehicles.

However, apportioning in this manner only gives a result about 4%

lower than using centerline miles. I lieu of any data suggesting one

method over the other, I decided to use centerline miles. Using this as

a weighting factor, I derived the fleet and mode-averaged emission

factors listed in Table 30. Most of these data were collected in 2000

and 2001, but there was no statistically significant difference between

the data collected in these two years. I made the assumption that I

could apply these to 1999 fuel sales data and still be within the bounds

of my error bars. However, my assessment may actually be slightly

low, since there is evidence that emission factors have been

decreasing in other cities in the past few years.[149] The major source of

error in these numbers is the uncertainty in determining the actual

slope of the relationship between each pollutant and CO_2.

Step 4 –

Determining fuel use within a given area is another source of uncertainty. State Department of Revenue fuel sales data are available on a state-wide basis, and since fuel use is proportional to the number people driving vehicles present in a given county, it makes sense to apportion the state-wide fuel sales by either population or vehicle registration percentage. In previous work by Harley[38] and Stedman,[39] the assumption has been made that the difference in vehicle registrations and population constitutes the uncertainty in fuel the sales data. This is the approach I used as well. The total population of El Paso County comprises 12% of the state's population[151], and 11% of the vehicles in Colorado are registered there.[152] This gives an uncertainty of 1% of the gasoline sales

	Composite Factors (g/gal)	**+/-**	**+/- (%)**
CO	149	25	17%
N₂O	4.1	0.78	19%
CH₄	4.0	1.2	31%
NH₃	1.1	0.28	25%
NO	19	1.3	7%

Table 30 - Fleet and Mode-Averaged Emission Factors for Colorado Springs (g/gal)

apportioned to El Paso County by population. This gives a total fuel

volume apportioned to El Paso County of (327,803,000 ± 3,278,000)

gallons of gasoline, gasohol and diesel. Because I am measuring the

aggregate emissions of all the vehicles passing by my site, my

emission factors will apply to the total of these three types of fuels.

	tons/day	tons/year	+/-
CO	143	52,200	17%
N_2O	3.9	1,400	19%
CH_4	3.8	1,400	31%
NH_3	1.1	402	25%
NO	19	6,900	7%

Table 31 - Mobile Source Emissions Inventory for El Paso County, 1999 (OPIEM)

Step 5 –

After determining the volume of gasoline to be applied to be the

basis of the inventory, one needs to calculate the amount of each

pollutant produced from it. This results in the following mobile source

emissions inventory for El Paso County for 1999:

By way of comparison, the Colorado Department of Public

Health and the Environment (CDPHE) has calculated an annual

inventory of emissions for El Paso County using the Mobile 5b

computer model. The method for computing this type of inventory is

explained in section 1.2.1, beginning on page 16. The results of this effort for CO and NOx, which are the only two substances that I can compare to my data, are reported in Table 32. The results of my fuel-based inventory are 20% lower than the modeled results for CO, but 51% higher for NOx. Part of the discrepancy regarding CO may be due to the fact that my data do not take cold start emissions into account; although it has been determined that Mobile 5b over-predicts the contributions of cold start emissions.[153]

Category	CO	NOx
On-road Vehicles	65,513	4564.7

Table 32 - Modeled Mobile Source Emissions Inventory (tons/year)[154]

A potentially significant result of the fuel-based emissions inventory is that vehicles may be contributing significantly to the nitrous oxide emissions budget, at least in Colorado. According to the EPA, mobile source emissions account for only 16% of the global N_2O budget. In Colorado, CDPHE's last estimate of state-wide N_2O emissions was 2,793 tons/year.[155] This is less than twice the estimated mobile source emission of N_2O in El Paso County alone, indicating that, at least in Colorado, mobile source production of nitrous oxide may rival or exceed other anthropogenic sources.

What about the potential for future predictions based upon emission factors and projected fuel use? This ability would be of the most interest to regulatory and planning agencies that need to project impacts of future changes to roadways or city expansion. I do not have the data necessary to make such a detailed prediction for Colorado Springs, but I can make an attempt based upon the results of some multi-year studies of automotive emissions in Denver, Chicago and Los Angeles, performed by Stedman, et al.[149] The results of this work have shown that the emission factors for CO, NO and HC have been dropping consistently over the past few years, as the fleets in each city have become populated with newer, cleaner vehicles. Figure 58 Figure 60 show these trends. The average changes, per year, in CO, NO and HC emission factors are: -9%, -3% and -5%, respectively. Figure 61 shows a plot of real-world ammonia emission factors, with a linear regression line through the points. This is a paltry amount of data to base a trend upon, but it is known that ammonia emissions have increased as three-way catalysts have become more prevalent. The average yearly increase in the ammonia emission factor has been 6% (see Appendix F for references). There is no appropriate source of data for making a similar projection for N_2O, so I will not attempt it. Applying these changes to the emission factors I measured in El Paso

County, I have projected the probable factors for the year 2010, in order to make a comparison with the modeled projection of emissions estimated by CDPHE. These projected factors, based upon my data, are listed in Table 33. Fuel use in Colorado is another quantity for which there is ample trend data. Since 1992, gasoline sales have risen at a fairly steady 3% per year, as shown in Figure 62.

Projected Factors (g/gal)	2010	+/- (%)
CO	103	17%
CH_4	1.9	31%
NH_3	2.1	25%
NO	13	7%

Table 33 – Projected Emission Factors for El Paso County, 2010 (OPIEM)

CO Emission Factors (g/gal)

Legend:
- ◆ Denver
- ■ Chicago
- ▲ LA
- ── Linear (Denver)
- ── Linear (Chicago)
- ── Linear (LA)

$y = -17.96x + 36025$
$R^2 = 0.8622$

$y = -20.391x + 40878$
$R^2 = 0.968$

$y = -26.249x + 52661$
$R^2 = 0.9304$
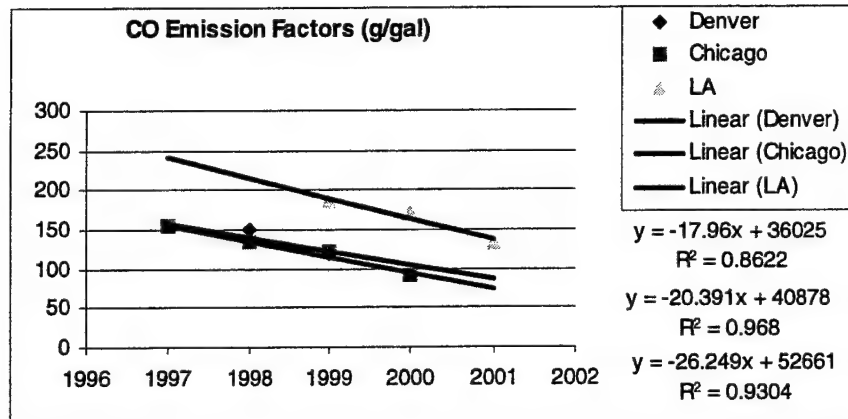
Figure 59 - Change in CO Emission Factors (g/gal) [149]

NO Emission Factor (g/gal)

Legend:
- ◆ Denver
- ■ Chicago
- ▲ LA
- ── Linear (Denver)
- ── Linear (Chicago)
- ── Linear (LA)

$y = -2.2104x + 4437.1$
$R^2 = 0.9231$

$y = -0.9394x + 1892$
$R^2 = 0.6964$

$y = 0.5526x - 1089.7$
$R^2 = 0.25$
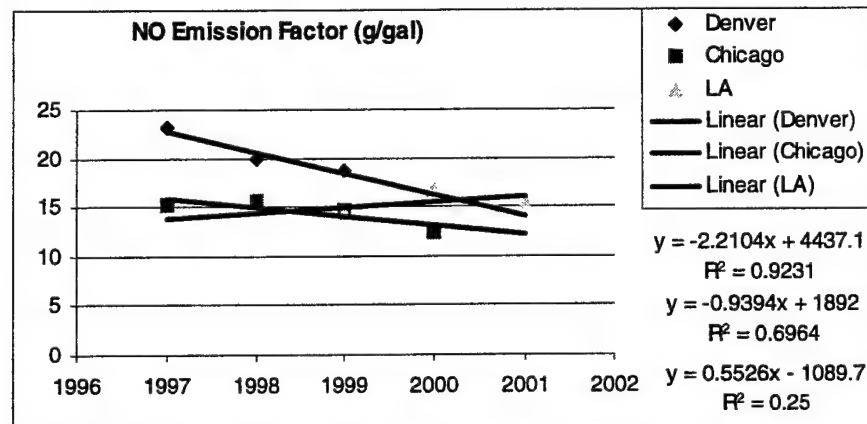
Figure 58 - Change in NO Emission Factors (g/gal) [149]

HC Emission Factors (g/gal)

Legend:
- ◆ Denver
- ■ Chicago
- ▲ LA
- ── Linear (Denver)
- ── Linear (Chicago)
- ── Linear (LA)

$y = -0.2763x + 558.6$
$R^2 = 0.75$

$y = -0.6908x + 1386.9$
$R^2 = 0.8993$

$y = -0.2763x + 555.74$
$R^2 = 0.75$
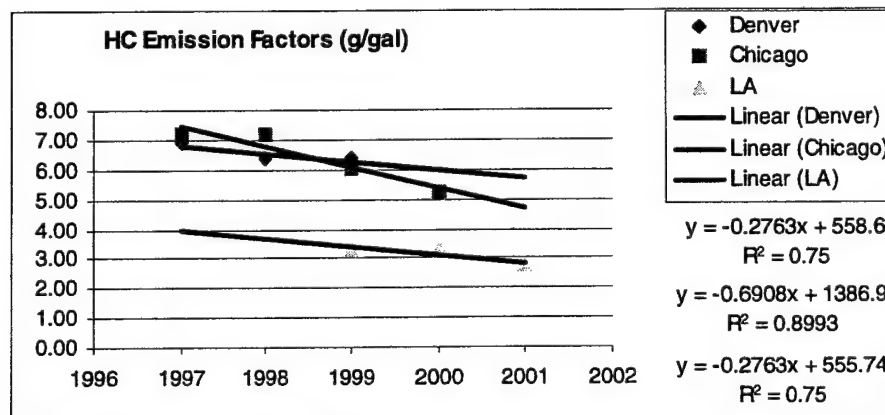
Figure 60 - Change in HC Emission Factors (g/gal) [149]

211

NH3 Emission Factor (g/gal)

$y = 0.1214x - 240.55$

$R^2 = 0.6985$
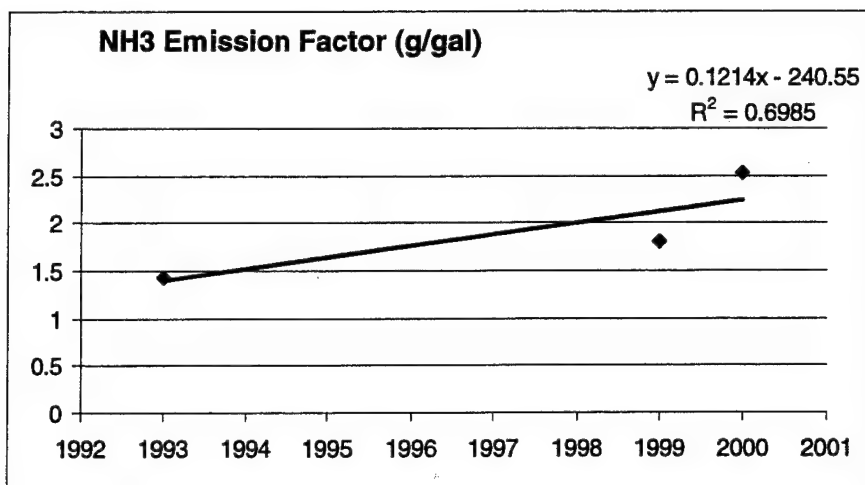
Figure 61 - Change in Ammonia Emission Factor

Gallons (gas+gasohol+diesel) Per Year

$y = 9E+07x - 2E+11$

$R^2 = 0.9736$
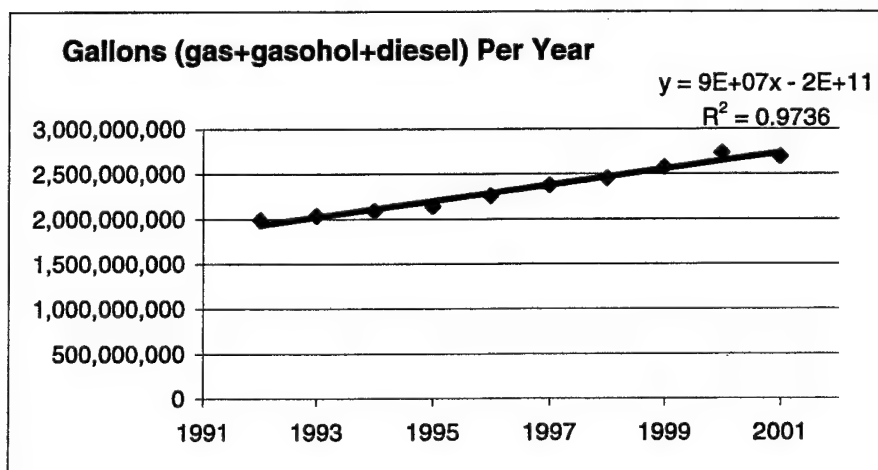
Figure 62 - Gasoline Sales in Colorado (Colorado Department of Revenue)

Using these projections, I have estimated a fuel-based inventory for the year 2010, which I have listed along with the CDPHE's modeled projections for CO and NOx, in Table 34. The CPDHE result is now much higher than mine, this time by nearly 150%. The modeled inventory for 2010 undoubtedly contains over-estimation of cold starts,

	tons/year	tons/day	+/-	CDPHE Estimate (tpd)
CO	28,300	77	17%	192.93
CH$_4$	1,200	3.3	21%	
NH$_3$	990	2.7	35%	
NO	6,900	19	7%	

Table 34 - Estimated Mobile Source Emissions for El Paso County (2010)

as does the current inventory does. An additional difference between the 1999 and 2010 inventories, is that the latter attempts to model the cumulative effects of the lack of oxygenated fuel use in the area. The city's redesignation request, honored by the EPA in 2001, eliminates oxygenated fuels from use in the winter. However, since Denver continues to use oxygenated fuels, it is certain that at least some amount of additional oxygen content will continue be present in the El Paso County fuel supply. This is an effect that neither estimate can

213

take into account at this time. As with the case of high-emitting

vehicles, this effect would be very difficult to model. It is also possible

that the modeled inventory over-estimates the effects of oxygenated

fuels. However, a consistent annual measurement campaign to

determine an actual measured inventory, as I have attempted above,

could easily determine the accuracy of such projections, and would

provide an invaluable database for future projections.

Another question of interest to someone who wants to measure

an emissions inventory is: "How many measurements do I need to

produce a useful inventory?" The answer to that question depends

upon many variables, not the least of which is the degree of accuracy

needed for the resulting inventory. Another variable is the number of

sites deemed necessary to adequately sample the vehicle fleet in the

given area. For any given measurement site, the error in any one

emission factor is driven almost entirely by the uncertainty in the slope

of the line when a given pollutant is plotted against CO_2. Therefore,

the average error in a group of measurements only depends on the

error in each individual measurement and there is not necessarily a

decrease in error with increasing numbers of measurements. The

individual errors are in turn affected by weather conditions like wind

and humidity, which may affect whether the emissions from the roadway are adequately sampled or whether adequate light arrives at the detector. One other parameter to consider is whether you believe the average estimate of the emission factor is an adequate estimation of the "true" emission factor, assuming it exists. One indication of this is the standard deviation of the measurements. In order to keep the situation as simple as possible I will consider only the CO emission factor at a single site, with the assumption that the results apply to any site and any emission factor. For this analysis, I have randomly selected four of the original 8 days of sampling at this particular site, and have constructed four random mixes of four numbers each. I then calculated the average emission factor with its associated error for each mix, and then the standard deviation of the four averages. I then repeated this analysis for sets of three and two. The results are listed in TABLE. The average emission factor for all eight days of measurements (in g/gal) is: $88.6 \pm 16\%$. None of the average emission factors calculated with smaller data sets differs significantly from this value. Also, in every case, three times the standard deviation of the range of values is smaller than the average error, meaning that the emission factors within each group are statistically identical. The

215

effect of decreasing the number of measurements is to increase the error, but, in this case, the error only increased to a maximum of 22%.

	Day 1	+/-	Day 2	+/-	Day 3	+/-	Day 4	+/-	Average	+/-	%
Mix 1	73.93	22.5	87.58	19.2	82.98	12.72	98.61	11.4	85.77	16.5	19%
Mix 2	87.58	19.2	97.34	9.73	71.27	12.19	108.55	8.23	91.18	12.3	14%
Mix 3	108.55	8.23	73.93	22.5	98.61	11.47	87.58	19.2	92.17	15.3	17%
Mix 4	82.98	12.7	87.58	19.2	108.55	8.23	71.27	12.1	87.59	13.0	15%
standard deviation										3.00	
	Day 1	+/-	Day 2	+/-	Day 3	+/-			Average	+/-	%
Mix 1	73.93	22.5	87.58	19.2	82.98	12.72			81.49	18.1	22%
Mix 2	87.58	19.2	97.34	9.73	71.27	12.19			85.40	13.7	16%
Mix 3	108.55	8.23	73.93	22.5	98.61	11.47			93.70	14.1	15%
Mix 4	82.98	12.7	87.58	19.2	108.55	8.23			93.03	13.4	14%
standard deviation										5.95	
	Day 1	+/-	Day 2	+/-					Average	+/-	%
Mix 1	73.93	22.5	97.34	9.73					85.63	16.1	19%
Mix 2	87.58	19.2	87.58	19.2					87.58	19.2	22%
Mix 3	108.55	8.23	73.93	22.5					91.24	15.4	17%
Mix 4	82.98	12.7	87.58	19.2					85.28	15.9	19%
standard deviation										2.73	

Table 35 - Effect of Smaller Sample Size on the Value of Emission Factors

Accurate mobile-source emissions inventories are an important tool in the effort to understand and control air pollution. In the past there was no convenient way to measure the emissions of large numbers of vehicles in the real world, leaving it to the modelers to attempt to calculate emissions inventories based on data from a relatively small number of vehicles. With the advent of remote sensing and tools such as the tunnel-less tunnel study, this is no longer the case. Once a history of fleet and mode-averaged emission factors and fuel use has been established for a particular region, it may even be possible to make accurate predictions about future emissions inventories. This type of simple "modeling" needs only to take into account a few factors instead of attempting to estimate future vehicle use rates or numbers of cold starts per day or any of the other myriad of inputs needed by such computer models as Mobile. Additionally, making real-world measurements of operational vehicles naturally takes into account variables such as high-emitters, which are difficult to quantify and model. The direct, nation-wide measurement of modal emission factors in units of mass/volume of fuel would also allow mobile-source emissions to be calculated like virtually every other type of emissions – on a fuel use basis.

CHAPTER 7. - IDEAS FOR FUTURE RESEARCH

There are a number of follow-on or extension projects regarding the use of open path spectrometry to measure automotive emissions that I think would be valuable to pursue. The most obvious of these, from my perspective, is to engage in a long-term study of either Colorado Springs or Denver. If measurements were taken at each site, and perhaps more sites could be included in the study, for a few days each month, an annual average could be computed and monthly variations could be studied over a longer period of time. Or, if that was prohibitive, only a few days study each year could be used to estimate the emission factors for the entire year.

Another interesting comparison would be between Denver and Colorado Springs, since the latter city has stopped using oxygenated fuels. The effect of oxygenated fuels has been studied in other locations, but there is still a great deal of uncertainty about their impact on real-world emissions. There would be some mixing of fleets, between these two cities, but there may be some measurable effect if similar measurement sites are used in each city. For example, a flat, multilane highway section could be the comparison site between the

218

cities -- perhaps a section of highway on the south side of Colorado Springs, and the north side of Denver. This would minimize fleet mixing, since the Colorado Springs traffic would be going to or from Pueblo, and the Denver traffic would be traveling to or from Boulder.

Severe altitude changes are also known to have an effect on automotive emissions, but it is not well quantified. This technique could provide a way to compare emission factors in a sea-level, or moderately elevated city with those in Denver or Colorado Springs. Actually, since Colorado Springs is approximately 1000 feet higher than Denver, there may be some discernible effect between these two cities as well. The tunnel-less tunnel study would be an excellent tool for this purpose because sites could be chosen to eliminate certain factors from consideration, such as roadway grade or acceleration, so that only the effect of altitude difference could be measured.

Other modes of vehicle operation could be studied in more detail, such as heavily congested intersections or severe accelerations on signalized interstate on-ramps. Long-term parking lots at airports would be an ideal place to study cold-start emissions, which could then be accounted for in a fuel-based inventory. Measurement sites near congested waterways and lakes would give the opportunity to quantify

219

the effects of watercraft, which are very difficult to measure otherwise. Additionally, the emissions of construction and earth-moving equipment could be directly measured, especially if the site was removed from a major roadway.

Finally, there are two instrumental changes, which may be a significant improvement to this technique. First, it may be possible to integrate temperature and pressure measurement along with the FTIR analysis software so that calibration files may be built for spectral analysis in real-time. This would ensure that each spectrum had a calibration set that accurately reflected the actual temperature and pressure during data collection. I have attempted to build a program that would take in temperature and pressure data from a file and build individual calibration files for each spectrum. However, I was not successful in getting this program to work. It may be that some software program other than GRAMS/32 needs to be used in order for this to be practical. The other change that might significantly improve the quality and perhaps the sensitivity of the data collected by this technique is the use of a higher-resolution FITR. I have been assembling a 0.1 cm^{-1} resolution spectrometer, which Dr. Stedman purchased from IdeaLab (Cambridge, MA). It is currently able to scan,

but the data-handling system is not completed. Dr. Scott McClaren, of
Apogee Scientific (Denver, CO), is completing this system, which may
be operational within the next few weeks. Using a system with 5 times
the resolution should allow us to better resolve the N_2O and CO_2
spectral features, and may lead to less cross-talk between them as well
as more accurate measurements of each.

ENDNOTES

[1] United States Census Data, Geospatial and Statistical Data Center. http:// fisher.lib.Virginia.edu (accessed June 2002)

[2] Heusner, Gary. "Common Questions and Answers about Horses." University of Georgia College of Agricultural and Environmental Sciences, http://www.ces.uga.edu/pubcd/B1113-W.HTML (accessed June 2002)

[3] Clean Air Act as Amended, 42 United States Code Section 7401, 1970

[4] U. S. EPA. "National Air Pollution Emission Trends: 1900 –1998", Appendix 3: "Trend Charts". http://www.epa.gov/ttn/chief/trends/trends98/ (accessed June 2002)

[5] U. S. EPA, Office of Air Quality Planning and Standards, National Ambient Air Quality Standards (NAAQS) Homepage. http://www.epa.gov/airs/criteria.html (accessed June 2002)

[6] Seinfeld, J. H. *Atmospheric Chemistry and Physics of Air Pollution* ; John Wiley and Sons, Inc., New York, 1986, pp. 119 - 134

[7] Ridley, B.; Atlas, E. in: *Atmospheric Chemistry and Global Change*; Brasseur, G. P.; Orlando, J. J.; Tyndall, G. S., Eds.;, Oxford University Press, New York, Oxford, 1999, pp. 259 - 267

[8] Pierson, W. R.; Brachaczek, W. W. Emissions of Ammonia and Amines from Vehicles on the Road. *Environmental Science and Technology* **1983**, *17*, 757 - 760

[9] Barthelmie, R. J.; Pryor, S. C. Implications of Ammonia Emissions For Fine Aerosol Formation from the Lower Fraser Valley, British Columbia. *Atmospheric Environment* **1998**, *32*, 345 - 352

[10] Fraser, M. P.; Cass, G. R. Detection of Excess Ammonia Emissions from In-Use Vehicles and the Implications for Fine Particle Control. *Environmental Science and Technology* **1998**, *32*, 1053 - 1057

[11] Kean, A. J.; Harley, R. A. On-Road Measurement of Ammonia and Other Motor Vehicle Exhaust Emissions. **2000**, *34*, 3535 - 3539

[12] U.S. Supreme Court Decision in the case of "Whitman, Administrator of the Environmental Agency, et. al. *v* the American Trucking Associations, Inc., et. al.," Feb 27, 2001, pg. 29

[13] Intergovernmental Panel on Climate Change, "Climate Change 2001 – Synthesis Report." p. 4, http://www.ipcc.ch/pub/tar/syr/004.htm (accessed June 2002)

[14] Intergovernmental Panel on Climate Change; *2001*, "Climate Change 2001 – Mitigation ," para. 3.3.2, http://www.ipcc.ch/pub/tar/wg3/021.htm (accessed June 2002)

[15] Excel Spreadsheet "Tier3_1999EmisFeb5_forWeb.xls", available from U.S. EPA - National Emission Inventory Trends Website: http://www.epa.gov/ttn/chief/trends/index.html

[16] Odaka, M.; Koike, N.; Suzuki, H. Influence of catalyst deactivation on N_2O emissions from automobiles. *Chemosphere: Global Change Science* **2000**, *2*, 3 - 4

[17] Zhao, Z.; Matsunami, A.; Kitagawa, K.; Arai, N. Gas Chromatographic evaluation of effects of rotational speed and mileage on N_2O emission from gasoline engines equipped with three-way catalytic converters. *Microchemical Journal* **2000**, *65*, 137 - 142

[18] Zachariadis, T.; Samaras, Z. An Integrated modeling system for the estimation of motor vehicle emissions. *Journal of the Air and Waste Management Association* **1999**, *49*, 1010 - 1026

[19] Reis, S.; Smipson, D.; Friedrich, R.; Jonson, J. E.; Unger, S.; Obermeier, A. Road traffic emissions - predictions of future contributions to regional ozone levels in Europe. *Atmospheric Environment* **2000**,*34*, 4701 - 4710

[20] Koike, N.; Odaka, M. Methane and Nitrous Oxide (N_2O) emission characteristics from automobiles. In *SP-1161(Engine Emissions and Emissions Measurement)*, Society of Automotive Engineers, 1996, pp. 1 - 8

[21] "National Air Pollution Emission Trends: 1900 –1998", U. S. EPA Report, http://www.epa.gov/ttn/chief/trends/trends98/, Chapter 8: "National Greenhouse Gas Emissions" (accessed June 2002)

[22] U.S. EPA, "Inventory of U.S. Greenhouse Gas Emissions and Sinks: 1990 – 1998," EPA-236-R-00-001, April 2000, Executive Summary, pg. 1 (accessed June 2002)

[23] Brasseur, G.; Schimel, D. in: *Atmospheric Chemistry and Global Change*; Brasseur, G. P.; Orlando, J. J.; Tyndall, G. S., Eds.;, Oxford University Press, New York, Oxford, 1999, ppg. 316 - 317

[24] International Panel on Climate Change, "Revised 1996 IPCC Guidelines for National Greenhouse Gas Inventories," Houghton, J. T.; Meira Filho, L. G.; Lim, B.; Treanton, K.; Mamaty, I; Bonduki,Y; Griggs, D. J.; Callender, B. A. (Eds), IPCC/OECD/IEA, 1996

[25] Guensler, R. *Evaluation of Ramp Metering Impacts on Air Quality: The Atlanta I-75 Case Study.* Report to the Georgia Department of Transportation, Report Number FHWA-GA-01-9814, 2001, Chapter 2, pp. 7 -10

[26] Colorado Department of Public Health and Environment, Air Pollution Control Division. *Revised Colorado Springs Area Carbon Monoxide Maintenance Plan*, 2000, pp. 6 - 8

[27] Colorado Department of Health and the Environment. Colorado Health Information Dataset Population Statistics webpage. http://www.cdphe.state.co.us/scripts/htmsql.exe/cohid/populationPub.hsql (accessed June 2002)

[28] Colorado Department of Revenue homepage. http://www.revenue.state.co.us/ (accessed June 2002)

[29] *Carbon Monoxide Emission Inventories for the Revised Colorado Springs Area Carbon Monoxide Maintenance Plan*, Colorado Department of Public Health and Environment, Air Pollution Control Division, Technical Services/Planning and Policy Programs, **2000**, Denver Colorado, pg. 1

[30] Kirchstetter, T. W.; Singer, B. C.; Harley, R. A. Impact of Oxygenated Gasoline Use on California Light-Duty Vehicle Emissions. *Environmental Science and Technology* **1996**, *30*, 661 - 670

[31] Pierson, W. R.; Gertler, A. W.; Bradow, R. L. Comparison of the SCAQS tunnel study with other on-road vehicle emission data. *Journal of the Air and Waste Management Association* **1990**, *40*, 1495 - 1504

[32] Fujita, E. M.; Croes, B. E.; Bennett, C. L.; Lawson, D. R.; Lurman, F. W.; Main, H. H. *Journal of the Air and Waste Management Association*, **1992**, *42*, 264 - 276

[33] Ingalls, M. N.; Smith, L. R.; Kirksey, R. E. *Measurement of on-road vehicle emissions factors in the California South Coast air basin. Volume I: regulated emissions,* Southwest Research Institute, San Antonio, TX, 1989

[34] National Research Council. *Modelling Mobile Source Emissions*, National Academy Press, Washington, DC, 2000, pg. 77

[35] Singer, B. C.; Harley, R. A. A Fuel-Based Motor Vehicle Emission Inventory, *Journal of the Air and Waste Management Association,* **1996**, *46*, pp. 581- 593

[36] Dreher, D. B.; Harley, R. A. A Fuel-based Inventory for Heavy-Duty Diesel Truck Emissions. *Journal of the Air and Waste Management Association*, **1998**, *48*, pp. 352 - 358

[37] Singer, B. C.; Harley, R.A. A Fuel-based inventory of motor vehicle exhaust emissions in the Los Angeles area during Summer 1997. *Atmospheric Environment*, **2000**, *34*, pp. 1783 - 1795

[38] Kean, A. J.; Swyer, R. F.; Harley, R. A. A Fuel-Based Assessment of Off-Road Diesel Engine Emissions. *Journal of the Air and Waste Management Association,* **2000**, *50*, pp. 1929 - 1939

[39] Pokarel, S. S.; Bishop, G. A.; Stedman, D. H. Fuel-Based On-Road Motor Vehicle Emissions Inventory for the Denver Metropolitan Area. *Atmospheric Environment*, in press

[40] Heywood, John B. *Internal Combustion Engine Fundamentals,* McGraw-Hill Publishing Co., New York, 1988, pg. 280

[41] Milton, B. E. "Control Technologies in Spark-Ignition Engines," in *Handbook of Air Pollution from Internal Combustino Engines*, Sher, E., Ed. Academic Press, New York, 1998, pg. 195

[42] Hilliard, J. C.; Wheeler, R. W. "Nitrogen Dioxide in Engine Exhaust," SAE paper #790691, *SAE Trans.,* 1979, *88*

[43] Coffin, David L. "Air Pollution: Present and Future Threat to Man and His Environment," in *Advances in Environmental Science and Technology*, Pitts, J. N.; Metcalf, R. L. Eds. Wiley Interscience, New York, 1971, v. 2, pg 19

[44] Metz, N. *Automobiltech. Z..* **1984**, *86*, 425

[45] Prigent, M.; De Soete, G. *Soc. Automot. Eng.,* **1989**, No. 890492

[46] Becker, K.H.; Lorzer, J. C.; Kurtenbach, R.; Wiesen, P.; Jensen, T. E.; Wallington, T. J. Nitrous Oxide Emissions from Vehicles, *Environmental Science and Technology,* **1999** *33,* 4134 - 4139

[47] U.S. EPA, "Inventory of U.S. Greenhouse Gas Emissions and Sinks: 1990 – 1998," EPA-236-R-00-001, April 2000, Annex C, pg. 2

[48] Zhao, Z.; Matsunami, A. Kitagawa, K.; Arai, N. Gas chromatographic evaluation of effects of rotational speed and mileage on N_2O emission from gasoline engines equipped with three-way catalytic converters.

[49] Odaka, M.; Koike, N.; Suzuki, H. Influence of catalyst deactivation on N_2O emissions from automobiles. *Chemosphere: Global Change Science*, **2000**, *2*, pp. 413 - 423

[50] U.S. EPA, "Inventory of U.S. Greenhouse Gas Emissions and Sinks: 1990 – 1998," EPA-236-R-00-001, April 2000, ch. 8, pg. 5

[51] U.S. EPA, "Inventory of U.S. Greenhouse Gas Emissions and Sinks: 1990 – 1998," EPA-236-R-00-001, April 2000, Executive summary, pg. 9 (accessed June 2002)

[52] Intergovernmental Panel on Climate Change; *2001*, "Climate Change 2001 – The Scientific Basis," Technical Summary, para. C.1 http://www.ipcc.ch/pub/tar/wg1/017.htm (accessed June 2002)

[53] Shores, R. C.; Walker, J. T. Jr.; Jones, Larry, G.; Rodegers, M. O.; Pearson, J, R,; McCulloch, R. B. Ammonia Emissions from the EPA's Light Duty Test Vehicle. *Society of Automotive Engineers SP-1644*, **2001**, pp. 107 - 201

[54] Pierson, W. R.; Brachaczek, W. W. Emissions of Ammonia and Amines from Vehicles on the Road. *Environmental Science and Technology*, **1983**, *17*, pp. 757 - 760

[55] Moeckli, M. A.; Fierz, M.; Sigrist, M. W. Emission Factors for Ethene and Ammonia from a Tunnel Study with a Photoacoustic Trace Gas Detection System. *Environmental Science and Technology*, **1996**, *30*, pp. 2864 - 2867

[56] Barthelmie, R. J.; Pryor, S. C. Implications of Ammonia Emissions for Fine Aerosol Formation and Visibility Impairment – A Case Study from the Lower Fraser Valley, British Columbia. *Atmospheric Environment*, **1998**, *32*, pp. 345 - 352

[57] Fraser, M. P.; Cass, G. R. Detection of Excess Ammonia Emissions from In-Use Vehicles and the Implication for Fine Particle Control. *Environmental Science and Technology*, **1999**, *32*, pp. 1053 - 1057

[58] Kean, A. J.; Harley, R. A. On-road Measurement of Ammonia and Other Motor Vehicle Exhaust Emissions. *Environmental Science and Technology*, **2000**, *34*, pp. 3535 - 3539

[59] Baum, M. M.; Kiyomiya, E. S.; Kumar, S.; Lappas, A. M. Multicomponent Remote Sensing of Vehicle Exhaust by Dispersive Absorption Spectroscopy. 2. Direct On-Road Ammonia Measurements. *Environmental Science and Technology*, **2001**, *35*, pp. 3735 - 3741

[60] McClaren, S. E. Open Path Spectrometers for Atmospheric Monitoring. Doctoral Thesis, University of Denver , Denver, Colorado, 1995, pp. 25, 26

[61] Stephens, E. R.; Hanst, P. L.; Doerr, R. C.; Scott, W. E. Reactions of nitrogen dioxide and organic compounds in air. *Industrial and Engineering Chemistry* **1956**, *48*, 1498 - 1504

[62] Hanst, P. L.; Stephens, E. R.; Scott, W. E. Reactions involving ozone, nitrogen dioxide and organic compounds at low concentrations in air. *Proceedings of the American Petroleum Institute* **1955**, *35*, 175 - 187

[63] Hanst, P. L.; Stephens, E. R.; Scott, W. E. Reactions involving ozone, nitrogen dioxide and organic compounds at low concentrations in air. *Air Repair* **1956**, *5*, 219 – 225, 244

[64] Stephens, E. R.; Hanst, P. L.; Doerr, R. C.; Scott, W. E. Recent developments in the study of the organic chemistry of the atmosphere. *Journal of the Air Pollution Control Association* **1956**, *6*, 159 - 165

[65] Stephens, E. R.; Hanst, P. L.; Doerr, R. C. Infrared Spectra of aliphatic peroxy acids. *Analytical Chemistry* **1957**, *29*, 776 - 777

[66] Stephens, E. R.; Hanst, P. L.; Doerr, R. C.; Scott, W. E. Auto Exhaust: composition and photolysis products. *Journal of the Air Pollution Control Association* **1959**, *8*, 333 - 335

[67] Pitts, J. N. Jr.; Finlayson-Pitts, B.; Winer, A.. *1977*, "Optical systems unravel smog chemistry," *Environmental Science and Technology*, **11**, *6*, p. 571, 572

[68] Hanst, P. L. Infrared Spectroscopy and infrared lasers in air pollution research and monitoring. *Applied Spectroscopy* **1970**, *24*, 161 - 174

[69] Hanst, P. L. Spectroscopic methods for air pollution measurement. *Advances in Environmental Science and Technology* **1971**, *2*, 91 - 213

[70] Hanst, P. L. Air Pollution measurement by long-path absorption spectroscopy. *Proceedings of the International Clean Air Congress* **1971**, 492 - 499

[71] Hanst, P. L.; Lefohn, A. S.; Gay, B. W. Jr. Detection of atmospheric pollutants at parts-per-billion levels by infrared spectroscopy. *Applied Spectroscopy* **1973**, *27*, 188 - 198

[72] Hanst, P. L. Air pollution measurement by Fourier transform spectroscopy. *Applied Optics* **1978**, *17,* 1360 - 1366

[73] Hanst, P. L., Wong, N. W., Bragin, J. A Long Path Infra-red Study of Los Angeles Smog. *Atmospheric Environment*, **1982**,*16*, 969 – 981

[74] Hanst, P. L. IR Spectroscopy of the atmosphere. *Fresenius' Z. Anal. Chem.* **1986**, *324*, 579 - 588

[75] Hanst, P. L. Analyzing air from a single-beam spectrum. *Spectroscopy* **1993**, *44*, 46 - 49

[76] Hanst, P. L.; Hanst, S. T.; Williams, G. M. Mouse-controlled air analysis using Grams-386. *Proceedings of SPIE – the International Society of Optical Engineers* **1996**, *2883*, 640 - 652

[77] Pate, C. T. ; Finlayson, B. J.; Pitts, J. N. Jr.. Long path infrared spectroscopic study of the reaction of methylperoxy free radicals with nitric oxide. *J. American Chemical Society* **1974**, *96,* 6554 - 6558

[78] Pitts, J. N. Jr.; McAfee, J. M.; Long, W. D.; Winer, A. M.. Long-path infrared spectroscopic investigation at ambient concentrations of the 2% neutral buffered potassium iodide method for the determination of ozone. *Environmental Science and Technology* **1976**, *10,* 787 - 793

[79] Tuazon, E. C.; Graham, R. A.; Winer, A. M.; Easton, R. R.; Pitts, J. N. Jr.; Hanst, P. L. A kilometer pathlength Fourier-transform infrared system for the study of trace pollutants in ambient and synthetic atmospheres. *Atmospheric Environment* **1978**, *12,* 865 – 875

[80] Tuazon, E. C.; Winer, A. M..; Pitts, J. N. Jr. Trace pollutant concentrations in a multi-day smog episode in the California South Coast Air Basin by long path length Fourier transform infrared spectroscopy. *Environmental Science and Technology* **1981**, *15* , 1232 - 1237

[81] Tuazon, E. C.; Graham, R. A.; Winer, A. M; Pitts, J. N. Jr. Atmospheric measurements of trace pollutants; long path Fourier transform infrared spectroscopy. Report (1981), (EPA-600/3-81-026), 104 pp.

[82] Biermann, H. W.; Tuazon, E. C.; Winer, A. M.; Wallington, T. J.; Pitts, J. N. Jr. Simultaneous absolute measurements of gaseous nitrogen species in urban ambient air by long pathlength infrared and ultraviolet-visible spectroscopy. *Atmospheric Environment* **1988**, *22*, 1545 - 1554

[83] New, D. L. Studies in Long Path Spectroscopy, Doctoral Thesis, University of Denver, Denver, Colorado, 1993, pp. 69 – 77, 126

[84] Stull, R. *Meteorology for Scientists and Engineers*, Brooks/Cole, Pacific Grove, CA, 2000, pp. 28

[85] Griffith, D. W. T.; Galle, B. Flux Measurements of NH_3, N_2O, and CO_2 using dual beam FTIR spectroscopy and the flux-gradient technique. *Atmospheric Environment* **2000**, *34*, 1087 - 1098

[86] James, T. A.; Meyer, D.; Ashbaugh, L. L.; Freitas, N. R. Field and laboratory estimates of ammonia emission from cattle production facilities. *Book of Abstracts,* 218th ACS National Meeting, New Orleans, Aug. **1999,** pp. 22-26

[87] Smith, K. A.; Clayton, H.; Arah, J. R.; Christensen, S.; Ambus, P.; Fouwler, D.; Hargreaves, K. J.; Skiba, U.; Harris, G. W. Micrometeorological and chamber methods for measurement of nitrous oxide fluxes between soil and the atmosphere: overview and conclusions. *Journal of Geophysical Research (Atmospheres)* **1994**, *99*, 16541 - 16548

[88] Gosz, J. R.; Dahm, C. N.; Risser, P. G. Long-path FTIR measurement of atmospheric trace gas concentrations. *Ecology* **1998**, *69*, 1326 -1330

[89] Griffith, D. W. T. Synthetic calibration and quantitative analysis of gas-phase FT-IR spectra. *Applied Spectroscopy* **1996**, *50*, 59 - 70

[90] Goode, J. G.; Yokelson, R. J.; Susott, R. A.; Ward, D. E. Trace gas emissions from laboratory biomass fires measured by open-path Fourier transform infrared spectroscopy. *Journal of Geophysical Research (Atmospheres)* **1999**, *104*, 21237 - 21245

[91] Yokelson, R. J.; Goode, J. G.; Ward, D. E; Susott, R. A.; Babbitt, R. E.; Wade, D. D.; Bertschi, I.; Griffith, D. W. T; Hao, W. M. Emissions of formaldehyde, acetic acid, methanol and other trace gases from biomass fires in North Carolina measured by airborne Fourier transform infrared spectroscopy. *Journal of Geophysical Research (Atmospheres)* **1999**, *104*, 30109 - 30125

[92] Yokelson, R. J.; Goode, J. G.; Ward, D. E; Susott, R. A.; Babbitt, R. E.; Wade, D. D.;Davies, M. A.; Hao, W. M. Measurements of excess O_3, CO_2, CO, CH_4, C_2H_4, C_2H_2, HCN, NO, NH_3, HCOOH, CH_3COOH, HCHO, and CH_3OH in 1997 Alaskan biomass burning plumes by airborne Fourier transform infrared spectroscopy (AFTIR). *Journal of Geophysical Research (Atmospheres)* **2000**, *105,* 22147 - 22166

[93] Personal conversations with Dr. Johan Mellqvist. 9 May 2002

[94] Bradley, K. S; Brooks, K. B.; Hubbard, L. K.; Popp, P. J.; Stedman, D. H. Motor Vehicle Fleet Emissions by OP-FTIR. *Environmental Science and Technology* **2000**, *34*, 897 - 899

95 Luening, R.; Baker, S. K.; Jamie, I. M.; Hsu, C. H.; Klein, L.; Denmead, O. T.; Griffith, D. W. T. Methane emission from free-ranging sheep: A comparison of two measurement methods. *Atmospheric Environment* **1999**, *33*, 1357 - 1365

96 Chang, T. Y.; Modzelewski, S. W.; Norbeck, J. M.; Pierson, W. R. Tunnel Air Quality and Vehicle Emissions. *Atmospheric Environment* **1981**, *15*, 1011 - 1016

97 Pierson, W. R.; Brachaczek, W. W. Emissions of ammonia and amines from vehicles on the road. *Environmental Science and Technology* **1983**, *17*, 757 - 760

98 Bishop, Gary A.; Zhang, Yi; McClaren, S. E.; Guenther, P. L.; Beaton, S. P.; Peterson, J. E.; Stedman, D. H.; Pierson, W. R.; Knapp, K. T. Enhancements of remote sensing for vehicle emissions in tunnels. *Air Waste* **1994**, *44*, 169 - 175

99 Pierson, W. R.; Gertler, A. W.; Robinson, N. F.; Sagabiel, J. C.; Zielinska, B.; Bishop, G.A.; Stedman, D. H.; Zweidlinger, R. B.; Ray, W. D. Real-world automotive emissions – summary of studies in the Fort McHenry and Tuscarora Mountain tunnels. *Atmospheric Environment* **1996**, *30*, 2233 - 2256

100 O'Connor, C. M.; Gertler, A. W.; Sagabiel, J. C. A comparison of ozone-forming potential of on-road emissions measured at the Sepulveda Tunnel between 1995 and 1996. *Proceedings, Annual Meeting of the Air and Waste Management Association* **1998**

101 Gofa, F.; Gertler, A. W.; Sagabiel, J. C. Changes in on-road emissions and emission factor model predictions for the Van Nuys Tunnel: 1987 to 1995. *Proceedings, Annual Meeting of the Air and Waste Management Association* **1998**

102 Kirchstetter, T. W.; Singer, B. C.; Harley, R. A.; Kendall, G. R.; Chan, W. Impact of Oxygenated Gasoline Use on California Light-Duty Vehicle Emissions. *Environmental Science and Technology* **1996**, *30*, 661 - 670

103 Kirchstetter, T. W.; Harley, R. A.; Littlejohn, D. Measurement of Nitrous Acid in Motor Vehicle Exhaust. *Environmental Science and Technology* **1996**, *30*, 2843 - 2849

104 Kirchstetter, T. W.; Harley, R.A.; Kreisberg, N. M.; Stolzenburg, M. R.; Hering, S. V. On-road measurement of fine particles and nitrogen oxide emissions from light- and heavy-duty motor vehicles. *Atmospheric Environment* **1999**, *33*, 2955 - 2968

105 Kean, A. J.; Harley, R. A.; Littlejohn, D.; Kendall, G. R. On-Road Measurement of Ammonia and Other Motor Vehicle Exhaust Emissions. *Environmental Science and Technology* **2000**, *34*, 3535 - 3539

106 Lindner, R,; Mueller, W.; Babelot, J. F.; Glatz, J. P.; Geiss, F.; Stangl, H.; Nicollin, B. O.; Rau, H.; Rogora, L.; Schlitt, H. Automobile exhaust emissions in the velocity range of 80 – 120 km/h. road measurements for a fleet of automobiles in the Pfaender Tunnel. *Comm. Eur. Communities, [Rep.] EUR* **1985**, 31 pp.

107 Allen, J. O.; Mayo, P. R.; Hughes, L.S.; Salmon, L. G.; Cass, G. R. Emissions of size-segregated aerosols from on-road vehicles in the Caldecott tunnel. *Environmental Science and Technology* **2001**, *35*, 4189 - 4197

108 Becker, K. H.; Lorzer, J. C.; Kurtenbach, R.; Wiesen, P. Nitrous Oxide (N_2O) Emissions fromVehicles. *Environmental Science and Technology* **1999**, *33*, 4134 - 4139

109 Moeckli, M. A.; Fierz, M.; Sigrist, M. W. Emission Factors for Ethene and Ammonia from a Tunnel Study with a Photoacoustic Trace Gas Detection System. *Environmental Science and Technology* **1996**, *30*, 2864 - 2867

[110] Fraser, M. P.; Cass, G. R. Detection of Excess Ammonia Emissions from In-Use Vehicles and the Implications for Fine Particle Control. *Environmental Science and Technology* **1998**, *32*, 1053 - 1057

[111] Bishop, G. A.; Starkey, J. R.; Ihlenfeldt, A.; Williams, W. J.; Stedman, D. H. IR Long-Path Photometry, A Remote Sensing Tool for Automobile Emissions. *Analytical Chemistry* **1989**, *61*, 671A – 677A

[112] Guenther, P. L.; Stedman, D. H.; Bishop, G. A.; Hannigan, J.; Bean, J.; Quine, R. Remote Sensing of Automobile Exhaust. American Petroleum Institute Publication Number 4538, Washington, D.C., **1991**

[113] Bishop, G. A.; Morris, J. A,; Stedman, D. H.; Cohen, L. H.; Countess, R. J.; Countess, S. J.; Maly, P.; Scherer, S. The Effects of Altitude on Heavy-Duty Diesel Truck On-Road Emissions. *Environmental Science and Technology* (2001), *35*, 1574 - 1578

[114] US Environmental Protection Agency. *FTIR Open-Path Guidance Document:;* EPA/600/R-96/040, National Exposure Research Laboratory, Research Triangle Park, Chapel Hill, NC, 1996, ch. 2, pg. 20

[115] Beer, A. *Ann.Physik.* **1852,** *86*, 78

[116] Walter, B. *Ann. Physik (Wiedemann)* **1889**, *36*, 502 - 518

[117] Ingle, J. D., Crouch, S. R.. *Spectrochemical Analysis*, Prentice Hall, Englewood Cliffs, NJ, 1988, pp. 34 – 45

[118] Chang, S.; Tso, T,; Lo, J. The Nonlinearity and Related Band Strength of Carbon Monoxide When Applied to Ambient Air Measurement Using Open Long-Path Fourier Transform Infrared Spectroscopy, *Journal of the Air and Waste Management Association* **2001**, *51*, 1332 - 1338

[119] Willard, H. H., Merritt, L. L., Dean, J. A., Settle, F. A. *Instrumental Methods of Analysis*, Wadsworth Publishing, Belmont, CA, 1981, pg 69

[120] *FTIR Open-Path Guidance Document:;* EPA/600/R-96/040; US Environmental Protection Agency, National Exposure Research Laboratory, Research Triangle Park, Chapel Hill, NC, 1996, ch. 2, pg. 3

[121] ORIEL Instrument Catalog, chapter 5, pages 4 - 5

[122] Griffiths, P. R., de Haseth, J. A. *Fourier Transform Infrared Spectrometry* John Wiley & Sons, New York, 1986, pg. 4

[123] Cooley, J. W., Tukey, J. W. An algorithm for the machine calculation of complex Fourier series, *Mathematics of Computation* **1969**, *19*, 297-301

[124] Patric, D. R. *Toxic Air Pollution Handbook*, Van Nostrand Reinhold, New York, 1994

[125] U. S. Environmental Protection Agency; *Preparation Aids for the Development of RREL Quality Assurance Plans (Category I Project Plans),* **EPA/600/8-91/003** (1991)

[126] White, J. U.; "Long Optical Paths of Large Aperture," *J. Optical Society of America* **1942,** *32*, 285

[127] Popp, P.J.; Bishop, G.A.; Stedman, D.H. Development of a High-Speed Ultraviolet Spectrometer for Remote Sensing of Mobile Source Nitric Oxide Emissions, *J. Air Waste Manage. Assoc.* **1999,** *49*, 1463-1468,

[128] Gill, Gerald C.; *1967*, Development and Use of the Gill UVW Anemometer, *3rd Symposium on Meteorological Observations and Instrumentation*, American Meteorological Society, Boston, MA, pp. 65 - 71

[129] Rothman, L. S., Rinsland, C. P., *et al.*, The HITRAN Molecular Spectroscopic Database and HAWKS (HITRAN Atmospheric Workstation): 1996 Edition

[130] Esler, M. B.; Griffith, D. W. T.; Wilson, S. R.; Steele, L. P. Precision Trace Gas Analysis by FT-IR Spectroscopy. 1. Simultaneous Analysis of CO_2, CH_4, N_2O and CO in Air. *Analytical Chemistry* **2000**, *72*, 206 - 215

[131] Yokelson, R. J.; Susott, R.; Ward, D. E.; Reardon, J.; Griffith, D. W. T. Emissions from smoldering combustion of biomass measured by open-path Fourier transform infrared spectroscopy. *Journal of Geophysical Research (Atmospheres)* **1997**, *102*, 18865 - 18877

[132] Griffith, D. W. T.; Esler, M. B.; Wilson, S. R. Isotopic analysis of atmospheric trace gases by FTIR spectroscopy. *AIP Conference Proceedings*, **1998**, *430*, 207 - 210

[133] Griffith, D. W. T.; Toon, G. C.; Sen, B.; Blavier, J.; Toth, R. A. Vertical profiles of nitrous oxide isotopomer fractionation measured in the stratosphere. *Geophysical Research Letter* **2000**,*27*, 2485 - 2488

[134] Rinsland, C. P.; Meier, A.; Griffith, D. W. T.; Chiou, L. S. Ground-based measurements of tropospheric CO C_2H_6 and HCN from Australia at 34°S latitude during 1997 – 1998. *Journal of Geophysical Research (Atmospheres)* **2001**, *106*, 20913 - 20924

[135] Ferm, M.; Galle, B.; Klemedtsson, L.; Kasimir-Klemedtsson, A; Griffith, D. W. T. Comparison of different techniques to measure ammonia emission after manure application. *IVL Report* **2000**, *B 1383*, Chapt i, ppg. 1 - 14

[136] Turatti, F. Griffith, D. W. T.; Wilson, S.R.; Esler, M. B.; Rahn, T.; Zhang, H.; Blake, G. A. Positionally dependent N fractionation factors in the UV photolysis of N_2O determined by high resolution FTIR spectroscopy. *Applied Spectroscopy* **2000**, *54*, 1303 - 1312

[137] Galle, B.; Samuelsson, J.; Svensson, B. H.; Boerjesson, G. Measurements of Methane Emissions from Landfills Using a Time Correlation Tracer Method Based on FTIR Absorption Spectroscopy. *Environmental Science and Technology* **2001**, *35*, 21 - 25

[138] Anderson, D. W.; McLaren, S. The use of carbon monoxide emissions measurement as a surrogate for formaldehyde emissions measurement. *Proceedings, Annual Convention – Gas Processors Association* **2001**, *80*, 342 - 352

[139] Haaland, D. M. "Multivariate Calibration Methods Applied to Quantitative FT-IR Analyses," in *Practical Fourier Transform Infrared Spectroscopy*, Ferrar, J. R.; Krishnan, K., Eds. Academic Press, San Diego, 1990

[140] Montgomery, D. C., Peck, E. P. *Introduction to Linear Regression Analysis.* John Wiley & Sons, New York, 1982, pg 347

[141] Chatterjee, S., Price, B. *Regression Analysis by Example*, Wiley-Interscience, New York, 1991, pp. 151 - 152

[142] Chatfield, C. *The Analysis of Time Serries, 5th Edition,* CRC Press, Boca Raton, FL, 1999, pp. 61 - 63

[143] Childers, J. W.; Thompson, E. L. Jr.; Harris, D. B.; Kirchgessner, D. A.; Clayton, M.; Natschke, D. F.; Phillips, W. J. Application of Standardized Quality Control Procedures to

Open-Path Fourier Transform Infrared Data Collected at a Concentrated Swine Production Facility, *Environmental Science and Technology*, **2001**, *35*, 1859 - 1866

[144] Okabe, H. *Photochemistry of Small Molecules.* John Wiley and Sons, New York, 1978, pg. 209

[145] Ikeda, Y.; Nakajima, T, Sher, E. "Air Pollution from Small Two-Stroke Engines and Technologies to Control It," in *Handbook of Air Pollution from Internal Combustion Engines.* Sher, E., Ed. Academic Press, New York, 1998, pp. 445 - 447

[146] Tsai, J. H.; Hsu, Y. C.; Weng, H. C.; Lin, ,W. Y.; Jeng, F. T. Air pollutant emission factors form new and in-use motorcycles. *Atmospheric Environment*, **2000**, *34*, 4747-4754

[147] National Institute of Standards and Technology On-line Webbook, http://webbook.nist.gov, ,accessed August, ,2002

[148] US EPA. *Emission Factor Documentation for AP-42 Section 1.4 – Natural Gas Combustion.* Technical Support Division, Office of Air Quality Planning and Standards, Research Triangle Park, N.C., 1997, Tables 1.4-1 and 1.4-2

[149] Pokharel, S. S.; Bishop, G. A.; Stedman, D. H. University of Denver, Denver, CO. Series of "On-Road Remote Sensing" reports from Chicago, Denver, Los Angeles and Phoenix. Prepared for the Coordinating Research Council, Inc.

[150] Colorado Department of Transportation Website, www.dot.state.co.us, Accessed Jan 2002

[151] United States Census Bureau Webpage, www.census.gov, accessed Jan 2002

[152] Colorado Department of Revenue Annual Report, 2000, pp. 53 - 55

[153] Beardsley, M. "Mobile 6: EPA's New Highway Emission Factor Model," *Proceedings of the 10th CRC On-Road Vehicle Workshop,* San Diego, CA, 2000

[154] Colorado Department of Public Health and the Environment, Air Pollution Control Division, Website. http://Puma.dphe.state.co.us, accessed April 2002

[155] Colorado Department of Public Health and the Environment. "Colorado Greenhouse Gas Emissions Inventory and Forecast," September, 1998

A - Replacing and Adjusting the Hamamatsu Photo-Diode Array

1) Remove the monochromator from the baseplate assembly by removing the cover and threaded hex rods inside the case.

2) Remove the four screws holding the PDA board onto the baseplate. The board and support will now only be attached by wiring, so be careful.

3) Detach the Hamamatsu C4070 circuit board from its support by removing the four corner screws.

4) **Carefully** pry the PDA chip from its socket. Be careful not to bend the chip.

5) Press the new PDA chip into the socket and re-attach the C4070 board to its support, but do not reattach the support to the baseplate.

6) Lay the C4070 board and support face down on the baseplate. This is to block the PDA from receiving any light. You will now be able to adjust the baseline dark-current output as well as minimizing internal switching noise induced by the driver board. This is important because, if the dark-current output is too low (<100), it will cause the software to lock up and stop responding.

7) Begin this process by starting the alignment program on the monochromator:

   a) Start the computer and run the program "TVTERM.exe." Follow the on-screen instructions to monitor the activity of the monochromator computer.
   b) Turn on the monochromator. After the boot-up sequence, press "ESC" on the computer keyboard to interrupt the automatically executed program.
   c) At the "A:" prompt, type the name of the appropriate alignment program name (i.e. - al512_50, or al128_50, etc.) If the program continues running, **proceed to step 8).**
   d) If the program will not start or if it begins and locks up immediately, then stand the PDA card assembly on its edge (so it can receive light), reboot the computer and mono following steps a), b) and c), above.
   e) If the PDA had to be put on its edge, you will need to turn off the lights in the room, but leave the hallway door open so that the PDA output doesn't get too low. Then, **go to step 9.**

8) If the number on the monochromator screen is between 200 and 400, then **proceed to step 10**. Otherwise, turn potentiometer VR3 on the Hamamatsu C4070 board counterclockwise to raise the reading or clockwise to lower it, until the reading on the LED screen is in the range of 200 - 400, **then proceed to step 10**.

9) Adjust potentiometer VR3 on the Hamamatsu C4070 board counterclockwise to increase the reading on the monochromator LED to about 1000, or as high as it will go. Attempt blocking out all light to the PDA and ensure that the LED reading stays between 200 and 400. You may need to turn VR3 dozens of times or more to accomplish this.

10) Turn off the monochromator and attach an oscilloscope to the C4070 board like so:

   a) Channel 1: wire on edge of board marked "Trig." This is the data collect trigger.
   b) Channel 2: center wire of coax attached to point marked "DV." This is the data signal.
   c) Ground lead: Any appropriate ground connection

11) Reboot the computer and follow steps 7) a), b) and c). Ensure that the PDA assembly is face down on the baseplate and the LED reading is between 200 and 400. Adjust the oscilloscope so Channel 1 is set on 1 volt (triggered), Channel 2 is set on 100 mV, and the time is set so you can see 1 or 2 trigger pulses on the screen. Ensure that both channels are DC coupled and are baselined together on the screen. Adjust VR2 on the C4070 board until the baseline of the Channel 2 signal is as flat as possible. Adjust VR1 to raise the baseline on the left side of the screen to about 100 mV above the baseline setting. If the LED reading falls below 200, adjust VR3 to raise it. If this is unresponsive, adjust VR1 slightly to put the LED reading between 200 and 400. When you are done, there should be two peaks on Channel 2 to the right of the trigger pulse. The first peak should be about 300 mV and the second about 500 mV.

12) Reassemble the monochromator and proceed with the optical alignment procedure in the manual.

B - Monochromator Alignment Procedure

DU Monochromator Alignment Procedure

This procedure describes re-alignment of the University of Denver ultraviolet monochromator for use in measuring nitric oxide. This procedure must be carried out in an absolutely dark room. Any light pollution in the room will make it very difficult to observe the absorption lines from the cadmium lamp. It may take 20 minutes for your eyes to adjust to the darkness. A computer is required for the final alignment, but it must not be turned on during the early steps, or it will pollute the room with. Embrace the darkness, keep your tools close at hand and keep a battery powered torch in the back pocket of your trousers.

1. Position the round tip of the fiber so that it is perpendicular to the window in the cadmium lamp. Maximize the light going into the monochromator, either using the alignment program if you can see the 228 nm Cd line on the screen, or by placing the fluorescent card on the first round mirror. Make sure that the fiber will stay in position in front of the Cd lamp window, and that light intensity does not drop as a result of misalignment of the fiber in front of the lamp.

2. Confirm that the light from the fiber is illuminating the collimating mirror. Do this by placing the fluorescent card in front of the mirror and seeing if it glows or if you can cast a shadow on it with your finger. This should not be a problem, but if it is not illuminated, ensure that the round fiber tip is in front of the lamp and that nothing (perhaps a bent light baffle or debris) is blocking the light. The light at this point is still somewhat polychromatic, having been only filtered by the beam splitters in the source and detector. The yellow card will appear more illuminated than glowing.

3. Place fluorescent card in front of the grating. A circle of light should fill the card, meaning the light is reflected from the collimating mirror to the grating. If it is not, the collimating mirror needs to be adjusted to center the circle of light on the diffraction grating.

4. Place the fluorescent card over the focussing mirror. Ideally, you should see a circle of light (228 nm) filling the mirror. This may be hard to see. The room must be absolutely dark, with no light pollution from the Cd lamp or a laptop computer screen. Don't confuse this light with another circle that will appear slightly above (even slightly overlapping with) the focussing mirror. This second circle of light is 326 nm light from the Cd lamp. It is only 85% of the intensity of the 228 nm line, but 326 nm light activates the fluorescent card much more, and it appears brighter. If the 228 nm light is not filling the focussing mirror, adjust the grating to make it so. It may be necessary to grind the appropriate size of Allen key (Imperial, not metric) to fit in the tight space behind the grating mount.

5. The 228 nm light from the focussing mirror should be focussing the image of the entrance slit on the detector. The active area of the detector is the dark area in the center of the detector, approximately 0.25 inches long. Place the thin strip of fluorescent card in the detector 'slot" (you will need to remover the baffle, don't forget to replace it). You should see the slit image on the card. If it is not visible,

use the larger card to locate it in the vicinity of the detector, and adjust the focussing mirror mount to relocate the slit image. The slit image is approximately 2 mm longer (remember, it's a horizontal slit) than the width of the detector on each side. Center the slit image on the detector so that the excess light on either side is balanced. This allows for slight misalignment in the x direction without a loss in signal. Visually center the slight vertically on the detector as well.

6.   Using the alignment program on the external computer, adjust the focussing mirror mount so that the 228 nm line is at diode 87. A smaller peak should be visible at 226.5 nm, slightly to the left. If this line is not visible, it is possible you have centered the 326 nm line. With the 228 nm line at diode 87, the g band of NO will be centered on the detector. After this final wavelength adjustment, confirm that the slit is still centered horizontally on the active area of the detector.

7.   Measure cars!

How to use a Cadmium lamp to adjust the monochromator.
(Step 6 in the previous instructions)

1) Have a PC with TVTERM.COM, MAX_128.EXE and the Borland Pascal graphic library files installed in a common directory.

2) Connect the communications cable between the PC and the Mono.

3) From the command line execute TVTERM with baud=19200, data bits=8, stop bits=1 and parity=none (i.e. TVTERM com1 b19200 d8 s1 pn).

4) Enter terminal mode by pressing ALT-rightshift-P.

5) Plug in mono and monitor boot progress. When UVMFEAT1.EXE loads and runs press the ESCAPE key to terminate its operation.

6) From the command line execute the program PDAG_128.EXE.

7) Return to the PC's command line by pressing ALT-rightshift-L and execute the program MAX_128.EXE. Remember to specify the com port you are using to talk to the mono (i.e. MAX_128 1 for com1).

8) Now power up the Cadmium lamp and gently press the lamp against the end of the fiber optic bundle until you see the Cadmium lines on the graph. The major cadmium line should be a diode 87 for optimum alignment.

9) Press the switch on the mono to end the programs. At this time both computers will now automatically reboot.

C - GRAMS/32 Array Basic Software for FTIR Spectral Analysis

All programs in this section are written in GRAMS/32 Array Basic

Program: OPIEM.ab
Purpose: To collect FTIR spectra, temperature and pressure data, wind data and UV Monochromator output.
Written by: D.W.T. Griffith's group at University of Wollangong, Australia.
Modified by: Dan Branan, University of Denver

```
'       Program OPIEM.AB, based on WOMBAT2.AB
'       By Dan Branan
'       Original form: May 2001
'       Last revised: June 2001
'

        ===========================================================
=======
'       Program written for Open Path IR operation under Midac-
Grams/32.
'       This is version 1, with primary emphases:
'               1.  Initiate instrument
'               2.  Check resolution and alignment of instrument
'               3.  Collect sample spectrum.
'               3.  Collect T,P, and Wind speed readings
'               4.  Collect NO data from UV monochromator
'               5.  Collect measurement from laser transmissometer
'               6.  Calculate absorbance spectrum.
'               7.  Use KFIT2.AB to analyze sample spectrum.
(commented out)
'               8.  Re-collect T, P, Wind, NO, and transmissometer
data
'               9.  Record results in Excel-readable *.csv file.
'               10.  Repeat sample/analyze loop for ncycles.
'

        ===========================================================
=======

        free

'       Perform initialization portouts

        portout -44,-1          'enables error messages
```

```
        portout -22,-1          'array/trace index bounds check
on
        portout -24,-1          'special input returns (keeps
default if no new input)

        setzero 1e-25           'zero for matrix inversion

'       Initialize arrays

        dim name(256)                   'core of spectra names
        dim namet(256)                  'transmission spectra
        dim namea(256)                  'absorption spectra
        dim spcname(256)
        dim log(256)
        dim check(256)                   'log filename, name.csv
        dim scratch9(256)
        dim calname(256)        'calibration file used by kp
'       dim ch4cal(256)          'ch4 calibration file
'       dim n2ocal(256)          'n2o calibration file
'       dim co2cal(256)          'co2 calibration file
'       dim nh3cal(256)          'nh3 calibration file
        dim comment(256)        'comment for start of new
logfile
        dim ref(256)                    'reference
        dim time(256)
'       dim ch4(256)                    'methane array
'       dim n2o(256)                    'nitrous oxide array
'       dim co2(256)                    'carbon dioxide array
'       dim co(256)                     'carbon monoxide array
'       dim h2o(256)                    'water array
'       dim nh3(256)                    'ammonia array
'       dim sf6(256)                    'sulfur hexafluoride
array
'       dim ch4err(256)
'       dim n2oerr(256)
'       dim co2err(256)
'       dim coerr(256)
'       dim h2oerr(256)
'       dim nh3err(256)
'       dim sf6err(256)
'       dim resch4(256)
'       dim resn2o(256)
'       dim resco2(256)
'       dim resnh3(256)
        dim csvrow12(256)       'long row for labels in csv file


'       Indicate to user that program is running

        blank : pauseoff
```

```
        printline 10
        print "OPIEM.AB: running."



     '  Define constants and initialize variables

        shour=0.0
        sminute=0.0
        ssec=0.0

        CH4=0 : N2O=0 : CO2=0 : CO=0 : H2O=0 : NH3=0 : SF6=0




        printline 10
        print "OPIEM.AB: running."

1       onerror 2                              'goto 2 if error occurs
        open #3,"c:\mdgrams\opiem.def"              'reads current
defaults
             input #3,"",$name
             input #3,"",$comment
'             input #3,"",$ch4cal
'             input #3,"",$n2ocal
'             input #3,"",$co2cal
'             input #3,"",$nh3cal
'             input #3, gosf6
             input #3, nscans
             input #3, path
             input #3, ncycles
             input #3, irscan
             input #3, tp
             input #3, wind
             input #3, Opacity
             input #3, NO
             input #3, NOpath
        close #3
        onerror -1                             'resets onerror
2       close #3                               'closes file if error

        dialogbeg "BEFORE YOU BEGIN"
           Print "BEFORE you proceed, make sure the following
items are OPERATING, and connected to this computer:"
           print ""
           print "   1.  MIDAC FTIR"
           print "   2.  Anemometer (if desired)"
           print "   3.  Temperature and Pressure devices (if
desired)"
```

```
            print "    4.  Transmissometer (if desired)"
            print "    5.  UV Monochromator (if desired)"
            print ""
            dialogask irscan,3+64+128,0,0,
"Are_you_planning_to_collect_infrared_spectra?: No Yes"
            dialogask tp,3+64+128,0,0,
"Are_you_planning_to_collect_temperature_and_pressure_data?:
No Yes"
            dialogask wind,3+64+128,0,0,
"Are_you_planning_to_collect_wind_data?: No Yes"
            dialogask Opacity,3+64+128,0,0,
"Are_you_planning_to_collect_Opacity_data?: No Yes"
            dialogask NO,3+64+128,0,0,
"Are_you_planning_to_collect_NO_concentration_data?: No Yes"
            dialogask NOpath,0,1,1, "What is the pathlength of
between the UV source and the receiving telescope? (m)"
            print ""
            print "NOTE:  Set up the Anemometer with the U vector
pointing across the road."
            print ""
3       dialogend 6, 0, 5

4       dialogoff -10 : goto 6

5       goto 3

6       dialogbeg "OPIEM Setup"
            dialogask $name,2,40,40, "Core file name (no
extension)"
            dialogask $comment,2,40,255, "Comment (<256
chars)"
'           dialogask $ch4cal,2,40,40, "CH4 Calibration file
(.cll)"
'           dialogask $n2ocal,2,40,40, "N2O Calibration file
(.cll)"
'           dialogask $co2cal,2,40,40, "CO2 Calibration file
(.cll)"
'           dialogask $nh3cal,2,40,40, "NH3/SF6 Calibration
file (.cll)"
'           dialogask gosf6,3+64+128,0,0, "Is_SF6_present?:
No Yes"
            dialogask nscans,0,1,1, "Number of scans for each
spectrum"
            dialogask path,0,1,1, "Optical path (m)"
            dialogask ncycles,0,1,1, "Number of spectra to
collect (steps in loop)"
7       dialogend 10, 0, 9

8       dialogoff -10 : goto 10
```

```
9       goto 7

'       Store last entered values as defaults.
10      open #3, "c:\mdgrams\opiem.def"
               print #3, $name
               print #3, $comment
'               print #3, $ch4cal
'               print #3, $n2ocal
'               print #3, $co2cal
'               print #3, $nh3cal
'               print #3, gosf6
               print #3, nscans
               print #3, path
               print #3, ncycles
               print #3, irscan
               print #3, tp
               print #3, wind
               print #3, Opacity
               print #3, NO
               print #3, NOpath

        close #3

        nsteps=ncycles-1

'       Timing dialog.

        dialogbeg "TIMING"
               dialogask delay,3+64+128,0,0, "Start_Immediately?:
Yes No"
               dialogask strthr,0,0,0, "Start time, hour"
               dialogask strtmn,0,0,0, "Start time, minute"
               dialogask wtcycl,3+64+128,0,0,
"Wait_Between_Cycles?: No Yes"
               dialogask intrvl,0,0,0, "Cycle time interval,
minutes"
11      dialogend 10, 0, 13

12      dialogoff -10 : goto 14

13      if delay>0 then dialogset 8, 2 : dialogset 8, 3
        if delay=0 then dialogset 16, 2 : dialogset 16, 3
        if wtcycl>0 then dialogset 8, 5
        if wtcycl=0 then dialogset 16, 5
        goto 11

14      if ((strthr=0) and (strtmn=0)) then goto 25

'       Wait until start time to begin.
```

```
             if wtcycl=0 then goto 33

             cyctim=clock(0)
             ctime=cyctim+(intrvl*60)

             if ctime>=86400 then ctime=ctime-86400 : mnflg1=1

     '       Set up spectrum file name.

     33      if ic=0 then string $namet = $namet + "01"
             if ic>0 then string $namet, 0         'increments name of
     cycle

     34      if irscan=0 then print "Collecting Environmental and/or
     NO data.  Press ESC to stop collection"
     '       Gather DAQ board readings if indicated
     '       BEFORE the IR spectrum is collected
             if tp=1 then 35 else 39

     35      gosub 5000
             pretemperature=temperature
             prepressure=pressure

     '       Gather wind speed data if indicated
     '       BEFORE the IR spectrum is collected
     39      if wind=1 then 40 else 41
     40      gosub 6000
             preu=u
             prevee=vee
             prew=w

     '       Gather NO concentration data if indicated
     '       BEFORE the IR spectrum is collected
     41      if NO=1 then 42 else 43
     42      gosub 7000
             preNO=NOppm/NOpath

     '       Gather opacity data if indicated
     '       BEFORE the IR spectrum is collected
     43      if Opacity=1 then 44 else 50
     44      gosub 8000
             preOpacity=ratio



     '       Collect sample spectrum.

     50      if irscan=0 goto 90
             driver 1,$namet,3,nscans,1,3,4000,700,0,1,1,"sample
     spectrum"
```

```
'       Call routine to calculate absorbance spectrum
75      gosub 20000

'       Call routine to do CLS fit   (COMMENTED OUT JUNE 2001,
DAN BRANAN)
'        gosub 30000


        if ic=nsteps goto 160             'end of loop

'       Wait until interval cycle time to start next cycle.

90      if wtcycl=1 then goto 100         'go through interval wait
code
        if wtcycl=0 then goto 160         'no interval wait, so end
of loop

100     if chwt=1 then goto 160           'start next cycle right
after chmbr action
        ccheck=clock(0)
        if mnflg1=0 goto 105
        if mnflg1=1 then ccheck=0 : mnflg1=2 : goto 105
        if mnflg1=2 goto 103
103     if ccheck>82800 goto 100
        if ccheck=0 then mnflg1=0 : goto 105

105     hcheck=int(ctime/3600)
        if hcheck >= 24 then htime=hcheck-24
        if hcheck < 24 then htime=hcheck
        mtime=int(((ctime/3600)-hcheck)*60)
        stime=ctime-(hcheck*3600)-(mtime*60)

        blank : pauseoff
        printline 5
        print "OPIEM.AB: waiting until next cycle."
'        print " "
        print "Current cycle is ";ic+1;" of ";ncycles
'        print " "
        if tp=1 then print "DAQ BOARD      TEMP : ";temperature;"
Kelvin"
        if tp=1 then print "                PRESS: ";pressure;"
Torr"
        if wind=1 then print "             Across Road Wind:
";u;" mph"
        if wind=1 then print "             Along Road Wind:
";v;" mph"
        if wind=1 then print "             Vertical Wind:
";w;" mph"
```

C-8

```
       print " "
'       print "FTIR            H2O : ";H2O(ic);" %"
'       print "               CO2 : ";CO2(ic);" ppm"
'       print "               N2O : ";N2O(ic);" ppm"
'       print "                CO : ";CO(ic);" ppm"
'       print "               CH4 : ";CH4(ic); " ppm"
'       print "               NH3 : ";NH3(ic);" ppm"
'       if gosf6=1 then print "                       SF6 : ";SF6(ic);"
ppm"
'       print " "
       print "Next cycle starts at
";htime;":";mtime;":";stime;"."
       printline 24
       print "Current time ";clock(-4);":";clock(-
3);":";clock(-2);"."
110    if(not(clock(1))) goto 110

       if ccheck<ctime then goto 100
       if ccheck>ctime then goto 150
       if ccheck=ctime then goto 160

150    dialogbeg "ERROR"
            print "Timing error!"
            print "Check interval."
            print " "
       dialogend
       stop

'      Loop back for next cycle.

'      Gather DAQ board readings if indicated
'      AFTER the IR spectrum is collected
       if irscan=0 then 200
       if tp=1 then 160 else 165
160     gosub 5000
       posttemperature=temperature
       postpressure=pressure

'      Gather wind speed data if indicated
'      AFTER the IR spectrum is collected
165.   if wind=1 then 170 else 171
170    gosub 6000
       postu=u
       postvee=vee
       postw=w

'      Gather NO concentration data if indicated
'      AFTER the IR spectrum is collected
171    if NO=1 then 172 else 173
172    gosub 7000
```

```
            postNO=NOppm/NOpath

'       Gather opacity data if indicated
'       AFTER the IR spectrum is collected
173     if Opacity=1 then 174 else 200
174     gosub 8000
        postOpacity=ratio



'       Call routine to write results out to CSV file
200     gosub 50000

        if irscan=0 goto 34
        if irscan=1 then next ic

'       End of program.

        dialogbeg "STOP"
              print "Successful completion of OPIEM.AB."
              print " "
        dialogend

        end

'=================================================================
=
'       Subroutine gather temperature and pressure data

5000    byte1=0
        byte2=0
        byte3=0
        byte4=0
        temp1=0
        temperature=0
        press1=0
        pressure=0
        i=0
        tpsamples=1000        'Number of samples to collect and
average

'       Read temperature from channel 0.
        for i=1 to tpsamples
          portout 770, 0     'set to read A/D chn 0
          portout 769,0        'clear registers start A\D
          portout 769,0
          portout 769,0
          portout 769,0
          portout 769,0
          portout 769,0
```

```
          portout 769,0
          portout 769,0

          portin 768, byte1          'byte1
          byte1=byte1/16      'shift first word to the right
          portin 769, byte2          'byte2
          byte2=byte2*16      ' shift second word to the left
          temp1=byte1+byte2      'combine the two words in the
proper order
          temperature=temperature+temp1

        next i

        i=0                    'Re-set index

'       Read pressure from channel 1
        for i=1 to tpsamples
          portout 770, 1  'set to read A/D chn 1
          portout 769,0       'clear registers start A\D
          portout 769,0        'several no-ops placed to clear A/D
coversion
          portout 769,0
          portout 769,0
          portout 769,0
          portout 769,0
          portout 769,0
          portout 769,0

          portin 768, byte3          'byte3
          byte3=byte3/16      'shift first word to the right
          portin 769, byte4          'byte4
          byte4=byte4*16      ' shift second word to the left
          press1=byte3+byte4      'combine the two words in the
proper order
          pressure=pressure+press1

        next i


'       Conversion factors
        temperature = (0.2244*(temperature/tpsamples))-707.91
        temperature = temperature+273

        pressure = (0.4191*(pressure/tpsamples))-796.53

        return

'=============================================================
=
'       Subroutine gather wind data
```

```
'       Read from channel 2, "U"

6000   r=0
       u=0
       utemp=0
       uneg=1
       vee=0
       vtemp=0
       vneg=1
       w=0
       wtemp=0
       byte5=0
       byte6=0
       byte7=0
       byte8=0
       byte9=0
       byte10=0
       i=0
       wsamples=1000

       portout 770, 2           'set to read A/D chn 2

       for i=1 to wsamples
         portout 769,0          'clear registers start A\D
         portout 769,0
         portout 769,0
         portout 769,0
         portout 769,0
         portout 769,0
         portout 769,0
         portout 769,0
         portin 768, byte5          'byte5
         byte5=byte5/16     'shift first word to the right
         portin 769, byte6          'byte6
         byte6=byte6*16     ' shift second word to the left
         utemp=byte5+byte6      'combine the two words in the
proper order
         u=utemp+u         'Running total of readings
       next i

       u=u/wsamples                   'Take average of 100
readings

       i=0               'Reset index


'       Read from channel 3, "V".

       portout 770, 3            'set to read A/D chn 3
```

C-12

```
        for i=1 to wsamples
          portout 769,0      'clear registers start A\D
          portout 769,0      'several no-ops placed to clear A/D
coversion
          portout 769,0
          portout 769,0
          portout 769,0
          portout 769,0
          portout 769,0
          portout 769,0
          portin 768, byte7       'byte7
          byte7=byte7/16     'shift first word to the right
          portin 769, byte8       'byte8
          byte8=byte8*16     ' shift second word to the left
          vtemp=byte7+byte8    'combine the two words in the
proper order
          vee=vtemp+vee            'Running total of readings
        next i

        vee=vee/wsamples

        i=0                  'Reset index


        'Read from channel 4, "W"

        portout 770, 4             'set to read A/D chn 4

        for i=1 to wsamples
          portout 769,0      'clear registers start A\D
          portout 769,0      'several no-ops placed to clear A/D
coversion
          portout 769,0
          portout 769,0
          portout 769,0
          portout 769,0
          portout 769,0
          portout 769,0
          portin 768, byte9       'byte9
          byte9=byte9/16     'shift first word to the right
          portin 769, byte10       'byte10
          byte10=byte10*16          'shift second word to the
left
        wtemp=byte9+byte10     'combine the two words in the
proper order
          w=wtemp+w          'Running total of readings
        next i
```

C-13

```
      w=(w/wsamples)
                                  'and apply correction factor
      i=0                  'Reset index

'Conversions
      u=0.02270*u-46.3698
      vee=0.02270*vee-46.3698
      w=1.25*(0.02270*w-46.3698)

'Determine larger of the U and V components
      if u<0 then uneg=-1 else uneg=1
      if vee<0 then vneg=-1 else vneg=1

      if abs(u)>abs(vee) then 6020 else 6030


6020    gosub 6100

goto 6040

6030    gosub 6200


6040    'End of Subroutine
         return



'sub-subroutines
' Apply correction factors to U and V components

6100    bigger=abs(u)
        smaller=abs(vee)
        gosub 6300
        u=bigger*uneg
        vee=smaller*vneg
        return 6040

6200    bigger=abs(vee)
        smaller=abs(u)
        gosub 6300
        u=smaller*uneg
        vee=bigger*vneg
        return 6040

6300    r=smaller/bigger

        'Calculate and apply correction factor for bigger value
        bcorrection=(0.1642*r^6)-(0.374*r^5)+(0.4567*r^4)-
(0.4365*r^3)+(0.3537*r^2)-(0.0347*r)+1.0003
```

C-14

```
        bigger=bigger*bcorrection

        'Calculate and apply correction factor for smaller value
        scorrection=(0.0836*r^6)-(0.7222*r^5)+(1.6481*r^4)-
(1.4847*r^3)+(0.383*r^2)-(.0281*r)+1.2502
        smaller=smaller*scorrection
        return


'================================================================
=
'       Subroutine gather NO data from UV monochromator

7000    NOppm=0
        NOtemp=0
        byte1=0
        byte2=0
        i=0
        nosamples=1000

'       Read from channel 5.
        for i=1 to nosamples      'same number of samples as
temperature and pressure
          portout 770, 5 'set to read A/D chn 0
          portout 769,0        'clear registers start A\D
          portout 769,0
          portout 769,0
          portout 769,0
          portout 769,0
          portout 769,0
          portout 769,0
          portout 769,0

          portin 768, byte1          'byte1
          byte1=byte1/16     'shift first word to the right
          portin 769, byte2          'byte2
          byte2=byte2*16     ' shift second word to the left
          NOtemp=byte1+byte2     'combine the two words in the
proper order
          NOppm=NOppm+NOtemp

        next i

        NOppm=NOppm/nosamples
        NOppm=(NOppm*0.7229)-1477.5      'NOTE: this is ppm-meters
and must
                                    'be divided by the pathlength
to get ppm.
        return
```

```
'================================================================
=
8000  '       Subroutine to gather opacity data from
transmissometer

'       Initialize local variables
        samplenum=1000
        i=0


'       Read reference from channel 6.
        byte1=0
        byte2=0
        ref1=0
        ref2=0

        for i=1 to samplenum
          portout 770, 6    'set to read A/D chn 0
          portout 769,0        'clear registers start A\D
          portout 769,0
          portout 769,0
          portout 769,0
          portout 769,0
          portout 769,0
          portout 769,0
          portout 769,0

          portin 768, byte1          'byte1
          byte1=byte1/16     'shift first word to the right
          portin 769, byte2          'byte2
          byte2=byte2*16     ' shift second word to the left
          ref1=byte1+byte2     'combine the two words in the
proper order
          ref2=ref2+ref1

        next i

        reference=ref2/samplenum
        i=0                    'Re-set index

'       Read sample from channel 7
        byte3=0
        byte4=0
        samp1=0
        samp2=0

        for i=1 to samplenum
          portout 770, 7  'set to read A/D chn 1
          portout 769,0        'clear registers start A\D
```

C-16

```
            portout 769,0        'several no-ops placed to clear A/D
coversion
            portout 769,0
            portout 769,0
            portout 769,0
            portout 769,0
            portout 769,0

            portin 768, byte3        'byte3
            byte3=byte3/16     'shift first word to the right
            portin 769, byte4        'byte4
            byte4=byte4*16     ' shift second word to the left
            samp1=byte3+byte4      'combine the two words in the
proper order
            samp2=samp2+samp1

        next i

        sample=samp2/samplenum
        i=0

'Conversions
        ratio=reference        '/sample

    return
'================================================================
===
'       Initialize log file

10000 open "C",#4,$log
        string $csvrow12="Date-Time,"
        string $csvrow12=$csvrow12 + "Spectrum,"
        if tp=1 then string $csvrow12=$csvrow12 + "T (K),"
        if tp=1 then string $csvrow12=$csvrow12 + "P (Torr),"
        if wind=1 then string $csvrow12=$csvrow12 + "Across Road
Wind (mph),"
        if wind=1 then string $csvrow12=$csvrow12 + "Along Road
Wind (mph),"
        if wind=1 then string $csvrow12=$csvrow12 + "Vertical
Wind (mph),"
        if NO=1 then string $csvrow12=$csvrow12 + "[NO] ppm,"
        if Opacity=1 then string $csvrow12=$csvrow12 +
"Opacity,"
'        string $csvrow12=$csvrow12 + "[H2O] %,"
'        string $csvrow12=$csvrow12 + "SE,"
'        string $csvrow12=$csvrow12 + "[CH4] ppm,"
'        string $csvrow12=$csvrow12 + "SE,"
'        string $csvrow12=$csvrow12 + "[N2O] ppm,"
'        string $csvrow12=$csvrow12 + "SE,"
```

```
'         string $csvrow12=$csvrow12 + "[CO2] ppm,"
'         string $csvrow12=$csvrow12 + "SE,"
'         string $csvrow12=$csvrow12 + "[CO] ppm,"
'         string $csvrow12=$csvrow12 + "SE,"
'         string $csvrow12=$csvrow12 + "[NH3] ppm,"
'         string $csvrow12=$csvrow12 + "SE,"
'         if gosf6=1 then string $csvrow12=$csvrow12 + "[SF6]
ppm,"
'         if gosf6=1 then string $csvrow12=$csvrow12 + "SE,"
'         string $csvrow12=$csvrow12 + "resCH4,"
'         string $csvrow12=$csvrow12 + "resN2O,"
'         string $csvrow12=$csvrow12 + "resCO2,"
'         string $csvrow12=$csvrow12 + "resNH3,"
        if tp=1 then string $csvrow12=$csvrow12 + "T (K),"
        if tp=1 then string $csvrow12=$csvrow12 + "P (Torr),"
        if wind=1 then string $csvrow12=$csvrow12 + "Across Road
Wind (mph),"
        if wind=1 then string $csvrow12=$csvrow12 + "Along Road
Wind (mph),"
        if wind=1 then string $csvrow12=$csvrow12 + "Vertical
Wind (mph),"
        if NO=1 then string $csvrow12=$csvrow12 + "[NO] ppm,"
        if Opacity=1 then string $csvrow12=$csvrow12 +
"Opacity,"

        print #4, $log
        print #4, "OPIEM run"
        print #4, $comment
        print #4, "Date:,"; clock(-6); "/"; clock(-5); "/";
clock(-7)
'        print #4, "CH4 calname:,";$ch4cal
'        print #4, "N2O calname:,";$n2ocal
'        print #4, "CO2 calname:,";$co2cal
'        print #4, "NH3 calname:,";$nh3cal
'        print #4, " "
        print #4, $csvrow12
        close #4

        return


'================================================================
===
'      Calculate absorbance spectrum.

20000 loadspc $namet
        #1=t2a(#1)
        string $namea=$namet + "a"
        savespc $namea
        noshow
        return
```

C-18

```
'===============================================================
===
'       Do CLS fit, and correct for T and P variations
'
'       All calibration files must be created before program is
run.
'       To avoid confusion, the following component ordering
scheme is
'       followed when creating the calibration files:
'              ** Components must be listed in MALT in numerical
order
'              by their HITRAN database identification number
(e.g.
'              H2O has id number 1, so it is always listed
first).

30000 string $spcname=$namea
      loadspc $spcname
      lshift=1              'do all fits with cm-1 shift

'       Do CH4 cal region (CH4 and H2O)
'       When creating cal file, ensure components match:
'       Yn(0) = H2O
'       Yn(1) = CH4

      string $calname = $ch4cal
      gosub 40000
      H2O(ic)=Yn(0)
      CH4(ic)=Yn(1)
      H2Oerr(ic)=SE(0)
      CH4err(ic)=SE(1)
      resCH4(ic)=rmsres
      noshow : noshow : noshow

'       Do N2O cal region (N2O and CO)
'       When creating cal file, ensure components match:
'       Yn(0) = H2O
'       Yn(1) = CO2
'       Yn(2) = N2O
'       Yn(3) = CO

      loadspc $spcname
      string $calname = $n2ocal.
      gosub 40000
      N2O(ic)=Yn(2)
      CO(ic)=Yn(3)
      N2Oerr(ic)=SE(2)
      COerr(ic)=SE(3)
      resN2O(ic) = rmsres
```

```
          noshow : noshow : noshow

'         Do CO2 cal region (CO2)
'         When creating cal file, ensure components match:
'         Yn(0) = H2O
'         Yn(1) = CO2
'         Yn(2) = N2O
'         Yn(3) = CO

          loadspc $spcname
          string $calname = $co2cal
          gosub 40000
          CO2(ic)=Yn(1)
          CO2err(ic)=SE(1)
          resCO2(ic) = rmsres
          noshow : noshow : noshow

          if gosf6=1 goto 35000

'         Do NH3 cal region (NH3)
'         When creating cal file, ensure components match:
'         Yn(0) = H2O
'         Yn(1) = NH3

          loadspc $spcname
          string $calname = $nh3cal
          gosub 40000
          NH3(ic)=Yn(1)
          NH3err(ic)=SE(1)
          resNH3(ic) = rmsres
          noshow : noshow : noshow
          return

'         Do NH3 cal region with SF6 present (NH3 & SF6)
'         When creating cal file, ensure components match:
'         Yn(0) = H2O
'         Yn(1) = NH3
'         Yn(2) = SF6

35000 loadspc $spcname
          string $calname = $nh3cal
          gosub 40000
          NH3(ic)=Yn(1)
          NH3err(ic)=SE(1)
          SF6(ic)=Yn(2)
          SF6err(ic)=SE(2)
          resNH3(ic)=rmsres
          noshow : noshow : noshow

          return
```

C-20

```
'================================================================
=
'       Subroutine to fit #s by CLS with wavenumber shift

40000 open "O",#1,$calname
      free cname, bands, flags, Kaug, Km, covm, Yn, SE
      dim flags(40)
      read #1, i,m,p,sp,sfp,slp,flags
      dim cname(m,15), bands(flags(1),4), Kaug(m+1,p),
Km(m,p), covm(m,m),
Yn(m),SE(m)
      read #1, cname,bands,Kaug
      close #1
      Km=Kaug
      ncpt=m
      fitleft=bands(0,0) : fitright=bands(0,1)

      ncpt = m
      fitleft=bands(0,0): fitright = bands(0,1)

      npt=npts(#s)

'       Fit spectrum without shift

      if lshift = 1 goto 40005
      chain "kp2.ab":
      return

'       Fit spectrum with shift
40005 shift=0
      dsig=abs(getffp()-getflp())/(npts(#s)-1)
      np=npts(#s(fitleft,fitright))
      n=1       '1024
40010 n=n*2
      if n<np goto 40010
      n=n*2
      nq=int((n-np)/2)
      x=int(fitleft/dsig)*dsig : if (fitleft-x)>(x+dsig-
fitleft) then x=x+dsig

      if fitleft>fitright then dsig=-dsig
      sigL1=x-nq*dsig                              'sigL1 &
sigR1 define the
      sigR1=sigL1+(n-1)*dsig                       'extended
region (spec+ramps)

      if dsig<0 goto 40020

      if getffp() > getflp() then XFLIP
```

```
        ffp = getffp() : flp = getflp()
        if ffp <= sigL1 then sigL2=sigL1 else sigL2=ffp
'sigL2 and sigR2
define the
        if flp >= sigR1 then sigR2=sigR1 else sigR2=flp
'region of #s to
be extracted
        goto 40030

40020 if getffp() < getflp() then XFLIP
        ffp = getffp() : flp = getflp()
        if ffp >= sigL1 then sigL2=sigL1 else sigL2=getffp()
        if flp <= sigR1 then sigR2=sigR1 else sigR2=getflp()

40030 'Create extended region with ramp for shifting in array
"scratch"
        dim scratch(n)
        scratch=0
        n1 = (sigL2-sigL1)/dsig
        n2 = (sigR2-sigL1)/dsig
        scratch(n1,n2) = #s(sigL2,sigR2)
'fill scratch with
#s(sigL2,sigR2)

        newspc scratch1(n) : setffp sigL1,sigR1
        #s=scratch
        savespc "scratch1" : noshow

'       Add ramp edges to "scratch"

        nrampts=n/4

        fillbeg 0
        fillinc scratch(nrampts)/nrampts
        scratch(0,nrampts-1)=fill(scratch)

        inc = scratch(n-1-nrampts)/nrampts
        fillbeg scratch(n-1-nrampts)-inc
        fillinc -inc
        scratch(n-1-nrampts,n-1)=fill(scratch)

        newspc scratch1(n) : setffp sigL1,sigR1
        #s=scratch
        savespc "scratch2"
        savespc "temp.spc"
        free scratch

        goto 40050

'       Diagnostics
```

```
          sigL3=sigL1+nrampts*dsig
          sigR3=sigL1+(3*nrampts-1)*dsig
'          dialogon
'           print "getffp, getflp",ffp,flp
'           print "fitleft, fitright", fitleft,fitright
'           print "rampleft,rampright",sigL3,sigR3
'           print "extended region", sigL1,sigR1
'           print "dsig",dsig
'           print "npts in disk spectrum", npt
'           print "nppts in fit region",np
'           print "npts in extended region",n
'           print "nq=point extension",nq
'           print "cm-1 extension", dsig*nq
'          dialogoff
          loadspc "scratch1"
          loadspc "scratch2"
          stop

'     End of new ramp calculation as per D.G. Oct 97

'     Continue

40050 count=0
      x=0                    'initial x
      xinc=dsig              'initial x increment
      blank
'      pauseoff
'      blank :printline 2
'      print "File: ";$spcname;
'      if ns>1 then print " #";nsub;
'      print "   Calibration: ";$calname
'      print "count","shift","increment","resid"
      chain "kp2.ab"
'      print count,x,xinc,rmsres
      x1=x
      r1=rmsres

'     main iteration loop
40100 count=count+1
      if count>200 then print "200 iterations -
stopped",dsig,xinc,r1,rmsres
: print #5, "too many interations": return
      x=x+xinc
      noshow
      noshow
      noshow
      loadspc "temp.spc"
      shift=x
      gosub 40400                'Shift #s by <shift> cm-1
```

```
'          print "File: ";$spcname;
'           if ns>1 then print " #";nsub;
'           printline 23
'           print "     Calibration: ";$calname
'           print "count","shift","increment","resid"
          chain "kp2.ab"
'           print count,x,xinc,rmsres
          if count=1 and rmsres>r1 then goto 40200
          if abs(r1/rmsres-1)<0.01 and abs(xinc)<abs(dsig)/64 goto
40300
          if rmsres<r1 then x0=x1 : r0=r1 : x1=x : r1=rmsres :
goto 40100
          if rmsres<r0 then xinc=xinc/2 else xinc=-xinc/2
          x=x1 : rmsres=r1 : goto 40100
          if rmsres<r1 then x1=x : r1=rmsres : goto 40100
          goto 40300

40200 r0=rmsres
      x0=x
      x=0
      rmsres=r1
      xinc=-xinc
      goto 40100

40300 if rmsres<r1 goto 40310
      loadspc "temp.spc"
      shift=x1
      gosub 40400                      ' Shift #s by <shift> cm-1
      chain "kp2.ab"

'40310 print count,x,xinc,rmsres
40310 return


'================================================================
===
'      Subroutine to shift #s by <shift> wavenumbers.
'
'      Uses IGM*complex exponential method
'      ref: AB manual p 60 for basis
'
'      Requires #s, <shift> to be pre-defined
'
40400 ds=abs(getffp()-getflp())/(npts(#s)-1)     ' Spectrum pt.
spacing
      rfft #s
      np=npts(#s)          ' # real points (power of 2)
      npc=np/2+1           ' # complex points
      dim cf(2,npc)
      fillbeg 0 : fillinc 1/(ds*np)          ' =
1/(2*ds*npc)=OPD/npc
```

```
            cf(0)=cos(-fill(cf(0))*2*pi_value*shift)
            cf(1)=sin(-fill(cf(1))*2*pi_value*shift)
            cf(1,0)=cf(0,npc-1)
            transpose cf
            #s=crmul(#s,cf)
            RIFFT #s
            free cf,ds,np,npc
            return


      '==================================================================
      =====
      '      Update CSV file with analysis information

      50000 open "O", #4, $log : seek #4, -0     'go to end of log
      file
            string $scratch9 = $namea + ".spc"
            print #4, clock(-6); "/"; clock(-5); "/"; clock(-7); "
      "; clock(-4); ":";clock(-3); ",";
            print #4, $scratch9; ",";
            if tp=1 then print #4, pretemperature;",";
            if tp=1 then print #4, prepressure;",";
            if wind=1 then print #4, preu;",";
            if wind=1 then print #4, prevee;",";
            if wind=1 then print #4, prew;",";
            if NO=1 then print #4, preNO;",";
            if Opacity=1 then print #4, preOpacity
      '       print #4, H2O(ic); ",";
      '       print #4, H2Oerr(ic); ",";
      '       print #4, CH4(ic); ",";
      '       print #4, CH4err(ic); ",";
      '       print #4, N2O(ic); ",";
      '       print #4, N2Oerr(ic); ",";
      '       print #4, CO2(ic); ",";
      '       print #4, CO2err(ic); ",";
      '       print #4, CO(ic); ",";
      '       print #4, COerr(ic); ",";
      '       print #4, NH3(ic); ",";
      '       print #4, NH3err(ic); ",";
      '       if gosf6=1 then print #4, SF6(ic); ",";
      '       if gosf6=1 then print #4, SF6err(ic); ",";
      '       print #4, resCH4(ic); ",";
      '       print #4, resN2O(ic); ",";
      '       print #4, resCO2(ic); ",";
      '       print #4, resNH3(ic); ",";
            if irscan=0 then 51000
            if tp=1 then print #4, ",";posttemperature;",";
            if tp=1 then print #4, postpressure;",";
            if wind=1 then print #4, postu;",";
            if wind=1 then print #4, postvee;",";
            if wind=1 then print #4, postw;",";
```

```
        if NO=1 then print #4, postNO;",";
        if Opacity=1 then print #4, postOpacity
51000

    close #4

    return
```

Program: DBFit.ab
Purpose: To fit FTIR Spectra with up to four calibration files and output the results to a comma-delimited ASCII file.
Written by: Dr. Kim Bradley, University of Denver
Modified by: Dan Branan, University of Denver

```
' Refitting program using 4 .cll files CH4,N2O,CO2,NH3
'=========================================================
'        Program DBFIT.AB (written for GRAMS/32)
'        By Daniel Branan
'        Based on BioReFIT.AB by Jeff Webber
'        Original Form: June 2001
'        Last Updated: June 2001
'=========================================================
'        This program reads in a text file containing the
'        names of absorbance spectra and the temperatures
'        and pressures at which they were collected, then
'        fits these spectra using 4 previously created
'        calibration files.  The output
'        from this program is a *.CSV file, which contains
'        component concentration information and fitting
'        statistics for each spectrum.
'=========================================================

        free
        portout -44,-1              'enables error messages
        portout -22,-1              'array/trace index bounds
check on
        portout -24,-1              'special input returns (keeps
default if no new input)

'       Initialize arrays

        dim infile(256)
        dim calname(256)
        dim spcname(256)
        dim output(256)
        dim text1(256)
        dim csvrow12(256)
        dim comma(15)
        dim test(10)
        dim labels(256)
        dim result(256)
        dim strnum(256)
        dim strtmp(256)
        dim strprs(256)
        dim species(6)
        dim stderr(6)
        dim ch4cal(256)
```

```
        dim n2ocal(256)
        dim co2cal(256)
        dim nh3cal(256)
        dim no2cal(256)

        setzero 1.0E-25

        species=0

        menufile $infile, "Select Input File: *.csv"

        menufile $output, "Select Output File: *.csv"

'       Identify defaults.  User feel free to change these.

        string $ch4cal=""
        string $n2ocal=""
        string $nh3cal=""
        string $no2cal=""

        numspec=10
        lshift=1


        dialogbeg "FMFIT.AB"
                dialogask numspec,0,1,1, "Number of spectra to
fit"
                dialogask lshift,3,0,0,"Fit_with_shift?"
              print " "
        dialogend

        menufile $ch4cal, "Select CH4 calibration file: *.cll"
        menufile $n2ocal, "Select N2O, CO, CO2 calibration
file: *.cll"
        menufile $nh3cal, "Select NH3 calibration file: *.cll"
'        menufile $no2cal, "Select NO2 calibration file:
*.cll"


'       Set up output file

        gosub 8000

        open "O",#3,$infile


100     for ic=1 to numspec

        input #3, "", $text1
```

```
'          gosub 9000

'          string $spcname=$text1(0,comma(1)-1)
'          string text1(comma(1)+1,comma(2)-1),-20 : tmp=v
'          string text1(comma(2)+1,255),-20 : press=v

          string $spcname=$text1


'          pauseon
'          printline 10
'          print "spcname is ",$spcname

'          Go analyze

          gosub 9500

'          Print results out to output file

          gosub 20000

          next ic

          dialogbeg
                  print "Successful completion of DBFIT.AB"
                  print " "
          dialogend

          noshow : noshow : noshow

          close #1
          close #3
          close #4

          stop
          end
'================================================================
=
'          Set up header for output file
'
8000      open "C",#4,$output
          string $csvrow12=$csvrow12 + "Spectrum,"
          string $csvrow12=$csvrow12 + "[H2O] %,"
          string $csvrow12=$csvrow12 + "SE,"
          string $csvrow12=$csvrow12 + "[CO2] ppm,"
          string $csvrow12=$csvrow12 + "SE,"
          string $csvrow12=$csvrow12 + "[CO] ppm,"
          string $csvrow12=$csvrow12 + "SE,"
          string $csvrow12=$csvrow12 + "[N2O] ppm,"
          string $csvrow12=$csvrow12 + "SE,"
```

C-29

```
          string $csvrow12=$csvrow12 + "[CH4] ppm,"
          string $csvrow12=$csvrow12 + "SE,"
          string $csvrow12=$csvrow12 + "[NH3] ppm,"
          string $csvrow12=$csvrow12 + "SE,"
'          string $csvrow12=$csvrow12 + "[NO2] ppm,"
'          string $csvrow12=$csvrow12 + "SE,"


          print #4, "DBFIT.ab Refits"
          print #4, "Date:,"; clock(-6); "/"; clock(-5); "/";
clock(-7)
          print #4, "CH4 calname:,";$ch4cal
          print #4, "N2O calname:,";$n2ocal
          print #4, "NH3 calname:,";$nh3cal
'          print #4, "NO2 calname:,";$no2cal
          print #4, " "
          print #4, $csvrow12

          close #4

          return


'================================================================
=
'          Find indices of commas in string text(256)

9000   j=0 : comma=0
       for i=0 to 255
          if text1(i)=44 then j=j+1 : comma(j)=i
          if j>13 then i=255
       next i
       return
'================================================================
===
'          Do CLS fit
'
'          All calibration files must be created before program
is run.
'          To avoid confusion, the following component ordering
scheme is
'          followed when creating the calibration files:
'                  ** Components must be listed in MALT in
numerical order
'                  by their HITRAN database identification
number (e.g.
'                  H2O has id number 1, so it is always listed
first).

9500   loadspc $spcname
```

```
            lshift=1                      'do all fits with cm-1 shift


'           Do CH4 cal region (CH4 and H2O)
'           For FORMLD.AB, get CH4 only here (H2O later).
'           When creating cal file, ensure components match:
'           Yn(0) = H2O
'           Yn(1) = CH4

'            pauseon
'            printline 20
'            print "ch4cal is ",$ch4cal

            string $calname = $ch4cal
            gosub 9700
            CH4=Yn(1)
            CH4err=SE(1)
            resCH4=rmsres
            noshow : noshow : noshow

'           Do N2O cal region (N2O, CO and CO2)
'           For FORMLD.AB get H2O here.
'           When creating cal file, ensure components match:
'           Yn(0) = H2O
'           Yn(1) = CO2
'           Yn(2) = N2O
'           Yn(3) = CO

            loadspc $spcname
            string $calname = $n2ocal

'            pauseon
'            printline 20
'            print "n2ocal is ",$n2ocal

            gosub 9700
            H2O=Yn(0)
            CO2=Yn(1)
            N2O=Yn(2)
            CO=Yn(3)
            H2Oerr=SE(0)
            CO2err=SE(1)
            N2Oerr=SE(2)
            COerr=SE(3)
            resN2O = rmsres
            noshow : noshow : noshow


'           Do NH3 cal region (NH3)
'           When creating cal file, ensure components match:
```

```
'          Yn(0) = H2O
'          Yn(1) = CO2
'          Yn(2) = NH3


          loadspc $spcname
          string $calname = $nh3cal

'          pauseon
'          printline 20
'          print "nh3cal is ",$nh3cal

          gosub 9700
          nh3=Yn(2)
          nh3err=SE(2)
          resnh3 = rmsres
          noshow : noshow : noshow

'          Do NO2 cal region (NO2)
'          When creating cal file, ensure components match:
'          Yn(0) = H2O
'          Yn(1) = CH4
'          Yn(2) = NO2


'          loadspc $spcname
'          string $calname = $no2cal

'          pauseon
'          printline 20
'          print "no2cal is ",$no2cal

'          gosub 9700
'          no2=Yn(2)
'          no2err=SE(2)
'          resno2 = rmsres
'          noshow : noshow : noshow


'          if gosf6=1 goto 35000

          return

'================================================================
=
'     Subroutine to fit #s by CLS with wavenumber shift

9700    open "O",#1,$calname
          free cname, bands, flags, Kaug, Km, covm, Yn, SE
          dim flags(40)
```

C-32

```
          read #1, i,m,p,sp,sfp,slp,flags
          dim cname(m,15), bands(flags(1),4), Kaug(m+1,p),
Km(m,p), covm(m,m), Yn(m),SE(m)
          read #1, cname,bands,Kaug
          close #1
          Km=Kaug
          ncpt=m
          fitleft=bands(0,0) : fitright=bands(0,1)

          ncpt = m
          fitleft=bands(0,0): fitright = bands(0,1)

          npt=npts(#s)

'         Fit spectrum without shift

          if lshift = 1 goto 10005
          chain "kp2.ab":
          return

'         Fit spectrum with shift
10005     shift=0
          dsig=abs(getffp()-getflp())/(npts(#s)-1)
          np=npts(#s(fitleft,fitright))
          n=1      '1024
10010     n=n*2
          if n<np goto 10010
          n=n*2
          nq=int((n-np)/2)
          x=int(fitleft/dsig)*dsig : if (fitleft-x)>(x+dsig-
fitleft) then x=x+dsig

      if fitleft>fitright then dsig=-dsig
      sigL1=x-nq*dsig
'sigL1 & sigR1 define the
      sigR1=sigL1+(n-1)*dsig
'extended region (spec+ramps)

      if dsig<0 goto 10020

      if getffp() > getflp() then XFLIP
      ffp = getffp() : flp = getflp()
      if ffp <= sigL1 then sigL2=sigL1 else sigL2=ffp
'sigL2 and sigR2 define the
      if flp >= sigR1 then sigR2=sigR1 else sigR2=flp
'region of #s to be extracted
      goto 10030

10020 if getffp() < getflp() then XFLIP
      ffp = getffp() : flp = getflp()
```

```
          if ffp >= sigL1 then sigL2=sigL1 else sigL2=getffp()
          if flp <= sigR1 then sigR2=sigR1 else sigR2=getflp()

10030 'Create extended region with ramp for shifting in array
"scratch"
          dim scratch(n)
          scratch=0
          n1 = (sigL2-sigL1)/dsig
          n2 = (sigR2-sigL1)/dsig
          scratch(n1,n2) = #s(sigL2,sigR2)
'fill scratch with #s(sigL2,sigR2)

          newspc scratch1(n) : setffp sigL1,sigR1
          #s=scratch
          savespc "scratch1" : noshow

'      Add ramp edges to "scratch"

          nrampts=n/4

          fillbeg 0
          fillinc scratch(nrampts)/nrampts
          scratch(0,nrampts-1)=fill(scratch)

          inc = scratch(n-1-nrampts)/nrampts
          fillbeg scratch(n-1-nrampts)-inc
          fillinc -inc
          scratch(n-1-nrampts,n-1)=fill(scratch)

          newspc scratch1(n) : setffp sigL1,sigR1
          #s=scratch
          savespc "scratch2"
          savespc "temp.spc"
          free scratch

          goto 10050

'      Diagnostics

          sigL3=sigL1+nrampts*dsig
          sigR3=sigL1+(3*nrampts-1)*dsig
          dialogon
              print "getffp, getflp",ffp,flp
              print "fitleft, fitright", fitleft,fitright
              print "rampleft,rampright",sigL3,sigR3
              print "extended region", sigL1,sigR1
              print "dsig",dsig
              print "npts in disk spectrum", npt
              print "nppts in fit region",np
              print "npts in extended region",n
```

C-34

```
            print "nq=point extension",nq
            print "cm-1 extension", dsig*nq
      dialogoff
      loadspc "scratch1"
      loadspc "scratch2"
      stop

'      End of new ramp calculation as per D.G. Oct 97

'         Continue

10050 count=0
      x=0                          'initial x
      xinc=dsig                    'initial x increment
      pauseoff
      blank :printline 2
      print "File: ";$spcname;
      if ns>1 then print " #";nsub;
      print "    Calibration: ";$calname
      print "count","shift","increment","resid"
      chain "kp2.ab"
      print count,x,xinc,rmsres
      x1=x
      r1=rmsres

'         main iteration loop
10100 count=count+1
      if count>200 then print "200 iterations -
stopped",dsig,xinc,r1,rmsres : print #5, "too many
interations": return
      x=x+xinc
      noshow
      noshow
      noshow
      loadspc "temp.spc"
      shift=x
      gosub 10400                       'Shift #s by <shift> cm-1
      print "File: ";$spcname;
      if ns>1 then print " #";nsub;
      printline 23
      print "    Calibration: ";$calname
      print "count","shift","increment","resid"
      chain "kp2.ab"
      print count,x,xinc,rmsres
      if count=1 and rmsres>r1 then goto 10200
      if abs(r1/rmsres-1)<0.01 and abs(xinc)<abs(dsig)/64 goto
10300
      if rmsres<r1 then x0=x1 : r0=r1 : x1=x : r1=rmsres :
goto 10100
      if rmsres<r0 then xinc=xinc/2 else xinc=-xinc/2
```

```
          x=x1 : rmsres=r1 : goto 10100
          if rmsres<r1 then x1=x : r1=rmsres : goto 10100
          goto 10300

10200 r0=rmsres
          x0=x
          x=0
          rmsres=r1
          xinc=-xinc
          goto 10100

10300 if rmsres<r1 goto 10310
          loadspc "temp.spc"
          shift=x1
          gosub 10400                              ' Shift #s by
<shift> cm-1
          chain "kp2.ab"

10310 print count,x,xinc,rmsres
          return


'================================================================
===
'       Subroutine to shift #s by <shift> wavenumbers.
'
'          Uses IGM*complex exponential method
'          ref: AB manual p 60 for basis
'
'          Requires #s, <shift> to be pre-defined
'
10400    ds=abs(getffp()-getflp())/(npts(#s)-1)   ' Spectrum pt.
spacing
          rfft #s
          np=npts(#s)                    ' # real points (power of 2)
          npc=np/2+1                     ' # complex points
          dim cf(2,npc)
          fillbeg 0 : fillinc 1/(ds*np)            ' =
1/(2*ds*npc)=OPD/npc
          cf(0)=cos(-fill(cf(0))*2*pi_value*shift)
          cf(1)=sin(-fill(cf(1))*2*pi_value*shift)
          cf(1,0)=cf(0,npc-1)
          transpose cf
          #s=crmul(#s,cf)
          RIFFT #s
          free cf,ds,np,npc
          return


'================================================================
===
'       Subroutine to print results from fit to output file
```

```
20000    open "O", #4, $output : seek #4, -0        'go to end
of log file
         print #4, $spcname; ",";
         print #4, H2O; ",";
         print #4, H2Oerr; ",";
         print #4, CO2; ",";
         print #4, CO2err; ",";
         print #4, CO; ",";
         print #4, COerr; ",";
         print #4, N2O; ",";
         print #4, N2Oerr; ",";
         print #4, CH4; ",";
         print #4, CH4err; ",";
         print #4, nh3; ",";
         print #4, nh3err; ",";
         print #4, no2; ",";
         print #4, no2err; ",";
         print #4, " "

         close #4

         return
```

Program: Weather.ab
Purpose: To interface with a ComputerBoards A/D card and collect temperature, pressure and wind data for storage in a comma-delimited ASCII file. All calibration curve corrections to data are made before the data points are stored.
Written by: Dan Branan, University of Denver

```
' CIO DAS08/Jr DAQ board for R.M. Young Gill-type UVW
anemometer
'=============================================================
===
'        Program WEATHER.AB
'        By: Dan Branan
'        Original form: OCT 2000
'        Last modified: June 2001
'=============================================================
===
'        Program written for a Computer Boards Inc., CIO-
DAS08/Jr board        plus auxilliary digital I/O attachment.
'        Correction factors for wind components taken from
Anemometer manual
'        Conversion factors for temperature and pressure
determined in the laboratory
'
'        PURPOSE:  To collect 1 Hz wind speed and direction
data, relative to the road surface and to collect
'                  temperature and pressure data once per minute.
'=============================================================
===

        free
        portout -44, -1          'enables error messages
        portout -22, 1           'enables bounds checking
        onerror 50               'goes to end of program and
closes log file on an error or ESC
        pauseoff                 'doesn't wait for a key after
a print statement

'Numerical Variables
        byte1=0
        byte2=0
        byte3=0
        byte4=0
        byte5=0
        byte6=0
        byte7=0
        byte8=0
        byte9=0
        byte10=0
```

```
        temp1=0
        temp2=0
        temperature=0
        press1=0
        press2=0
        pressure=0
        bcorrection=0              'correction factor for bigger
componenet
        scorrection=0              'correction factor for smaller
component
        interval=0
'Index Variables
        r=0
        i=0
        c=0
        samples=500      'Number of times to sample a given
channel and average the readings
'Text Variables"
        dim filename(80), comment(256), udirection(2),
vdirection(2)
        dim op_udirection(2), op_vdirection(2)   'These are the
directions for negative windspeeds
        dim mainwind(2), perpwind(2), vertwind(2)
' Wind Variables
        u=0                'Along the wind axis component
        utemp=0
        uneg=1             'neg variables are flags which indicate
direction
        udir=0             'indicates direction of "U",
        vee=0               'Perpendicular component
        vtemp=0
        vneg=1
        vdir=0             ' same as udir
        w=0                'Vertical component
        wtemp=0
'==============================================================
=

'Get initial information for data collection
        dialogbeg "Anemometer Setup"
                dialogask $filename,2,40,40, "Include path,
but no extension"
                dialogask $comment,2,40,255, "Comment (<256
chars)"
                print ""
                print "What approximate direction is the U
vector pointing (across the road)?"
                menu udir, "N NE E SE S SW W NW"
        dialogend
```

```
dialogbeg "Timing Message"
        print "This program will collect weather data every
second until you press the ESC key."
dialogend

'Set directions for "U" and "V"
        if udir=0 then goto 0
        if udir=1 then goto 1
        if udir=2 then goto 2
        if udir=3 then goto 3
        if udir=4 then goto 4
        if udir=5 then goto 5
        if udir=6 then goto 6
        if udir=7 then goto 7
        goto 8

0       string udirection="NO"
        string vdirection="WE"
        string op_udirection="SO"
        string op_vdirection="EA"
        goto 8

1       string udirection="NE"
        string vdirection="NW"
        string op_udirection="SW"
        string op_vdirection="SE"
        goto 8

2       string udirection="EA"
        string vdirection="NO"
        string op_udirection="WE"
        string op_vdirection="SO"
        goto 8

3       string udirection="SE"
        string vdirection="NE"
        string op_udirection="NW"
        string op_vdirection="SW"
        goto 8

4       string udirection="SO"
        string vdirection="EA"
        string op_udirection="NO"
        string op_vdirection="WE"
        goto 8

5       string udirection="SW"
        string vdirection="SE"
        string op_udirection="NE"
        string op_vdirection="NW"
```

```
            goto 8

6           string udirection="WE"
            string vdirection="SO"
            string op_udirection="EA"
            string op_vdirection="NO"
            goto 8

7           string udirection="NW"
            string vdirection="SW"
            string op_udirection="SE"
            string op_vdirection="NE"


8           'Open file and print header
            string filename=$filename+".csv"
            Open #1, $filename
            print #1, $comment
            print #1, "Date:,"; clock(-6); "/"; clock(-5); "/";
clock(-7)
            print #1,""
            print #1,"Time,";"Temp(C),";"Press(T),";"Cross-
Road(mph),";"From the:,";"Along-Road(mph),";"From
the:,";"V_Wind(mph),";"Direction:"


9  ' Begin Data collection

'   Set Variables to initial values
'   Numeric Variables
            byte1=0
            byte2=0
            byte3=0
            byte4=0
            byte5=0
            byte6=0
            byte7=0
            byte8=0
            byte9=0
            byte10=0
            temp1=0
            temp2=0
            temperature=0
            press1=0
            press2=0
            pressure=0
            bcorrection=0              'correction factor for bigger
componenet
            scorrection=0              'correction factor for smaller
component
```

C-41

```
          interval=0
'Index Variables
          r=0
          i=0
          c=0
' Wind Variables
          u=0                   'Along the wind axis component
          utemp=0
          uneg=1                'neg variables are flags which indicate
direction
          udir=0                'indicates direction of "U",
          vee=0                   'Perpendicular component
          vtemp=0
          vneg=1
          vdir=0                ' same as udir
          w=0                   'Vertical component
          wtemp=0


'print "                              COLLECTING WEATHER DATA.    PRESS
ESC TO QUIT"

'         Read temperature from channel 0.

          for i=1 to samples
            portout 770, 0           'set to read A/D chn 0
            portout 769,0              'clear registers start A\D
            portout 769,0
            portout 769,0
            portout 769,0
            portout 769,0
            portout 769,0
            portout 769,0
            portout 769,0

            portin 768, byte1        'byte1
            byte1=byte1/16           'shift first word to the
right
            portin 769, byte2        'byte2
            byte2=byte2*16           ' shift second word to the
left
            temp1=byte1+byte2        'combine the two words in the
proper order
            temp2=temp2+temp1

          next i

          temperature=temp2/samples
          i=0                            'Re-set index
```

C-42

```
'          Read pressure from channel 1
11        for i=1 to samples
              portout 770, 1          'set to read A/D chn 1
              portout 769,0            'clear registers start A\D
              portout 769,0            'several no-ops placed to
clear A/D coversion
              portout 769,0
              portout 769,0
              portout 769,0
              portout 769,0
              portout 769,0
              portout 769,0

              portin 768, byte3       'byte3
              byte3=byte3/16          'shift first word to the
right
              portin 769, byte4       'byte4
              byte4=byte4*16          ' shift second word to the
left
              press1=byte3+byte4      'combine the two words in the
proper order
              press2=press2+press1

          next i

          pressure=press2/samples
          i=0


'          Read from channel 2, "U"

13        portout 770, 2              'set to read A/D chn 2

          for i=1 to samples
            portout 769,0                'clear registers start A\D
            portout 769,0
            portout 769,0
            portout 769,0
            portout 769,0
            portout 769,0
            portout 769,0
            portout 769,0

            portin 768, byte5         'byte5
            byte5=byte5/16            'shift first word to the
right
            portin 769, byte6         'byte6
            byte6=byte6*16            ' shift second word to the
left
```

C-43

```
        utemp=byte5+byte6      'combine the two words in the
proper order
        u=utemp+u              'Running total of readings
      next i

      u=u/samples

      i=0                      'Reset index


'       Read from channel 3, "V"

      portout 770, 3           'set to read A/D chn 3

      for i=1 to samples
        portout 769,0              'clear registers start A\D
        portout 769,0              'several no-ops placed to
clear A/D coversion
        portout 769,0
        portout 769,0
        portout 769,0
        portout 769,0
        portout 769,0
        portout 769,0

        portin 768, byte7        'byte7
        byte7=byte7/16           'shift first word to the
right
        portin 769, byte8        'byte8
        byte8=byte8*16           ' shift second word to the
left
        vtemp=byte7+byte8      'combine the two words in the
proper order
        vee=vtemp+vee                'Running total of
readings
      next i

      vee=vee/samples                'Take average of 100
readings

      i=0                      'Reset index



'Read from channel 4, "W"

      portout 770, 4          'set to read A/D chn 4

      for i=1 to samples
        portout 769,0              'clear registers start A\D
```

```
          portout 769,0              'several no-ops placed to
clear A/D coversion
          portout 769,0
          portout 769,0
          portout 769,0
          portout 769,0
          portout 769,0

          portin 768, byte9         'byte9
          byte9=byte9/16            'shift first word to the
right
          portin 769, byte10         'byte10
          byte10=byte10*16           'shift second word to the
left
          wtemp=byte9+byte10        'combine the two words in the
proper order
          w=wtemp+w                  'Running total of readings
        next i

        w=(w/samples)
                                        'and apply correction
factor
        i=0                        'Reset index

'Conversions
        u=0.02270*u-46.3698
        vee=0.02270*vee-46.3698
        w=1.25*(0.02270*w-46.3698)
        temperature=((temperature)*.2244)-707.91
        pressure=((pressure)*.4191)-796.53


'Determine larger of the U and v components
        if u<0 then uneg=-1 else uneg=1
        if vee<0 then vneg=-1 else vneg=1

        if abs(u)>abs(vee)then 20 else 30


20      gosub 100

goto 40

30      gosub 200


40      'Determine directions from polarities
        if uneg=1 then string mainwind=$udirection else string
mainwind=$op_udirection
```

```
         if vneg=1 then string perpwind=$vdirection else string
perpwind=$op_vdirection
         if w>0 then string vertwind="UP" else string
vertwind="DN"

' write to file
     print #1, clock(-4);":";clock(-3);":";clock(-
2);",";temperature;",";pressure;",";u;",";$mainwind;",";vee;",
";$perpwind;",";w;",";$vertwind

' write to screen
     print "Weather Data:    Time: ";clock(-4);":";clock(-
3);":";clock(-2);"   Temp:";temperature;"   Press:";pressure;"
U:";u;"   V:";vee;"   W:";w


!WAIT #1000000/#TICK    'Waits until 1 second passes

goto 9

50 Close #1
   end




'subroutines
' Apply correction factors to U and v components

100      bigger=abs(u)
         smaller=abs(vee)
         gosub 300
         u=bigger*uneg
         vee=smaller*vneg
         return 40

200      bigger=abs(vee)
         smaller=abs(u)
         gosub 300
         u=smaller*uneg
         vee=bigger*vneg
         return 40

300      r=smaller/bigger


         'Calculate and apply correction factor for bigger
value
         bcorrection=(0.1642*r^6)-(0.374*r^5)+(0.4567*r^4)-
(0.4365*r^3)+(0.3537*r^2)-(0.0347*r)+1.0003
         bigger=bigger*bcorrection
```

```
         'Calculate and apply correction factor for smaller
value
         scorrection=(0.0836*r^6)-(0.7222*r^5)+(1.6481*r^4)-
(1.4847*r^3)+(0.383*r^2)-(.0281*r)+1.2502
         smaller=smaller*scorrection
         return
```

D - Software for UV/Vis Monochromator

Program: UVMLP1.exe
**Purpose: To collect dark, background and calibration scans with the
512-element PDA and then collect sample scans until the program is
manually terminated. Analyzes the spectra for NO and NH₃
concentration.**
Written and Maintained by: Dr. Gary Bishop

```
Program UVMLP512;

{5/15/02}

{9/26/01 - Modified UVMRoad4 to save the dark and reference
scans to solid state   }
{           disk for reuse if desired. Changed name to UVM_LP1
(Long Path).           }

{6/15/99 - Modified UVMRoad1 to use a 25msec sample clock to
eliminate light        }
{           saturation. Also change alignment readout from
diode 50 to diode 90.   }
{           This should help prevent saturation in the data and
baseline areas.     }
{           Eliminated the summing display since it is not
necessary.               }

{4/5/99 - Version 0.9 of UVMRoad1 adapated from UVMFEAT1.
}

{3/17/99 - Version 1.01
}
{           1) changed a repeat until statement to clean up a
Flip display problem.}
{           2) modified if then statement in analysis routine
to eliminate the      }
{              possiblity of taking the ln of a negative
number.                      }
{           3) modified NO_err calculation equation to get the
units correct.       }

{2/26/99 - Version 1.0 features cemented. }

uses crt, Dos, drvr6430, dio5812, util_512, irqutils, pcl4p;

const
   avg_spectra_count      = 100;
```

```
    BASE_ADDRESS           = 768;
{Base address of DM6430}
    CHANNEL                = 0;
{A/D channel}
    Com1                   = 0;
    Com2                   = 1;
    Flatness_spec          = 1.5;
{Count ratio limit for Dark/Reference Spectra data}
    GAIN                   = 0;
{Gain}
    IRQ1_Channel           = 10;
    IRQ2_Channel           = 11;
    max_extreme_shift      = 37;
{upper extreme diode shift boundary}
    max_diode_shift        = 25;
{maximum diode shift allowed for operation}
    min_extreme_shift      = -37;
{lower extreme diode shift boundary}
    min_cell_vs_master     = 0.499;
{min conc drop allowed from master cell for operation}
    NH3_cal_conc_ppm              = 10;
{NH3 cell in ppb meters}
    NH3a_offset            = 199;
    NH3b_offset                          = 145;
    NH3a_upper_offset      = 35;
    NH3b_upper_offset      = 38;
    NO_lower_BL_end        = 11;
{Baseline correct uses first and last 11 points}
    NO_peak_start          = 300;
{NO maximum diode search starting point}
    NO_upper_BL_start      = 37;
{Relative starting diode for baseline correction}
    NO_upper_BL_end        = 47;
{Relative ending baseline diode for upper region}
    Peak_offset            = 23;
{Start offset from tallest NO peak}
    lower_peaka_end        = 10;
    upper_peaka_start      = 26;
    upper_peaka_end        = 36;
    lower_peakb_start      = 37;
    lower_peakb_end        = 47;
    upper_peakb_start      = 64;
    upper_peakb_end        = 75;
    sample_spectra_count   = 40;
{1 second data collection of 25ms data}
    SE_DIFF                = 0;
{Single-ended A/D voltage hookup}
    skip_num               = 0;
{Readings skiped to sync with FEAT}
```

```
    spin_delay              = 350;
{Controls Flip spinner speed}
   NO_diode_offset          = 46;
{Width of spectra analysis region}

   array_bytes              = sample_spectra_count * 4 + 2;
{number of bytes transfered}
   NO_elements: word        = NO_diode_offset + 1;
{Range of diode elements for NO fit}
   samples                  = sample_spectra_count + skip_num;
{A/D readings taken per car}

Type
   Spectra                  = array[1..Max_diode_number] of Word;
   Spectra_total            = array[1..Max_diode_number] of
Longint;

Var
   adjustment_factor        : single;
   answer                   : char;
   BL_slope_denominator     : single;
   BufPtr                   : pointer;
{TX & RX buffer setup variables}
   BufSeg                   : word;
   cal_check                : boolean;
   Cal_FileName             : String;
   CalInputFile             : Text;
   Cal_ready                : boolean;
   Clock_counts             : word;
   com_check                : boolean;
   counts_str               : string;
   data_out                            : string[30];
   denominator              : extended;
   diode_number             : integer;
   Diode_shift              : integer;
   disk_error               : integer;
   element_count            : integer;
   Erase_file               : boolean;
   error_str                : string[5];
   exit_request             : boolean;
   fit_count                : integer;
   fit_status               : boolean;
   fit_str                  : string;
   i                        : integer;
   IO_complete              : boolean;
   lower_diode_avg          : single;
   lower_diode_count        : single;
   lower_peaka_avg          : single;
   lower_peaka_count        : single;
   lower_peakb_avg          : single;
```

```
    lower_peakb_count      : single;
    NH3                    : real;
    NH3a_end               : integer;
    NH3b_end                               : integer;
    NH3_error              : real;
    NH3_error_str                 : string[5];
    NH3_error_sum          : real;
    NH3_intercept          : single;
    NH3_intcpt_err         : single;
    NH3a_lower_diode       : integer;
    NH3b_lower_diode       : integer;
    NH3_sigma                      : single;
    NH3_slope                      : single;
    NH3_slope_err          : single;
    NH3a_start             : integer;
    NH3b_start                     : integer;
    NH3_str                        : string[6];
    NH3_sum                : real;
    NH3a_upper_diode       : integer;
    NH3b_upper_diode       : integer;
    NO                     : real;
    NO_cal_conc_ppm        : Single;
{cal spectra ppm concentration}
    NO_end                 : integer;
    NO_error               : real;
    NO_error_sum           : real;
    NO_intercept           : single;
    NO_intcpt_err          : single;
    NO_lower_diode         : integer;
    NO_sigma               : single;
    NO_slope               : single;
    NO_slope_err           : single;
    NO_start                       : integer;
    NO_str                 : string[6];
    NO_sum                 : real;
    NO_upper_diode         : integer;
    Old_IRQ1_vector        : word;
    Old_IRQ2_vector        : word;
    Out_pointer                    : PChar;
    peaka_slope_denominator : single;
    peakb_slope_denominator : single;
    Reset1st               : boolean;
    Reset2nd               : boolean;
    Restart                : boolean;
    RetCode                : integer;
    ring_state             : boolean;
    S                      : string;
    Sampling               : boolean;
    Scan                   : integer;
```

```
    SpecPtr                  : PChar;
{Data_transfer pointer variable}
    spin_counter             : integer;
    spin_segment             : integer;
    Start_tics               : Longint;
    temp_err                 : extended;
{intermediate result place holder}
    temp_NO                  : extended;
{intermediate result place holder}
    terminate                : boolean;
    timer_continue           : boolean;
    timer_expired            : boolean;
    transfer_done            : boolean;
    upper_diode_avg          : single;
    upper_diode_count        : single;
    upper_peaka_avg          : single;
    upper_peaka_count        : single;
    upper_peakb_avg          : single;
    upper_peakb_count        : single;
    waste_time                          : single;

    Data                                : Spectra;
    Ref_spec, Dark_spec                 : absorbance_array;
    Master_Cal, Cal_spec                : absorbance_array;
    x_master_NO, x_cal_NO               : absorbance_array;
    x_master_NH3, x_cal_NH3             : absorbance_array;
    y_NO, y_NH3                         : absorbance_array;
    Alignment_counts                    : array[1..3] of word;
{Intensity counts for diode 50}
    Alignment_transfer                  : array[1..6] of byte
absolute Alignment_counts;

procedure LSTSQR4 (var x_data, y_data, slope, sl_err, intcpt,
int_err, sigma; xy_num : word);far;external;
{$L LSTSQR4.OBJ}

procedure Service_PDA; Interrupt;

var
    diode_number : integer;

begin
    Sampling := FALSE;
    diode_number := 0;
    while (not IsADFIFOEmpty6430) do
        begin
            diode_number := diode_number + 1;
            Data[diode_number] := ReadADData6430;
        end;
```

```
        ClearIRQ16430;
{Clear first IRQ on DM6430.}
        EndOfIT(IRQ1_CHANNEL);
{VERY IMPORTANT !!!}

{'End of Interrupt' command.}
end;


procedure Service_timer; Interrupt;

begin
    if timer_continue then
        ClockDivisor6430(1, Clock_counts)
{Restart counter for next count}
    else
        Port[$21] := Port[$21] and $FE;
{Last scan, turn clock interupt back on.}
        ClearIRQ26430;
{Clear second IRQ on DM6430.}
        EndOfIT(IRQ2_CHANNEL);
{VERY IMPORTANT !!!}
        Timer_expired := TRUE;
end;
{'End of Interrupt' command.}


procedure start_scan;
{Routine to start timer and take first data scan}

var
    dummy : real;
    short_delay : integer;

begin
    Port[$21] := Port[$21] or $01;
{Mask off timer interupts}
    ClockDivisor6430(1, Clock_counts);
{Restart counter for next count}
    RetCode := SioDTR(Com1, 'C');
{Signal Mono has started data collection}
    WriteDIO5812(0, 0, $01);
{Trigger PDA scan}
    for short_delay := 1 to 25 do
{30 usec delay when run on a 100 Mhz 486}
        dummy := 3.1435 * short_delay;
    WriteDIO5812(0, 0, $00);
    Sampling := TRUE;
{Set sampling flag}
    Timer_expired := False;
{Clear timer flag}
```

```pascal
    Timer_continue := True;
{Set timer continue flag}
    while Sampling do;
end;

procedure PDA_scan;

var
  dummy : real;
  short_delay : integer;

begin
    WriteDIO5812(0, 0, $01);
{Trigger PDA scan}
    for short_delay := 1 to 25 do
{30 usec delay when run on a 100 Mhz 486}
        dummy := 3.1435 * short_delay;
    WriteDIO5812(0, 0, $00);
    Sampling := TRUE;
{Set sampling flag}
    Timer_expired := False;
{Clear timer flag}
    while Sampling do;
end;

procedure Spinner;

begin
    if spin_counter = spin_delay then
        begin
            case spin_segment of
                0 : FlipData_out(chr($1B)+chr(19)+chr($F6), 3);
                1 : FlipData_out(chr($1B)+chr(19)+chr($2F), 3);
                2 : FlipData_out(chr($1B)+chr(19)+chr($2D), 3);
                3 : FlipData_out(chr($1B)+chr(19)+chr($5C), 3);
                4 : FlipData_out(chr($1B)+chr(19)+chr($F6), 3);
                5 : FlipData_out(chr($1B)+chr(19)+chr($2F), 3);
                6 : FlipData_out(chr($1B)+chr(19)+chr($2D), 3);
                7 : FlipData_out(chr($1B)+chr(19)+chr($5C), 3);
            end;
            spin_segment := spin_segment + 1;
            if spin_segment = 8 then
                spin_segment := 0;
            spin_counter := 0;
        end
    else
        spin_counter := spin_counter + 1;
end;
```

```pascal
procedure ErrorCheck(Code : Integer; program_position:
string);

begin
   case Reset2nd of
      TRUE : if Code < 0 then
{trap PCL error codes}
                  begin
                     FlipData_out(chr($15), 1);
{clear display and Home cursor}
                     Flipdata_out('ERROR:
'+chr($19)+chr($31)+chr($04)+' HALTING'

+chr($19)+chr($32)+chr(10)+chr(13), 22);

Flipdata_out(chr($1B)+chr(18)+program_position, 4);
                     case Code of
                        -18 : FlipData_out('ISR limit exceeded',
18);
                        -17 : FlipData_out('No such IRQ', 11);
                        -16 : FlipData_out('ISR already in use',
18);
                        -15 : FlipData_out('Port Already
enabled', 20);
                        -14 : FlipData_out('Bad or missing
UART', 19);
                        -13 : FlipData_out('UART undefined',
14);
                        -12 : FlipData_out('LOOP_BACK test
fails', 20);
                        -11 : FlipData_out('Bad baud rate code',
18);
                        -10 : FlipData_out('Bad buffer size
code', 20);
                         -9 : FlipData_out('Bad wordlength
code', 19);
                         -8 : FlipData_out('Bad stop bits code',
18);
                         -7 : FlipData_out('Bad parity code',
15);
                         -6 : FlipData_out('Bad 2nd argument',
16);
                         -5 : FlipData_out('Bad 2nd argument',
16);
                         -4 : FlipData_out('No such port', 12);
                         -3 : FlipData_out('No buffer
available', 19);
                         -2 : FlipData_out('Port not enabled',
16);
                         -1 : FlipData_out('I/O Timeout', 11);
```

```
                                end;
                                delay(2000);
                                if Reset1st then RetCode := SioDone(Com1);
                                if Reset2nd then RetCode := SioDone(Com2);
                                Halt;
                            end
                    else if (Code and (FramingError or ParityError or
OverrunError)) <> 0 then
                        begin (* Port Error *)
                            if (Code and FramingError) <> 0 then
FlipData_out('Framing Error', 13);
                            if (Code and ParityError)  <> 0 then
FlipData_out('Parity Error', 12);
                            if (Code and OverrunError) <> 0 then
FlipData_out('Overrun Error', 13);
                            delay(2000);
                            if Reset1st then RetCode := SioDone(Com1);
                            if Reset2nd then RetCode := SioDone(Com2);
                            Halt;
                        end;
        False : if Code < 0 then
{trap PCL error codes}
                        begin
                            alarm(5);
                            if Reset1st then RetCode := SioDone(Com1);
                            if Reset2nd then RetCode := SioDone(Com2);
                            Halt;
                        end
                    else if (Code and (FramingError or ParityError or
OverrunError)) <> 0 then
                        begin (* Port Error *)
                            alarm(5);
                            if Reset1st then RetCode := SioDone(Com1);
                            if Reset2nd then RetCode := SioDone(Com2);
                            Halt;
                        end;
    end;
end;

procedure Setup_Com;

begin
    RetCode := SioParms(Com2, NoParity, OneStopBit,
WordLength8);
    RetCode := SioReset(Com2, Baud19200);
{reset COM2}
    if RetCode <> 0 then ErrorCheck(SioReset(Com2, Baud19200),
'E1'); {if error then try one more time}
    Reset2nd := TRUE;
    RetCode := SioFifo(Com2, Level_1);
```

```
    ErrorCheck(SioRxClear(Com2), 'E2');
    ErrorCheck(SioTxClear(Com2), 'E3');
    RetCode := SioParms(Com1, NoParity, OneStopBit,
WordLength8);
    RetCode := SioReset(Com1, Baud19200);
{reset COM1}
    if RetCode <> 0 then ErrorCheck(SioReset(Com1, Baud19200),
'E4');  {if error then try one more time}
    Reset1st := TRUE;
    ErrorCheck(SioRxClear(Com1), 'E5');
{flush ports}
    ErrorCheck(SioTxClear(Com1), 'E6');
    RetCode := SioFifo(Com1, Level_4);
end;

procedure Cmd_handshake(const Cmd : char; const
program_position : string);

var
    Com_link  : boolean;
    time_outs : integer;

begin
    time_outs := 0;
    repeat
        RetCode := SioPutc(Com1, Cmd);
{send data}
        if RetCode = -1 then ErrorCheck(SioPutc(Com1, Cmd),
program_position);
        transfer_done := False;
        Start_tics := SioTimer;
        com_link := False;
        repeat
            RetCode := SioGetc(Com1, 0);
            if RetCode > 0 then
                if Cmd = chr(RetCode) then
                    begin
                        transfer_done := True;
                        com_link := True;
                    end
                else
                    transfer_done := True;
            if (SioTimer - Start_tics) > 20 then
                begin
                    if Time_outs > 10 then
                        begin
                            if Reset2nd then RetCode :=
Siodone(Com2);
                            if Reset1st then RetCode :=
SioDone(Com1);
```

```pascal
                        Halt;
                    end
                else
                    Time_outs := Time_outs + 1;
                transfer_done := True;
            end;
        until transfer_done;
    until com_link;
end;

procedure Baseline_correct(var spectra: absorbance_array);

var
  i                                  : integer;
  Baseline_slope, Baseline_intercept : single;
  lower_abs_sum, lower_abs_avg       : single;
  upper_abs_sum                      : single;

begin
    lower_abs_sum := 0; upper_abs_sum := 0;
    for i := 1 to NO_Lower_BL_end do
        lower_abs_sum := lower_abs_sum + spectra[i];
    lower_abs_avg := lower_abs_sum / Lower_diode_count;
    for i := NO_upper_BL_start to NO_upper_BL_end do
        upper_abs_sum := upper_abs_sum + spectra[i];
    Baseline_slope := (lower_abs_avg - (upper_abs_sum /
Upper_diode_count)) / BL_slope_denominator;
    Baseline_intercept := lower_abs_avg - (Baseline_slope *
lower_diode_avg);
    for i := 1 to NO_elements do
        spectra[i] := spectra[i] - (Baseline_slope * i +
Baseline_intercept);
end;

procedure NH3_Baseline_correct(var master, cal :
absorbance_array;
                                    const level : integer);

var
  i                                  : integer;
  Baseline_slope, Baseline_intercept : single;
  lower_abs_sum, lower_abs_avg       : single;
  upper_abs_sum                      : single;

begin
   if level = 0 then
{skip master file correction?}
      begin
         lower_abs_sum := 0; upper_abs_sum := 0;
                                {master cal peak a correction}
```

```
                    for i := 1 to Lower_peaka_end do
                        lower_abs_sum := lower_abs_sum + master[i];
                    lower_abs_avg := lower_abs_sum / Lower_peaka_count;
                    for i := upper_peaka_start to upper_peaka_end do
                        upper_abs_sum := upper_abs_sum + master[i];
                    Baseline_slope := (lower_abs_avg - (upper_abs_sum /
upper_peaka_count)) / peaka_slope_denominator;
                    Baseline_intercept := lower_abs_avg - (Baseline_slope
* lower_peaka_avg);
                    for i := 1 to upper_peaka_end do
                        master[i] := master[i] - (Baseline_slope * i +
Baseline_intercept);
                    lower_abs_sum := 0; upper_abs_sum := 0;
                                                    {master cal peak b
correction}
                    for i := Lower_peakb_start to Lower_peakb_end do
                        lower_abs_sum := lower_abs_sum + master[i];
                    lower_abs_avg := lower_abs_sum / Lower_peakb_count;
                    for i := upper_peakb_start to upper_peakb_end do
                        upper_abs_sum := upper_abs_sum + master[i];
                    Baseline_slope := (lower_abs_avg - (upper_abs_sum /
upper_peakb_count)) / peakb_slope_denominator;
                    Baseline_intercept := lower_abs_avg - (Baseline_slope
* lower_peakb_avg);
                    for i := lower_peakb_start to upper_peakb_end do
                        master[i] := master[i] - (Baseline_slope * i +
Baseline_intercept);
                end;
            lower_abs_sum := 0; upper_abs_sum := 0;
                                                {calibration peak a
correction}
            for i := 1 to Lower_peaka_end do
                lower_abs_sum := lower_abs_sum + cal[i];
            lower_abs_avg := lower_abs_sum / Lower_peaka_count;
            for i := upper_peaka_start to upper_peaka_end do
                upper_abs_sum := upper_abs_sum + cal[i];
            Baseline_slope := (lower_abs_avg - (upper_abs_sum /
upper_peaka_count)) / peaka_slope_denominator;
            Baseline_intercept := lower_abs_avg - (Baseline_slope *
lower_peaka_avg);
            for i := 1 to upper_peaka_end do
                cal[i] := cal[i] - (Baseline_slope * i +
Baseline_intercept);
            lower_abs_sum := 0; upper_abs_sum := 0;
                                                {calibration peak b
correction}
            for i := Lower_peakb_start to Lower_peakb_end do
                lower_abs_sum := lower_abs_sum + cal[i];
            lower_abs_avg := lower_abs_sum / Lower_peakb_count;
            for i := upper_peakb_start to upper_peakb_end do
```

```
      upper_abs_sum := upper_abs_sum + cal[i];
   Baseline_slope := (lower_abs_avg - (upper_abs_sum /
upper_peakb_count)) / peakb_slope_denominator;
   Baseline_intercept := lower_abs_avg - (Baseline_slope *
lower_peakb_avg);
   for i := lower_peakb_start to upper_peakb_end do
      cal[i] := cal[i] - (Baseline_slope * i +
Baseline_intercept);
end;

procedure Dark_Scan(var Dark : absorbance_array);

var
   Dark_ratio                   : Single;
   Spectra_number, diode_number : integer;
   exit_request                 : boolean;
   dark_accepted                : boolean;
   Spectra_sum                  : Spectra_total;

begin
   repeat
      for Diode_number := 1 to Max_diode_number do
                              {clear array}
         Spectra_sum[diode_number]:= 0;
      FlipData_out(chr($15), 1);
{clear display and Home cursor}
      FlipData_out('Collect dark scan'+chr(13), 18); .
      FlipData_out(chr(10)+'Block &
'+chr($19)+chr($31)+chr($02)+'press'+chr($19)+chr($32)+'
switch', 26);
      repeat until Button_pressed;
      FlipData_out(chr($15), 1);
      FlipData_out('...Collecting.....', 18);
      start_scan;
{Start timer}
      while (not Timer_expired) do;
      PDA_Scan;
      For Spectra_number:= 1 to avg_spectra_count do
{collect Dark Spectra}
         Begin
            while (not Timer_expired) do;
            PDA_Scan;
            for Diode_number := 1 to Max_diode_number do
               Spectra_sum[diode_number]:=
Spectra_sum[diode_number] + Data[diode_number];
         end;
      timer_continue := FALSE;
      For Diode_number:= 1 to Max_diode_number do
         Dark[Diode_number] :=
Spectra_sum[diode_number]/avg_spectra_count;
```

```
        Dark_ratio := Dark[Max_diode_number]/Dark[1];
        if Dark_ratio < Flatness_spec then
           dark_accepted := True
        else
           begin
              FlipData_out(chr($15), 1);
              FlipData_out('Dark Scan Error'+chr($0A)+chr($0D),
17);
              FlipData_out('Is beam blocked?', 16);
              Alarm(5);
              delay(5000);
              dark_accepted := False;
           end;
     until dark_accepted;
     FlipData_out(chr($15), 1);
     FlipData_out('Dark Scan Collected'+chr($0A)+chr($0D), 21);
     exit_request := False;
     repeat
        FlipData_out('Remove Blocker'+chr($0D), 15);
        Start_tics := SioTimer;
        repeat
           if button_pressed then exit_request := True;
        until ((SioTimer - Start_tics) > 25) or exit_request;
        FlipData_out(chr($19)+chr($36)+chr($2)+'Press
switch!'+chr($0D)+chr($0E), 18);
        Start_tics := SioTimer;
        repeat
           if button_pressed then exit_request := True;
        until ((SioTimer - Start_tics) > 25) or exit_request;
     until exit_request;
     FlipData_out(chr($15), 1);
end;

procedure Reference_Scan(var Ref : absorbance_array; const
Dark : absorbance_array);
var
   Spectra_number, diode_number : integer;
   Ref_ratio                    : Single;
   Ref_accepted                 : boolean;
   Spectra_sum                  : Spectra_total;

begin
   repeat
      for Diode_number := 1 to Max_diode_number do
                            {clear array}
         Spectra_sum[diode_number]:= 0;
      FlipData_out(chr($15), 1);
{clear display and Home cursor}
      FlipData_out('Collect Reference'+chr($0D), 18);
```

```
      FlipData_out(chr($0A)+chr($19)+chr($31)+chr($04)+'Press'+chr($
19)+chr($32)+' switch & begin', 26);
        repeat until Button_pressed;
        FlipData_out(chr($15), 1);
        FlipData_out('...Collecting.....', 18);
        start_scan;
{Start timer}
        while (not Timer_expired) do;
        PDA_Scan;
        For Spectra_number:= 1 to avg_spectra_count do
{collect Dark Spectra}
            Begin
                while (not Timer_expired) do;
                PDA_Scan;
                for Diode_number := 1 to Max_diode_number do
                    Spectra_sum[diode_number]:=
Spectra_sum[diode_number] + Data[diode_number];
                if Spectra_number = 50 then
                    Alignment_counts[1] := Data[250];
            end;
        timer_continue := FALSE;
        For Diode_number:= 1 to Max_diode_number do
            Ref[Diode_number] :=
(Spectra_sum[diode_number]/avg_spectra_count) -
Dark[Diode_number];
        Ref_ratio := Ref[Max_diode_number]/Ref[1];
        if Ref_ratio > Flatness_spec then
            Ref_accepted := True
        else
            begin
                FlipData_out(chr($15), 1);
                FlipData_out('Reference Scan Error', 20);
                FlipData_out('Is beam blocked?', 16);
                Alarm(5);
                delay(5000);
                Ref_accepted := False;
            end;
    until Ref_accepted;
    FlipData_out(chr($15), 1);
    FlipData_out(chr($1B)+chr(20)+'Reference
Collected'+chr(10)+chr(13), 23);
    delay(3000);
    FlipData_out(chr($15), 1);
end;

procedure PDA_align;

begin
```

```
      FlipData_out(chr($15), 1);
{clear display and Home cursor}
      FlipData_out('Alignment Mode'+chr(13), 15);

FlipData_out(chr(10)+chr($19)+chr($31)+chr($04)+'Press'+chr($1
9)+chr($32)+' switch to exit', 26);
      delay(5000);
      FlipData_out(chr($15), 1);
      start_scan;
{Start timer}
      repeat
          PDA_scan;
          Flip_display(Data[250]);
{Using an upper diode to prevent saturation in data area}
             LoadDAC6430(Data[250]);
{Sending analog output data.}
          while (not Timer_expired) do;
          Timer_expired := False;
      until button_pressed;
      Timer_continue := False;
      LoadDAC6430(0);
{Zero DAC}
      FlipData_out(chr($15), 1);
end;

function Cal_accepted : boolean;

var
  seconds       : string[2];
  ticks         : integer;
  exit_request  : boolean;

begin
   Cal_accepted := False;
   exit_request := False;
   FlipData_out(chr($15)+chr($1B)+chr(20), 3);

FlipData_out(chr($19)+chr($31)+chr($04)+'Press'+chr($19)+chr($
32)+' switch to keep', 25);
   FlipData_out(chr($1B)+chr(18)+'25', 4);
   for ticks := 24 downto 0 do
       begin
           Start_tics := SioTimer;
           repeat
               if button_pressed then
                   begin
                       Cal_accepted := True;
                       exit_request := True;
                       break;
{Exit repeat}
```

D-16

```
                    end;
            until (SioTimer - Start_tics) > 18;
            if exit_request then break;
{Exit for/next loop}
            str(ticks, seconds);
            case ticks of
                0..9 : FlipData_out(chr($1B)+chr(18)+' '+seconds,
4);
                else
                    FlipData_out(chr($1B)+chr(18)+seconds, 4);
            end;
        end;
    FlipData_out(chr($15), 1);
    case exit_request of
        True  : FlipData_out('Calibration Accepted', 20);
        False : FlipData_out('Calibration Rejected', 20);
    end;
    delay(3000);
end;

procedure Cal_compress(const master, cal : absorbance_array;
                       var x_master, x_cal : absorbance_array;
                       const Start_cal, End_cal, Start_master,
End_master : integer);

var
    element_count, diode_number : integer;

begin
    element_count := 0;
    for diode_number := Start_cal to End_cal do
        begin
            element_count := element_count + 1;
            x_cal[element_count] := Cal[diode_number];
        end;
    element_count := 0;
    for diode_number := Start_master to End_master do
        begin
            element_count := element_count + 1;
            x_master[element_count] := Master[diode_number];
        end;
end;

procedure NH3_compress(const master, cal : absorbance_array;
                       var x_master, x_cal : absorbance_array;
                       const Start_a, End_a, Starta_master,
Enda_master,

Start_b, End_b, Startb_master, Endb_master : integer);
```

```pascal
var
    element_count, diode_number : integer;

begin
    element_count := 0;
    for diode_number := Start_a to End_a do
        begin
            element_count := element_count + 1;
            x_cal[element_count] := Cal[diode_number];
        end;
    for diode_number := Start_b to End_b do
        begin
            element_count := element_count + 1;
            x_cal[element_count] := Cal[diode_number];
        end;
    element_count := 0;
    for diode_number := Starta_master to Enda_master do
        begin
            element_count := element_count + 1;
            x_master[element_count] := Master[diode_number];
        end;
    for diode_number := Startb_master to Endb_master do
        begin
            element_count := element_count + 1;
            x_master[element_count] := Master[diode_number];
        end;
end;

procedure Cal_compare(const cal_slope, cal_sigma, cell_ppm :
single; const shift, species : integer);

var
    shift_str, slope_str        : string[3];
    fit_str                     : string[5];
    cal_str                     : string[4];
    i : integer;

begin
    FlipData_out(chr($15), 1);
    str(shift:3, shift_str);
    FlipData_out('SHIFT:'+shift_str, 9);
    FlipData_out(chr($1B)+chr(9), 2);
    str(cal_sigma:5:3, fit_str);
    FlipData_out('   '+chr($8F)+ ' '+fit_str, 10);
    FlipData_out(chr($1B)+chr(20), 2);
    str(cal_slope*100:3:0, slope_str);
    if cell_ppm > 999.9 then
        str(cell_ppm:4:0, cal_str)
    else
        str(cell_ppm:3:0, cal_str);
```

```
     case species of
         0 : FlipData_out('[NO]/'+cal_str+' = '+slope_str+'%',
12+length(cal_str));
         1 : FlipData_out('[NH3]/'+cal_str+' =
'+slope_str+'%',13+length(cal_str));
     end;
     if (abs(shift) < max_diode_shift) and (cal_slope >
min_cell_vs_master) then
         FlipData_out(chr($1B)+chr(38)+'OK', 4)
     else
         FlipData_out(chr($1B)+chr(37)+'BAD', 5);
     delay(10000);
end;

function Calibration(const Ref, Dark : absorbance_array; var
Cal : absorbance_array): boolean;

var
     element_count                  : integer;
     Spectra_number, diode_number : integer;
     exit_request, Cal_collected  : boolean;
     cal_transmittance              : single;
     Spectra_sum                    : spectra_total;

begin
     for Diode_number := 1 to Max_diode_number do
                                     {clear array}
         Spectra_sum[diode_number]:= 0;
     FlipData_out(chr($15), 1);
     FlipData_out('Collect Calibration'+chr($0A)+chr($0D), 21);
     exit_request := False;
     repeat
         FlipData_out('Insert Cal Cell'+chr($0D), 16);
         Start_tics := SioTimer;
         repeat
             if button_pressed then exit_request := True;
         until ((SioTimer - Start_tics) > 25) or exit_request;
         FlipData_out(chr($19)+chr($36)+chr($2)+'Press
switch!'+chr($0D)+chr($0E), 18);{Erase and display on bottom
line}
         Start_tics := SioTimer;
         repeat
             if button_pressed then exit_request := True;
         until ((SioTimer - Start_tics) > 25) or exit_request;
     until exit_request;
     FlipData_out(chr($15), 1);
     FlipData_out('...Collecting.....', 18);
     start_scan;
{Start timer}
     while (not Timer_expired) do;
```

```
     PDA_Scan;
     For Spectra_number:= 1 to avg_spectra_count do
{collect Spectra}
        Begin
            while (not Timer_expired) do;
            PDA_Scan;
            for Diode_number := 1 to Max_diode_number do
                Spectra_sum[diode_number]:=
Spectra_sum[diode_number] + Data[diode_number];
        end;
     timer_continue := FALSE;
     Cal_collected := True;
   ' For Diode_number := 1 to Max_diode_number do
        begin
            cal_transmittance := Ref[Diode_number] /
((Spectra_sum[diode_number]/avg_spectra_count) -
Dark[Diode_number]);
            if cal_transmittance <> 0 then
                Cal[Diode_number] := ln(cal_transmittance)
            else
                begin
                    Cal_collected := FALSE;
                    break;
                end;
        end;
     FlipData_out(chr($15), 1);
     if Cal_collected then
        begin
            FlipData_out(chr($1B)+chr(20)+'Cal
Collected'+chr(10)+chr(13), 17);
            Calibration := True;
        end
     else
        begin
            FlipData_out(chr($1B)+chr(20)+'Cal
Aborted'+chr(10)+chr(13), 15);
            Calibration := False;
            Alarm(5);
        end;
     delay(3000);
end;

begin
   Escape_Hatch;
   Clock_counts := $61A7;
{set timer to 25ms counter}
   spin_segment := 0;
   Reset1st := FALSE;
   Reset2nd := FALSE;
   Out_pointer := @data_out[1];
```

```
{Define parameters for NO Baseline Correction}
   lower_diode_avg := (NO_Lower_BL_end - 1)/2 + 1;
   lower_diode_count := NO_Lower_BL_end;
   upper_diode_avg := (NO_upper_BL_end - NO_upper_BL_start)/2
+ NO_upper_BL_start;
   upper_diode_count := NO_upper_BL_end - NO_upper_BL_start +
1;
   BL_slope_denominator := lower_diode_avg - upper_diode_avg;

{Define parameters for NH3 Baseline Correction}
   lower_peaka_avg := (Lower_peaka_end - 1)/2 + 1;
   lower_peaka_count := Lower_peaka_end;
   upper_peaka_avg := (Upper_peaka_end - Upper_peaka_start)/2
+ Upper_peaka_start;
   upper_peaka_count := Upper_peaka_end - Upper_peaka_start +
1;
   peaka_slope_denominator := lower_peaka_avg -
upper_peaka_avg;
   lower_peakb_avg := (Lower_peakb_end - Lower_peakb_start)/2
+ Lower_peakb_start;
   lower_peakb_count := Lower_peakb_end - Lower_peakb_start +
1;
   upper_peakb_avg := (Upper_peakb_end - Upper_peakb_start)/2
+ Upper_peakb_start;
   upper_peakb_count := Upper_peakb_end - Upper_peakb_start +
1;
   peakb_slope_denominator := lower_peakb_avg -
upper_peakb_avg;

   GetMem(BufPtr,128+16);
{setup 128 byte receive buffers}
   BufSeg := Seg(BufPtr^) + ((Ofs(BufPtr^)+15) SHR 4);
   ErrorCheck(SioRxBuf(Com1, BufSeg, Size128), 'M1');
   GetMem(BufPtr,128+16);
{setup 128 byte receive buffers}
   BufSeg := Seg(BufPtr^) + ((Ofs(BufPtr^)+15) SHR 4);
   ErrorCheck(SioRxBuf(Com2, BufSeg, Size128), 'M2');

   GetMem(BufPtr,4096+16);
{setup 512 byte transmit buffers}
   BufSeg := Seg(BufPtr^) + ((Ofs(BufPtr^)+15) SHR 4);
   ErrorCheck(SioTxBuf(Com1, BufSeg, Size4096), 'M3');
   GetMem(BufPtr,128+16);
{setup 128K transmit buffers}
   BufSeg := Seg(BufPtr^) + ((Ofs(BufPtr^)+15) SHR 4);
   ErrorCheck(SioTxBuf(Com2, BufSeg, Size128), 'M4');

   Setup_Com;
```

D-21

```pascal
    Disk_check(disk_error);
{Check disk operation and master cal file}
    if disk_error <> 0 then
        case disk_error of
            2 : begin
                    alarm(5);
                    FlipData_out(chr($15), 1);
                    FlipData_out('NO Master Cal File', 18);
                    FlipData_out(chr($0A)+chr($0D)+'Program
Halted!', 17);
                    delay(2000);
                    if Reset1st then RetCode := SioDone(Com1);
                    if Reset2nd then RetCode := SioDone(Com2);
                    Halt;
                 end;
        else
            begin
                alarm(5);
                FlipData_out(chr($15), 1);
                str(disk_error:3, error_str);
                FlipData_out('Disk Error #'+error_str, 15);
                FlipData_out(chr($0A)+chr($0D)+'Program Halted!',
17);
                delay(2000);
                if Reset1st then RetCode := SioDone(Com1);
                if Reset2nd then RetCode := SioDone(Com2);
                Halt;
            end;
        end;

FlipData_out(chr($18)+chr($F6)+chr($81)+chr($04)+chr($12)+chr(
$48)+chr($00), 7);{User defined character}
    FlipData_out(chr($15)+chr($0E), 2);
{Clear display and turn off cursor}
    SetBaseAddress(BASE_ADDRESS);
    InitBoard6430;
{Board initializing}

    SetPort0Direction5812(0, 1);
{Initialize port 0 for output}
    SetPort1Direction5812(1, 0);
{Initialize port 1 for input}
    WriteDIO5812(0, 0, $00);
    delay(20);
{Wait for PIC/PDA to reset}

    SetChannelGain6430(CHANNEL, GAIN, SE_DIFF);
{Set channel and gain.}
```

```
   SetConversionSelect6430(1);
{Set conversion select to pacer clock}
   SetStartTrigger6430(0);
{Set Start Trigger to Software.}
   SetStopTrigger6430(0);
{Set Stop Trigger to Software.}
   SetPacerClockSource6430(1);
{Set Pacer Clock Source External}

   SelectTimerCounter6430(1);
{Select user T/C}
   ClockMode6430(0,2);
{Set Clock 0 to mode 2}
   ClockMode6430(1,0);
{Set Clock 1 to mode 0, interrupt on TC}
   ClockDivisor6430(0,8);
{Set Clock 0 Divider to 8, 1 Mhz}
   LoadADSampleCounter6430(Max_diode_number);
{Set Sample Counter for 128 readings}

   SetIRQ16430(0,IRQ1_CHANNEL);
{Set Board first IRQ Source to A/D sample counter.}

   InitHostIT(@Service_PDA, @Old_IRQ1_vector, IRQ1_CHANNEL);
{Set the Interrupt Service Routine}

{and enable the appropriate IRQ channel}
   ClearIRQ16430;
{Clear IRQ on DM6430.}
   SetIRQ26430(13,IRQ2_CHANNEL);
{Set Board second IRQ Source to User TC out 1}

   InitHostIT(@Service_Timer, @Old_IRQ2_vector, IRQ2_CHANNEL);
{Set the Interrupt Service Routine}

{and enable the appropriate IRQ channel}
   ClearIRQ26430;
{Clear IRQ on DM6430}

   ClearADFIFO6430;
{Clear FIFO}
   StartConversion6430;
{Arm A/D convertor}
   FlipData_out(chr($15)+chr($0E), 2);
{clear display and Home cursor}
   FlipData_out('UVM_LP1'+chr(13)+chr(10), 9);
   repeat
      FlipData_out('Press switch '+chr($0D), 14);
{Display on bottom line}
      Start_tics := SioTimer;
```

```
      repeat
          if button_pressed then exit_request := True;
      until ((SioTimer - Start_tics) > 25) or exit_request;
      FlipData_out('to begin.....'+chr($0D), 14);
{Display on bottom line}
      Start_tics := SioTimer;
      repeat
          if button_pressed then exit_request := True;
      until ((SioTimer - Start_tics) > 25) or exit_request;
    until exit_request;

    RetCode := SioDTR(Com1, 'S');
{Signal CPU ready to begin communications}
    Make_Cal_filename(Cal_filename);
    If Cal_file_check(Cal_filename) then
        begin
            FlipData_out(chr($15), 1);
{clear display and Home cursor}
            FlipData_out('Daily Cal file'+chr(13)+chr(10), 16);
            FlipData_out('detected!', 9);
            Cal_check := True;
            Alarm(6);
            delay(4000);
            if cal_accepted then
                Erase_file := FALSE
            else
                Erase_file := TRUE;
        end
    else
        Cal_check := False;
    Read_Cal_file(Master_Cal, 'Cal.Mas', no_cal_conc_ppm,
diode_shift);{Load Master NO spectra}
    repeat
        PDA_Align;
        delay(1000);
        if Cal_check then
            if Erase_file then
                begin
                    Erase_Cal_file(Cal_filename);
                    Dark_Scan(Dark_spec);
                    delay(1000);
                    Reference_Scan(Ref_spec, Dark_spec);
                    if Calibration(Ref_spec, Dark_spec, Cal_spec)
then
                        begin
                            diode_shift :=
Special_Max_diode(Cal_spec, NO_peak_start) -
Special_Max_diode(Master_Cal, NO_peak_start);
                            if (diode_shift > min_extreme_shift) and
(diode_shift < max_extreme_shift) then
```

```
                              begin
                                NO_start :=
Special_Max_diode(Master_Cal, NO_peak_start) - peak_offset;
{Define NO extraction zones}
                                NO_end := NO_start +
NO_Diode_offset;
                                NO_Lower_Diode := NO_start +
diode_shift;
                                NO_Upper_Diode := NO_Lower_Diode +
NO_Diode_offset;
                                Cal_compress(master_cal, cal_spec,
x_master_NO, x_cal_NO,
                                        NO_Lower_Diode,
NO_Upper_Diode, NO_start, NO_end);
                                Baseline_correct(x_Cal_NO);
                                Baseline_correct(x_Master_NO);
                                lstsqr4(x_Master_NO, x_cal_NO,
no_slope, no_slope_err, no_intercept,
                                        no_intcpt_err, no_sigma,
NO_elements);
                                Cal_compare(no_slope, no_sigma,
no_cal_conc_ppm, diode_shift, 0);
                                NH3a_start := NO_start -
NH3a_offset;
                                NH3a_end := NH3a_start +
NH3a_upper_offset;
                                NH3a_lower_diode := NO_lower_diode
- NH3a_offset;
                                NH3a_upper_diode :=
NH3a_lower_diode + NH3a_upper_offset;

      NH3b_start := NO_start - NH3b_offset;
                                NH3b_end := NH3b_start +
NH3b_upper_offset;
                                NH3b_lower_diode := NO_lower_diode
- NH3b_offset;
                                NH3b_upper_diode :=
NH3b_lower_diode + NH3b_upper_offset;
                                NH3_compress(master_cal, cal_spec,
x_master_NH3, x_cal_NH3,
                                        NH3a_lower_diode,
NH3a_upper_diode, NH3a_start, NH3a_end,

                    NH3b_lower_diode, NH3b_upper_diode,
Nh3b_start, NH3b_end);
                                NH3_baseline_correct(x_master_NH3,
x_cal_NH3, 0);   {corrrect both files}
                                lstsqr4(x_Master_NH3, x_cal_NH3,
NH3_slope, NH3_slope_err, NH3_intercept,
```

```
                                        NH3_intcpt_err, NH3_sigma,
upper_peakb_end);
                                  Cal_compare(NH3_slope, NH3_sigma,
NH3_cal_conc_ppm, diode_shift, 1);
                                  if Cal_accepted then
                                      begin
                                          Cal_ready := True;
                                          Save_cal_file(Cal_filename,
Cal_spec, NO_cal_conc_ppm, diode_shift);

Save_DkRef_files('Dk_ref.spc', Dark_spec, Ref_spec);
                                      end
                                  else
                                      Cal_ready := False;
                              end
                          else
                              begin
                                  Excess_shift_warning;
                                  Cal_ready := False;
                              end;
                      end
                  else
                      Cal_ready := False;
{Reject cal for ln(0) problem}
                      Cal_check := False;
{Allow only one erasure}
              end
          else
              begin
                  Read_Cal_file(Cal_spec, Cal_filename,
no_cal_conc_ppm, diode_shift);{Load Master NO spectra}
                  Read_DkRef_files(Dark_spec, Ref_spec,
'Dk_ref.spc');
                  NO_start := Special_Max_diode(Master_Cal,
NO_peak_start) - peak_offset; {Define NO extraction zones}
                  NO_end := NO_start + NO_Diode_offset;
                  NO_Lower_Diode := NO_start + diode_shift;
                  NO_Upper_Diode := NO_Lower_Diode +
NO_Diode_offset;
                  Cal_compress(master_cal, cal_spec, x_master_NO,
x_cal_NO,
                                  NO_Lower_Diode, NO_Upper_Diode,
NO_start, NO_end);
                  Baseline_correct(x_Cal_NO);
                  NH3a_start := NO_start - NH3a_offset;
                  NH3a_end := NH3a_start + NH3a_upper_offset;
                  NH3a_lower_diode := NO_lower_diode -
NH3a_offset;
                  NH3a_upper_diode := NH3a_lower_diode +
NH3a_upper_offset;
```

```
                                    NH3b_start := NO_start -
NH3b_offset;
                NH3b_end := NH3b_start + NH3b_upper_offset;
                NH3b_lower_diode := NO_lower_diode -
NH3b_offset;
                NH3b_upper_diode := NH3b_lower_diode +
NH3b_upper_offset;
                NH3_compress(master_cal, cal_spec,
x_master_NH3, x_cal_NH3,
                                NH3a_lower_diode,
NH3a_upper_diode, NH3a_start, NH3a_end,

NH3b_lower_diode, NH3b_upper_diode, Nh3b_start, NH3b_end);
                NH3_baseline_correct(x_master_NH3, x_cal_NH3,
1);           {Don't need to correct the master}
                Cal_ready := True;
                FlipData_out('Cal file loaded', 15);
                delay(2000);
            end
      else
        begin
            Dark_Scan(Dark_spec);
            delay(1000);
            Reference_Scan(Ref_spec, Dark_spec);
            if Calibration(Ref_spec, Dark_spec, Cal_spec) then
                begin
                    diode_shift := Special_Max_diode(Cal_spec,
NO_peak_start) - Special_Max_diode(Master_Cal, NO_peak_start);
                    if (diode_shift > min_extreme_shift) and
(diode_shift < max_extreme_shift) then
                        begin
                            NO_start :=
Special_Max_diode(Master_Cal, NO_peak_start) - peak_offset;
{Define NO extraction zones}
                            NO_end := NO_start + NO_Diode_offset;
                            NO_Lower_Diode := NO_start +
diode_shift;
                            NO_Upper_Diode := NO_Lower_Diode +
NO_Diode_offset;
                            Cal_compress(master_cal, cal_spec,
x_master_NO, x_cal_NO,
                                            NO_Lower_Diode,
NO_Upper_Diode, NO_start, NO_end);
                            Baseline_correct(x_Cal_NO);
                            Baseline_correct(x_Master_NO);
                            lstsqr4(x_Master_NO, x_cal_NO,
no_slope, no_slope_err, no_intercept,
                                        no_intcpt_err, no_sigma,
NO_elements);
```

```
                              Cal_compare(no_slope, no_sigma,
no_cal_conc_ppm, diode_shift, 0);
                              NH3a_start := NO_start - NH3a_offset;
                              NH3a_end := NH3a_start +
NH3a_upper_offset;
                              NH3a_lower_diode := NO_lower_diode -
NH3a_offset;
                              NH3a_upper_diode := NH3a_lower_diode +
NH3a_upper_offset;
                                                     NH3b_start :=
NO_start - NH3b_offset;
                              NH3b_end := NH3b_start +
NH3b_upper_offset;
                              NH3b_lower_diode := NO_lower_diode -
NH3b_offset;
                              NH3b_upper_diode := NH3b_lower_diode +
NH3b_upper_offset;
                              NH3_compress(master_cal, cal_spec,
x_master_NH3, x_cal_NH3,
                                       NH3a_lower_diode,
NH3a_upper_diode, NH3a_start, NH3a_end,

           NH3b_lower_diode, NH3b_upper_diode, Nh3b_start,
NH3b_end);
                              NH3_baseline_correct(x_master_NH3,
x_cal_NH3, 0);
                              lstsqr4(x_Master_NH3, x_cal_NH3,
NH3_slope, NH3_slope_err, NH3_intercept,
                                       NH3_intcpt_err, NH3_sigma,
upper_peakb_end);
                              Cal_compare(NH3_slope, NH3_sigma,
NH3_cal_conc_ppm, diode_shift, 1);
                              if Cal_accepted then
                                  begin
                                     Cal_ready := True;
                                     Save_cal_file(Cal_filename,
Cal_spec, NO_cal_conc_ppm, diode_shift);
                                     Save_DkRef_files('Dk_ref.spc',
Dark_spec, Ref_spec);
                                  end
                              else
                                  Cal_ready := False;
                       end
                  else
                     begin
                        Excess_shift_warning;
                        Cal_ready := False;
                     end;
              end
          else
```

```
                      Cal_ready := False;
{Reject cal for ln(0) problem}
          end;
   until Cal_ready;
   RetCode := SioDTR(Com1, 'S');
{Signal FEAT ready to begin communications}
   FlipData_out(chr($15), 1);
   FlipData_out(chr($1B)+chr(0), 2);
{Move cursor to beginning of line 1}
   start_scan;
   repeat
      NO_sum := 0;
{Clear sum variables}
      NO_error_sum := 0;
      NH3_sum := 0;
      NH3_error_sum := 0;
      fit_count := 0;
      For Scan := 1 to samples do
         begin
            while (not Timer_expired) do;
{collect sample Spectra}
            PDA_Scan;
            element_count := 0; fit_status := True;
            For diode_number:= NO_lower_diode to
NO_upper_diode do
               begin
                  element_count := element_count + 1;
                  Denominator := Data[diode_number]-
Dark_spec[diode_number];
                  if (Denominator > 0) and
(Ref_spec[diode_number] > 0) then
                     y_NO[element_count] :=
ln(Ref_spec[diode_number]/Denominator)
                  else
                     begin
                        fit_status := FALSE;
                        break;
                     end;
               end;
            if fit_status then
               begin
                                                  {extract
NH3 peak A}
                     element_count := 0;
                     For diode_number:= NH3a_lower_diode to
NH3a_upper_diode do
                     begin
                           element_count := element_count +
1;
```

```pascal
                                    Denominator :=
Data[diode_number]-Dark_spec[diode_number];
                                    if (Denominator > 0) and
(Ref_spec[diode_number] > 0) then
                                    y_NH3[element_count] :=
ln(Ref_spec[diode_number]/Denominator)
                                    else
                                    begin
                                          fit_status := FALSE;
                                          break;
                                    end;
                              end;
                  end;
            if fit_status then
                  begin
                                                      {extract
NH3 peak B}
                              For diode_number:= NH3b_lower_diode to
NH3b_upper_diode do
                              begin
                                    element_count := element_count +
1;
                                    Denominator :=
Data[diode_number]-Dark_spec[diode_number];
                                    if (Denominator > 0) and
(Ref_spec[diode_number] > 0) then
                                    y_NH3[element_count] :=
ln(Ref_spec[diode_number]/Denominator)
                                    else
                                    begin
                                          fit_status := FALSE;
                                          break;
                                    end;
                              end;
                  end;
            if fit_status then
                  begin
                        Baseline_Correct(y_NO);
                        lstsqr4(x_cal_NO, y_NO, no_slope,
no_slope_err, no_intercept,
                              no_intcpt_err, no_sigma,
NO_elements);
                        temp_NO := NO_slope * NO_cal_conc_ppm;
                        temp_err := NO_slope_err * NO_cal_conc_ppm;
                        NO_sum := NO_sum + (0.9275 * temp_NO +
0.0001933 * temp_NO * temp_NO);
                        NO_error_sum := NO_error_sum + (0.9275 *
temp_err + 0.0003866 * temp_err * temp_NO);
                        NH3_baseline_correct(x_master_NH3, y_NH3,
1);          {don't correct master file}
```

```
                    lstsqr4(x_cal_NH3, y_NH3, NH3_slope,
NH3_slope_err, NH3_intercept,
                            NH3_intcpt_err, NH3_sigma,
upper_peakb_end);
                    NH3_sum := NH3_sum + NH3_slope *
NH3_cal_conc_ppm;
                    NH3_error_sum := NH3_error_sum +
NH3_slope_err * NH3_cal_conc_ppm;
                    fit_count := fit_count + 1;
                end;
         end;
         if fit_count > 0 then
             begin
                 NO := NO_sum / fit_count;
                 NO_error := NO_error_sum / fit_count;
                 NH3 := NH3_sum /fit_count;
                 NH3_error := NH3_error_sum / fit_count;
             end
         else
             begin
                 NO := 0;
                 NO_error := -1;
             end;
         str(NO:6:1, NO_str);
         str(NH3:6:1, NH3_str);
         data_out := '';
         if NO_error > 1000.0 then
             error_str := '*****'
         else
             str(NO_error:5:1, error_str);
         if NH3_error > 1000.0 then
             NH3_error_str := '*****'
         else
             str(NH3_error:5:1, NH3_error_str);
         data_out := NO_str+'  '+error_str+'   '+NH3_str+'
'+NH3_error_str+chr(13)+chr(10);
         RetCode := SioPuts(Com1, out_pointer, 30);
         FlipData_out(' [NO] '+NO_str+' '+chr(158)+'
'+error_str+'[NH3] '+
                                      NH3_str+' '+chr(158)+'
'+NH3_error_str+chr($1B)+chr(0), 42);
   until button_pressed;
   Timer_continue := False;
{Stop data collection}
   RetCode := SioDTR(Com1, 'C');
{Signal FEAT Mono not enabled}
   FlipData_out(chr($15)+chr($0F), 2);
{Clear display and turn on cursor}
   delay(2000);
{Wait till last command is finished}
```

```
   RestoreHostIT(@Old_IRQ1_vector, IRQ1_CHANNEL);
{Restores the IT vector and disable

{the appropriate IRQ channel.}
   SetIRQ16430(0,0);
{Disable board IRQ.}
   RestoreHostIT(@Old_IRQ2_vector, IRQ2_CHANNEL);
{Restores the IT vector and disable

{the appropriate IRQ channel.}
   SetIRQ26430(0,0);
{Disable board IRQ.}
   RetCode := SioDone(Com1);
   RetCode := SioDone(Com2);
end.
```

E - Durbin-Watson Statistics

Distribution of Durbin–Watson d:
5% Significance Points of d_L and d_U

n	$k = 1$ d_L	d_U	$k = 2$ d_L	d_U	$k = 3$ d_L	d_U	$k = 4$ d_L	d_U	$k = 5$ d_L	d_U
15	1.08	1.36	0.95	1.54	0.82	1.75	0.69	1.97	0.56	2.21
16	1.10	1.37	0.98	1.54	0.86	1.73	0.74	1.93	0.62	2.15
17	1.13	1.38	1.02	1.54	0.90	1.71	0.78	1.90	0.67	2.10
18	1.16	1.39	1.05	1.53	0.93	1.69	0.82	1.87	0.71	2.06
19	1.18	1.40	1.08	1.53	0.97	1.68	0.86	1.85	0.75	2.02
20	1.20	1.41	1.10	1.54	1.00	1.68	0.90	1.83	0.79	1.99
21	1.22	1.42	1.13	1.54	1.03	1.67	0.93	1.81	0.83	1.96
22	1.24	1.43	1.15	1.54	1.05	1.66	0.96	1.80	0.86	1.94
23	1.26	1.44	1.17	1.54	1.08	1.66	0.99	1.79	0.90	1.92
24	1.27	1.45	1.19	1.55	1.10	1.66	1.01	1.78	0.93	1.90
25	1.29	1.45	1.21	1.55	1.12	1.66	1.04	1.77	0.95	1.89
26	1.30	1.46	1.22	1.55	1.14	1.65	1.06	1.76	0.98	1.88
27	1.32	1.47	1.24	1.56	1.16	1.65	1.08	1.76	1.01	1.86
28	1.33	1.48	1.26	1.56	1.18	1.65	1.10	1.75	1.03	1.85
29	1.34	1.48	1.27	1.56	1.20	1.65	1.12	1.74	1.05	1.84
30	1.35	1.49	1.28	1.57	1.21	1.65	1.14	1.74	1.07	1.83
31	1.36	1.50	1.30	1.57	1.23	1.65	1.16	1.74	1.09	1.83
32	1.37	1.50	1.31	1.57	1.24	1.65	1.18	1.73	1.11	1.82
33	1.38	1.51	1.32	1.58	1.26	1.65	1.19	1.73	1.13	1.81
34	1.39	1.51	1.33	1.58	1.27	1.65	1.21	1.73	1.15	1.81
35	1.40	1.52	1.34	1.58	1.28	1.65	1.22	1.73	1.16	1.80
36	1.41	1.52	1.35	1.59	1.29	1.65	1.24	1.73	1.18	1.80
37	1.42	1.53	1.36	1.59	1.31	1.66	1.25	1.72	1.19	1.80
38	1.43	1.54	1.37	1.59	1.32	1.66	1.26	1.72	1.21	1.79
39	1.43	1.54	1.38	1.60	1.33	1.66	1.27	1.72	1.22	1.79
40	1.44	1.54	1.39	1.60	1.34	1.66	1.29	1.72	1.23	1.79
45	1.48	1.57	1.43	1.62	1.38	1.67	1.34	1.72	1.29	1.78
50	1.50	1.59	1.46	1.63	1.42	1.67	1.38	1.72	1.34	1.77
55	1.53	1.60	1.49	1.64	1.45	1.68	1.41	1.72	1.38	1.77
60	1.55	1.62	1.51	1.65	1.48	1.69	1.44	1.73	1.41	1.77
65	1.57	1.63	1.54	1.66	1.50	1.70	1.47	1.73	1.44	1.77
70	1.58	1.64	1.55	1.67	1.52	1.70	1.49	1.74	1.46	1.77
75	1.60	1.65	1.57	1.68	1.54	1.71	1.51	1.74	1.49	1.77
80	1.61	1.66	1.59	1.69	1.56	1.72	1.53	1.74	1.51	1.77
85	1.62	1.67	1.60	1.70	1.57	1.72	1.55	1.75	1.52	1.77
90	1.63	1.68	1.61	1.70	1.59	1.73	1.57	1.75	1.54	1.78
95	1.64	1.69	1.62	1.71	1.60	1.73	1.58	1.75	1.56	1.78
100	1.65	1.69	1.63	1.72	1.61	1.74	1.59	1.76	1.57	1.78

Source: J. Durbin and G. S. Watson, *Biometrika*, **38** (1951).

E-1

F - Emission Factors from Literature

Reference	Component	Factor	Factor (+/-)	Units	Location	g/km	g/mi	g/L	g/gal
Rogak, et al, JAWMA, 1998, 48:604	NOx	0.87	0.26	g/km	Cassiar Tunnel, 1995	0.87	0.92	5.22	19.75
		0.72		g/km	Cassiar Tunnel, 1993	0.72	0.76	4.32	16.35
					Cassiar Average	0.80	0.84	4.77	18.05
		0.24		g/km	Tuscorora Tunnel, 1992	0.24	0.25	1.44	5.45
		0.79		g/km	Ft McHenry, 1992, uphill	0.79	0.84	4.74	17.94
		0.38		g/km	Ft McHenry, 1992, downhill	0.36	0.38	2.16	8.17
					Ft McHenry Average	0.58	0.61	3.45	13.05
		1.10		g/km	Gubrist, SW, 1993	1.10	1.17	6.60	24.97
Pierson, Gertler, et al.	NO	29.00	4.00	g/gal	Ft McHenry, 1992, uphill	0.55	0.88	4.98	18.85
Atmos. Environ., 30:12, pp. 2233-225 canister		21.00	2.00	g/gal	Ft McHenry, 1992, downhill	0.40	0.64	3.61	13.65
(adjusted from "as NO$_2$" to "as NO")		14.00	10.00	g/gal	Tuscarora Tunnel, 1992	0.26	0.43	2.40	9.10
FEAT Studies	NO	7.59	0.48	g/gal	Austin, 1998	0.22	0.35	2.01	7.59
used reported relative errors of		15.20	0.95	g/gal	Chicago, 1997	0.44	0.71	4.01	15.20
5% (CO, NO) and 15% (HC) to calculate		15.75	0.99	g/gal	Chicago, 1998	0.46	0.74	4.16	15.75
an overall relative error of 6.28%		14.64	0.92	g/gal	Chicago, 1999	0.43	0.68	3.87	14.64
		12.43	0.78	g/gal	Chicago, 2000	0.36	0.58	3.28	12.43
					Chicago Average	0.42	0.68	3.83	14.51
		23.21	1.46	g/gal	Denver, 1999	0.67	1.08	6.13	23.21
		19.89	1.25	g/gal	Denver, 2000	0.58	0.93	5.26	19.89
		18.79	1.18	g/gal	Denver, 2001	0.55	0.88	4.96	18.79
					Denver Average	0.60	0.96	5.45	20.63
		14.37	0.90	g/gal	Los Angeles, 1999	0.42	0.67	3.80	14.37
		16.58	1.04	g/gal	Los Angeles, 2000	0.48	0.77	4.38	16.58
		15.47	0.97	g/gal	Los Angeles, 2001	0.45	0.72	4.09	15.47
					Los Angeles Average	0.45	0.72	4.09	15.47
		22.43	1.41	g/gal	Phoenix, 1999	0.65	1.05	5.93	22.43
					Overall FEAT Average	0.47	0.75	4.26	16.13

Reference	Component	Factor	(+/-)	Factor Units	Location	g/km	g/mi	g/L	g/gal
Cadle, Steven, et.al. ES&T, 33:14, pg 2328 (FTP on dyno)	NOx				Denver, '96/'97 (summer)				
ir of Automobiles (#): 1971 - 1980 (6)		2.52		g/mi		1.57	2.52	14.25	53.93
1981 - 1985 (7)		1.59		g/mi		0.99	1.59	8.99	34.03
1986 - 1990 (9)		1.50		g/mi		0.93	1.50	8.48	32.10
1991 - 1996 (5)		0.46		g/mi		0.29	0.46	2.60	9.84
(aggregate of 23 cars ranging from 1971 - 1996, all tested on dyno)	NOx				Denver, '96/'97 (winter)				
ir of Automobiles (#): 1971 - 1980 (8)		1.82		g/mi		1.13	1.82	10.29	38.95
1981 - 1985 (8)		2.07		g/mi		1.29	2.07	11.70	44.30
1986 - 1990 (6)		1.38		g/mi		0.86	1.38	7.80	29.53
1991 - 1996 (5)		0.73		g/mi		0.45	0.73	4.13	15.62
Heeb, N.V., et. al. Atmos. Environ., 34(2000), pg 1123 (without Catalytic Converter, average of 15 readings over speeds of 5 to 145 km/hr)	NO	1.80		g/km	Switz., FTP dyno ('96)	1.80	1.91	10.81	40.92
Heeb, N.V., et. al. Atmos. Environ., 34(2000), pg 1123 (WITH Catalytic Converter, average of 15 readings over speeds of 5 to 145 km/hr)	NO	0.14		g/km	Switz., FTP dyno ('96)	0.14	0.15	0.87	3.29
Heeb, N.V., et. al. Atmos. Environ., 34(2000), pg 1123 (Hypothetical fleet with 70% cars having effective catalytic converters)	NO	0.61		g/km	Switz., Calculated ('96)	0.61	0.65	3.67	13.89

Reference	Component	Factor	(+/-)	Factor Units	Location	g/km	g/mi	g/L	g/gal
Kirchstetter, Singer, Harley ES&T (1999) 33:2, pg 318 (readings are est. from a bar graph)	NOx	8.00		g/L	Caldecott Tunnel (1994)	0.88	1.42	8.00	30.28
		7.00		g/L	Caldecott Tunnel (1995)	0.77	1.24	7.00	26.50
		6.50		g/L	Caldecott Tunnel (1996)	0.71	1.15	6.50	24.60
		6.40		g/L	Caldecott Tunnel (1997)	0.70	1.13	6.40	24.23
					Caldecott Tunnel Average	0.77	1.23	6.98	26.40
Corvalan and Urrutia JAWMA 50, pp. 2102-2111	NOx Dyno	0.66	converted to "as NO"	g/km	Santiago, Chile, 1998 to 200	0.43	0.46	2.57	9.74
Average for United States LDV Nitric Oxide Emissions:						0.54	0.77	4.38	16.58
Singer and Harley, 1996, JAWMA, 46:	CO	364.00		g/gal	7 sites in SOCAB, 1991, by IR Remote	10.57	17.01	96.16	364.00
Singer and Harley Atmos. Environ., 2000, 34, pp. 1783-:	CO	80.00	7.00 g/l		Los Angeles, 1997	8.79	14.15	80.00	302.83
Bishop, Stedman, McLaren, Pierson, Atmos. Environ., 30:12, pp. 2307-231 (FTIR)	CO	150.19	10.66 g/gal		Ft. McHenry Tunnel, 1992	6.62	7.02	39.68	150.19
Rogak, et al, JAWMA, 1998, 48:604	CO	4.84	0.88	g/km	Cassiar Tunnel, 1995	4.84	5.13	29.03	109.89
		67.00	20.00	g/L	Cassiar Tunnel, 1995	11.17	11.85	67.00	253.62
		49.00	20.00	g/L	Cassiar Tunnel, 1994	8.17	8.67	49.00	185.48
					Cassiar Tunnel Average	8.06	8.55	48.34	183.00
		78.20		g/L	*Caldecott Tunnel, 1994*	13.04	13.83	78.20	296.01
		47.80		g/L	*Tuscorora Tunnel, 1992*	7.97	8.46	47.80	180.94
		55.30		g/L	Ft McHenry, 1992, uphill	9.22	9.78	55.30	209.33
		46.80		g/L	Ft McHenry, 1992, downhill	7.80	8.28	46.80	177.15
					Ft McHenry, Average	8.51	9.03	51.05	193.24

Reference	Component	Factor	(+/-)	Factor Units	Location	g/km	g/ml	g/L	g/gal
Pierson, Gertler, et al.	CO	210.00	9.00	g/gal	Ft McHenry, 1992, uphill	6.10	9.81	55.48	210.00
Atmos. Environ., 30:12, pp. 2233-225		177.00	2.00	g/gal	Ft McHenry, 1992, downhill	5.14	8.27	46.76	177.00
(adjusted from "as NO$_2$" to "as NO"					Ft McHenry, Average	5.62	9.04	51.12	193.50
		181.00	10.00	g/gal	Tuscarora Tunnel, 1992	5.26	8.46	47.82	181.00
FEAT Studies	CO	135.58	8.51	g/gal	Austin, 1998	5.97	6.34	35.82	135.58
used reported relative errors of		154.18	9.68	g/gal	Chicago, 1997	6.79	7.20	40.73	154.18
5% (CO, NO) and 15% (HC) to calculate		135.39	8.50	g/gal	Chicago, 1998	5.96	6.33	35.77	135.39
an overall relative error of 6.28%		122.13	7.67	g/gal	Chicago, 1999	5.38	5.71	32.26	122.13
		90.63	5.69	g/gal	Chicago, 2000	3.99	4.23	23.94	90.63
					Chicago Average	5.53	5.87	33.18	125.58
		154.73	9.72	g/gal	Denver, 1999	6.82	7.23	40.88	154.73
		149.20	9.37	g/gal	Denver, 2000	6.57	6.97	39.42	149.20
		118.81	7.46	g/gal	Denver, 2001	5.23	5.55	31.39	118.81
					Denver Average	6.21	6.58	37.23	140.92
		185.12	11.63	g/gal	Los Angeles, 1999	8.15	8.65	48.91	185.12
		171.31	10.76	g/gal	Los Angeles, 2000	7.55	8.01	45.26	171.31
		132.63	8.33	g/gal	Los Angeles, 2001	5.84	6.20	35.04	132.63
					Los Angeles, Average	7.18	7.62	43.07	163.02
		72.22	4.54	g/gal	Phoenix, 1999	3.18	3.37	19.08	72.22
					Overall FEAT Average	5.61	5.96	33.67	127.46

Reference	Component	Factor	(+/-)	Factor Units	Location	g/km	g/mi	g/L	g/gal
Cadle, Steven, et.al. ES&T, 33:14, pg 2328 (FTP on dyno)	CO				Denver, '96/'97 (summer)				
ir of Automobiles (#): 1971 - 1980 (8)		63.70		g/mi		39.58	63.70	360.12	1363.18
1981 - 1985 (7)		21.40		g/mi		13.30	21.40	120.98	457.96
1986 - 1990 (9)		6.46		g/mi		4.01	6.46	36.52	138.24
1991 - 1996 (5)		3.44		g/mi		2.14	3.44	19.45	73.62
(aggregate of 23 cars ranging from 1971 - 1996, all tested on dyno)	CO				Denver, '96/'97 (winter)				
ir of Automobiles (#): 1971 - 1980 (6)		59.60		g/mi		37.03	59.60	336.94	1275.44
1981 - 1985 (6)		45.30		g/mi		28.15	45.30	256.10	969.42
1986 - 1990 (6)		14.90		g/mi		9.26	14.90	84.24	318.86
1991 - 1996 (5)		17.00		g/mi		10.56	17.00	96.11	363.80
Bonsang, B. and Touaty, M. Atmos. Environ., 34(2000), pg 985	CO	12.97		g/mi	Paris, Thials Tunnel ('96)	8.06	12.97	73.32	277.56
		6.58		g/mi	Fort McHenry Tunnel ('96)	4.08	6.56	37.09	140.38
		4.96		g/mi	Tuscarora Tunnel ('96)	3.08	4.96	28.04	106.14
Kirchstetter, Singer, Harley ES&T (1999) 33:2, pg 318	CO	84.00		g/L	Caldecott Tunnel (1994)	9.23	14.86	84.00	317.97
(readings are est. from a bar graph)		70.00		g/L	Caldecott Tunnel (1995)	7.69	12.38	70.00	264.97
		65.00		g/L	Caldecott Tunnel (1996)	7.14	11.50	65.00	246.05
		66.00		g/L	Caldecott Tunnel (1997)	7.25	11.67	66.00	249.83
					Caldecott Tunnel average	7.83	12.60	71.25	269.70
Moeckli, M.A., Fierz, M, and Sigrist, M. ES&T (1996) 30:9, pg 2864	CO	5.20	0.50	g/km	Gubrist Tunnel, 1995	5.20	5.52	31.19	118.06
Corvalan and Urrutia JAWMA 50, pp. 2102-2111	CO Dyno	6.51		g/km	Santiago, Chile, 1998 to 200	6.51	6.91	39.05	147.80
Average for United States LDV Carbon Monoxide Emissions:						7.12	9.85	55.68	210.76

Reference	Component	Factor	Factor (+/-)	Units	Location	g/km	g/mi	g/L	g/gal
Bishop, Stedman, McLaren, Pierson, HC Atmos. Environ., 30:12, pp. 2307-231 (FTIR)	HC	18.39	6.07	g/gal	Ft. McHenry Tunnel	0.81	0.86	4.86	18.39
Cadle, Steven, et.al. ES&T, 33:14, pg 2328 (FTP on dyno)	HC				Denver, '96/97 (summer)				
r of Automobiles (#): 1971 - 1980 (6)		6.60		g/mi		4.10	6.60	37.31	141.24
1981 - 1985 (7)		2.65		g/mi		1.65	2.85	14.98	56.71
1986 - 1990 (9)		0.77		g/mi		0.48	0.77	4.35	16.48
1991 - 1996 (5)		0.24		g/mi		0.15	0.24	1.36	5.14
(aggregate of 23 cars ranging from 1971 - 1996, all tested on dyno)	HC				Denver, '96/97 (winter)				
r of Automobiles (#): 1971 - 1980 (6)		4.42		g/mi		2.75	4.42	24.99	94.59
1981 - 1985 (6)		4.05		g/mi		2.52	4.05	22.90	86.67
1986 - 1990 (6)		1.17		g/mi		0.73	1.17	6.61	25.04
1991 - 1996 (5)		1.39		g/mi		0.86	1.39	7.86	29.75
FEAT Studies	HC								
used reported relative errors of 5% (CO, NO) and 15% (HC) to calculate an overall relative error of 6.28%		7.18	0.45	g/gal	Chicago, 1997	0.32	0.34	1.90	7.18
		7.18	0.45	g/gal	Chicago, 1998	0.32	0.34	1.90	7.18
		6.08	0.38	g/gal	Chicago, 1999	0.27	0.28	1.61	6.08
		5.25	0.33	g/gal	Chicago, 2000	0.23	0.25	1.39	5.25
					Chicago Average	*0.28*	*0.30*	*1.70*	*6.42*
		6.91	0.43	g/gal	Denver, 1999	0.30	0.32	1.82	6.91
		6.36	0.40	g/gal	Denver, 2000	0.28	0.30	1.68	6.36
		6.36	0.40	g/gal	Denver, 2001	0.28	0.30	1.68	6.36
					Denver Average	*0.29*	*0.31*	*1.73*	*6.54*
		3.32	0.21	g/gal	Los Angeles, 1999	0.15	0.15	0.88	3.32
		3.32	0.21	g/gal	Los Angeles, 2000	0.15	0.15	0.88	3.32
		2.76	0.17	g/gal	Los Angeles, 2001	0.12	0.13	0.73	2.76
					Los Angeles, Average	*0.14*	*0.15*	*0.83*	*3.13*
		7.29	0.46	g/gal	Phoenix, 1999	0.32	0.34	1.93	7.29
					Overall FEAT Average	*0.26*	*0.27*	*1.54*	*5.85*
Average for United States LDV Hydrocarbon Emissions:						0.55	0.78	4.43	16.77

Reference	Component	Factor	(+/-)	Factor Units	Location	g/km	g/mi	g/L	g/gal
Moeckli, M.A., Fierz, M, and Sigrist, M. ES&T (1996) 30:9, pg 2864	NH3	0.02	0.00	g/km	Gubrist Tunnel, 1995	0.02	0.02	0.09	0.34
Kean, Harley, et al. ES&T, 2000, 34, pg 3535	NH3	0.48	29.00	g/L	Caldecott Tunnel (1999)	0.05	0.08	0.48	1.80
Fraser, M.P, Cass, G.R. ES&T, 1998, 32, pg 1053	NH3	0.38		g/L	Sherman Way Tunnel Van Nuys, CA (1993	0.04	0.07	0.38	1.44
Baum, et al. ES&T, 2001, 35, pp. 3735-3741	NH3 IR Remote	0.67	0.06	g/L	LA Freeway ramp	0.07	0.12	0.67	2.52
Durbin, Wilson, et al. Atmos. Environ., 2002, 36:9, pp.1475	NH3 FTP, Dyno FTIR	0.05		g/mi	Lab, non-cat to ULEV	0.03	0.05	0.31	1.16
Average for United States LDV Ammonia Emissions:						0.05	0.08	0.46	1.73
Bradley, et al. ES&T, 2000, 34, pp 897-899	N2O	0.59 / 0.41	0.04 / 0.04	g/kg / g/kg	Denver,CO (10Jul 1997) / Tech Rpt EPA-420-R-009	0.05 / 0.03	0.08 / 0.05	0.43 / 0.30	1.63 / 1.13
Becker et al. ES&T 1999, 33, pp 4134-4139	N2O	0.01	0.00	g/km	Ford FTIR dyno study, 1997	0.01	0.01	0.07	0.25
Jimenez, JL., et al. Chemosphere: Global Change Science 2000, 2, pp. 397 - 412 (assumed CO/CO2 = 0.028 to calc emission factor)	N2O	1.08	0.02	g/gal	Manchester, NH (1998)	0.05	0.05	0.29	1.08
Average for United States LDV Nitrous Oxide Emissions:						0.03	0.05	0.27	1.02

G - Colorado Springs Traffic Volume Map

(Obtained from Colorado Department of Transportation, www.dot.state.co.us)

G-1
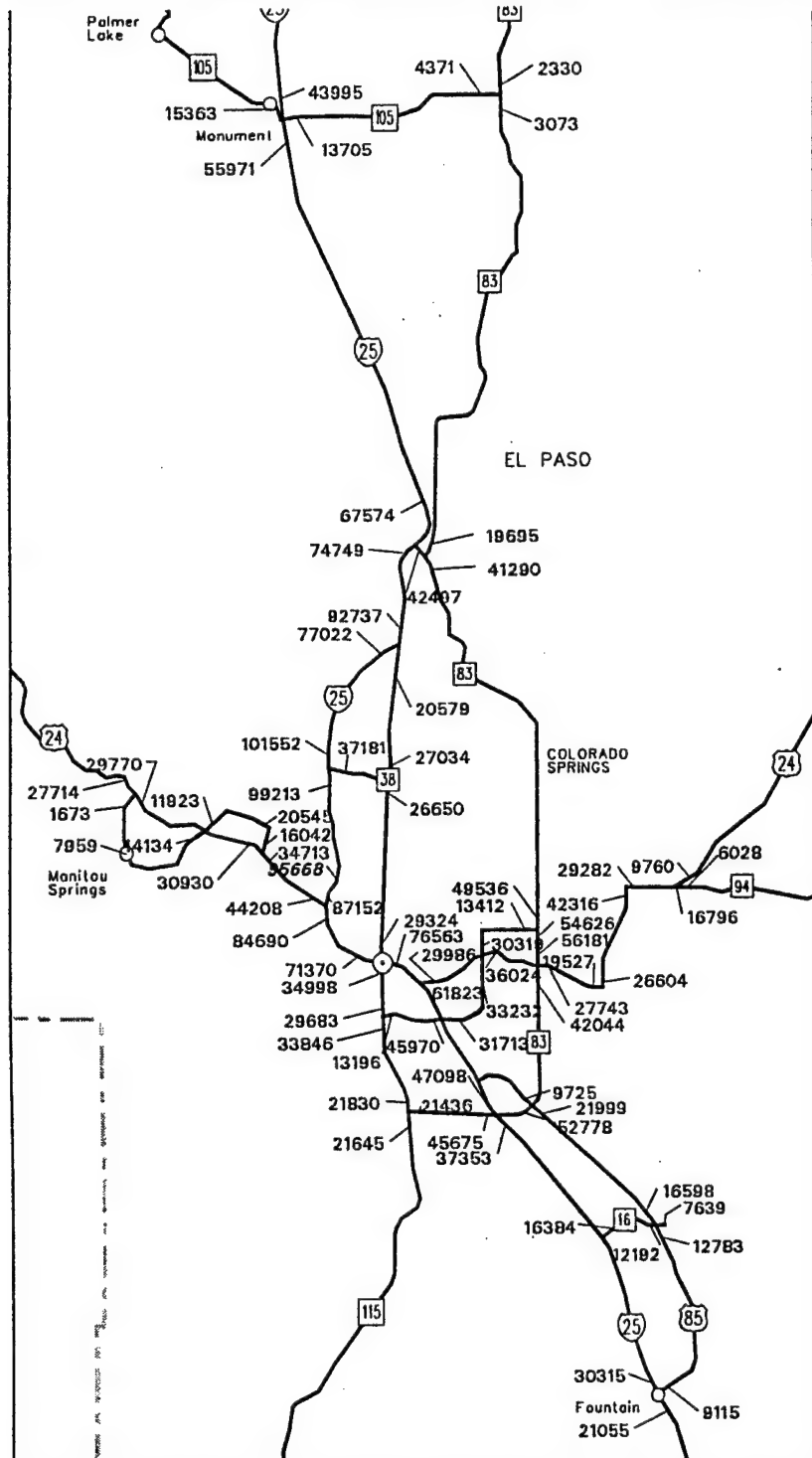
CHARACTERIZING MOTOR VEHICLE FLEET EMISSIONS BY
OPEN-PATH SPECTROSCOPY

—————

An Abstract of a Dissertation

Presented to

the Faculty of Natural Sciences, Mathematics, and Engineering

University of Denver

—————

In Partial Fulfillment

of the Requirements for the Degree

Doctor of Philosophy

—————

by

Daniel M. Branan

August 2002

This work presents a cheaper, easier and more flexible alternative to other types of real-world automotive emissions measurement techniques by the use of open-path spectroscopy. The "Tunnel-less Tunnel Study" is described as a method for the direct measurement of fleet and mode-averaged emission factors for CO, N_2O, CH_4, NH_3 and NO.

Through several measurement campaigns in Colorado, 2363 FTIR spectra were collected and analyzed in the cities of Denver and Colorado Springs, as well as in the Rocky Mountain foothills. This technique is shown to be flexible and robust, yielding results that are in general agreement with the literature. The detection-limits and sensitivities of this new application are also investigated and quantified.

The application of these measurements is the creation of a first-ever calculation of a fuel-based mobile-source emissions inventory for the Colorado Springs Area. The table below shows the inventories for carbon monoxide and nitrous oxide for both the fuel-based method and the computer modeling method currently employed by the Colorado Department of Public Health and the Environment (CDPHE).

Finally, as justification for this method being potentially easier and cheaper than existing methods, the case is made for minimizing the number of days required for an estimation of the fleet averaged emission factors at a particular site. After decreasing the number of sampling days to sets of four, three and two by randomly selecting from the available days at the given site, it was discovered that the uncertainty in the estimate of the CO emission factor increased from 17% to 22%,

and that the standard deviation of the group of emission factors calculated in each case was much less than this uncertainty.

Fuel-based Results		
1999	tons/year	tons/day	+/-
CO	52,300	143	23
NO	6,800	19	1.1
2000			
CO	55,500	152	24
NO	7,200	20	1.2
2001			
CO	54,700	150	24
NO	7,100	20	1.2
CDPHE Computer Modeling Results			
1999	tons/year	tons/day	+/-
CO	65,513	179.5	N/A
NO	7,023	19.2	N/A
2000			
CO	105,576	289.2	N/A
NO	11,978	32.8	N/A
2001			
CO	Not Available		
NO			

Table 1 - Mobile Source Emissions Inventories for Colorado Springs, CO

This work presents a cheaper, easier and more flexible alternative to other types of real-world automotive emissions measurement techniques by the use of open-path spectroscopy. The "Tunnel-less Tunnel Study" is described as a method for the direct measurement of fleet and mode-averaged emission factors for CO, N_2O, CH_4, NH_3 and NO.

Through several measurement campaigns in Colorado, 2363 FTIR spectra were collected and analyzed in the cities of Denver and Colorado Springs, as well as in the Rocky Mountain foothills. This technique is shown to be flexible and robust, yielding results that are in general agreement with the literature. The detection-limits and sensitivities of this new application are also investigated and quantified.

The application of these measurements is the creation of a first-ever calculation of a fuel-based mobile-source emissions inventory for the Colorado Springs Area. The results of this inventory are compared to those generated by the computer model used by the Colorado Department of Public Health and the Environment. The only emissions common between both methods are those for carbon monoxide (CO) and nitric oxide (NO). In actuality, the State calculates total nitrogen oxides (NOx) and reports in units of tons NO_2. The fuel-based method measures NO directly, but these figures are reported as tons of NO_2 for comparison's sake.

Finally, as justification for this method being potentially easier and cheaper than existing methods, the case is made for minimizing the number of days required for an estimation of the fleet averaged emission factors at a particular site. After

decreasing the number of sampling days to sets of four, three and two by randomly selecting from the available days at the given site, it was discovered that the uncertainty in the estimate of the CO emission factor increased from 17% to 22%, and that the standard deviation of the group of emission factors calculated in each case was much less than this uncertainty.